Towards A Better Understanding of Lithium Ion Local Environment in Pure, Binary and Ternary Mixtures of Carbonate Solvents : A Numerical Approach

Veerapandian Ponnuchamy

UNIVERSITÉ DE GRENOBLE

THÈSE

Pour obtenir le grade de

DOCTEUR DE L'UNIVERSITÉ DE GRENOBLE

Spécialité : **Physique**

Arrêté ministériel : 7 Aôut 2006

Présentée par

Veerapandian PONNUCHAMY

Thèse dirigée par **Valentina Vetere**
et codirigée par **Stefano Mossa**

préparée au sein **Laboratoire des Composants pour Piles combustibles et Electrolyseurs et de Modlisation (CEA LITEN)**
et de **Ecole Doctorale Physique**

Towards A Better Understanding of Lithium Ion Local Environment in Pure, Binary and Ternary Mixtures of Carbonate Solvents: A Numerical Approach

Thèse soutenue publiquement le **23 January 2015**,
devant le jury composé de :

Prof. Timothy ZIMAN
CNRS DR1, LPMMC, UMR 5493, Maison des Magistéres CNRS, 38042 Grenoble, France, Président

Prof. Laurent JOUBERT
Universit de Rouen, COBRA UMR CNRS 6014, Rue Tesnire 76821 Mont Saint-Aignan Cedex, France, Rapporteur

Prof. Jean-Sebastian FILHOL
Institut Charles GERHARDT - CNRS 5253 Universit Montpellier 2, 34095 Montpellier Cedex 5, France, Rapporteur

Dr. Valentina VETERE
Chercheur, CEA/LITEN/DEHT, 38054 Grenoble, France , Directeur de thèse

Dr. Stefano MOSSA
Chercheur, CEA/INAC/SPrAM, 38054 Grenoble, France , Co-Directeur de thèse

Abstract

Due to the increasing global energy demand, eco-friendly and sustainable green resources including solar, or wind energies must be developed, in order to replace fossil fuels. These sources of energy are unfortunately discontinuous, being correlated with weather conditions and their availability is therefore strongly fluctuating in time. As a consequence, large-scale energy storage devices have become fundamental, to store energy on long time scales with a good environmental compatibility. Electrochemical energy conversion is the key mechanism for alternative power sources technological developments. Among these systems, Lithium-ion (Li^+) batteries (LIBs) have demonstrated to be the most robust and efficient, and have become the prevalent technology for high-performance energy storage systems. These are widely used as the main energy source for popular applications, including laptops, cell phones and other electronic devices.

The typical LIB consists of two (negative and positive) electrodes, separated by an electrolyte. This plays a very important role, transferring ions between the electrodes, therefore providing the electrical current. This thesis work focuses on the complex materials used as electrolytes in LIBs, which impact Li-ion transport properties, power densities and electrochemical performances. Usually, the electrolyte consists of Li-salts and mixtures of organic solvents, such as cyclic or linear carbonates. It is therefore indispensable to shed light on the most important structural (coordination) properties, and their implications on transport behaviour of Li^+ ion in pure and mixed solvent compositions.

We have performed a theoretical investigation based on combined density Functional Theory (DFT) calculations and Molecular Dynamics (MD) simulations, and have focused on three carbonates, cyclic ethylene carbonate (EC) and propylene carbonate (PC), and linear dimethyl carbonate (DMC). DFT calculations have provided a detailed picture for the optimized structures of isolated carbonate molecules and Li+ ion, including pure clusters $Li^+(S)_n$ (S=EC, PC, DMC and n=1-5), mixed binary clusters, $Li^+(S_1)_m(S_2)_n$ (S1, S2 =EC, PC, DMC, with m+n=4), and ternary clusters $Li^+(EC)_l(DMC)_m(PC)_n$ with l+m+n=4. Pure solvent clusters were also studied including the effect of PF_6^- anion. We have investigated in details the structure of the coordination shell around Li^+ for all cases.

Our results show that clusters such as $Li^+(EC)_4$, $Li^+(DMC)_4$ and $Li^+(PC)_3$ and $Li^+(PC)_4$ are the most stable, according to Gibbs free energy values, in agreement with previous experimental and theoretical studies. The calculated Gibbs free energies in binary mixtures suggest that the clusters such as $Li^+(EC)_2(PC)_2$, $Li^+(EC)_3(DMC)$ and $Li^+(PC)_3(DMC)$ are more preferable one in their corresponding binary mixtures. In the case of ternary mixtures, $Li^+(EC)_2(DMC)(PC)$ is most preferable and the DMC molecule cannot replace EC and PC, while PC can easily substitute both EC and DMC molecules. Our

study shows that PC tends to substitute EC in the solvation shell.

We have complemented our ab-initio studies by MD simulations of a Li-ion when immersed in the pure solvents and in particular solvents mixtures of interest for batteries applications, e.g., EC:DMC (1:1) and EC:DMC:PC(1:1:3). MD is a very powerful tool and has allowed us to clarify the relevance of the cluster structures discovered by DFT when the ion is surrounded by bulk solvents. Indeed, DFT provides information about the most stable structures of isolated clusters but no information about their stability or multiplicity (entropy) when immersed in an infinite solvent environment. The MD data, together the DFT calculations have allowed us to give a very comprehensive picture of the local structure of solvent mixtures around Lithium ion, which substantially improve over previous work. Some preliminary information about the dynamics of these long-lived local structures is also given.

Résumé

En raison de l'augmentation de la demande d'énergie, ressources écologiques respectueux de l'environnement et durables (solaires éoliennes) doivent être d éveloppées afin de remplacer les combustibles fossiles. Ces sources d'énergie sont discontinues, étant corrélés avec les conditions météorologiques et leur disponibilité est fluctuant dans le temps. En conséquence, les dispositifs de stockage d'énergie à grande éechelle sont devenus incontournables, pour stocker l'énergie sur des échelles de temps longues avec une bonne compatibilité environnementale. La conversion d'énergie électrochimique est le mécanisme clé pour les développements technologiques des sources d'énergie alternatives. Parmi ces systèmes, les batteries Lithium-ion (LIB) ont démontré être les plus robustes et efficaces et sont devenus la technologie courante pour les systèmes de stockage d'énergie de haute performance. Ils sont largement utilisés comme sources d'énergie primaire pour des applications populaires (ordinateurs portables, téléphones cellulaires, et autres). La LIB typique est constitué de deux électrodes, séparés par un électrolyte. Celui-ci joue un rôle très important dans le transfert des ions entre les électrodes fournissant la courante électrique. Ce travail de thèse porte sur les matériaux complexes utilisés comme électrolytes dans les LIB, qui ont un impact sur les propriétés de transport du ion Li et les performances électrochimiques. Habituellement l'électrolyte est constitué de sels de Li et de mélanges de solvants organiques, tels que les carbonates cycliques ou linéaires. Il est donc indispensable de clarifier les propriétés structurelles les plus importantes, et leurs implications sur le transport des ions Li^+ dans des solvants purs et mixtes. Nous avons effectué une étude théorique basée sur la théorie du fonctionnelle densité (DFT) et la dynamique moléculaire (MD), et nous avons consideré des carbonates cyclique (carbonate d'éthylène, EC, et carbonate de propylène, PC) et le carbonate de diméthyle, DMC, linéaire. Les calculs DFT ont fourni une image détaillée des structures optimisées de molécules de carbonate et le ion Li^+, y compris les groupes pures $Li^+(S)_n$ (S =EC,PC,DMC et n=1-5), groupes mixtes binaires, $Li^+(S_1)_m(S_2)_n$ (S_1,S_2=EC,PC,DMC, m+n=4), et ternaires $Li^+(EC)_l(DMC)_m(PC)_n$ (l+m+n=4). L'effet de lanion PF_6^- a également été étudié. Nous avons aussi étudié la structure de la couche de coordination autour du Li^+, dans tous les cas. Nos résultats montrent que les complexes $Li^+(EC)_4$, $Li^+(DMC)_4$ et $Li^+(PC)_3$ sont les plus stables, selon les valeurs de l'énergie libre de Gibbs, en accord avec les études précédentes. Les énergies libres de réactions calculés pour les mélanges binaires suggèrent que l'ajout de molécules EC et PC aux clusters Li^+-DMC sont plus favorables que l'addition de DMC aux amas Li^+-EC et Li^+-PC. Dans la plupart des cas, la substitution de solvant aux mélanges binaires sont défavorables. Dans le cas de mélanges ternaires, la molécule DMC ne peut pas remplacer EC et PC, tandis que PC peut facilement remplacer EC et DMC. Notre étude montre que PC tend à substituer EC dans la couche de solvation. Nous avons complété nos études ab-initio par des simulations MD d'une ion Li^+ immergé dans les solvants purs et dans des mélanges de

solvants d'intérêt pour les batteries, EC:DMC(1: 1) et EC:DMC:PC(1:1:3). MD est un outil très puissant et nous a permis de clarifier la pertinence des structures découvertes par DFT lorsque le ion est entouré par des solvants mélangés. En effet,la DFT fournit des informations sur les structures les plus stables de groupes isolés, mais aucune information sur leur stabilité ou de la multiplicité (entropie) lorsqu'il est immergé dans un environnement solvant infinie. Les données MD, ainsi que les calculs DFT nous ont permis de donner une image très complète de la structure locale de mélanges de solvants autour le ion lithium, sensiblement amélioré par rapport aux travaux précédents.

"Dedicated
to my beloved Parents
and to my beloved wife Esakkiammal Sudha"

Acknowledgements

First of all, I would like to thank my thesis advisors Dr. Valentina Vetere and Dr. Stefano Mossa for providing me all the opportunities for completing this work. Their knowledge, care, and inspiration for this work pushed me to expand my knowledge and research potential, without their constant support I would have never reached this academic achievement. Since, they come from the two different fields (Chemistry and Physics), I have developed my knowledge in Chemistry and I have learned physics as well. My boss (Stefano) always telling I am a lucky person and of course I am, because I have got quite nice bosses for my academic degree. I also would like to thanks my previous group leader Dr. Arnaud Buhot for an occasional discussions.

I would like to thank my all past and current members in both petit SPrAM/GT and DEHT/LITEN groups, I particularly thank to my senior post-doc Dr. Ioannis Skarmoutsos for the wide discussions in my work, and my colleagues Daiane Damasceno Borges and Timothée Menais and other Members: Benjamin, Pablo, Luiz, Yoshinori. I am also grateful to Senthinathan anna for my computational work.

I would like to express my special thanks to Prof. P. Venuvanalingam (Master thesis supervisor) and Mrs. J . Jeyachristi Bai (My high school chemistry teacher) who have helped and inspired me in many ways and I wish to extend my great thanks to *udan pirava annans* Kalyanraman Balasubramanian and Ramachandran Balasubramanian for helping me navigate my life through good times and for being as a good brothers, and I would very grateful to thank my dearest akka-anna Sri Devi-Rajasekar for their constant support both in work and also in life and also thanks to Vijay Solomon, Sabareesh, Manikandan, Velavan and my Grenoble friends, Master and Bachelor friends.

Moreover, I would like to express my gratitude to the CEA for the financial and admistrative support over the last three years, without which I would never have been able to undertake this research project.

I would like to say tons of thanks to my amma Muthumariammal and my appa Ponnuchamy for their love and unselfish support and their hard working all over their lives always impacts me deeply Without them, this dissertation would have never been accomplished. I would also very grateful to my Periappa Kalimuthu, Periamma Ramuthai for their constant support. Also, I would like to thank my Mamiyar (mother-in-law) Parvathi for her wishes, my sister Sangeetha, and my sister-in-laws Devi- Prabhakaran and Indra for their well-wishes.

My special thanks go to my beloved wife Esakkiammal Sudha, My study and life in France as well as in India is more wonderful, of course she is the backbone of my everything. Without her endless love and courage, this thesis would be impossible to publish.

Contents

List of Figures

List of Tables

1

Introduction and Motivations

In the first section of this chapter, we briefly discuss the most important devices that are used for energy storage. In the following, we mainly focus on rechargeable batteries, particularly lithium-ion batteries, and their main components such as the electrolyte. Next, we give a general overview and the state of the art of the properties and applications of different carbonate solvents such as ethylene carbonate, dimethyl carbonate and propylene carbonate in pure and in the presence of salts, like $LiPF_6$. In the following sections, we will discuss the motivations for introducing solvent mixtures and provide an overview of the most recent literature. Finally, we will state our main motivations for this work and provide a general overview of the manuscript.

1.1 Introduction

An increasing global energy demand and the associated environmental implications are most important issues in modern society. In the past two decades, the need of efficient energy storage has increased dramatically. Indeed, devices such as cars, electric vehicles, cell phones, televisions, are used in everyday life, but a considerable fraction of the energy needed for their functioning still comes from the fossil fuels like oil, natural gas or coal. Unfortunately, these classes of fuels are the most important responsible for producing greenhouse gases, which severely arm the environment. In order to reduce the large amount of carbon-dioxide emission in atmosphere, alternative energy sources are needed. Various technologies have been introduced in the past, such as solar cells, batteries, fuel cells and super capacitors. Green electricity or renewable energies have been successfully generated from wind or solar natural sources, which are unfortunately correlated to weather conditions and therefore strongly fluctuating in time. As a consequence, large-scale energy storage devices are now fundamental, to store energy on long time scales with a good environmental compatibility. Electrochemical energy conversion is the key mechanism for alternative power sources in technological investigation.

Conversion and electrochemical energy storage devices include fuel cells, batteries, and super-capacitors. These technologies are widely used in several applications such as portable devices, transportations, industries [3–7]. Although the conversion mechanisms and energy storage strategy used in these devices are different, they show common features like an energy-providing process which takes place at the inter-phase between three segments: anode, electrolyte and cathode. More precisely, all devices are composed by two electrodes which are separated by the electrolyte solution [3, 4, 6, 8, 9]. The chemical energy is converted into electric energy through redox reactions in batteries and fuel cells. In the case of electrochemical super-capacitors, the energy is stored from the accumulation of charges at the interface between electrodes and electrolyte, in which there is no chemical reaction occur inside the system. In the following, we briefly discuss composing materials, energy conversion mechanisms and functioning of all devices.

Fuel Cells [9] are devices that convert the chemical energy supplied as a fuel into electric energy, by a chemical reaction with oxidizing oxygen. We show an example of fuel cell [1] in Figure 7.1(b). This device sensibly differs from batteries, requiring constant sources of fuels and oxygen for the chemical reaction to occur. Fuel cells supply energy with an efficiency of more than 80%, are environment friendly and are mainly used in stationary applications [10] and transportations. Polymer electrolyte (or proton exchange) membrane fuel cells (PEMFC)[11] are mostly used in stationary, automotive and portable devices. In PEMFCs, high protonic conductivity is obtained in presence of water. Other properties include: oxidative stability, electro-osmosis, low water transport and low electronic conductivity [8]. The PEMFC role is that it allows proton transport from anode to the cathode. This membrane is mostly made of organic polymers which contains acid functional groups such as sulfonic, carboxylic and phosphonic acids. In which, it dissociates with presence of water to allow H_3O^+ hydrated proton transport[11]. The main drawback of a fuel cell is that it can continuously produce electricity as long as the fuel is provided. Batteries are therefore required to storage the electricity produced, as we will see below.

Primary batteries[8, 12] are devices that can be used only once and are subsequently discarded, as they cannot be re-charged with electricity as secondary batteries do. The electrochemical reactions which occur in the cell are not reversible and the battery stops working when the reactions complete. In 1860, Leclanché invented the first primary battery, consisting of a carbon-zinc cell[2], as shown in Figure 7.1(a). Natural manganese dioxide-carbon black was employed as the cathode and the electrolyte was a combination of ammonium chloride-zinc chloride contain in a zinc can. Synthetic manganese oxide has subsequently given better performance than natural manganese oxide. The carbon-zinc with zinc chloride electrolyte primary battery has same performance as zinc-manganese and outsold worldwide in 2003. Alkaline electrolyte potassium hydroxide (KOH) in zinc-manganese is mostly used in primary batteries, because it provides a better performance

[1] http://en.wikipedia.org/wiki/Fuel-cell
[2] http://www.daviddarling.info/encyclopedia/L/Leclanche-cell.html

than carbon-zinc cell. Moreover, the same electrolyte was used in several electronic devices and also more reliable in high energy applications. There are several sort of primary cells: lithium thionyl chloride, zinc-silver oxide, lithium-sulfur dioxide cells. Lithium primary cells are more widely used than alkaline cells, due to high energy density. The lithium metal is used as the anode in lithium cells and the voltage exceeds 3.7 V, due to the strong negative potential of lithium. The drawback of lithium cells is a lower rate capability, due to a non-aqueous electrolyte with low conductivity. The solid electrode interphase (SEI) (electronically insulating film which selectively allows lithium ion transport) can easily be formed in lithium cells. Other primary cell $Li-SOCl_2$ and $Li-SO_2$ system are used in long range temperature applications and also in applications like transponders, military and car electronics.

Recently, *Electrochemical capacitors* [6] or *Ultra capacitors* [13, 14] have significantly attracted because of their high power density, long cycle-life (>100000 cycles), fast charge and discharge and high output power. Its power delivery performance which perfectly fills the gap [15] between batteries/fuel cells (high energy storage) and traditional dielectric capacitors(high power output) [14]. They also act as temporary energy storage devices, when coupled with fuel cells and batteries. A electrochemical super-capacitor [3] is shown in Figure 7.1(c). There are however some disadvantages, such as high production costs and low energy density. Two main classes of electrochemical capacitors are used, such as redox super-capacitors of *pseudo*-capacitor and electric double-layer capacitors (EDLC). The difference of these capacitor is that the reversible redox reactions involve between electrolyte and electro-active species on the electrode surface in *pseudo*-capacitor but no reaction in EDLC [13].

Recently, lithium-ion capacitors (LICs) have more attention to researchers in order to achieve battery level energy density with power density super-capacitors. However, the kinetic imbalance of electrodes in LICs remains a problem and in order to overcome this issue functionalized graphene is used to balance the kinetics and leads to storage of lithium [16]. Moreover, the oxide functional groups in graphene cathode greatly act as radical centers which stores lithium at high potential.[17]

This thesis work particularly focused on secondary lithium-ion batteries that we discuss in the following section.

1.2 Rechargeable Batteries

Among the different storage technologies, batteries are the most efficient and robust devices. Batteries convert chemical energy into electrical energy or vice-versa, via electrochemical reversible oxidation-reduction reactions.The first reported rechargeable battery was based on Nickel-Cadmium (Ni-Cd) electrodes and alkaline (KOH) solution was an

[3] https://gigaom.com/2011/07/12/how-ultracapacitors-work-and-why-they-fall-short

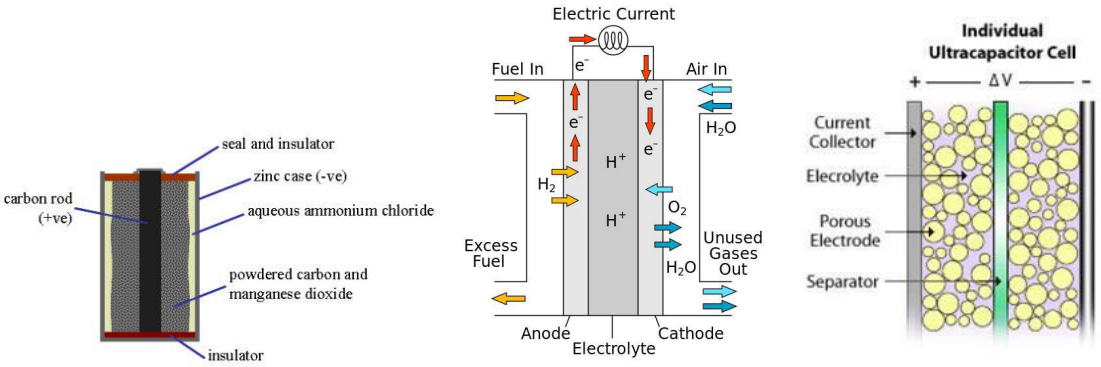

(a) Primary (Leclanché) Cell (b) Fuel Cell (c) Capacitor

FIGURE 1.1: Electrochemical Devices such as a) Primary or Leclanché cell, consists of an anode(zinc rod) and cathode a carbon plate surrounded by packed manganese dioxide and the electrodes were dipped into a solution of ammonium and zinc chlorides b) proton conducting fuel cell c) Schematic diagram of Ultracapacitors also have two metal plates called electrodes immersed in an electrolyte

electrolyte [8]. The Ni metal constitutes the positive electrode (cathode), whose function is to insert/de-insert protons while charging/discharging. The Ni cathode actually exists as a $Ni(OH)_2$ electrode. Cd constitutes the negative electrode (anode), which works reversibly, and the discharge product is $Cd(OH)_2$. Due to toxic character of Cd and a poor energy density, this device has been replaced by the Nickel-Metal hydride (Ni-MH) cell. Although, Ni-MH has a higher energy storage capability and weightless as well. This,however, failed to properly work at low temperatures although it played an important role in the developments in electric vehicles, motors and portable electronic device market.

Due to the above drawbacks of Nickel-metal batteries a new type of battery was developed, the **lithium battery**. In particular, Lithium-ion batteries(LIBs) have been used since a few decades and with particular success in a wide range of technologies, including portable electronic devices and novel automotive applications, due to their high energy efficiency(>90 %), power density storage, and long cycling life (>5000 cycle). Other explored technologies, such as lead acid, nickel-cadmium and nickel-hybrid [2, 18–22] batteries have been demonstrated not to be well suited for such applications, due to low energy density as compared to lithium-ion batteries. Comparison of energy densities of different classes of batteries are shown in Figure 7.2 The development of the electrochemistry of the Li-ion has been mostly due to its small ionic radius and low molecular weight, both beneficial for diffusion. Moreover, it has a low redox potential $E^{\circ}(Li^{+}/Li) = -3.04V$ [23] compared to SHE (Standard Hydrogen Electrode) so it can easily reduced. This process make a potential difference between the electrodes and lithium transport also obtained. Also Lithium is more stable against non-aqueous solvents. Initially, lithium has been used in primary batteries, and after some decades it is by now the main component of rechargeable batteries[12]. The capacity and operating

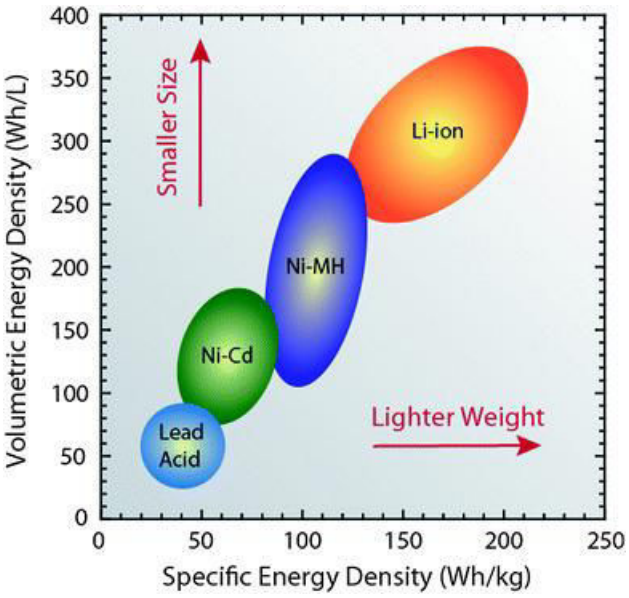

FIGURE 1.2: Comparison of rechargeable battery technologies as a function of volumetric and specific energy densities. Figure from the Reference [1]

voltage of LIB are 700 to 2400 mA.h and $\sim$ 3.6 V, respectively. The operating temperature of LIBs ranges in 15-60 °C [24]. Unfortunately, at low temperature, ($<$ 15 °C), the capacity becomes quite low, while at high temperature, ($>$ 60 °C), degradation of the electrode materials becomes important. The pioneering scientists Whittingham and Goodenough [25] had been developed lithium-ion battery cathode materials in 1970.The first commercial lithium-ion battery was produced by Sony Co. in 1991 [26] and was based on $LiCoO_2$ and petroleum coke. We show a schematic diagram of a Lithium-ion battery in Figure 7.3(a).

After 1991, development of LIBs has substantially grown, especially during the last two decades. LIBs are exploited in high energy density applications and their potential is being explored for use in electric (EV), hybrid electric (HEV) and plug-in hybrid (PHEV)[24] vehicles, as replacements of internal combustion(IC) engines that used fossil fuels, diesels or gasoline to produce electricity.

A normal Lithium-ion battery is composed of a negative carbon (generally graphite) anode and a solid layered metal oxide (e.g. LiT^MO_2, where T is Transition metal) as the cathode. These two electrodes are the sources of chemical reactions and are separated by an electrolyte (lithium-ion conductive medium), which consists of Lithium-salts (e.g., $LiPF_6$) and organic solvents(e.g., ethylene carbonate). The reactions are started when the electrodes are connected to an external load and the electron flow occurs from anode to the cathode. By reversing the process, the battery can be recharged by applying an external current. While charging, the lithium ions are deintercalated (intercalation host) from the cathode(for example, layered $LiCoO_2$[27]) which intercalated between the graphite layers which passes through electrolyte. The discharging is reverse process.

During intercalation/deintercalation, reactions occur in the electrolyte, which decomposes and forms the solid electrolyte inter-phase (SEI)[28–34]. The SEI is formed at the graphite anode surface, where the graphite is turned into an other form LiCx, where LiC_6 is the highest degree of intercalation. The SEI have been studied using X-ray and it comprises the compounds such as lithium oxalate ($Li_2C_2O_4$), lithium methoxide ($LiOCH_3$) and lithium succinate ($LiO_2CCH_2CH_2CO_2Li$)[35] respectively. Moreover, The performance of the graphite anode is largely determined by the specific features of the SEI film. Numerous factors control the chemical composition of SEI, e.g., the choice of solvents and of the electrolyte salt, operating temperature, nature of the surface, type of anode etc. The SEI layer prevents the electrode surface corrosion from decomposition reaction of the electrolyte. During the study of SEI layer formation, the ethylene carbonate solvent involved in the SEI later formation. An in-depth control of composition, morphology and structure of the SEI are needed in order to design better electrodes and electrolyte compositions [27], which is the most important goal in the LIB technology. The SEI have been studied using X-ray and it comprises the compounds such as lithium oxalate ($Li_2C_2O_4$), lithium methoxide ($LiOCH_3$) and lithium succinate ($LiO_2CCH_2CH_2CO_2Li$)[35] respectively. Moreover, The performance of the graphite anode is largely determined by the specific features of the SEI film.

Metal air batteries: The intercalation/deintercalation reactions affect the energy density of lithium-ion batteries. This issue has driven the development of an alternative approach, metal-air batteries [36–40]. In this batteries, the cathode intercalation material is replaced with catalytically oxygen reduction reaction (ORR) and oxygen evolution reaction (OER). The metal-air batteries such as Li-air and Zn-air batteries are widely used because of their high energy density, environment friendliness and low cost. A Li-air battery [4] is shown in Figure 7.1(b).

It generates electricity via redox reaction between metal and oxygen in air. Metal-air batteries also face some issues like a low efficiency of the anode, a limited energy density of the cathode, and high corrosion of the anode in contact with the electrolyte. The formation of hydroxides, metal oxides and other species which accumulate at the anode surface prevents the discharging process. In the following sections, we will se the electrolytes involved in batteries.

1.3 Electrolytes in Batteries: Fundamentals

Electrolytes are a crucial component for all electrochemical devices as discussed above. Electrolytes are composed by salts (solutes) dissolved in solvents and they act as the conductive medium which transfer the charges or ions between the electrodes. Performances of the devices depend on both the electrolyte and electrode materials. The electrolyte material must be chemically compatible when the electrodes to avoid stability issues

[4] http://www.transportation.anl.gov/features/2009-Li-air-batteries.html

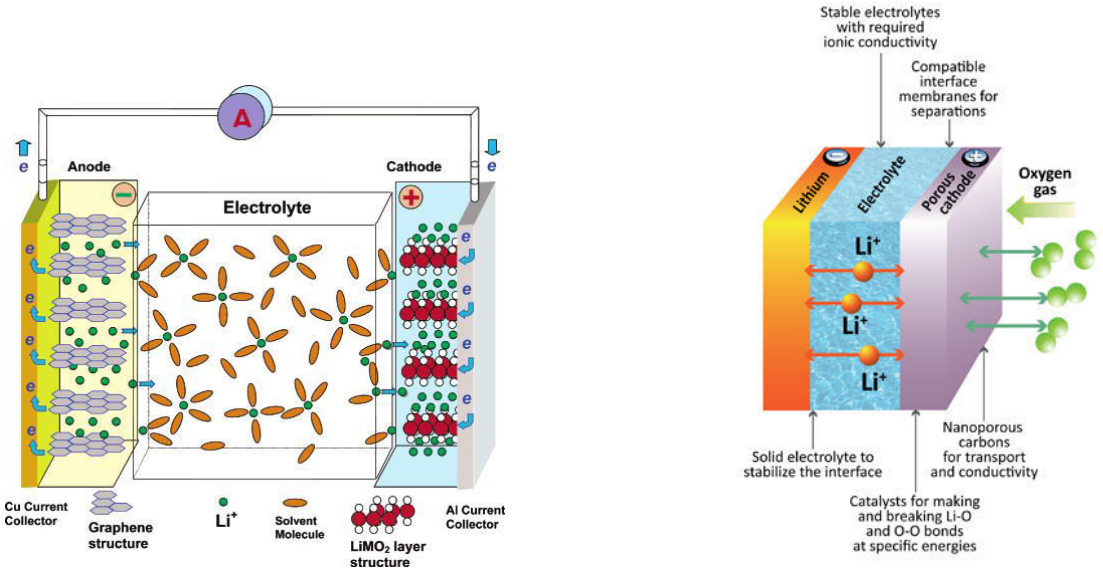

(a) Lithium-ion Battery

(b) Lithium-Air Battery

FIGURE 1.3: Lithium Batteries types : a) Schematic diagram of lithium ion battery (LIB) consisting of the positive electrode (Li-intercalation compound and negative electrode (graphitic carbon) separated by electrolyte, Figure from Reference [2], b) Li-air battery consists of catalytic air cathode that supplies oxygen, an electrolyte, and a lithium anode)

and the chemical reactions taking place in the electrolyte control both quantity and speed of the energy released towards the electrodes. Also, electrolytes must be highly stable or completely inert when on contact with the electrode surface, otherwise they fail to produce high energy densities. The reaction rate of the reductive and oxidative decomposition is controlled by the electrolyte concentration.

In order to develop better electrolytes a few issues should be considered [12]: *1)* temperature range for stability. For instance, the EC solvent is solid at room temperature, therefore affecting conductivity and reactivity of the salt, e.g., $LiPF_6$; *2)* flammability, it is therefore crucial to consider safety problems; *3)* solvent efficiency in dissolving lithium salts; and *4)* considerable loss of concentration of lithium-ion in electrolytes, because those lithium ions are involved in the formation of SEI. The electrolyte must therefore fulfil many requirements, such as being environment friendly, inert toward electrode substrates and cell separator, highly efficient for oxidative and reductive decomposition, and show a good ionic conductivity.

Electrolytes in Batteries: Electrolytes are in close interaction with both electrodes and play a crucial role in LIBs. They provide the ion-conductive medium of the lithium-ion battery, where the Li^+ shuttles between the electrodes. The electrolytes must be characterized a high chemical stability, that prevents decomposition when oxidizing at the cathode or reducing at the anode. Some important properties, like non-toxicity, low melting point, high boiling point, the absence of explosive reaction, are required for a

good electrolyte in batteries applications. Three types of electrolytes have been used in batteries: *aqueous*, *non-aqueous* and *solid*.

An *aqueous electrolyte* consists of a strong acid or base, due to the more polarity those exist as ions like positive and negative in solution. These electrolytes are stable in particular voltage ranges, while beyond these limits, they start to decompose. The stability of the provided voltage is controlled by the electrolyte composition degree of purity. High ionic conductivities can be achieved in aqueous electrolytes when dielectric constant and solvating power of the materials are reasonably high.

Non-aqueous electrolytes are formed by carbonate solvents with common lithium salts such as $LiBF_4$, $LiClO_4$, $LiPF_6$, $LiAsF_6$, LiTFSI (lithium bis-(trifluoromethane sulfonyl) iodide) and LiBOB (lithium bis-oxalato borate). The conductivity of non-aqueous electrolytes are in the range of 10^{-2}-10^{-3} Scm^{-1}. More specifically, these electrolytes are non-aqueous aprotic (unable of acting as proton donors) organic solvents, combined with lithium salts. They are characterized by low toxicity and melting point, good ion conductivity and electrochemical stability towards the electrodes. The two classes of electrolytes that have been used in batteries are: *i)* linear alkyl carbonates (dimethyl carbonate (DMC), ethyl methyl carbonate (EMC), and diethyl carbonate (DEC)) and *ii)* cyclic alkyl carbonates (ethylene carbonate (EC), vinylene carbonate (VC), and propylene carbonate (PC)). A large number of studies have been devoted to their decomposition, electrochemical properties, and the formation and structure of the first solvation shell around lithium ions[33, 41–44]. Due to lower dielectric constant and lower solvating power of some solvents, the formation of ion pairs is enhanced, resulting in a lower ionic conductivity. Indeed, in this case ions are bound to each other and no longer freely diffuse in solution. At present, mixtures of solvents with different compositions are used to enhance the conductivity, and to achieve good low temperature performances. Pure solvents and solvent mixtures are discussed in the following sections.

Carbonates such as EC and PC have failed to be used as solvents in *lithium-air batteries* because of their decomposition reaction with O_2. In particular, super-oxides or radicals are formed during initial reduction of O_2[45]. Less volatile ether-based compounds such as dimethylether(DME) or larger ether compound electrolytes have been preferred as good candidates for lithium-air batteries [46, 47].

Beyond carbonates, silicon liquids have also received substantial attention. Several studies have focused on carbonate-modified electrolytes [48–50], siloxane and silyl ether[35, 51, 52] and ethylene-glycol[53–55] compounds. Instead of carbonate solvents mixed with lithium salts, polymer and copolymer electrolytes have also been considered, formed by poly(ethylene)oxide (PEO) and lithium salts ($LiPF_6$ or $LiCF_3SO_3$)[56–58].

In the past 15 years, Ionic Liquids (IL) [59–61] have attracted much attention as lithium-ion battery electrolytes. Indeed, ILs are interesting alternatives to organic solvents in

batteries due to their unique properties such as electrochemical stability, low or no toxicity, low flammability, low vapour-pressure properties, high charge density and tunable polarity. ILs with a melting temperature higher or close to room temperature are called room-temperature ionic liquids (RTILs). ILs are charged molecules and other than some advantages, it has relatively high viscosity which will affect the ionic conductivity. ILs are entirely comprised of cation with basis amines such as pyridinium, imidazolinium , piperidinium, pyrrolidinium and morpholinium [62–64]. The anion can be inorganic like BF_4^-, PF_6^-, CN^- or AsF_6^-. The IL properties also based on the nature of the substituents whose affect the ionicity and salt solubility. The alkyl chain lengths[62] or branching chain length increases the conductivity of the IL upto 1 $mScm^{-1}$.

The peculiar effect of ion-ion interactions, molecular charge distribution and molecular shapes are the main properties of IL in both bulk solutions and at the interfaces. Contrary to what happens in normal solvents, the ion-pair effects are not predominant in ILs, and therefore the molar conductivity rises up to 0.1 Scm^2mol^{-1}. ILs also have low dielectric constant and vapour pressure. ILs show, however, moisture sensitivity, properties associated with halogen atoms and moderately high viscosity.

Different classes of ILs are used in a large electrochemical window and can achieve high charge densities. A virtually infinite number of IL electrolytes can be produced, by mixing different ILs or mixing ILs with other inorganic or organic polar solvents.

In the following section, we start our discussion of the organic solvents most used in applications as the main component of electrolytes.

1.4 Organic Solvents and Salts

In this section we briefly discuss the pure solvents we have considered in this work, EC, DMC and PC, and their physical properties. We also discuss previous work on the Li^+-carbonate interaction. In particular we will first focus on the bibliography reporting mostly theoretical calculation without a specific salt in pure clusters. Next we will present additional results highlighting the role played by chosen from the chosen Li salts ($LiPF_6$, $LiClO_4$, $LiBF_4$, and others).

1.4.1 Physical Properties of Ethylenecarbonate (EC), Dimethylcarbonate (DMC), Propylenecarbonate(PC)

Among all organic solvents, the most widely used in LIBs cyclic and linear carbonates. In particular, the EC solvent is very commonly used as the main component in electrolytes, due to its high dipole moment (4.9 D), dielectric constant ($\varepsilon \sim 89$), and miscibility with most of the non-aqueous solvents [65, 66]. Some physical properties of the EC are shown in Table 7.1. At room temperature EC is solid (melting point temperature

36.4°), therefore it is mixed with other carbonate solvents in order to lower the overall melting point temperature. In most cases, a small percentage of linear carbonates, like DMC, is added to EC to turn the resulting mixture into the liquid state at room temperature. DMC is chosen because of its low viscosity, low boiling point and low dielectric constant (values are shown in Table 7.1). The combination of EC and DMC in different concenrations forms a homogeneous mixture characterized by low viscosity and high ion conductivity. This mixture is stable up to 5.0 V at the cathode surface.

The PC solvent is another attractive cyclic carbonate, characterized by a higher dielectric constant ($\varepsilon \sim 64.9$) than linear carbonates. The ionic conductivity and static stability over a wide temperature range, make PC as a preferred solvent for lithium. PC is a five member ring molecule, like EC with an extra methyl group in the side chain. However, PC behaves differently than EC. For instance, several studies have shown that EC plays an important role in the formation of the Solid Electrolyte Interfaces (SEI), which in particular protects, protects graphite anodes from further decomposition. The SEI is formed during the first slow charge of a battery, and the quality of its strcuture strongly impacts the lifetime of the system. In contrast, in systems only containing pure PC, no SEI is effectively formed on the graphite electrode surface [67]. Also, PC undergoes a susceptible reduction reaction after a single electron transfer [68] from lithium which impacts the cycling efficiency of the system. Despite these issues, PC molecule has also been considered as a promising solvent due to high anodic stability. In fact, the first commercial battery (produced by Sony and co.) was developed based on a PC solvent electrolyte. Structure and some physical properties of PC are shown in Table 7.1. Based on the data shown in the Table, PC appears to have a slightly higher viscosity than EC, therefore PC cannot lower the viscosity of EC as DMC does.

In the last decades, several theoretical an experimental work has been published on the coordination properties of EC, PC and DMC with Li^+ ions. In fact, the understanding of the solvation properties of carbonate electrolytes with Li^+ is crucial to understand a number of physical phenomena occurring in LIBs, like transport properties, stability in redox environment, and degradations phenomena. For instance, Masia et al., [69] studied the solvation structure of Li^+ with EC molecules, using DFT and MD methods. The DFT results have shown that a 4-coordinated complex $Li^+(EC)_4$, is the dominant species. Similarly, they also found the same coordination number ($Li^+(EC)_4$) in MD simulations. A similar result have been obtained by Wang et al.,[70] by a DFT study, confirming the $Li^+(EC)_4$ species as the most stable complex for the $Li^+(EC)_{1\text{-}4}$ series. They also studied the $Li^+(DMC)_{1\text{-}3}$ complexes and found that $Li^+(DMC)_3$ is the most stable conformation. Moreover they have also studied addition and substitution reaction on mixed complexes with EC and DMC solvents, concluding that the addition of DMC to the $Li^+(EC)_n$ with n=1-3 complexes is favourable, while substitution of DMC to the $Li^+(EC)_2$ complex is forbidden.

According to Hiroto et al.,[71] studies on EC with Li^+ ion by AIMD (ab-initio molecular

TABLE 1.1: Structure, Chemical formula, Dielectric constant, Viscosity and Melting Point (Mp) and Boiling point (Bp) of Solvents such as EC, DMC and PC

Solvent	Structure	Dielectric Constant, ε	Viscosity η (cP)	Mp/Bp (°C)
EC ($C_3H_4O_3$)	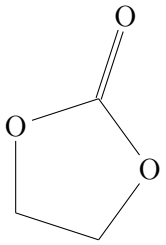	89	1.85 (40° C)	36.4/248
DMC ($C_3H_6O_3$)	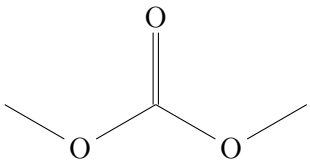	3.1	0.78 (30° C)	4.6/91
PC ($C_4H_6O_3$)	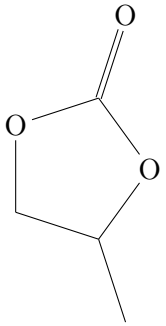	64	2.53 (30° C)	-48.8/242

dynamics), the Li^+ ion is solvated by four EC molecules in the first solvation shell. In the case of $Li^+(EC)_5$, only four molecules are coordinated with Li^+ ion while the 5^{th} molecule displaced with an average distance of 5.09 Å from the Li^+ ion. Similar results have been obtained by Cho et al.,[72]by DFT calculations. In both papers the authors conclude that the maximum coordination number in the first solvation sphere is 4 and additional EC molecules can be only arranged in the second solvation shell.

Mahesh et al., [73] studied the Li^+ ion with EC solvent by DFT and MD simulation. Gibbs free energy were computed using B3LYP/6-311++G(d,p) on the addition reaction of EC to $Li^+(EC)_n$ (where n = 0 to 5) cluster gives negative values or spontaneous reactions for $Li^+(EC)_{1\text{-}4}$ clusters and positive Δ G value for the $Li^+(EC)_5$ complex. Therefore, they concluded that the formation of a coordination shell with 5 molecules is energetically unfavourable. Also, the AIMD simulation revealed that the coordination number is 4 around Li^+ ion within a range of ∼4 Å. They also reported that there is no exchange of EC molecules once the solvation structure is formed. The same authors also published in following work [74] for PC complexes that $Li^+(PC)_3$ is the leading component, by calculating Gibbs free energy formation. From heat of formation and Gibbs free energy calculations, they concluded that EC acts as a better solvent than PC. Using the

same discussion on ΔG energies, with different DFT approaches, Balbuena et al.,[34] and Wang et al., agreed on the same conclusions, thus confirming a maximum coordination number of 4 for $Li^+(EC)_n$ solvation and explaining that $Li^+(PC)_4$ is unlikely to exist and $Li^+(PC)_2$, $Li^+(PC)_3$ are the main components in solution.

Mostly, the conventional electrolytes consists of lithium salt like $LiPF_6$, $LiClO_4$, $LiBF_4$ etc, and a binary or ternary mixture of carbonates.

1.5 Mixtures of Organic Solvents

Among a variety of solvent electrolytes for LIBs, nowadays mixtures of carbonates containing EC are mostly used with success, due to the following reasons: *i)* even at high concentration of salt (up to 1.0 M), EC molecule can easily dissolve lithium salts, due to its high dielectric constant; *ii)* low melting point of the electrolyte; *iii)* low viscosity of linear carbonate electrolytes with improved chemical stability, ionic trans- port and dielectric permittivity; *iv)* high ionic conductivity at room temperature, which is higher than up to $10^{-3}\Omega^{-1}cm^{-1}$ [75, 76] . This greatly impacts battery performances and is compatible with battery voltage. The mixture compositions are used in a wide temperature range for operations as well as storage applications and cell performance. The choice of the electrolyte is of crucial importance to develop better conventional devices. Therefore, the high dielectric constant of EC molecule is mixed with both liquid carbonate solvent (such as linear carbonates) and PC (cyclic carbonate) to overcome these issues. The ternary mixt ures have been used to enhance at lower-temperature performance of batteries. Mixture of EC and DMC with $LiPF_6$ allows the largest number of charge-discharge processes without loss of capacity.

In the past two decades, very extended research works have been published focusing on EC containing electrolytes. Before the 1970s, EC was used as a co-solvent in electrolytes, in order to obtain good ionic conductivity. In the 1970s, a little amount of PC was added, in order to lower the melting point of EC molecule resulting in a mixture high ionic conductivity in the bulk solution. In early 1990s, conventional LIBs employed with EC solvents and despite of EC high boiling point, little amounts of different co-solvents were added, including PC, THF (tetrahydrofuran), DEE (diethoxyethane). These solvents do not perform satisfactorily, due to the fact that PC causes side reactions affecting the irreversible capacity of the LIBs. Moreover, ether solvent are unstable during oxidation at the charged cathode. After 1994, Tarascon and Guyomard [77, 78] found that the linear carbonate DMC molecule acts as a better co-solvent with EC to form an effective electrolyte.

Indeed, the addition of linear carbonate DMC to EC forms homogeneous mixtures resulting in the decreasing of EC melting temperature [78, 79]. As a result, EC viscosity becomes very low, enhancing ion transport mechanisms and, therefore, increasing ion

conductivity. The addition of EC and PC solvents in adapted ratios has also been used to decrease the melting point of the electrolyte, due to the high permittivity and low melting temperature (-49°) [80] of PC solvent. Further development and improvement of lithium ion batteries still implies to overcome limitations of the above binary mixtures, mainly due to low thermal stability of solvents and high vapour pressure. To date, there of lot of research works have been published in various mixtures with different salts that we discuss below. Some results could be dependent not only from the choice of the electrolyte mixture but also from the salts . For that reason we will discuss bibliography for each salt in separate paragraphs.

1.5.1 EC,PC,DMC + $LiClO_4$

Earlier experimental Raman spectroscopic studies by Hyodo et al., [81] in 1989 focused on the local structure of Li^+ ion solvation in EC and PC with $LiClO_4$ salt. They proposed a coordination number around 4 for Li^+ in EC with a high concentration of 1 M $LiClO_4$ and this value becomes 4.9 at lower concentration, 0.1 M $LiClO_4$. Moreover, they also examined EC:PC mixtures. They reported 3.3 EC molecules and 0.7 molecules of PC at higher concentration (5:1). On the other hand Li^+-EC molecule coordination decreases with increasing the molar ratio of PC. At 1:1 ratio, the number of EC molecule coordinated to Li^+ is 1.9 (on a total coordination number 3.8) meaning that in this case both EC and PC are bound to Li^+ in a 50:50 ratio and there is no preferential solvation in the first solvation shell. Nevertheless, theoretical studies by Klassen et al., [76] investigating the heat of formation of the reactions of Li^+ ion with EC and PC, showed that EC/ Li^+ has a higher solvation energies than PC/ Li^+. They concluded that EC selectively solvates Li^+ in the EC/PC/ $LiClO_4$ solutions. Also DFT and MD studies on $LiClO_4$ with EC, PC and mixtures by Balbuena et al. [82], demonstrated that EC tends to substitute PC in the first solvation shell. They also demonstrated that the EC molecules have a coordination number of 4.1 with $LiClO_4$ in diluted solutions, but it decreases to 3.8 in concentrated solutions. Also, the coordination numbers are 4 and 4.4 in the mixture of EC:PC in 1:1 and 3:1 ratio, respectively. In the first solvation shell, they found 38% of PC bound to Li^+ ion in the 1:1 mixture, and 16% in the 3:1 mixture.

Lithium ion solvation in EC with $LiClO_4$ has been studied by Cazzanelli et al. [83], using NMR techniques, with a concentration defined by the ratio R=[Li^+]/[EC]. They found a solvation number ∼7 at R=0.1 concentration, while at higher concentration (R= 0.33), the Li^+-EC complex formed with ∼3 solvent molecules. Most of the work cited above therefore suggest that the coordination is around 4 for $Li^+(EC)_n$. In contrast, Huang et al., [84] studied the solvation of $LiClO_4$ in EC by Raman and IR spectroscopy and suggested that the average solvation number for Li^+ ions in EC is 6. Also, Matsuda et al., [85] measured the solvation of Li^+ ion in EC and PC with $LiClO_4$ by Electrospray Ionization - Mass spectroscopy (ESI-MS) and showed that $Li^+(EC)_2$ and $Li^+(EC)_3$ are

the main solvation species in 1 mM $LiClO_4$ solution. Similar result were obtained for PC molecules.

In 2002 Inaba et al., [86] studied the linear carbonate (DEC and DMC) co-solvents effect on EC-based solutions, with 1 M $LiClO_4$ by Atomic Force Microscopy (AFM). They reported that 4.6 is the apparent solvation number of Li^+ in EC and this solvation number decreases to 4.2 (3.1 EC+1.1 DEC) and 3.1 (2.9 EC + 0.2 DMC) in EC:DEC(1:1) and EC:DMC(1:1) solutions, respectively. Their results revealed that EC molecule dominantly participate in the first solvation shell over linear carbonates.

1.5.2 EC, PC, DMC + $LiBF_4$

The molecular dynamics simulation studies of Soetans et al., [87] focused on $LiBF_4$ salt in EC, DMC and PC. They performed simulation on Li^+- (EC), Li^+- (DMC) and Li^+- (PC) at different temperatures, in simulations boxes containing 214 solvent molecules for one Li^+ and one BF_4^-, corresponding to 0.1 M concentration. They showed that the typical solvation shell is formed by both EC and PC around Li^+, with a coordination number of 4.

On the other hand, the MD studies of Prezhdo et al., [88] reported that 6 individual carbonate molecules (EC, PC and DMC) can coordinate around Li^+ ion at low concentration (0.1 M) of $LiBF_4$. The coordination decreases to 5 at 1 M concentration. They also described the solvation shell for binary mixtures. Particularly in PC-DME mixtures, lithium ion was found to coordinate with 6 PC molecules, due to absence of the C=O group in DME. In the case of EC-DMC mixtures, 5 EC and 1 DMC molecule were found to solvate Li^+ ion. At higher concentrations, they also found some interaction with the counter anion. In particular, they discussed that the counter anion BF_4^- acts as a monodentate in PC-DME mixtures, and as a bidentate ligand in EC-DMC mixtures.

Sono et al., [89] studied the solvation of Li^+ ion in PC solutions with $LiBF_4$ salt, by Raman and NMR techniques. They reported that Li^+ ion is bound to 1.08 PC molecules, at a concentration over 1 M. This small coordination number is evidence of a more important formation of contact-ion pairs of Li^+- BF_4^-. Recent studies on $LiBF_4$ in PC by Sono et al., [90] demonstrated that at 1 M concentration the total coordination can be attributed as 2.66 for Li^+-O(PC) and 1.38 for Li^+-F (BF_4^-). The Li^+- PC coordination number increases to 3.14 in 0.5 M concentration, while Li^+-F decreases to 0.91, which means that the counter anion BF_4^- interaction is smaller in the first solvation shell.

1.5.3 EC, PC, DCM + LiTFSI

Borodin and Smith et al., [91] studied solvation and transport of Li^+ ion in EC by using MD simulations. They considered LiTFSI (lithium bistrifluoromethane sulfonamide) salt

for the Li^+ ion and studied the system at 313 K. They reported that 2.7-3.2 EC molecules and 0.67-1.05 TFSI anions are bound to Li^+ ion in the first solvation shell. However, approximately 3.8 EC molecules solvated to Li^+ in completely dissociated electrolytes with a typical RDF distance of the Li-O(=C in EC) ∼1.95 Å for all concentrations.

1.5.4 EC, PC, DMC + $LiPF_6$

Morita et al., [92] analysed, by using Raman spectroscopy, Li^+ ion solvation for 3 different concentration of $LiPF_6$ salt in EC. They found coordination numbers of 4.4, 4.1 and 3.9, corresponding to the 3 concentration of $LiPF_6$ 0.5 M, 1.0 M and 1.5 M, respectively. For the EC:DMC mixture in 1 M $LiPF_6$ they obtained a total coordination number of 4.1, which includes 3.0 EC molecules and 1.1 DMC. From this result they concluded that EC coordination with Li^+ ion is preferred over the DMC one.

Tasaki et al., [93] computational studies on $LiPF_6$ salt association with a variety of solvents concluded that solvation numbers of EC, PC and DMC are 3.53, 3.46 and 2.84 and the corresponding Li^+ distances are 2.06, 2.05 and 2.05, respectively. Also, they reported that the PF_6^- ion also participates in the solvation shell around Li^+ ion. Sono et al., [89] studied the solvation of Li^+ ion in PC solution with $LiPF_6$ salt by Raman and NMR techniques and reported that Li^+ ion is bound to 4.3 PC molecule in the diluted solution. They also showed that at higher concentration (2.5M), the ratio of PC/ Li^+ is 4, and almost 25% of PC molecules are free in the solution. However, they also obtained the distorted orientation of PC to Li^+ ion. At the highest concentration 3.29 M, the PC/ Li^+ ratio decreased to 2.85. They also reported in following paper on the same $LiPF_6$ salt [94] that the coordination number is 3 for PC/ Li^+ cluster at 1 M concentration.

Sono et al.,[90] focused on the ion-ion interaction of $LiPF_6$ and $LiBF_4$ in PC solutions. The results show that the $LiPF_6$/ PC solution has a higher ionic conductivity compared to the $LiBF_4$ ones, and they attributed this phenomena to a weaker ion-pair formation. The average solvation number of 1M $LiPF_6$ salt in PC was found to be 3.72. At 0.5 M concentration the solvation number was determined to be 3.97 which indicates that there are fewer formed contact ion pairs than in the 1 M case. In both cases, PF_6^- ion acts as a monodentate ligand.

A Neutron diffraction study of $LiPF_6$ solution in PC by Yasuhiro et al., [95] revealed that 4.5 PC molecules are strongly bound to Li+ ion in the first solvation shell (10 mol % $LiPF_6$ solution in PC). Detailed quantum chemistry and MD simulation studies have also been published by Borodin et al., [96] on the solvation properties of binary mixtures of EC and DMC solvents with $LiPF_6$. The typical MD simulation box contained 480 solvent molecules with 1M $LiPF_6$, and simulations were performed at various temperatures. The results revealed that 3.8 EC molecules are present in the first solvation shell (defined by a cut off radius of 2.8 Å) at 298 K. At higher temperature (333 K), the solvation number

of EC reduces to 3.3. A coordination number of 2.7 is obtained for DMC with $LiPF_6$ at 1 M which is slightly lower than in the EC case. In the case of binary EC:DMC (1:1) mixtures, the same authors found a solvation shell with higher content of DMC than EC. In the first shell, however, there is still some considerable contribution coming from the counter anion PF_6^-. In the same work they also made an interesting discussion about the role played by the DMC conformation, and showed that, for instance, the Li^+-DMC complex prefers a cis-trans conformation for the DMC fragment than the cis-cis one. Nevertheless they found that the $EC_3DMC(cis-cis)/\ Li^+$ complex is more stable than the $EC_4/\ Li^+$ species and that the $EC_3DMC(cis-trans)/\ Li^+$ is less stable than $EC_4/\ Li^+$ because of unfavourable dipole-dipole interactions.

Ganesh et al., [97] performed simulation of EC and PC solvents with $LiPF_6$. The typical distance between Li-O(=C) was found to be about ∼1.94 Å in PC and ∼ 1.92 Å in EC at 310 K (400 K). At higher temperature (400 K), the EC solvation shell was found to be non-spherical to allow some free space inside the shell. The neighbour counter-ion distance of Li^+- PF_6^- is ∼6.0 in EC and ∼9.0 in PC. In the same work it was demonstrated that the apparent solvation number is 4 for PC molecules at 310 and 400 K. In contrast, in the case of EC molecule, the solvation number was shown to be temperature dependent, with 4 EC molecules at 310 K within 3 Å. The authors concluded that EC more effectively solvates Li^+ ion than PC, due to the higher dielectric constant of EC.

Kang Xu [98] performed ^{17}O NMR experiments on EC and DMC with 1 M $LiPF_6$, and found that a maximum of 6 EC molecules can coordinate to Li^+ ion in the primary solvation shell. They also performed the same experiment on EC:DMC(50:50 with 1 M $LiPF_6$) mixtures and showed that around 70 % of the DMC molecule bond to Li^+ ion in the first solvation shell.

On the basis of MD simulations, Tenney et al., [99] studied the Li^+ solvation number in EC, DMC and in the mixture EC:DMC, with $LiPF_6$ salt . These results show that the coordination number varies with concentration and temperature. At the very low concentration of 0.1 M $LiPF_6$, the coordination number of EC around Li^+ are 5.2, 5.0 and 4.2 at 300 K, 350 K, 400 K, respectively. Therefore, the coordination numbers decreases with increasing temperature at fixed concentration. At 1 M $LiPF_6$, the apparent solvation number of EC is 4 at room temperature (300 K) but it decreased to 2.9 at the higher temperature of 400 K. This effect has been explained by observing that at higher temperature, the coordination decreases to 2.9 because the counter anion joins the first solvation shell, thus obtaining a solvation shell formed by 2.9 EC and 1.6 PF_6^- molecules around the Li^+ ion. For DMC, the typical coordination number is 2.3 at 1.0 M (300K) and slightly increases to 2.6 at lower concentration (0.1 M). They also observed that the counter anion PF_6^- involved in both 0.1 M and 1 M concentration. For instance, in the case of pure EC ($LiPF_6$- EC) clusters, the Li^+-PF_6^- coordination numbers were 0.4 and

1.1 in 0.1 M and 1 M at 300 K , respectively. However, in the case of pure DMC($LiPF_6$-DMC) clusters, they found that the Li^+-PF_6^- coordination numbers were 1.7 and 2.1 in 0.1 and 1 M. In the case of 1:1 EC:DMC mixtures (300 K), the coordination numbers of EC and DMC are 3.0 and 2.6 at 0.1 M $LiPF_6$, which decreases to 1.6 for both EC and DMC with 1 M $LiPF_6$. Further contact ion pair study (Li^+ with counter ion) has been performed by Takeuchi [100], who reported a monodentate linkage obtained for PF_6^- in PC solution.

1.6 Motivation and Overview

In the following work of my thesis, I concentrate my study on typical carbonate electrolytes used in LIB technology. In particular, I focused my attention on EC, PC and DMC that are largely used in commercial devised and in recent experimental developments. Although, we presented in previous paragraphs, several studies have already been published on such carbonyl electrolytes, some discrepancy between experimental and theoretical results still remains, and the role of different carbonates mixtures in the solvation shell of Li^+ still matter of debate. From experimental point of view, there is no perfect measurement for how many number of solvents participate in the first solvation shell. However, there have been different solvation numbers available but the results are contrasting to one another. To date, several experimental and theoretical studies devoted to the interactions of Li^+ with pure and mixed carbonate-based electrolytes have already been published, the solvation structure and dynamics of lithium cations in these solvents is still a subject of debate. Interestingly, even the determination of the coordination number around the lithium ions in pure carbonate-based solvents has not been definitely resolved. While the generally accepted picture comprises a tetrahedral coordination of the carbonyl oxygen atoms around Li^+, some experimental and theoretical studies propose the existence of local structures exhibiting slightly higher coordination numbers(several theoretical studies [76, 83, 86, 87, 89, 90, 92, 95, 97] agreed on coordination 4 around Li^+, some experimental and theoretical results [84, 88, 98, 99, 101] shows a coordination that can go to up to 6).

The dependence of this local coordination number on the ion concentration is also somehow controversial. However, it should be emphasized that designing experimental methods or theoretical models to analyze the experimental data in order to provide a direct measurement of the coordination number is an extremely complicated task. On the other hand, since the validation of molecular simulation results strongly depends on the direct comparison with experimental data, the development of experimental methods proving a direct determination of the coordination number becomes indispensable in order to obtain a clear picture about the local structural effects in liquid solvents.

Moreover, the study of binary mixtures EC/DMC needs to better describe the role of DMC in the solvation shell and ternary mixtures EC/DMC/PC that are very used in recent developments have never been explored from a theoretical point of view.

This work is devoted to the investigation of different mixture of carbonate solvents for this work to clarify the contributions of solvent molecules to the lithium solvation shell. After a presentation of the theoretical approaches used in this work, Chapter 2, we will present in Chapter 3, the DFT calculations for pure clusters formed by a single solvent clusters with lithium-ion $Li^+(S)_n$ (S= EC, DMC and PC, n=1-5) . In the same chapter, we will also describe and analyse DFT results obtained for binary mixtures $Li^+(S_1)_n(S_2)_m$, (S_1 , S_2 =EC, PC, DMC, with m+n=4), and ternary clusters $Li^+(EC)_l(DMC)_m(PC)_n$ with l+m+n=4. In particular, we will try to describe structures, coordination around Li^+, bonding interaction and we will also analyse thermodynamic properties in order to discuss the stability and preferential arrangement. The role of the salt, $LiPF_6$, will be discussed in Chapter 4. In particular, we will discuss the change in the first solvation shell by the presence of the PF_6^- counter ion. In Chapter 5, DFT results will be coupled with realistic results and the typical MD systems formed by pure EC/Li^+, DMC/Li^+, PC/Li^+ and mixed binary EC:DMC/Li^+ (1:1) and ternary solvent EC:DMC:PC/Li^+ (1:1:3) electrolytes at dilute concentration. From MD results, we will rationalize the results including radial distribution functions, coordination numbers, local mole fractions and dipole distributions etc.

2

Numerical Techniques

This chapter focuses on the theoretical methodologies developed for solving the Schrödinger equation for many-body systems, such as the Hartree-Fock method and density functional theory. Also we briefly discuss the basis sets which will be used to perform the calculations with theoretical functionals. Finally, we will discuss the Amsterdam Density Functional (ADF) package formalism and the solvent effects using COSMO method. The ADF software package is used for all our electronic structure calculations. Finally, we also give a few details about the molecular dynamics simulation method.

2.1 Density Functional Theory

2.1.1 Outline of Electronic Structure Calculations

The quantum mechanics have been developed since the discovery of the electron in 1896 by Lorentz and Zeeman, and in 1897 by Thomson. The quantum field has been established in 1930s, when the band theory was developed for the case of independent electrons. Also in the 1930s, methods such as Hartree-Fock, orthogonalized plane wave, augmented plane wave and effective potential method were proposed. Although, Band structure calculations were used until 1950s for solid systems, this theory fails to study semiconductors. The quantum fields were rapidly developed in the 1960s after the formulation of density functional theory(DFT) based on the Hohenburg-Kohn (HK) theorem. This states that the many-body system properties are completely determined by the ground state charge density. However, the DFT have become useful after the development of the Kohn-Sham approach that concerns the wave function rather than density. Due to lack of adequate powerful computer facilities, DFT calculations were very limited until th 1980s. With the advances of computer technology, the DFT method electronic structure calculations became more popular and are now widely used

in quantum chemistry and material science. Nowadays, the Kohn-Sham approach combined with Born-Oppenheimer approximation for accurate DFT calculation which have been made another approximation called exchange-correlation (XC) potential. This describes the effect of Coulomb interactions and of the and Pauli principle to pure electrostatic interaction of electrons. Unfortunately, It is very hard to calculate the exact exchange-correlation potential by solving many-body problem. Therefore, additional approximations called the local density approximation (LDA) and the generalized gradient approximation(GGA) have been developed using the local electron density. In the following sections, we briefly discuss the most imporatant quantum chemistry theorems and methods.

2.1.2 Schrödinger Equation

Schrödinger equation[102] is the starting point of any discussion of quantum mechanics . The time-independent form of this equation is

$$\hat{H}\Psi = E\Psi, \tag{2.1}$$

where $\hat{H}$ is the *Hamiltonian operator*, E is the total energy of the system and Ψ is the many body wave function.

Consider a system formed by M nuclei and N electrons. Particles such as electrons and nuclei interact among each other, i.e., the coulomb potential and consequently the Schrödinger equation $\hat{H}$ (atomic units) can be written as:

$$\hat{H} = -\sum_{i=1}^{N} \frac{1}{2} \bigtriangledown_i^2 - \sum_{A=1}^{M} \frac{1}{2M_A} \bigtriangledown_A^2 - \sum_{i=1}^{N}\sum_{A=1}^{M} \frac{Z_A}{r_{iA}} + \sum_{i=1}^{N}\sum_{j>i}^{N} \frac{1}{r_{ij}} + \sum_{A=1}^{M}\sum_{B>A}^{M} \frac{Z_A Z_B}{R_{AB}} \tag{2.2}$$

where R_A and r_i are the position of M(nuclei) and N(electrons), respectively. The distance between nucleus A and electron i, is r_{iA} = | r_i - R_A | the distance between electrons i and j is r_{ij} = | r_i - r_j |, and the distance between nuclei A and B is R_{AB} = | R_A - R_B |. Z_A is the atomic number of nucleus, while M_A is its mass in units of the mass of an electron. $\bigtriangledown_A^2$ and $\bigtriangledown_i^2$ are the Laplacian operators, therefore, in the above equation, the first two terms represent the kinetic energy of the electrons and nuclei, respectively. The third term is the Coulomb attraction between nuclei and electrons, while the repulsion between electrons and between nuclei is accounted for by the fourth and fifth terms respectively.

2.1.3 The Born-Oppenheimer (BO) Approximation

The Schrödinger equation can be solved easily for the simplest molecular species(H_2^+) only, but it is very complicated to solve in the case of molecular systems. In these cases, the Born-Oppenheimer Approximation[103] is used, which plays an important role in electronic structure calculations. It consists in separating the Schrödinger equation into nuclear and electronic parts. This approximation is based on the fact that the masses of the nuclei are much greater than the masses of the electron, e.g., the lightest nuclei(the proton) is 1836 times heavier than the mass of the electron. Hence, in most cases the nuclei can be considered as fixed points and the electrons move subject to the fixed external potential produced by the nuclei. The electronic wavefunction, therefore is only depends on the positions of the nuclei and not on their momenta. Under this approximation the second term in eq 2.2 is neglected and the repulsion between the nuclei, the last term can be considered as a constant for fixed nuclei. The remaining terms are the electronic Hamiltonian($\hat{H}_{elec}$) that can be written as:

$$\hat{H}_{elec} = -\sum_{i=1}^{N} \frac{1}{2} \bigtriangledown_i^2 - \sum_{i=1}^{N}\sum_{A=1}^{M} \frac{Z_A}{r_{iA}} + \sum_{i=1}^{N}\sum_{j>i}^{N} \frac{1}{r_{ij}} \tag{2.3}$$

The total electronic wavefunction for the molecule therefore is,

$$\hat{H}_{elec}\Psi_{elec} = E_{elec}\Psi_{elec} \tag{2.4}$$

and the general solution of Eq 2.2 can be finally written as:

$$\Psi_{tot}(nuclei, electrons) = \Psi(electrons)\Psi(nuclei). \tag{2.5}$$

The total energy is obviously the sum of electronic and nuclear energy(the electrostatic repulsion between the positively charged nuclei).

The electronic energymis the sum of potential and kinetic energy of the electrons. The electrons are moving in the electrostatic field generated by the nuclei and are subject to the electro-electron repulsion:

$$E_{tot} = E_{elec} + \sum_{A=1}^{M}\sum_{B>A}^{M} \frac{Z_A Z_B}{R_{AB}} \tag{2.6}$$

This approximation breaks down on the multiple potential energy surfaces those are close to each other in energy and also if the reactions involving with hydrogen bonds and proton transfer reactions. In which, the solving above equation 2.3 is still complex

for many-electron wave function contains 3N variables. In order to solve this many-electrons problem special approaches have been developed, including the Thomas-Fermi theory and Hartree Fock theories.

2.1.4 Hartree-Fock Theory

The Hartree-Fock method was introduced at the end of the 1920s and developed 1927 by D. R. Hartree. This is an approximation for the determination of the wave function and the energy of a many-body system in a stationary state[104]. This theory simplifies the electron-electron interaction, by expanding the many electron wave function into a product of single electron wave function. The ground state wave function of a system of N electrons is written as a single Slater determinant in N dimensions, Ψ_{SD}, with the one electron wave functions (ψ_i) as the components. The Slater determinant is:

$$\Psi_{HF}(\{\mathbf{x}_i\}) = \frac{1}{\sqrt{N!}} \begin{vmatrix} \psi_1(\mathbf{x}_1) & \psi_1(\mathbf{x}_2) & \cdots & \psi_1(\mathbf{x}_n) \\ \psi_2(\mathbf{x}_1) & \psi_2(\mathbf{x}_2) & \cdots & \psi_2(\mathbf{x}_n) \\ \vdots & \vdots & \ddots & \vdots \\ \psi_n(\mathbf{x}_1) & \psi_n(\mathbf{x}_2) & \cdots & \psi_n(\mathbf{x}_n) \end{vmatrix} \tag{2.7}$$

With this wave function, the full Hartree-Fock equation can be written as:

$$E[\Psi_{HF}] = \left(-\frac{1}{2} \bigtriangledown^2 + \upsilon_{ext} \right) \psi_i(\mathbf{x}) + \sum_j \int \mathrm{d}\mathbf{x}' \frac{\mid \psi_j(\mathbf{x}') \mid^2}{\mid r - r' \mid} - \sum_j \delta_{\sigma_i \sigma_j} \int \mathrm{d}\mathbf{x}' \frac{\psi_j^*(\mathbf{x}') \psi_i(\mathbf{x}')}{\mid r - r' \mid} \psi_j \mathbf{x}'. \tag{2.8}$$

and consists of four terms. The first two terms represent the kinetic energy contribution and the electron-ion potential. The third term is also known as the Hartree term and is the electrostatic potential generated from the charge distribution of N electrons. The fourth term, or exchange term, results from the inclusion of the Pauli principle. The Hartree-Fock approximation assumes a single-electron picture of the electronic structure, i.e., the distribution of the N electrons is given by the sum of the one-electron distributions $|\psi|^2$. However, the Hartree-Fock theory was established by assuming a single-determinant form for the wavefunction, and it also neglects the correlation between electrons. Therefore, The average non-local potential of electrons arising from the other electrons is not considered, leading to a poor description of the electronic structure of the molecule. Although the HF theory is qualitatively correct for various materials and compounds, it is not adequate to make accurate quantitative predictions.

The many electron wavefunction in HF is built by using antisymmetric electron wavefunctions. Since in HF methods, the electron correlations are neglected and they produce

large band gaps, higher energies and too small band widths, the HF approach is particularly suited for small organic molecules and oxides, which have a small number of localized electrons. However, this HF approximation is less appropriate for high electron density transition materials. Due to the interaction of average charge density of electrons, the ground-state energy calculated in HF theory is normally higher than the true ground-state energy. The theory fails in delocalized electron systems because this method ignores the collective Coulomb screening. Following these weakness of HF theory, the DFT method was developed, which deals with electron density.

2.1.5 Thomas-Fermi Theory

Llewellyn Thomas and Enrico Fermi proposed (1927) a quantum mechanical theory for solving the electronic structure of many body system[105, 106]. This theory is formulated in terms of the electron density, $\rho(r)$, instead of the wave function. The total energy of a system comprises three terms:

$$E_{TF}[\rho(r)] = A_1 \int \rho(r)^{\frac{5}{3}} \mathrm{d}r + \int \rho(r) V_{ext}(r) \mathrm{d}r + \frac{1}{2} \int \int \frac{\rho(r)(\rho(r)'}{\mid r - r' \mid} \mathrm{d}r \mathrm{d}r', \tag{2.9}$$

where the first term represents the kinetic energy of the non-interacting electrons in a homogeneous electron gas, with $\mathrm{A}_1 = \frac{1}{10}(3\pi^2)^{\frac{2}{3}}$, and the second term is the electrostatic energy between nucleus-electron interaction. The $\mathrm{V}_{ext}(r)$ is the static coulomb potential generated by the nuclei, while the third term is the classical electrostatic Hartree energy originating from the classical Coulomb repulsion between electrons.

This method has been used to account for a rough description of electrostatic potential and the charge density. The inclusion of correlation energy was developed as an approximation. For realistic systems, this scheme allows for poor quantitative predictions, and it does not reproduce any usual shell structure of atoms in various complex systems. The approximation of the kinetic energy is the main source in this model. The TF model over-simplifies the description of the electron-electron intreaction, which is treated classically, exchange interaction is not taken into account. This theory was used as a precursor to develop the modern density functional theory.

2.1.6 Density Functional Theory (DFT)

DFT is the most important method and it has been widely used due to its good accuracy and high computational efficiency. It takes into account the structure of molecules, surfaces, crystals and their interactions. This method works based on the electronic-charge density distribution rather than many-electron wave function. The advantage of using electron density is a much reduced dimensionality compared to that of the wave function. Indeed, this method is easy to apply to larger systems because it works with electron

density. Detailed discussions of DFT can be found in many books[107, 108] and review articles[109–111]. Although, the DFT method is accurate for ground states it insufficiently accounts for the form of exchange-correlation functional. Some approximation are therefore used to refine the model for the exchange-correlations interactions.

2.1.6.1 Hohenberg and Kohn Theorems

Modern DFT theory of many-body systems was introduced by Hohenberg and Kohn [112] in 1964. This theory is based on two two theorems: The first states that the ground state energy of any interacting many particle system in an external potential $\mathrm{V}_{ext}(\mathbf{r})$ which determines uniquely by its ground state density. This theorem is also valid for systems with degenerate ground states. Assume that there are two different potentials $\mathrm{V}_{ext}(\mathbf{r})$ and $\mathrm{V}'_{ext}(\mathbf{r})$, they differ by a constant, and give the same ground state electron density $\mathrm{n}_0(\mathbf{r})$. These two external potentials will give two different Hamiltonians, $\hat{H}$ and $\hat{H}'$, and these Hamiltonians will have the same ground state electron density $\mathrm{n}_0(\mathbf{r})$, but the normalized ground state wave functions, Ψ and Ψ' are different. Then it follows that

$$E_0 = E'_0 + \int n_0(\mathbf{r})[V_{ext}(\mathbf{r}) - V'_{ext}(\mathbf{r})]\mathrm{d}\mathbf{r} \tag{2.10}$$

where E_0 and E'_0 are the ground state energies for $\hat{H}$ and $\hat{H}'$ respectively. Similarly,

$$E'_0 = E_0 + \int n_0(\mathbf{r})[V'_{ext}(\mathbf{r}) - V_{ext}(\mathbf{r})]\mathrm{d}\mathbf{r} \tag{2.11}$$

The second theorem states that the universal functional of the density is independent of the external potential $\mathrm{V}_{ext}(\mathbf{r})$. The exact ground state density of the system is the global minimum value of this functional, and the exact ground state density $\mathrm{n}_0(\mathbf{r})$ minimizes the functional. In other words the calculation of the ground state density will minimize the energy.

The universal functional $\mathrm{F}[n(r)]$ is independent on the external potential and it can be written as

$$F[n(\mathbf{r})] \equiv T[n(\mathbf{r})] + E_{int}[n(\mathbf{r})], \tag{2.12}$$

where $\mathrm{T}[n(\mathbf{r})]$ is the kinetic energy and $\mathrm{E}_{int}[n(\mathbf{r})]$ represents the interaction energy of the particles. For another wave function Ψ', the energy functional $\mathrm{E}[\Psi']$ can be calculated using variational principle:

$$E[\Psi'] \equiv \langle \Psi' \mid \hat{T} + \hat{V}_{int} + \hat{V}_{ext} \mid \Psi' \rangle \tag{2.13}$$

If Ψ' is the ground state wavefunction, Ψ_0, the above has its global minimum and the total number of particles is conserved. According to the HK theorem I and the variational principle:

$$\begin{aligned} E[\Psi'] &= \int n_0(\mathbf{r}) V_{ext}(\mathbf{r}) \mathrm{d}\mathbf{r} + F[n_0(\mathbf{r})] \\ &= E[n = 0(\mathbf{r})] \end{aligned} \tag{2.14}$$

Therefore, the above energy attains the minimum only when the electron density is equal to ground state energy.

2.1.6.2 The Kohn-Sham Formulation

In order to apply DFT formalism one needs a good approximation for the F[n**(r)**] functional. The accurate Kohm-Sham(KS) [113] approximation consists in the replacing the problem of the original many body system with an auxiliary independent particles system that will have the same ground state density but is easier to solve. The main advantage of this approximation is that it allows to calculate the kinetic energy in a simplest way. It clearly provides a picture of one-particle interacting electronic systems. This method was introduced in 1965 and Kohn was awarded with Nobel prize in chemistry in the 1998, together with John Pople.

The auxiliary independent-particle Hamiltonian is:

$$\hat{H}_{KS} = -\frac{1}{2} \bigtriangledown^2 + V_{KS}(\mathbf{r}) \tag{2.15}$$

In order to evaluate the kinetic energy of a system with N independent particles, they obtained the corresponding potential $V_{KS}(\mathbf{r})$, by solving the system of N one-electron Schrödinger equations:

$$(-\frac{1}{2} \bigtriangledown^2 + V_{KS}(\mathbf{r}))\psi_i(\mathbf{r}) = \varepsilon_i \psi_i(\mathbf{r}) \tag{2.16}$$

Each of the N orbital $\psi_i(\mathbf{r})$ has one electron with the lowest eigen values ε_i, with the density is

$$\rho(\mathbf{r}) = \sum_{i=1}^{N} \mid \psi_i(\mathbf{r}) \mid^2 \tag{2.17}$$

The normalisation condition is

$$N = \int \rho(\mathbf{r}) \mathrm{d}\mathbf{r} \tag{2.18}$$

The independent-particle kinetic energy $T_S[\rho(\mathbf{r})]$ of the non-interacting particles is

$$T_S[\rho(\mathbf{r})] = -\frac{1}{2} \sum_{i=1}^{N} \int \psi_i^*(\mathbf{r}) \bigtriangledown^2 \psi_i(\mathbf{r}) \mathrm{d}\mathbf{r} \tag{2.19}$$

The universal functional $F[\rho(\mathbf{r})]$ is

$$F[\rho(\mathbf{r})] = T_S[\rho(\mathbf{r})] + E_H[\rho(\mathbf{r})] + E_{XC}[\rho(\mathbf{r})], \tag{2.20}$$

where $E_H[\rho(\mathbf{r})]$ represents the classic electrostatic energy of the electrons,

$$E_H[\rho(\mathbf{r})] = \frac{1}{2} \int \int \frac{\rho(\mathbf{r})\rho(\mathbf{r}')}{\mid \mathbf{r} - \mathbf{r}' \mid} \mathrm{d}\mathbf{r}\mathrm{d}\mathbf{r}' \tag{2.21}$$

and $E_{XC}[\rho(\mathbf{r})]$ is the exchange-correlation energy.

The Hartree potential $V_H(\mathbf{r})$

$$\begin{aligned} V_{KS}(\mathbf{r}) &= V_{ext}(\mathbf{r}) + V_H(\mathbf{r}) + V_{XC}(\mathbf{r}) \\ &= V_{ext}(\mathbf{r}) + \frac{\delta E_H[\rho(\mathbf{r})]}{\delta \rho(\mathbf{r})} + \frac{\delta E_{XC}[\rho(\mathbf{r})]}{\delta \rho(\mathbf{r})} \end{aligned} \tag{2.22}$$

where $V_H(\mathbf{r})$ is

$$V_H(\mathbf{r}) = \int \frac{\rho(\mathbf{r}')}{\mid \mathbf{r} - \mathbf{r}' \mid} \mathrm{d}\mathbf{r}' \tag{2.23}$$

and the exchange-correlation potential is

$$V_{XC}(\mathbf{r}) = \frac{\delta E_{XC}[\rho(\mathbf{r})]}{\delta \rho(\mathbf{r})} \tag{2.24}$$

Equations (2.16), (2.17) and (2.22) are KS equations. These equations are solved self-consistently because $V_{XC}(\mathbf{r})$ depends on the density.

The definition of the XC energy functional is

$$E_{XC}(\mathbf{r}) = T[\rho(\mathbf{r})] - T_S[\rho(\mathbf{r})] + E_{int}[\rho(\mathbf{r})] - E_H[\rho(\mathbf{r})] \tag{2.25}$$

where $T[\rho(\mathbf{r})]$ and $E_{int}[\rho(\mathbf{r})]$ represent kinetic and electron-electron interaction energies of the interacting system, respectively.

2.1.6.3 Exchange-Correlation Functional

The above equations provide a good method for finding the ground state energy of an interacting system when the form of E_{XC} is known. However, the form of E_{XC} has been exactly calculated for only a few simple systems, therefore this term is generally unknown. The E_{XC} term is commonly approximated in electronic structure calculations within the local density approximation or the generalised-gradient approximation. In the last decades hundreds of authors have been publishing different forms for the E_{XC} functional. The first method was proposed by Perdew and is also called the Jacob's ladder[114]. He introduced the simple types of exchange-correlation functional which are the following:

Local-Density Approximation (LDA) The most widely used, and simplest method to obtain the exchange-correlation energy is called the Local-density approximation (LSDA is also be used, for Local Spin Density Approximation). In this method, the contribution to the exchange-correlation energy from each volume in space and the same density of homogeneous electron gas. The total exchange-correlation energy E_{xc} can be obtained by integrating over the entire space:

$$E_{xc}^{LDA}[\rho(\mathbf{r})] = \int \rho(\mathbf{r})\varepsilon_{xc}(\rho(\mathbf{r}))\mathrm{d}\mathbf{r} \tag{2.26}$$

where $\varepsilon_{xc}(\rho(\mathbf{r}))$ represents the exchange-correlation energy per electron. The Exchange-correlation functional can be obtained by differentiating this equation:

$$V_{xc}(\mathbf{r}) = \rho(\mathbf{r})\frac{\mathrm{d}\varepsilon_{xc}(\rho(\mathbf{r}))}{\mathrm{d}\rho(\mathbf{r})} + \varepsilon_{xc}(\rho(\mathbf{r})) \tag{2.27}$$

In this approximation, the point $\mathbf{r}$ is to be assumed in the inhomogeneous electron distribution. At this point the electron density $\rho(\mathbf{r})$ in both $V_{xc}\rho(\mathbf{r})$ and $\varepsilon_{xc}\rho(\mathbf{r})$, has the same value as in the homogeneous electron gas. Initially, Ceperley and Alder [115] have been calculated the exchange-correlation energy for the homogeneous electron gas using Monte Carlo methods and after the parametrisation was done by Perdew and Zunger [116]. LDA only predicts the limit of slowly-varying densities. However, the density is rapidly varying in most systems, and the LDA is clearly a crude approximation in these cases. However, the LDA method can still be used in predicting physical properties in real systems. In the following equation, we establish the connection of the interacting and non-interacting systems using the coupling constant variable λ (which varies in

the range of [0, 1]) in the presence of the external potential $V_\lambda(\mathbf{r})$. The corresponding Hamiltonian[117] is

$$\hat{H}_\lambda = -\frac{1}{2}\sum_i \nabla_i^2 + \frac{1}{2}\sum_i \sum_{j\neq i} \frac{\lambda}{\mid \mathbf{r}_i - \mathbf{r}_j \mid} + \hat{V}_{ext} + \hat{V}_\lambda \tag{2.28}$$

The exchange-correlation hole $n_{\mathrm{xc}}(\mathbf{r}, \mathbf{r}')$ is defined with density $n(\mathbf{r})$ in terms of pair correlation function and scaled Coulomb interaction[118, 119] as

$$n_{\mathrm{xc}}(\mathbf{r}, \mathbf{r}') = n(\mathbf{r}') \int_0^1 \mathrm{d}\lambda \left[g(\mathbf{r}, \mathbf{r}'; \lambda) - 1\right] \tag{2.29}$$

The exchange-correlation energy can be written in the form of a classical electrostatic interaction

$$E_{\mathrm{xc}}[n] = \frac{1}{2}\int \mathrm{d}\mathbf{r}\mathrm{d}\mathbf{r}' \left|\mathbf{r} - \mathbf{r}'\right| \tag{2.30}$$

The following sum rule holds which arises from pair correlation function

$$\int \mathrm{d}\mathbf{r}' n_{\mathrm{xc}}(\mathbf{r}, \mathbf{r}') = -1 \tag{2.31}$$

It shows that the exchange-correlation energy depends on the shape of the exchange-correlation hole. These two facts account for the success of the LDA. In spite of success of the LDA, it has some limitations. Indeed, which means if systems density varies slowly, the LDA performs well, and chemical properties are well reproduced. However, in strongly correlated systems, where an independent particle approach breaks down, the LDA is very inaccurate. Moreover, the LDA gives a very poor description of hydrogen bonding and it does not account for van der Waals bonding. Recently, the LDA functional has been developed and it differs only in their contribution to the many-body electron gas. The most common LDA functionals are Perdew-Wang (PW)[120], Perdew-Zunger (PZ)[121] and Vosko-Wilk-Nusair (VWN)[122] for varying densities.

Generalised-Gradient Approximation (GGA) The LDA method neglects the real charge density in inhomogeneous system which differs from that of homogeneous electron gas. A simple term E_{xc} have been raised for local derivatives of the electron density is called Gradient Expansion Approximation (GEA), however this is ineffective on the accuracy of DFT. The electron density as well as the each coordinate of the system take into account from the gradient of the density and it is called as Generalised-Gradient Approximation (GGA). It includes higher derivatives of the electron density and density gradient gives better results than the LDA method in many cases, such as binding energy

of molecules, bond lengths, crystal lattice constants and so on. The more general form is

$$E_{xc}^{GGA}[\rho(\mathbf{r})] = \int \rho(\mathbf{r})\varepsilon_{xc}(\rho(\mathbf{r})) \bigtriangledown \rho(\mathbf{r})\mathrm{d}\mathbf{r} \tag{2.32}$$

The above equation should satisfy some fundamental conditions such as reduce to LDA, respect the sum rule for the exchange-correlation hole and respect limits for small and large gradients. However, the exchange GGA functionals are written in the forms of LDA exchange and F_x enhancement factor, which depend on the local magnitude of the density gradient. This gradient is scaled according to the electron density,

$$E_x^{GGA} = F_x(s^2)E_x^{LDA} \tag{2.33}$$

where s is the measure of inhomogeneity of the system,

$$s = \frac{|\bigtriangledown n|}{2k_f n}. \tag{2.34}$$

The above s term is a logarithmic derivative of density and density is measured by changing as compared to the Fermi factor.

Over the years several exchange functionals have been developed in GGA. The most important functionals such as B88 (Becke, 1988 [123]), PBE (Perdew et al., 1996) have earned great attention by physicists and chemists communities and they have been used in the construction of hybrid functionals. The Beck's B88 exchange functionals is

$$F_x^{B88}(s) = 1 + \frac{\beta c_2(c_1 s)^2}{1 + 6\beta(c_1 s)sinh^{-1}(c_1 s)'} \tag{2.35}$$

where

$$c_1 = 2(6\pi^2)^{\frac{1}{3}} \tag{2.36}$$

$$c_2 = \frac{4}{3}\left(\frac{4\pi}{3}\right)^{\frac{1}{3}} \tag{2.37}$$

and the parameter $\beta = 0.0042$ is an empirical parameter which is fitted from the Hartree-Fock exchange energies of noble gas atoms.

Perdew [124] and Perdew, Burke, Ernzerhof (PBE)[125] of GGA-PBE exchange component is

$$F_x^{PBE}(s) = 1 + \kappa - \left(\frac{\kappa}{1 + \frac{\mu s^2}{\kappa}} \right) \tag{2.38}$$

which, for small s^2

$$F_x^{PBE}(s) \sim 1 + \mu s^2 \tag{2.39}$$

where $\mu \approx 0.21951$

and in the large s^2 limit

$$F_x^{PBE}(s) \sim 1 + \kappa \tag{2.40}$$

the proposed value of $\kappa = 0.804$. After the introduction of PBE functionals, several functionals have been proposed to give accurate predictions using modified correlation and exchange functionals. However, the GGA functionals has always large and small s limit but it differs only in changing of the functional of μ value. Another functional such as revPBE has the same form as PBE and it varies the value of κ to 1.245. This revPBE functional is used to calculate the accurate atomization energy. The functional of revPBE[126, 127] is

$$F_x = 1 + \kappa - \left(1 - exp\frac{mus^2}{\kappa} \right) \tag{2.41}$$

Also, the PBEsol functional can be used to improve calculations on solids and it is able to account for the structure of solids with high accuracy. This PBEsol functional use the same correlation enhancement factor and a different $\beta = 0.046$ value. The corresponding PBEsol[128] functional is

$$F_x = 1 + \kappa - \left(\frac{\kappa}{1 + \frac{\mu s^2}{\kappa}} \right) \tag{2.42}$$

RGE2 [129]functional uses the same μ as PBEsol functional and κ is taken from the PBE functional. The RGE2 functional form is

$$F_x = 1 + \kappa - \frac{\kappa}{\left[1 + \frac{\mu s^2}{\kappa} + \left(\frac{\mu s^2}{\kappa} \right)^2 \right]} \tag{2.43}$$

The RPBE [130] exchange functional use the PBE correlation functional with PBEsol β to get

$$F_x = 1 + \kappa \left(1 - \frac{1}{2} \frac{1}{1 + \frac{\mu s^2}{\kappa} - \frac{1}{2} e^{\frac{-\mu s^2}{\kappa}}} \right) \tag{2.44}$$

2.1.7 Basis Sets

The basis sets are composed of atomic functions and are commonly used in quantum mechanical calculations. A basis set is a mathematical description[131] of the orbitals within system and each linear combinations of single electron describes in the Equation 2.45.

$$\psi_i = \sum_{\nu=1}^{K} c_{\nu i} \phi_\nu \tag{2.45}$$

where ϕ_ν or one-electron orbitals which are called *basis functions* and correspond to the atomic orbitals and K is the basis functions orbitals.

The Slater Type Orbitals (STOs) are the most used to represent the basis functions. The STOs were introduced by Slater in 1930 and are more convenient than atomic orbitals. Gaussian type orbitals (GTO) are also used in quantum chemistry calculations. However, the GTOs fail to represent the near-nucleus region and fall very rapidly with comparison to STO. Since GTOs take into account energetically important electrons rather than core electrons those are not involved in the reactions. STOs provided reasonable representations of atomic orbitals including near core region electrons.

STO and GTO functions are

$$\begin{aligned} \phi_{abc}^{STO}(x, y, z) &= N x^a y^b z^c e^{-\zeta r} \\ \phi_{abc}^{GTO}(x, y, z) &= N x^a y^b z^c e^{-\zeta r^2} \end{aligned} \tag{2.46}$$

where N is a normalization constant and a, b, c are control angular momentum (L = a+b+c), and ζ represents the width of the orbital.

The normalised form of STOs are:

$$\phi_{1s} = \left(\frac{\zeta_1^3}{\pi} \right)^{\frac{1}{2}} exp(\zeta_1 r) \tag{2.47}$$

$$\phi_{2s} = \left(\frac{\zeta_2^5}{96\pi} \right)^{\frac{1}{2}} r exp\left(-\frac{\zeta_2 r}{2} \right) \tag{2.48}$$

$$\phi_{2p_x} = \left(\frac{\zeta_2^5}{32\pi}\right)^{\frac{1}{2}} xexp\left(-\frac{\zeta_2 r}{2}\right) \tag{2.49}$$

To date, hundreds of basis sets have been reported. The smallest basis sets are called *minimal basis sets*. Normally, the minimal basis set includes all atomic orbitals in the shell. A single s-type function is required for the hydrogen and helium atoms but in the case of lithium to neon the 1s, 2s, 2p functions are used. The minimal basis set problem can be addressed if each orbital used more than one function. The *Double zeta* basis set was introduced in which it doubles the number of functions in the minimal basis set. For example, it assigned twice in function for each orbital 1s, 1s, 2s, 2s, 2p, 2p due to accuracy and efficiency. Alternatively, the Pople basis set, or *split valence* basis sets, approach is used to describe the valence electrons by increasing to double the number of functions but the inner shells are kept in a single function. This basis set does not affect the chemical properties because this approach is mainly for core orbitals rather than valence orbitals. Using these functions Triple Zeta (TZ), Quadruple Zeta (QZ) and Quintuple Zeta (5Z) and also higher functions have been developed. However, in order to account polarisation of orbitals during chemical bond formation, polarization functions also known as higher angular momentum functions are required. Diffuse functions are also used for all elements, s and p type functions with small components. These basis functions are used to account for the energies of the system with high accuracy and also give more information the region that is far away from the nuclei. In the next section, we introduced the quantum chemistry DFT package (ADF) formalism which we used for all electronic calculations included in this thesis work.

2.1.8 Amsterdam Density Functional (ADF)

In early 1970s, Hartree-Fock Slater (HFS) [132] was introduced to exploit the DFT and later was called the Amsterdam Density Functional (ADF) [133]. This package has been developed by theoretical research groups in Amsterdam [132, 134–145] and Calgary [144–150]. The ADF program supports a variety of exchange-correlation functional and also includes relativistic effects with ZORA. In this package, the basis set works with Slater type functions. It includes basis sets from minimal to doubly polarized triple-zeta basis. This program calculate the energy minima of the molecule, reaction paths and harmonic frequencies and also takes into account the effect of solvation and of the dielectric field environment. It can also compute properties such as NMR, ESR and excitation energies (TD-DFT), dispersion coefficients and Raman intensities.

2.1.8.1 Formalism

Numerical Integration: To calculate the exchange-correlation (XC) potential the ADF uses the Gaussian quadrature method [135–137]. This method works by partitioning

the space in atomic cells and it contains a core-region sphere. In terms of spherical coordinates of nucleus:

$$\int_{cell} f(\mathbf{r})\mathrm{d}\mathbf{r} = \int_0^R r^2\mathrm{d}r \int_0^{4\pi} f(r,\Omega)\mathrm{d}\Omega + \int_{cell-without-sphere} f(\mathbf{r})\mathrm{d}\mathbf{r} \tag{2.50}$$

where r^2 is the Jacobian factor and removes at the nuclear position by coulomb singularity of the integrand. More precise numerical integration evaluated with different point in the different region such as cells, atomic sphere and outer region. In order to obtain higher precision (close to machine), of-course the scaling of computation time also the double the number. Numerical approach has some advantages like more efficient and reduced errors.

Basis Sets: ADF mainly works with Slater-type functions (STOs)

$$f(\mathbf{r})\mathrm{d}\mathbf{r} = Y_{lm}(\Omega)r^n e^{-\alpha r} \tag{2.51}$$

where Y_{lm} are the spherical harmonics and the long-range decay of the function is determined by the exponential factor α. STOs possesses cusp behaviour and appropriate long range decay compared to the over than Gaussian-type orbitals (GTOs). STOs are used to build high quality basis set with small numbers of functions, but in the case of GTOs the same basis set needs a factor of 3 more functions. The ADF package contains a larger number of basis set for all elements, ranging from single-ζ to triple-ζ doubly polarized (TZ2P) basis set. It also extends to diffuse functions for polarizability calculations [151–155] and relativistic ZORA formalism [140–143, 156], also used to account for deep-core functions.

The *Frozen Core Approximation* has been used to reduce the computational time. The *molecular symmetry* is used to enhance the computational efficiency, because the numerical integral applies only symmetry-unique region. The calculation of Coulomb potential matrix needs two-electron integrals with n^4 scaling, and it is reduced to n^3 by using numerical integration and density fitting. The *Coulomb potential* is derived at each point $\mathbf{r}$ by the following expression (2.52).

$$F_{\mu\nu}\sum_k w_k\chi_\mu(\mathbf{r}_k)\left\{-\frac{1}{2}\bigtriangledown^2 + V_{Coulomb}(\mathbf{r}_k) + V_{XC}(\mathbf{r}_k) + \cdots\right\}\chi_\nu(\mathbf{r}_k) \tag{2.52}$$

Where the exchange-correlation potential $V_{XC}(\mathbf{r})$ and the single numerical integration evaluate the Fock-metrix and the Fock operator. The summation of all integration runs over points ($\mathbf{r}_k$).

The *Self Consistent Field* is used to obtain the solution of the Kohn-Sham equations.

The Fock matrix F^j is computed from the trial density matrix P^k and, after diagonalization, the eigenvectors(MOs) are obtained. The occupied MOs gives a new trial density matrix P^{k+1} etc, and forms until P^k and P^{k+1} are identical, when self-consistency reached.

In ADF, the *Fragment Approach* offers some advantages. This approach clearly describes the picture of bonding and reduces the degree of mixing of complicated basis functions. For the case of fragments, the energies are calculated directly by a single numerical integral of the energy density ($\varepsilon[\rho,\mathbf{r}]-\sum_A \varepsilon_A[\rho,\mathbf{r}]$). It also improves numerical precision. ADF follows Mokokuma-type method [157–160] to calculate the bond energy (ΔE).

$$\Delta E[\rho] = \int \left(\varepsilon[\rho,\mathbf{r}] - \sum_A \varepsilon_A[\rho,\mathbf{r}] \right) \mathrm{d}\mathbf{r} \tag{2.53}$$

The bond energy is divided into two major parts, the preparation energy and the interaction energy. The preparation energy (ΔE_{prep}) is the amount of energy needed to deform into separated fragments. The corresponding energy term partitioned into form a equilibrium structure to geometry ($\Delta E_{prep,geo}$) and excite to their valence electronic configuration($\Delta E_{prep,el}$). The interaction energy (ΔE_{int}) is calculated between the fragments,

$$\begin{aligned} \Delta E &= \Delta E_{prep} + \Delta E_{int} \\ &= \Delta E_{prep,geo} + \Delta E_{prep,el} + \Delta E_{int} \end{aligned} \tag{2.54}$$

The interaction energy ΔE_{int} is further splitted into three terms

$$\begin{aligned} \Delta E_{int} &= \Delta V_{elst} + \Delta E_{Pauli} + \Delta E_{oi} \\ &= \Delta E^0 + \Delta E_{oi} \end{aligned} \tag{2.55}$$

Here the ΔV_{elst} term represents the classical electrostatic interaction of the prepared fragments. The ΔE_{Pauli} defines the Pauli repulsion and combine ΔV_{elst} and ΔE_{Pauli} with a term ΔE^0. The ΔE_{oi} is the associated orbitals interaction energy which accounts for the charge transfer (HOMO-LUMO interactions), electron pair bonding and polarization, $\Delta E_{oi} = \sum_\Gamma \Delta E_{oi,\Gamma}$, where Γ is the irreducible representation of the interacting system.

In ADF, the *Atomic Charges* gives additional insight to understand bonding and reactivity by investigating the wave function. There are three different approaches to compute atomic charges in ADF: Mulliken population analysis [161, 162], Voronoi deformation density (VDD) [163] method and the Hirshfield scheme [164, 165].

In order to calculate the self-consistent equations of the exchange correlation potential (Kohn-Sham equation) derived from the expression of E_{XC}. Various levels of approximations are implemented in ADF such as local density approximation(LDA) and the generalised gradient approximation(GGA). For LDA level approximation, the Vosko-Wilk-Nusair (VWN) [115, 166] can be chosen for the parameterization of the electron gas data. In the case of GGA, the Becke (exchange), Perdew (correlation), Lee-Yang-Parr (correlation), Perdew-Wang (both) [167–170] are used. The default method BFGS (Broy-den Fletcher Goldfarb Shanno) [171] used for geometry optimization in ADF. For instance, for the particular geometry, the first derivatives of the energy are calculated by using nuclear displacement at the end of the SCF procedure [144, 172] and initial estimate of the Hessian are carried out by Newton-type procedure. In each step of the geometry optimization , the Hessian is updated from the difference of the current and previous gradients results in the different geometries.

In ADF, *IR frequencies* are calculated using equation 2.57 below [145, 173]. It computes the second derivatives of the energy with respect to nuclear displacements. The analytically computed first derivatives (gradients) are used for numerical differentiation. The matrix of force constants express in mass-weighted Cartesian coordinates(q_i).

$$F_{ij} = \frac{\partial^2 E}{\partial q_i \partial q_j} \tag{2.56}$$

$$\begin{aligned} q_1 &= x^{(1)}\sqrt{m^{(1)}}, \qquad & q_2 &= y^{(1)}\sqrt{m^{(1)}}, \\ q_3 &= z^{(1)}\sqrt{m^{(1)}}, \qquad & q_4 &= x^{(2)}\sqrt{m^{(2)}}, \qquad \ldots \end{aligned} \tag{2.57}$$

Diagonalization of F, the normal mode eigenvector vectors obtained after projecting translations and rotations. The eigenvalues and harmonic frequencies relationship is

$$\nu_k = \frac{\sqrt{\lambda_k}}{2\pi} \tag{2.58}$$

The IR intensities are calculated by

$$A_k = (974.86) g_i \left(\frac{\partial \mu}{\partial Q_i} \right)^2 \tag{2.59}$$

where Q_i represents the normal mode (masses in atomic units and mass-weighted Cartesian coordinates in atomic units) with degeneracy g_i. μ is the dipole moment and A_i is the absorption intensity. These IR intensities are obtained both with an nalytic approach and a numerical approach using second derivatives.

2.1.8.2 Solvent Effects: Conductor-like Screening Model (COSMO)

The COSMO method [174, 175] was originally developed by Klamt and Schüürmann [176]. and was implemented in ADF by Pye and Ziegler [177]. This method includes the solvent effects for reaction and compounds which have to be studied in solvent environment, and for material properties in solution. The specific solvent is handled as dielectric field medium which induces the charge polarization onto a defined surface around a molecule. The sphere size of the solvent molecules has to be assumed and it can penetrate into the occupied molecule region. This effective molecular region is called Solvent Accessible Surface (SAS). The series of sphere [174, 178, 179] in the SAS are atomic centred with Van der Waals-type radii, which slightly larger than usual Van der Waals radii.

Tomasi et al., [180] reported, the finite value of the dielectric constant (ϵ) and the ideal charge density are scaled by a proper function,

$$\sigma(s) = f(\epsilon)\sigma^*(s) \tag{2.60}$$

where $f(x)$ is the scaling function and is determined by comparing electrostatic-solute solvent energies and COSMO. The suggested formula is

$$f(\epsilon) = \frac{\epsilon - 1}{\epsilon + k} \tag{2.61}$$

Klamt suggested $k = 0.5$ and k depends on the cavity shape. Pye and Ziegler introduced COSMO into ADF with the default of $k = 0$ and they also leave the users to select the value.

2.2 Molecular Dynamics Simulations

In this section, we give a few details about Molecular Dynamics simulation method, restricting the discussions to the techniques actually used in this work only. The Molecular dynamics (MD) simulation technique is widely used to study equilibrium and transport properties of atomic and molecular systems. MD gives a very detailed description of the individual particle motions as a function of time. MD is an important tool for understanding structure at the mesoscale and also addresses systems that are difficult to study experimentally. Typically, MD simulations starts from initial coordinates that are obtained from experimental methods such as X-ray crystallography or NMR and uses a force field in order to approximate the potential energy. The time evolution of the system is determined by solving the Newton equations of motion which specify the time dependence of position and velocity of the particles in the system varies with time. The

trajectory is obtained by solving a set of the N differential equations of motion of the form

$$\frac{dx_i^2}{dt^2} = \frac{F_i}{m_i} \tag{2.62}$$

In this equation m_i describes the mass of a particle with coordinate x_i and F_i represents force applied on particle and a is the acceleration.

The output of an MD simulation is the trajectory, i.e., coordinates and velocities of all atoms in the system which provide a high quality information only limited by the accuracy of the used force-fields. The trajectory is next analysed to obtain various geometrical, thermodynamical, dynamical quantities of the interest.

2.2.1 Algorithm for integration of equation of motion

One important stage of an MD simulation is the integration of the equations of motion. The intermolecular interactions in realistic models are very simple but they make a many-body problem that is impossible to solve analytically. Under this circumstances the equations of motion have to be solved by numerical integration methods. Several algorithms have been used in for integrating equations of motion using finite difference methods. MD requires many time steps and the integration is performed in many small time steps. One of the most widely used algorithm is called the Verlet algorithm [181]. The algorithm is derived using Taylor series expansions,

$$\mathbf{r}(t + \Delta t) = 2\mathbf{r}(t) - \mathbf{r}(t - \Delta t) + \mathbf{a}(t)(\Delta t)^2 \tag{2.63}$$

$$\mathbf{v}(t + \Delta t) = 2\mathbf{v}(t) - \mathbf{a}(t - \Delta t) + \mathbf{b}(t)(\Delta t)^2 \tag{2.64}$$

This Verlet algorithm is stable and also time-reversible, however, these integrators suffer from instability.

Runge-Kutta integrator methods are also used in some occasions. However, this method presents that forces must be calculated several times per time step, which is highly insufficient. In molecular cases, with molecules considered rigid, the equations of motion for the molecular centers of mass are solved by the verlet algorithm, while rotations are solved by using the quaternion formalisms. This is the technique used in this work.

Quaternions method The orientation of the molecule can be expressed [182], in terms of the Euler angles θ, ψ and ϕ. Here ψ is the rotation of the body about the axis and θ, ϕ defines the orientation of a body axis which is relative to the space fixed frame.

The rotation matrix is

$$A = \begin{pmatrix} \cos\psi\cos\phi - \cos\theta\sin\phi\sin\psi & \cos\psi\sin\phi + \cos\theta\cos\phi\sin\psi & \sin\psi\sin\theta \\ -\sin\psi\cos\phi - \cos\theta\sin\phi\cos\psi & -\sin\psi\sin\phi + \cos\theta\cos\phi\cos\psi & \cos\psi\sin\theta \\ \sin\theta\sin\phi & -\sin\theta\cos\phi & \cos\theta \end{pmatrix} \tag{2.65}$$

The rotational dynamical equation written in terms of A shows singularities for θ close to 0° or 180°. In order to overcome this issue, a larger reductant set of four variables called quaternions used. Quaternions can be defined in terms of the Euler angles as:

$$Q_x = \sin\frac{\theta}{2}\cos\frac{\phi-\psi}{2} \tag{2.66}$$

$$Q_y = \sin\frac{\theta}{2} sin\frac{\phi-\psi}{2} \tag{2.67}$$

$$Q_z = \cos\frac{\theta}{2}\sin\frac{\phi+\psi}{2} \tag{2.68}$$

$$Q_4 = \cos\frac{\theta}{2}\cos\frac{\phi+\psi}{2} \tag{2.69}$$

with the normalisation condition

$$\sum_{\alpha=1}^{4} Q_\alpha^2 = 1 \tag{2.70}$$

As a consequence, A can be written as:

$$A_{ii} = Q_4^2 + Q_i^2 - \sum_{j\neq i} Q_j^2 \tag{2.71}$$

$$A_{ij} = 2Q_iQ_j + \varepsilon_{ijk}Q_4Q_k if i \neq j \tag{2.72}$$

When i = 1,2,3. The rotation matrix in the quaternions forms can therefore be written as [183]:

$$A = \begin{pmatrix} Q_x^2 - Q_y^2 - Q_z^2 + Q_4^2 & 2Q_xQ_y + 2Q_4Q_z & 2Q_xQ_z - 2Q_4Q_y \\ 2Q_xQ_y - 2Q_4Q_z & -Q_x^2 + Q_y^2 - Q_z^2 + Q_4^2 & 2Q_yQ_z + 2Q_4Q_x \\ 2Q_xQ_z + 2Q_4Q_y & 2Q_yQ_z - 2Q_4Q_x & -Q_x^2 - Q_y^2 + Q_z^2 + Q_4^2 \end{pmatrix} \tag{2.73}$$

The time evaluation of quaternions is therefore

$$\dot{Q}_i = \frac{1}{2}(Q_4\omega_i + \varepsilon_{ijk}Q_j\omega_k), i = 1, 2, 3 \tag{2.74}$$

$$\dot{Q}_4 = -\frac{1}{2}Q_i\omega_i \tag{2.75}$$

with w_i is the angular velocity

2.2.2 Ensembles

MD simulation can be performed in the micro-canonical ensemble, where number of particles (N), volume (V) and total energy (E) are constant. Also, other techniques exist to produce the time evaluation at constant pressure and temperature (NPT) or constant volume and temperature (NVT). These two ensembles can be generated by using extended Lagrangian formalism, in the form of the Parrinello-Rahman barostat and Nosé-Hoover thermostat.

Nosé -Hoover Thermostat Nosé[184] introduced a well designed form of a thermostat in 1984, which was further developed by Hoover[185]. The Nosé Hamiltonian for the N particle extended system is written as:

$$H_N = \sum_i \frac{p_i^2}{2m_i s^2} + U(r_i) + N_{df}k_BTlns + \frac{p_s^2}{2Q} \tag{2.76}$$

Here s represents an additional degree of the freedom of the system, p_i is the momentum, N_{df} is the number of degrees of the freedom in N-body system and Q is the Nosé mass parameter. This thermostat mechanism is also called an extended system method. From the above Hamiltonian, we can derive the equation of motion as follows

$$\dot{r}_i = \frac{\partial H_N}{\partial p_i} = \frac{p_i}{m_i s^2} \tag{2.77}$$

$$\dot{p}_i = -\frac{\partial H_N}{\partial r_i} = F_i(r) \tag{2.78}$$

$$\dot{s} = \frac{\partial H_N}{\partial p_s} = \frac{p_s}{Q} \tag{2.79}$$

$$\dot{p}_s = \frac{\partial H_N}{\partial s} = \left(\sum_i \frac{p_i^2}{m_i s^2} - N_{df}k_BT\right)/s \tag{2.80}$$

Nosé's thermostat is not able to account for the correct calculation of velocity correlation functions, due to rescaling of momenta. In order to overcome this problem, Nosé developed a coordinates transformation, further developed by Hoover, and re-wrote the equation of motion in a more convenient form. The resulting form of the Nosé-Hoover thermostat therefore is

$$\dot{r}_i = \frac{p_i}{m_i s^2} \tag{2.81}$$

$$\dot{p}_i = F_i(r) - \zeta p_i \tag{2.82}$$

$$\dot{\zeta}_i = \frac{1}{Q}\left[\sum_{i=1}^{N} \frac{p_i^2}{m_i} - N_{df} k_B T\right] = \frac{T(t) - T_0}{Q} \tag{2.83}$$

The above term is the time derivative which can be calculated from both the reference(target) temperature (T_0) and the instantaneous temperature T(t), which Q determines the strength of the coupling.

Parrinello-Rahman Barostat This approach resembles the Nosé-Hoover temperature coupling and generates configurations confirming to the NPT ensemble [186] by rescaling in a controlled way the simulation box side lengths. The box vectors are represented by the matrix H which evolves the equation of motion:

$$\frac{d^2 H}{dt^2} = V W^{-1} \left(\frac{dH}{dt}\right)^{-1} (P - P_{ref}) \tag{2.84}$$

Here W^{-1} describes the strength of the coupling and the matrices P_{ref} and P are the reference and current pressures respectively. The corresponding equation of motion for the particles change to,

$$\frac{d^2 r_i}{dt^2} = \frac{F_i}{m_i} - M \frac{f r_i}{dt} \tag{2.85}$$

where,

$$M = H^{-1} \frac{d}{dt}\left[H \frac{dH}{dt}\right] \left(\frac{dH}{dt}\right)^{-1} \tag{2.86}$$

and

$$(W^{-1})_{ij} = \frac{4\pi^2 \beta_{ij}}{3\tau_p^2 L} \tag{2.87}$$

Here τ_p is the coupling constant, controlling the relaxation of the current pressure towards the reference one, and β is the isothermal compressibility.

3

Study of Lithium ion Coordination with Carbonate Solvents

This chapter is dedicated to the DFT study of Li^+ ion solvation in EC, PC and DMC solvents. In particular, $Li^+(S)_{1\text{-}4}$(S=EC,PC,DMC) structures have been investigated. Next, we have examined binary solvent structures such as $Li^+(EC)_m(PC)_n$, $Li^+(EC)_m(DMC)_n$ and $Li^+(PC)_m(DMC)_n$ where $m+n=4$, followed by the study of mixed solvent clusters $[Li^+(EC)_l(PC)_m(DMC)_n]$ $(l+m+n=4)$.

3.1 Ethylene carbonate(EC)

We have started our DFT calculations by examing the structure properties of the isolated EC molecule. DFT calculations are performed by ADF, using GGA/PBE functional with the TZP basis set. An isolated EC molecule has two symmetry structures, such as planar, with C_{2V} symmetry, and non-planar with C_2 symmetry. In 1953, the first crystal structure of isolated EC was determined by *Brown et al.,*[187] who reported the EC is not planar. They also shown that the alkyl carbon atoms C-C joining to the CO_3 group(planar) makes an angle of 20°. However, the planar structure of EC with C_{2V} symmetry has been reported by *Angell et al.,*[188], based on infra-red spectroscopy in gaseous and liquid state and from the disappearance of some bands in the infra-red spectra. Neutron diffraction studies by *Matiaz et al.,*[189] found that the EC structure has a non planar conformation with C_2 symmetry. Theoretical studies on EC by *Blint et al.,*[190] reported that the isolated EC is planar, by using HF/D95V** basis, and similar results were published by *Klassen et al.,*[76] with HF/6-311++G(d,p) basis. Recent theoretical studies by *Soetens et al.,*[191] and *Wang et al.,* [34] have found that EC is non planar, using higher level abinitio calculation with MP2/6-311G** and B3PW91/6-31g(d). We have computed the isolated structure of EC molecule in both planar with C_{2V} symmetry and non planar with C_2 symmetry conformations. Our results show that

the planar C_{2V} symmetry gives one imaginary frequency and non planar C_2 symmetry gives all positive eigen frequencies. Nevertheless, the energy barrier between these two configurations is only 0.4 kcal/mol. This is in agreement with experimental results. Indeed, the low energy difference between the planar C_2 and the transition C_{2V} state makes the molecule extremely floppy at room temperature. This explains why several experiments in liquid or gas phase found an average planar structure. In solid state experiments could easily access the non-planar ground state. In C_2 symmetry, the methylene group is slightly deviated from the plane of the $-CO_3$ group by 23.9° which almost agrees with an experiment. Some bond parameters are listed in Table 3.1 and atom numbers are shown in Figure 3.1a. From the Table 3.1, the isolated EC optimized geometry parameters are in good agreement with experiment results taken from *Mahesh et al*[73]. Our dipole moment of EC is 5.29 D,a value which is in good agreement with the experimental value 5.35±0.15D reported by *Alonso et al.*,[192].

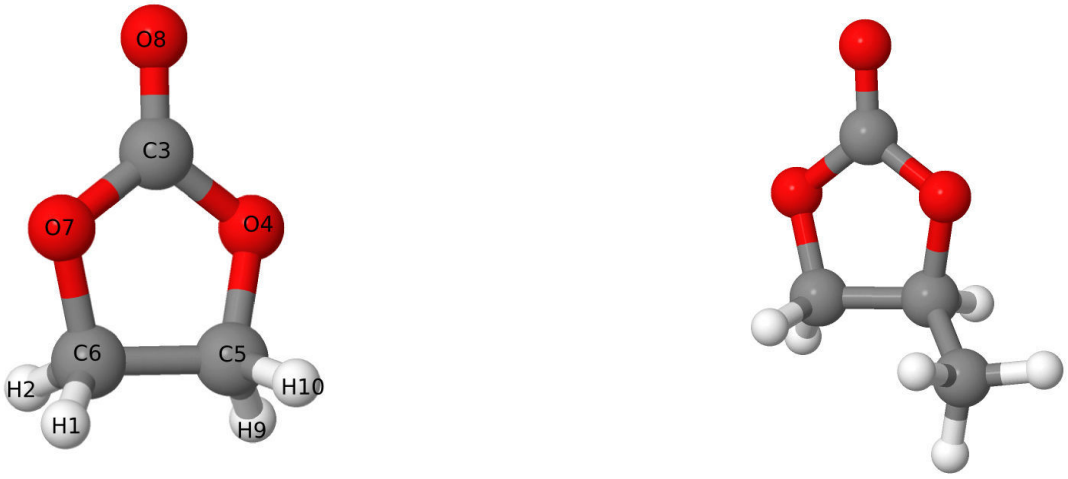

(a) Ethylene Carbonate (EC) (b) Propylene Carbonate (PC)

FIGURE 3.1: Isolated optimized geometry structures of Ethylene carbonate and Propylene carbonate, colours Gray = Carbon, Red= Oxygen, White = Hydrogen

3.2 Propylene carbonate (PC)

The isolated geometry of PC was optimized using GGA/PBE level of theory and the calculated structural parameters are presented in Table 3.2. Due to the fact that no experimental data are available for PC, we compared our structural parameters with previously computed results[191] using high level MP2/6-311G** theory. The bond parameters are in good agreement with this reference work. The optimized geometry of PC molecule is shown in Figure 3.1 showing that PC has a non-planarity of ring with C_2 symmetry, similar to the case of EC.

TABLE 3.1: Comparison between calculated and experimental parameters of EC molecule (bond lengths in angstrom, bond and dihedral angles in degree)

Parameters	**Calculated**		**Experimental**
	Isolated EC	EC Crystal	
Bond length			
O_8-C_3	1.20	1.22	1.20
C_3-O_4/C_3-O_7	1.38	1.36	1.34
O_4-C_5/O_7-C_6	1.44	1.46	1.46
C_5-C_6	1.53	1.53	1.52
C_5-H_9	1.10	1.09	1.09
Bond angle			
$O_8-C_3-O_4$	124.80	124.30	124.17
$C_3-O_4-C_5$	108.70	108.93	108.71
$O_4-C_3-O_7$	110.50	111.39	111.67
$H_9-C_5-H_{10}$	109.90	110.36	111.67
$C_6-C_5-H_9$	113.70	113.36	113.94
Dihedral angle			
$C_3-O_4-C_5-C_6$	20.20	-18.44	21.25
$C_3-O_4-C_5-H_{10}$	141.10	-138.95	141.81
$O_4-C_5-C_6-O_7$	-24.10	21.65	-24.80
$O_4-C_3-O_7-C_6$	-8.30	7.57	-8.73

3.3 Dimethyl Carbonate (DMC)

The DMC molecule show three conformers with respect to the hindered rotation on the planar $(CH_3)-O-C=O$ bond, which generates cis and trans conformers such as $cis-cis$, $cis-trans$ and $trans-trans$. The conformational features of of DMC have been investigated by spectroscopic techniques[193] [194] and dielectric measurements and ab-initio[195], molecular dynamics simulation[196]. These results show that two isomers, cis-cis and cis-trans, are local minimum structures and the cis-cis is the most stable conformer. However, our numerical results show the existance of one negative eigen frequency for the trans-trans conformer, which confirms that this is not a local minimum but a transition state. We optimized the three conformers of DMC (shown in Figure 3.2) using GGA/PBE functional with TZP basis set, and the results are presented in Table 3.3. As we can see from the Table, there is a contraction on the C=O bond length moving from the cis-cis to trans-trans structure. The electron delocalization and the lack of repulsive interaction with methyl groups can be the reasons for this small contraction. According to our results, conformers such as cis-cis and cis-trans exist in local minimum states which is confirmed by frequencies calculation. In contrast the case of trans-trans, shows a negative frequency, meaning that this conformer exists in a transition state. Moreover, the cis-cis is more stble than the cis-trans one, with

TABLE 3.2: Structural parameters of PC molecule (bond lengths in angstrom, bond and dihedral angles in degree)

Parameters	Calculated	Reference[191]
Bond length		
O=C	1.201	1.190
$(CH_2)O-C_{/}(CH)O-C$	1.376/1.371	1.362/1.361
$CH_2-O_{/}CH-O$	1.442/1.457	1.427/1.435
CH_2-CH	1.531	1.521
$CH-CH_3$	1.512	1.509
Bond angle		
O−C=O	124.5/125.0	124.8
O-C-O	110.5	110.2
$CH_2-O-C_{/}CH-O-C$	108.5/109.1	108.2/108.8
CH_2-CH-O	102.0	102.9
$CH_2-CH-CH_3$	115.6	115.3
Dihedral angle		
$O-CH_2-CH-O$	23.9	28.3
$(O=)C-O-CH_2-C$	-20.2	-23.7
$(O=)C-O-CH-CH_2$	-20.1	-24.1
$O-(O=)C-O-CH$	8.4	9.8

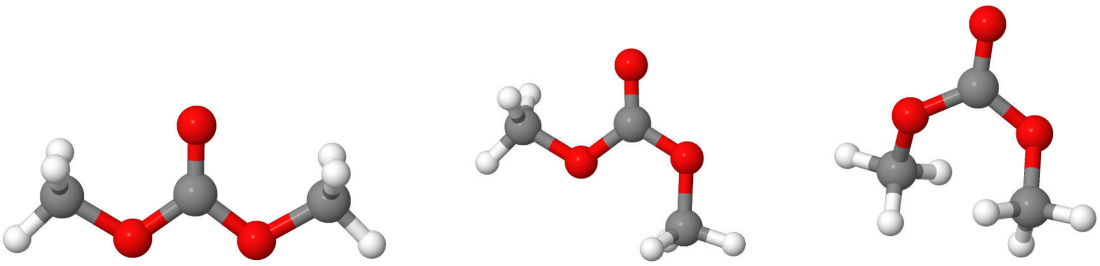

(a) cis-cis (b) cis-trans (c) trans-trans

FIGURE 3.2: Three different conformers of DMC such as cis-cis, cis-trans and trans-trans

the energies of 3.0 and 15 kcal/mol, respectively. In addition to the optimization, we confirmed the local structures of all DMC conformers by frequency analysis.

3.4 $Li^+(EC)_{1-6}$ complexes

3.4.1 Structural Properties

In this paragraph we discuss our results for the $Li^+(EC)_n$ (n=1 to 6) complexes. The optimized structural parameters are presented in Table 3.4 and geometries in Figure 3.3

TABLE 3.3: Comparison between the structural parameters of stable DMC conformers (bond lengths in angstrom, bond and dihedral angles in degree)

Parameters	**cis-cis**	**cis-trans**	**trans-trans**
Bond length			
C=O	1.217	1.212	1.207
C-O/C-O	1.353	1.364/1.352	1.368/1.369
O-C	1.446	1.448	1.447
C-H	1.097	1.097	1.096
Bond angle			
O=C-O	126.4	125.6/122.3	121.3
C-O-C	113.5	113.2/118.9	119.5
Dihedral angle			
O=C-O-C	0.0	0.0/180.0	143.1/142.5
Dipole moment/D	0.355	3.501	5.025
Δ H(kcal/mol)	0.0	2.98	15.50
ΔG(kcal/mol)	0.0	3.0	15.61

and we can clealry see from the Figure that the geometries are arranged in a symmetrical manner. In the first coordination of a single EC with Li^+ ion, the dihedral angle (O-C-C-O) in EC molecule decrease from 23.9° to 17.4°, while the carbonyl bond length increases from 1.201 Å to 1.235 Å. A linear arrangements is obtained for atoms Li^+-O=C in Li^+(EC) and $Li^+(EC)_2$ complexes with carbonyl group (178.8° and 176.2°).

In the $Li^+(EC)_2$ geometry, the two planes of the EC molecules are arranged perpendicular to each other, with an angle of ((C=)O- Li^+-O(=C)) 177.1°, which gives the most stable structure . In the $Li^+(EC)_3$ complex, the trigonal plane is obtained between intermolecular (C=)O- Li^+-O(=C) atoms, with an angle of ∼120°. A tetrahedral arrangement is formed by four coordinated complex with an angle of ∼106°. The bond between Li^+-O(=C) increases from 1.733 Å ($Li^+(EC)_3$) to 1.951 Å ($Li^+(EC)_4$) but the opposite result is obtained for the O=C bond. In the case of $Li^+(EC)_5$ complex, four EC molecules interact with the Li^+ ion in a tetrahedral way, with an average distance of 1.951 Å. The 5^{th} EC molecule is located in the second sphere of solvation with an average distance of 5.225 Å (Li^+– O=(C)). Similarly, for $Li^+(EC)_6$ complex two EC molecules are pointing to the $Li^+(EC)_4$ complex with distance of ∼ 5.1Å from Li^+ ion. However, these two complexes are stabilized by hydrogen bonds at a distance of ∼ 2.4 Å between EC molecules. In addition, we have also tried several optimization calculations from different starting structures, in order to look for 5 and 6 coordinated EC in the first solvation shell but without success. The steric repulsion only allows these additional EC molecules into the second solvation shell. These results seems that the EC molecules are participated in the second solvation shell. Despite of strong interation of Li^+ with EC molecules, coordination number increases, the EC molecule nearly attains isolated geometry. The dipole moment also increases from 1 to 6. The interaction between Li^+

TABLE 3.4: Structural parameters of $Li^+(EC)_{1\text{-}6}$ complexes (bond lengths in angstrom, bond and dihedral angles in degree)

Atoms	EC	$Li^+(EC)$	$Li^+(EC)_2$	$Li^+(EC)_3$	$Li^+(EC)_4$	$Li^+(EC)_5$	$Li^+(EC)_6$
Bonds							
Li^+-O(=C)		1.733	1.784	1.876	1.951	1.929	1.920
O=C	1.201	1.235	1.226	1.220	1.215	1.218	1.215
C-O	1.372	1.330	1.337	1.344	1.352	1.349	1.353
O-C	1.441	1.469	1.464	1.459	1.455	1.461	1.460
C-C	1.543	1.533	1.532	1.531	1.529	1.530	1.529
Angles							
Li^+-O=C		178.8	176.2	144.8	136.9	140.5	151.6/131.6
O-C-O	124.6	122.8	123.2	123.2	123.5	123.4	124.1
O-C(=O)-O	110.8	114.3	113.6	112.8	112.2	112.4	112.3
Dihedral							
O-C(=O)-O	180.0	173.9	173.6	172.9	172.1	173.0	172.0
O-C-C-O	-23.9	-17.4	-18.5	-20.2	-21.2	-20.7	-21.6
DPM/D	5.29	9.37	19.29	20.57	21.94	23.68	24.11
BE/ΔE		-47.94	-41.56	-34.86	-29.56	-24.45	-22.50

DPM = Dipole moment, BE = Binding Energy in kcal/mol

ion and the solvents molecules can be characterized by the average calculating binding energy (BE) of all complexes using following equation:

$$\Delta E_{BE} = \{E_{total}[Li^+(S)_n] - E[Li^+] - nE[S]\}/n \tag{3.1}$$

where ΔE is the binding energy of the complexes and S is the solvent molecule, n is the number of solvent molecules and $E_{total}[Li^+(S)_n]$, E[Li^+], $nE[S]$ are the total energy of the Li^+-S cluster, Li^+ ion and isolated solvent molecule respectively.

The gas phase Binding energy of $Li^+(EC)_{1\text{-}6}$ complexes are shown in Table 3.4. The average binding energy decreases going from n=1 to 6. The strongest interaction(EC/ Li^+) is obtained for the Li^+-EC and by adding extra EC molecules the charge/dipole interaction is shared on different cluster thus reducing the average interaction in following clusters.

3.4.2 Frequency and Mulliken Charge Analysis

We have also studied the vibrational frequencies of the isolated EC molecule and of the $Li^+(EC)_n$ complexes are given in Table 3.5. Two frequencies of the isolated EC molecule are particularly affected by the coordination with Li^+, the C=O stretching and the asymmetric C-O stretching. As we discussed before for the BE, also the C=O

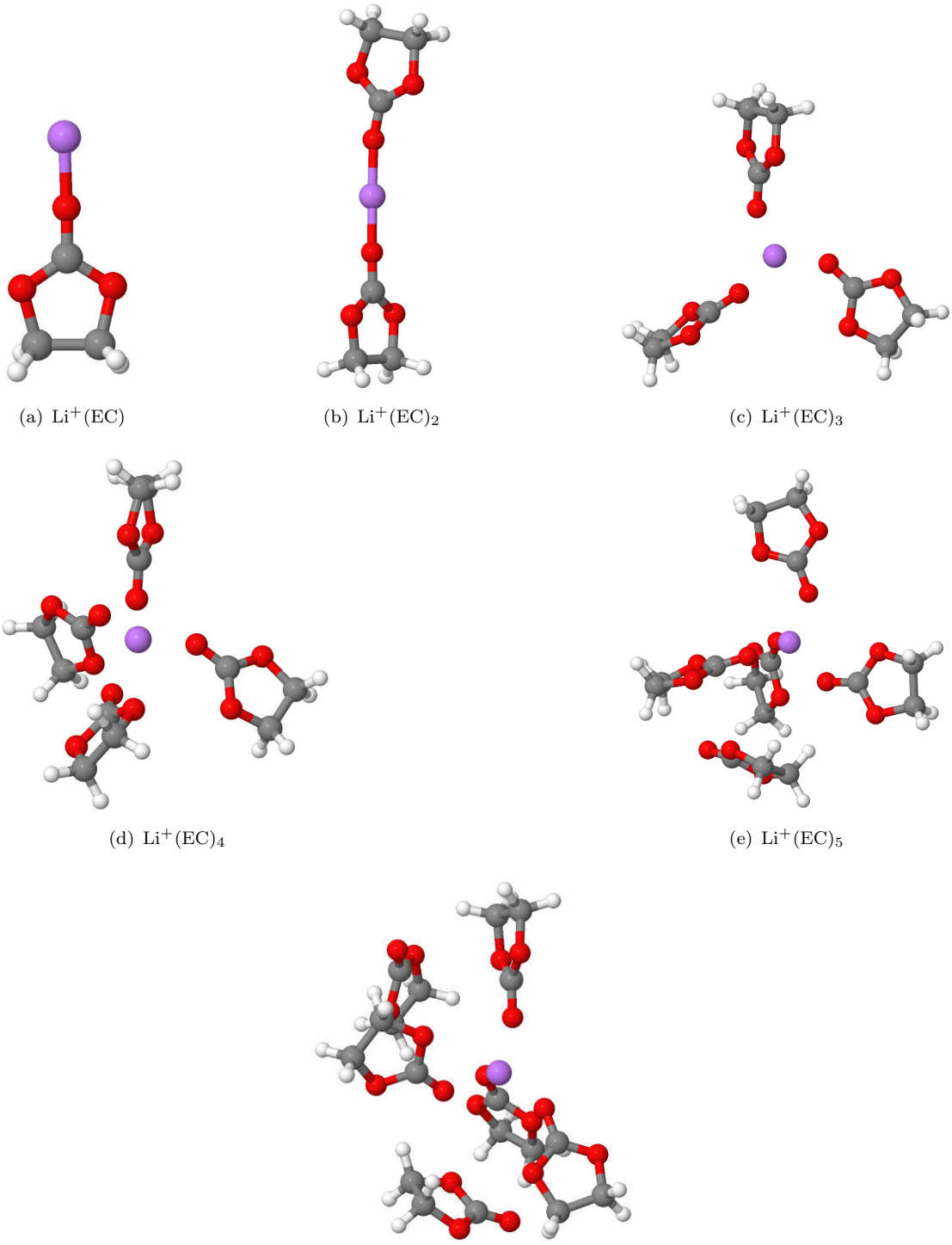

(a) $Li^+(EC)$ (b) $Li^+(EC)_2$ (c) $Li^+(EC)_3$

(d) $Li^+(EC)_4$ (e) $Li^+(EC)_5$

(f) $Li^+(EC)_6$

FIGURE 3.3: Gas phase optimized Solvation Structures of $Li^+(EC)_{1-6}$

and C-O frequency results are in agreement with the strongest interaction fro the single coordination (Li^+-EC bonds) respect to the following $Li^+(EC)_n$ coordination. In fact for the Li^+-EC system the C=O frequency EC decrease by -100cm^{-1} after addition of Li^+ ion. This confirms a strong Li^+-O(=C) interaction, where C=O act as donor of

TABLE 3.5: Vibrational modes(in cm^{-1}) and Mulliken charges of $Li^+(EC)_{1-6}$ complexes

Atoms	EC	$Li^+(EC)$	$Li^+(EC)_2$	$Li^+(EC)_3$	$Li^+(EC)_4$	$Li^+(EC)_5$	$Li^+(EC)_6$
Modes							
C=O	1833	1733	1748	1763	1776	1760/1790	1760/1793
C-O	1074	1209	1182	1164	1146	1150/1116	1148/1117
Charges							
Li^+		0.814	0.706	0.666	0.641	0.630	0.635
O(=C)	-0.540	-0.601	-0.578	-0.574	-0.564	-0.561	-0.552/-0.605
C(=O)	0.946	0.955	0.936	0.946	0.951	0.951	0.945/0.999
$O(CH_2)$	-0.508	-0.454	-0.461	-0.470	-0.482	-0.493	-0.486

electrons lowering the π interaction thus increasing the bond length and decreasing the stretching mode. The corresponding C-O frequency increases of about $135cm^{-1}$. For the higher coordination (n $\geq$ 2) this phenomenon (reduction of the C=O frequency, increasing of C-O one) is lower and lowered with increasing of EC. The normal modes of EC are tend to approach as an isolated molecule with increasing coordination number. In case of n=5 and 6 for which 1 and 2 EC molecules are in the second solvation sphere, two different frequencies are obtained for C=O and C-O atoms.

Moreover, we have analysed the charge distribution by Mulliken charge analysis and our results are also shown in Table 3.5. As we could imagine the distribution of all charges on EC molecule are affected by the Li^+ ion coordination and the positive charge on Li^+ also decreases. The negative charge on O of the C=O group increases respect to the isolated EC molecule. But in case of Li^+ ion, the positive charge decrease from +1 to 0.814, it shows the main interaction through carbonyl oxygen atom. The general charge trend is a full of electrons going from EC to Li^+, thus reducing the electron density on $O(CH_2)$ groups, lowering the π bond character. The charges on Li^+ decreases EC molecules. But the reverse results are obtained in C(=O) and ethereal oxygen and also on alkyl carbon. Indeed, we could suggest that in all EC molecule O(=C) atoms are contributed some electron charge towards Li^+ ion results decrease of charge on Li^+ ion. There are two sort of charges are obtained in n=5 and 6 complexes due to lack of coordination of 5th and 6th EC molecule. In the particular EC molecules, the negative charge on O(=C) is higher than the coordinated EC molecules that also confirms the participation towards second solvation shell.

3.4.3 Frontier Molecular Orbital(FMO) analysis

We have calculated the frontier molecular orbital energy(FMO) gaps in the gas phase which are shown in Figure 3.4. In the approximation of Koopman's theorem the HOMO energy should represent the ionization potential (IP) (the first ionization energy of a

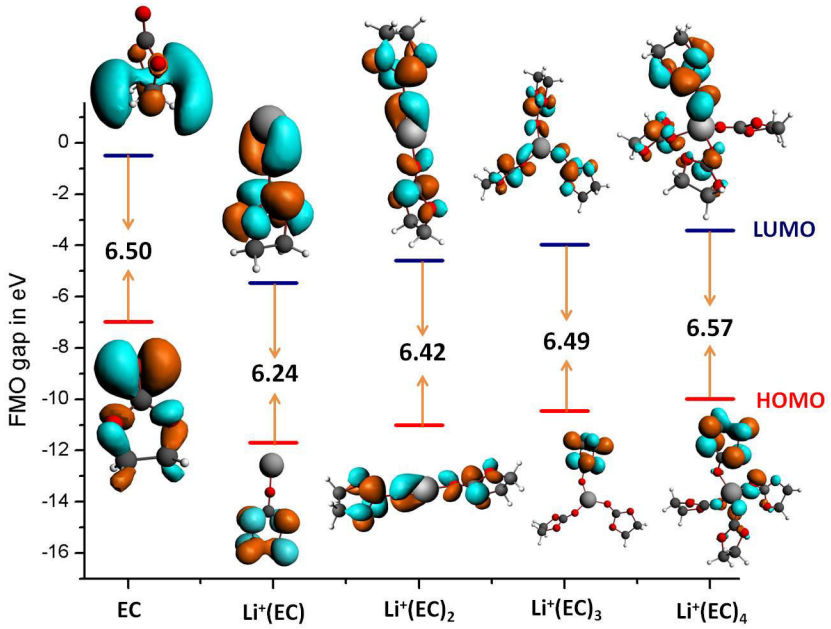

FIGURE 3.4: Frontier molecular orbitals energy (HOMO-LUMO) gap and corresponding molecular orbitals of EC and its complexes $Li^+(EC)_{1-6}$

molecular system is equal to the negative of the orbital energy of the highest occupied molecular orbital (HOMO)) and the LUMO the electron affinity. Using this description, the HOMO level on EC are stongly stabilized by the interaction with Li^+. So the IP values, for the lose of electrons, becomes higther in the complexes with Li^+. On the other hand, the LUMO energy is stabilized in order to capture one electron. From Figure 3.4, the gap for isolated EC is 6.5 eV and for $Li^+(EC)_4$ complex is almost stable with values between 6.24 and 6.57 eV. From a general point of view the EC molecule both isolated or coordinated to Li^+ should be stable to redox reaction occuring in LIBs where typical voltage (difference of potential between electrods) are around 3.6 V.

3.5 $Li^+(DMC)_{1-5}$ complexes

3.5.1 Structural Properties

In this section we will discuss our results on $Li^+(DMC)_{1\text{-}5}$ clusters. In the case of linear DMC like carbonates, there are two possibility for Li^+ ion coordination. One is through the carbonyl oxygen (O=C) the second is via two ether oxygen atoms, as shown in Figure 3.5. We have therefore consider these two conformations, and calculated the binding energy based on the above equation (3.1). Our results show that the Li^+ ion prefers to coordinate through the carbonyl oxygen rather than the ether oxygen, with an energy difference of about 3.0 kcal/mol.

TABLE 3.6: Selected structural parameters of $Li^+(DMC)_{1-5}$ complexes (bond lengths in angstrom, bond and dihedral angles in degree)

Parameters	DMC	$Li^+(DMC)$	$Li^+(DMC)_2$	$Li^+(DMC)_3$	$Li^+(DMC)_4$	$Li^+(DMC)_5$
Bond length						
Li^+-O		1.729	1.793	1.852	1.945	1.950/1.964
O=C	1.212	1.252	1.245	1.237	1.234	1.232
C-O	1.353	1.318	1.324	1.330	1.335	1.338
$O-CH_3$	1.446	1.456	1.453	1.450	1.450	1.448
Bond angle						
Li^+-O=C		178.5	176.5	173.5	143.1	139.6-161.2
O=C-O	126.4	125.0	125.3	125.7	124.3	125.8
$C-O-CH_3$	113.5	117.3	116.8	116.0	102.0	108.1
Dihedral angle						
$O=C-O-CH_3$	0.0	0.0	0.0	0.0	1.2	0.7
O=C-O-O	180.0	180.0	179.8	179.9	179.7	179.5
DPM/D	0.35	10.18	7.65	1.56	2.32	1.49
BE/ΔE		-42.09	-36.98	-30.97	-25.80	-21.70

DPM = Dipole moment, BE = Binding Energy in kcal/mol

Some selected bond parameters for $Li^+(DMC)_{1\text{-}4}$ are presented in Table 3.6, and our optimized geometries are shown in Figure 3.6 . The general trend that we can extract from the data in the Table, is that compared to the isolated DMC molecule, the coordination with Li^+ generates an elongation of the bond, O=C and $O-C(H_3)$. For low coordination numbers smaller then 3DMC, Li^+-O=C is almost linear, but angles of 143° are observed for coordination 4. Dipole moments have also been calculated for all structures. For the isolated DMC, the dipole is low (0.355 D), while coordination with Li^+ generate much higher dipole for coordinations 1 and 2 (around 7-10 D). Dipole next decreases for higher coordination numbers.

In the case of $Li^+(DMC)_2$ complexes, the Li^+ ion is linearly coordinated with two DMC molecules ((C=)O- Li^+-O(=C)) with an angle of 179.3°. In the $Li^+(DMC)_3$ complex,

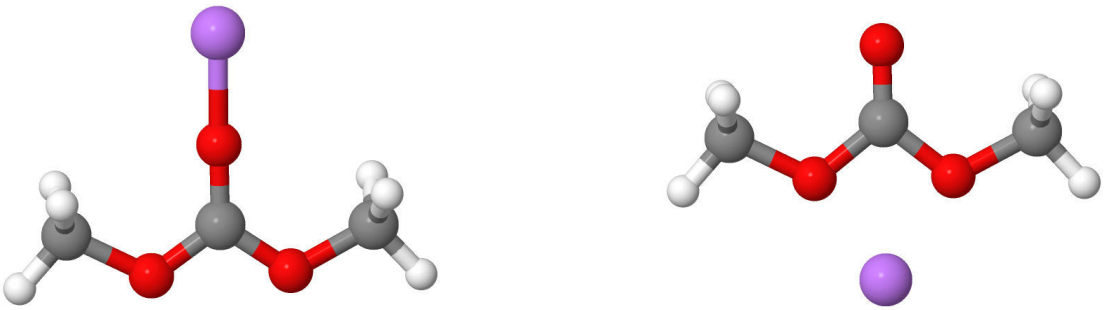

(a) Carbonyl coordination of $Li^+(DMC)$ (b) Ether coordination of $Li^+(DMC)$

FIGURE 3.5: Possible coordination structures of DMC with Li^+ ion

the 3 DMC molecules arrange on a trigonal geometry around the Li^+ ion. For instance, the angle (C=)O - Li^+-O(=C) are found to be around 120.0°. Due to the fact that 3 DMC molecules point towards Li^+ ion, the entire cluster dipole moment decreases(it falls to 1.56D to be compared to the value 7.6 observed for the $Li^+(DMC)_2$ complex) . In the $Li^+(DMC)_4$ complex, the Li^+-O=C angle takes a value of 143°. Also, DMC molecules are arranged around Li^+ with the four oxygens of the carbonyls groups organized in a tetrahedral-like geometry with an approximate angle of 112°. As we have already seen in the case of the $Li^+(EC)_5$ complex, we tried to obtain a $Li^+(DMC)_5$ complex with 5 DMC directly linked to Li^+ atoms. However, our calculations always converged to structures with the fifth DMC molecule weakly interacting with the Li^+ ion, at a distance of 4.59 Å. Indeed, the fifth DMC molecule has been found to interact through on hydrogen bond with other DMC molecules in the $Li^+(DMC)_5$ cluster but should be considered as pertaining to the second solvation shell. The four DMC molecules in the first shell still keep a pseudo tetrahedral geometry around Li.

The average binding energy of all complexes have been calculated in the gas phase, using equation 3.1, and are also shown in Table 3.6. The average binding energy decreases in $Li^+(DMC)_n$ complexes with n=1 to 5, meaning that the interaction between the Li^+ ion and a DMC molecule becomes weaker. By comparing these data to the average binding energies of $Li^+(EC)_{1\text{-}5}$ (from Table 3.4) complexes, we conclude that the Li^+-EC binding energies are a few kcal/mol higher than those of the Li^+-DMC complexes. Concluding, at this level of theory our result is that the Li^+ ion prefer to link with EC molecules rather than DMC ones.

3.5.2 Frequency and Mulliken Charge Analysis

We now discuss the vibrational modes of both isolated DMC and $Li^+(DMC)_{1\text{-}5}$ clusters in the gas phase. We focus on the two important frequencies, corresponding to stretching C=O and asymmetric stretching C-O modes. Our data are reported in Table 3.7. Comparison of data for the isolated DMC molecule and Li^+(DMC) shows that a strong interaction corresponds to the O=C group. In particular, the stretching frequency of C=O decreases significantly from 1736 cm^{-1} to 1640 cm^{-1}, which indicates that the C=O bond strength tends to become weaker following the interaction with Li^+. In contrast, the C-O mode frequency increases from 1241 cm^{-1} to 1345 cm^{-1}. The frequency variations are also directly related to the corresponding bond length changes, i.e., C=O is stretched (1.212 Å to 1.252 Å) while the C-O bond is contracted (1.353 Å to 1.318 Å) . This also explains the increase of electrons localisation in the DMC molecule. The C=O stretching frequency increases upon increasing the cluster size from n=2 to 4, due to the interaction between Li^+ and DMC molecules which become weaker making C-O frequency decrease, thus DMC modes approach to isolated molecules. In the $Li^+(DMC)_5$ complex, due to the weaker interaction of Li^+ ion with fifth DMC molecule (second solvation shell) and thus we obtain two different frequencies.

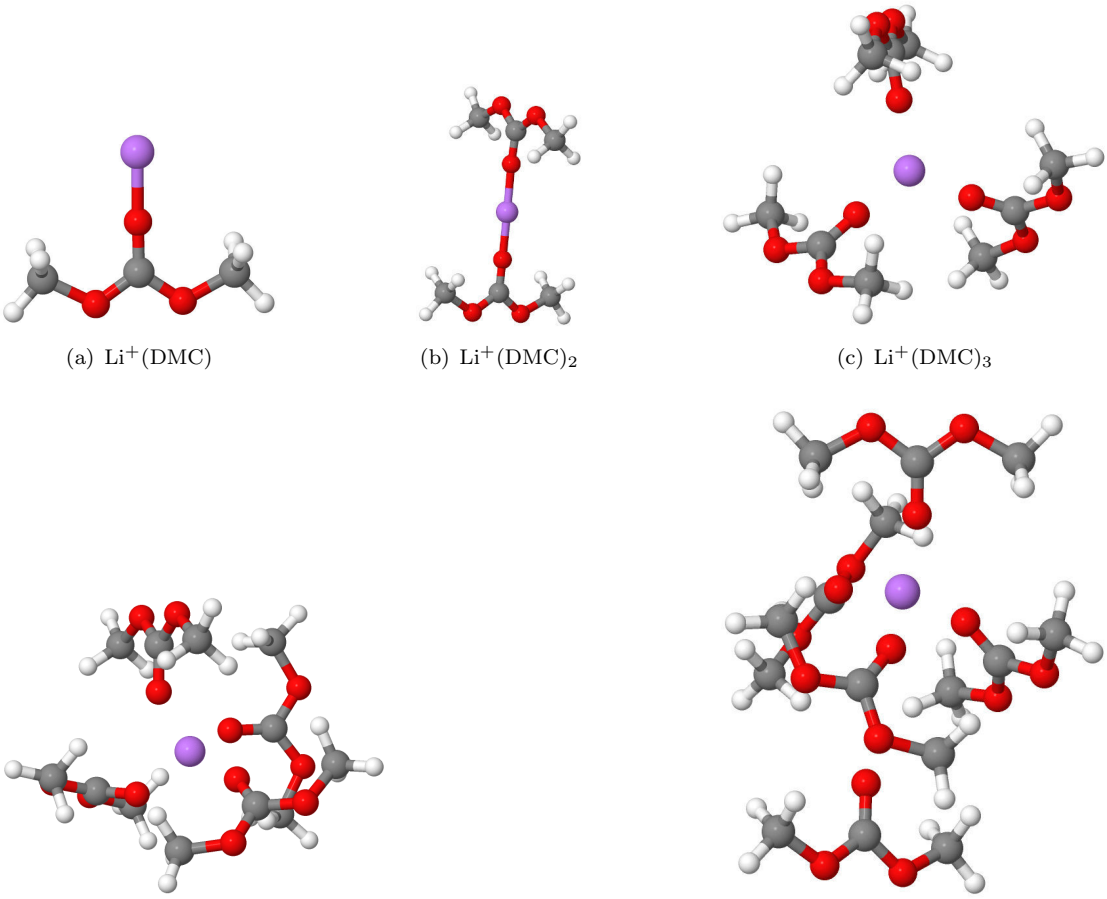

(a) $Li^+(DMC)$ (b) $Li^+(DMC)_2$ (c) $Li^+(DMC)_3$

(d) $Li^+(DMC)_4$ (e) $Li^+(DMC)_5$

FIGURE 3.6: Gas phase optimized solvation geometries of $Li^+(DMC)_{1-5}$

TABLE 3.7: Vibrational modes(in cm^{-1}) and Mulliken charges of $Li^+(DMC)_{1-5}$ clusters

Atoms	DMC	$Li^+(DMC)$	$Li^+(DMC)_2$	$Li^+(DMC)_3$	$Li^+(DMC)_4$	$Li^+(DMC)_5$
Frequencies						
C=O	1736	1640	1673	1710	1715	1720
C-O	1241	1345	1330	1315	1296	1291
Charges						
Li^+		0.799	0.695	0.654	0.642	0.656
O(=C)	-0.622	-0.658	-0.646	-0.625	-0.638	-0.622/-0.658
C(=O)	1.071	0.988	0.967	0.952	0.971	0.952-0.994
O	-0.501	-0.438	-0.449	-0.462	-0.482	-0.474/-0.495
C	0.582	0.708	0.717	0.732	0.751	0.742-0.762

We have also performed Mulliken charge analysis to account for the charge distribution in the $Li^+(DMC)_{1\text{-}5}$, clusters and the results are also reported in Table 3.7. Due to the strong interaction between Li^+ ion and the DMC molecule, we can expect significant charge variation on both DMC and Li^+ ion. The addition of Li^+ ion to a DMC molecule

shows that the positive charge on Li^+ ion decreases from +1 to 0.799 while the corresponding negative charge on O in O=C group increases. Therefore, the DMC molecule electron density moves towards Li^+ ion, resulting in a charge decrease. As we can see from the data in the Table, the positive charge on C in the methyl group increases following addition of Li^+ ion, therefore suggesting that the electrons are pulled by carbonyl fragment. The negative electron density on O (C=O) and the positive charge on C (=O) decrease upon addition of 2 to 4 DMC molecules. These results also explain the strong interaction occurring between Li^+-O=C. In the case of $Li^+(DMC)_5$ cluster, in agreement with the previous discussion on the fifth DMC molecule, charge analysis also shows values similar to the isolated DMC molecule, thus demonstrating that this is too far to be part of the first solvation shell.

3.5.3 Frontier Molecular Orbital(FMO) analysis

We have also analysed the HOMO-LUMO gap for isolated DMC and $Li^+(DMC)_{1\text{-}5}$ complexes in order to account for redox reactions, This could be of interest for applications in Li-ion batteries. Our results for the HOMO-LUMO calculations are shown in Figure 3.7. Going from the isolated DMC molecule to the Li^+ complexes, the HOMO-LUMO gap is slightly lowered in energy, and the $Li^+(DMC)_{1\text{-}4}$ complexes show energy gaps between 6.10 eV to 6.52 eV. What is interesting to underline here is that the nature of the orbitals changes. Indeed, from the data shown in the Figure is clear that, the DMC molecule electronic distribution of HOMO can be mainly atributed to carbonyl oxygen and ether oxygen atoms while the LUMO is distributed over all atoms. In contrast, after addition of Li^+ ion, the HOMO can be attributed to the ethereal oxygens and methyl groups.

3.6 $Li^+(PC)_{1-5}$ complexes

3.6.1 Structural Properties

In this section we will study the structural properties of $Li^+(PC)_{1\text{-}5}$ complexes. As we discussed in the state of the art included in Chapter 1 (7), previous results on Li^+-PC complexes, both from experiments and DFT calculations, showed that the $Li^+(PC)_3$ is the most stable structure, although, a few MD studies have found that a fourth PC molecule can also be involved in the first solvation shell. Therefore, similar to what we have done for other structures, we have considered the $Li^+(PC)_n$ complexes with n is 1 to 5. The optimized geometries, in the gas phase at the level of GGA/PBE using TZP basis, are shown in Figure 3.8 and the structural parameters are reported in Table 3.8. In $Li^+(PC)_n$ complexes, due to the strong interaction of Li^+ with the carbonyl oxygen the C=O bond length increases. The π character of C=O bond therefore becomes weaker

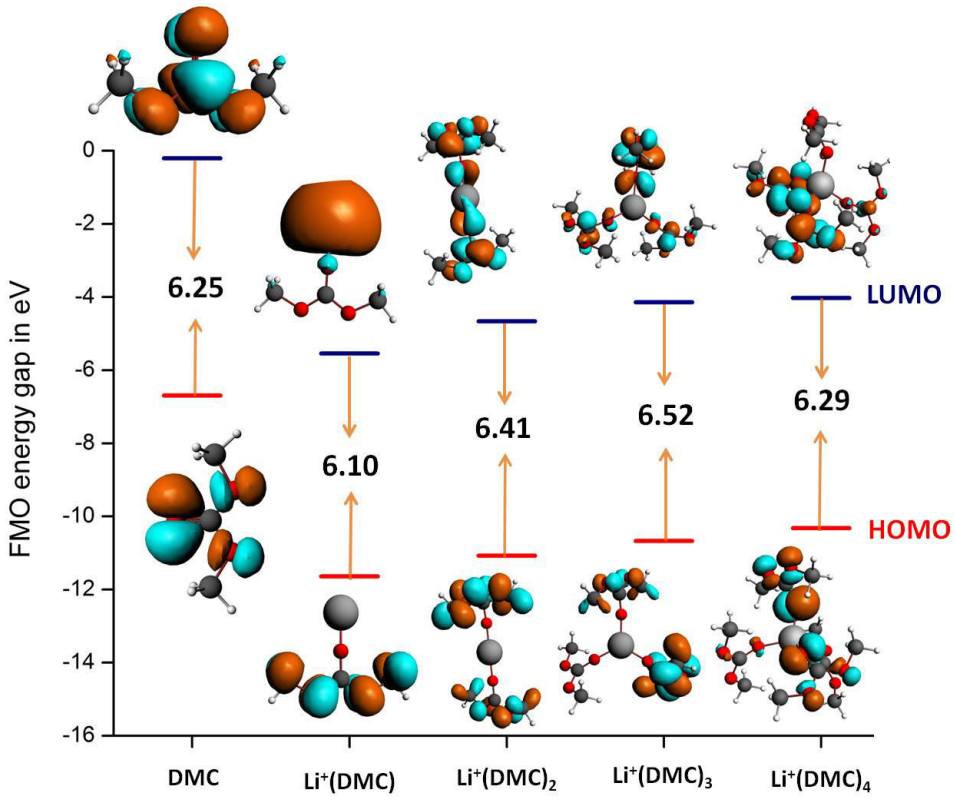

FIGURE 3.7: Frontier molecular orbitals energy (HOMO-LUMO) gap and corresponding orbitals of DMC and its complexes $Li^+(DMC)_{1-4}$

while the corresponding C-O bond distance decreases. The Li^+ ion interaction also inuences the bond angle O=C-O, which slightly decreases to 123.1° from 125° (isolated) molecule. However, the dihedral plane of the carbonyl group O-C(=O)-O is fept planar in all clusters (n = 1 to 5). The dihedral angle of O-C-C-O (ring) is slightly twisted by the Li^+ ion coordination, and remains almost the same for all clusters.

According to the data Table 3.8, as we expected the distance Li^+-O(=C) increases by increasing n, whereas, the reverse result is obtained for C=O bond. For instance, for the $Li^+(PC)_2$ cluster the two PC molecules are almost linearly linked with Li^+ ion with an angle (C=)O- Li^+-O(=C) of 177.0°. Similarly, the $Li^+(PC)_3$ and $Li^+(PC)_4$ complexe show a (C=)O- Li^+-O(=C) angle of 145.5° and 136.6°, respectively. Also, the carbonyls oxygens show respectively a trigonal and pseudo tetrahedral arrangement around Li^+. In $Li^+(PC)_4$ complex, all PC molecules are twisted in order to overcome the repulsion of methyl groups. Similar to our results for $Li^+(EC)_5$ and $Li^+(DMC)_5$ clusters, also for $Li^+(PC)_5$ the fifth PC molecule pertains to the second solvation shell, with a distance of 4.933 from Li^+.

The average binding energy of $Li^+(PC)_{1\text{-}5}$ complexes are calculated in the gas phase, using the equation (3.1) and the values are shown in Table 3.8. The average binding energy decreases by increasing n. By comparing of the average binding energy of $Li^+(PC)_{1\text{-}5}$ and $Li^+(EC)_{1\text{-}5}$ complexes, we conclude that the difference is very small,

TABLE 3.8: Selected Structural parameters of $Li^+(PC)_{1-5}$ geometries (bond lengths in angstrom, bond and dihedral angles in degree)

Parameters	PC	Li^+(PC)	$Li^+(PC)_2$	$Li^+(PC)_3$	$Li^+(PC)_4$	$Li^+(PC)_5$
Bond length						
Li^+-O		1.731	1.780	1.870	1.954	1.950/1.997/4.933
O=C	1.201	1.237	1.228	1.222	1.217	1.218/1.210
C-O($CHCH_3$)	1.372	1.325	1.333	1.340	1.348	1.346/1.361
C-O(CH_2)	1.376	1.333	1.339	1.348	1.355	1.455/1.450
O-C(CH_3)	1.457	1.491	1.480	1.473	1.470	1.465
O-C(H_2)	1.442	1.466	1.460	1.456	1.453	1.450
C(H_2)-C(H)	1.531	1.535	1.541	1.540	1.532	1.532
C-C(H_3)	1.512	1.507	1.512	1.514	1.510	1.510
Bond angle						
Li^+-O=C		173.8	177.0	145.5	136.6	121.1-148.3
O=C-O($CHCH_3$)	125.0	123.1	123.4	123.4	123.7	123.6-123.7
O=C-O(CH_2)	124.5	122.4	122.9	123.7	124.0	123.0-124.0
C-O-C(H)	109.3	108.5	109.1	109.2	108.8	108.3
C-O-C(H_2)	108.5	107.9	108.6	108.6	108.3	108.8
Dihedral angle						
O-C(=O)-O	180.0	180.0	179.9	180.0	180.0	179.2-179.9
O-C-C-O	20.4	24.1	13.3	15.0	18.0	21.3
DPM/D	5.59	10.11	19.34	21.58	2.56	3.59
BE/ΔE		-49.50	-42.65	-35.50	-30.32	-25.76

DPM = Dipole moment, BE = Binding Energy in kcal/mol

which means the PC solvent molecule could possibly substitute EC molecule (and vice-versa) in the first solvation shell.

3.6.2 Frequency and Mulliken Charge Analysis

We have also studied the vibrational frequencies of the isolated PC molecule and the $Li^+(PC)_{1\text{-}5}$ clusters. The calculated frequencies are shown in Table 3.9. The two important frequencies associated to the C=O stretching and the asymmetric C-O stretching are strongest affected by the coordination with Li^+ ion. According to BE, the strongest interaction obtained for Li^+-(PC) cluster, the corresponding C=O and C-O modes are more affected than in the case of other coordinated clusters ($Li^+(PC)_{2\text{-}5}$). The difference for the C=O stretching between the isolated PC and the Li^+-(PC) is around 100 cm^{-1}. Also, the π bond character of C=O tends to decrease and this results in an increase of the bond length. However, the corresponding C-O stretching increases of about 350cm^{-1}, due to ethe lectron distribution throughout the molecule, which leads to a shorter bond length. While the addition of 2 to 5 PC molecules, affects the interaction between Li^+

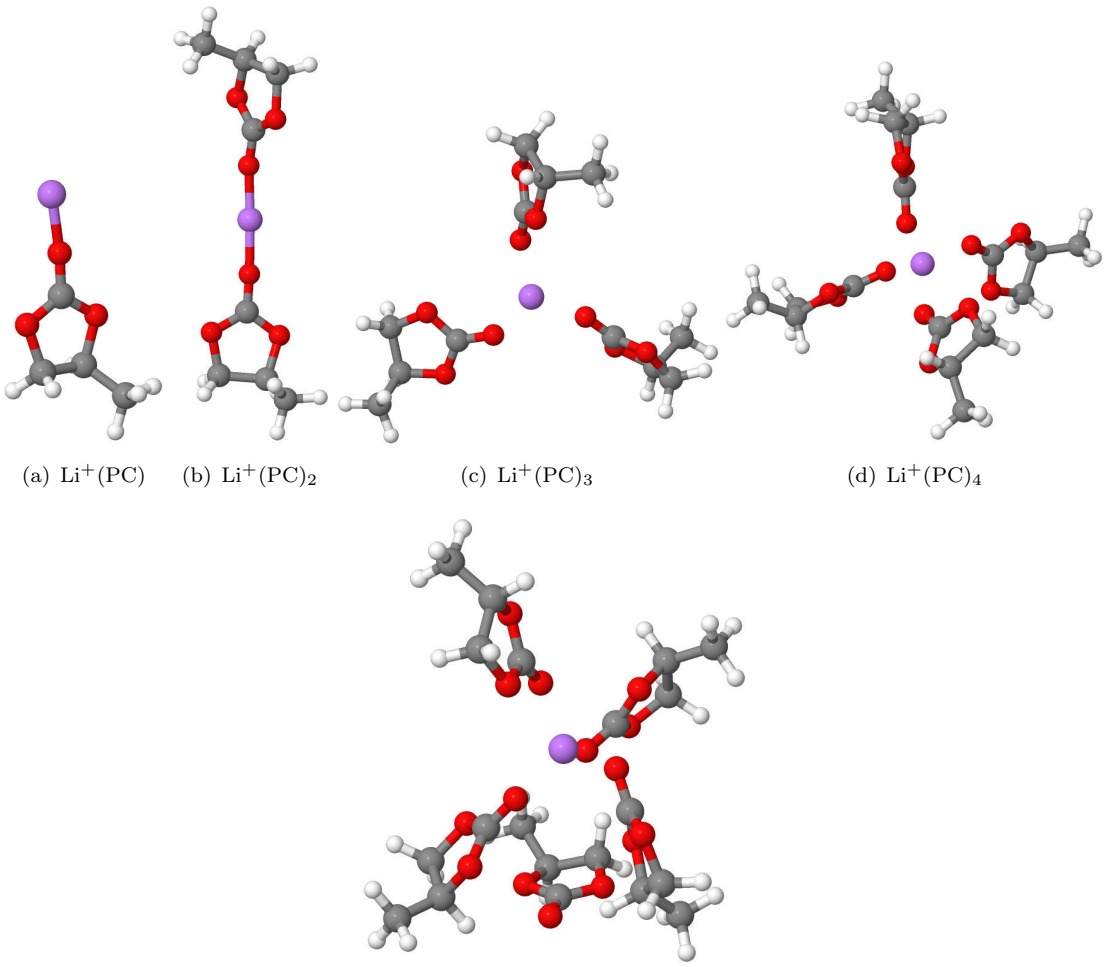

(a) $Li^+(PC)$ (b) $Li^+(PC)_2$ (c) $Li^+(PC)_3$ (d) $Li^+(PC)_4$

(e) $Li^+(PC)_5$

FIGURE 3.8: Gas phase optimized solvation clusters of $Li^+(PC)_{1-5}$

ion and PC which becomes increasingly weaker, the C=O frequency increases. The reverse result is obtained for the asymmetric C-O stretching. In particular, from the data shown in the Table, the $Li^+(PC)_5$ complex shows two sort of stretching modes for the PC molecule. This confirms, also for this case, then fifth PC molecule participates to the second solvation shell.

We have also investigated the Mulliken charge distribution for the PC molecule and the $Li^+(PC)_{1\text{-}5}$ clusters, and the values are reported in Table 3.9. As we could have expected that the strong interaction with Li^+ ion impacts the charge distribution on the entire PC molecule. In the case of the $Li^+(PC)$ cluster, the charge on the Li^+ ion decrease from +1 e to 0.814 e, while the corresponding negative charge on O of C=O increases. This clearly explains the main interaction associated to the O=C bond. Similarly, the positive charge on C in C=O increases. It therefore seems that the electrons move towards the Li^+ ion. Nevertheless, the negative charge on ether oxygen reduced upon Li^+ addition, thus confirming the electron distributions occur in the entire molecule. The addition of PC molecules decreases the positive charge of Li^+ and a similar trend have also been

TABLE 3.9: Vibrational modes(in cm^{-1}) and Mulliken charges of $Li^+(PC)_{1-4}$ geometries

Atoms	PC	$Li^+(PC)$	$Li^+(PC)_2$	$Li^+(PC)_3$	$Li^+(PC)_4$	$Li^+(PC)_5$
Frequencies						
C=O	1829	1724	1763	1783	1801	1796
C-O	1070	1404	1393	1380	1370	1347
Charges						
Li^+		0.811	0.703	0.667	0.652	0.647
O(=C)	-0.492	-0.607	-0.585	-0.580	-0.570	-0.576/-0.592
C(=O)	0.840	0.955	0.942	0.950	0.948	0.944/0.987
$O(CH_2)$	-0.487	-0.449	-0.467	-0.485	-0.482	-0.492/-0.521
$O(CHCH_3)$	-0.497	-0.466	-0.462	-0.473	-0.496	-0.488/-0.497

observed in the other cases. As we can see for the $Li^+(PC)_5$ complex, two different charges are obtained for PC molecules, due to the fifth PC molecule participating to the second solvation shell. The higher negative charge on O of the C=O bond in the fifth PC molecule describes the consequence of the lack of direct coordination to the Li^+ ion.

3.6.3 Frontier Molecular Orbital(FMO) analysis

We have also analysed the HOMO-LUMO gaps for PC and the $Li^+(PC)_{1\text{-}4}$ complexes. Our data are shown in Figure 3.9. From the Figure, it is evident that there is not a considerable change of the HOMO-LUMO energy gaps if considering isolated PC molecule on the $Li^+(PC)_{1\text{-}4}$ complexes. Our conclusion therefore is that redox stability of PC should not be affected by coordination with Li^+.

3.7 Thermodynamic parameters of $Li^+(S)_{1-5}$ complexes: (S=EC,DMC and PC)

In this section we report our study of the thermodynamic parameters including entropy, enthalpy and Gibbs free energy for all investigated clusters $Li^+(S)_n$ (n = 1 to 5) and S = EC, DMC, PC. In order to provide an estimation of the preferable coordination number around the lithium cation, the most favorable path between these clusters $Li^+(S)_n$ has to be determined in terms of free energy changes. To do so, the free energies of the aggregates $Li^+(S)_n$ + m S (n+m=constant=5 in this case) were estimated, in order to define the aggregate exhibiting the lowest free energy value. In this way, if the fragment $Li^+(S)_n$ + m S has the lowest free energy value, all paths of the type:

$$Li^+(S)_k + l.S \rightarrow Li^+(S)_n + m.S, k + l = m + n \tag{3.2}$$

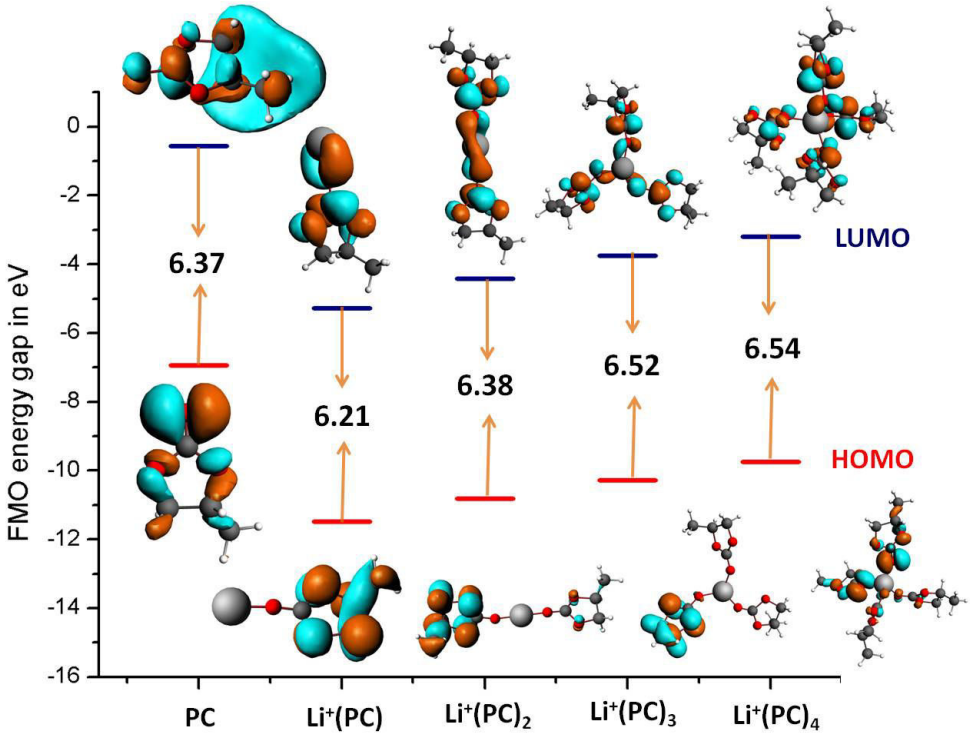

FIGURE 3.9: Frontier molecular orbitals energy gap and corresponding orbitals of PC and its complexes $Li^+(PC)_{1-4}$

will exhibit a negative free energy change ΔG, thus indicating that all possible paths leading to the cluster $Li^+(S)_n$ are favorable and, therefore, this cluster could be considered the most preferable one in terms of the free energy changes. Note that the paths depicted in Eq. 2 can correspond to both additions or subtractions of solvent molecules from one particular cluster leading to another, depending on the relative difference $m\ l$. If $m\ \ l < 0$, then the transition is being achieved through solvent addition, otherwise through solvent subtraction.

The calculated enthalpy and entropy values of all complexes are given in Table 3.10, and the corresponding free energy value changes are reported in Table 3.11. From the free energy values, it can be clearly seen that in the cases of EC and DMC, the tetra coordinated Li^+ ion is predicted to be more favourable structure. Similar conclusions have been drawn in the DFT study of Bhatt et al, studying the solvation of Li+ in EC. In the case of PC the free energy difference for the path going from $Li^+(PC)_3$ to $Li^+(PC)_4$ is very small. This is an indication that although the $Li^+(PC)_3$ cluster has been predicted to be the most favorable one, both structures could possibly exist in the bulk phase. From the data presented in Tables it might be also seen that in the cases of the tetracoordinated clusters the binding energies decrease in the order $E(Li^+(PC)_4)$ $>E(Li^+(EC)_4)$ $>E(Li^+(DMC)_4)$, which is reasonable taking into account that the dipole moments of PC, EC and DMC molecules decrease in the same order (5.6, 5.3 and 0.35 D, respectively). It should be also noted that the entropic contributions to the free

TABLE 3.10: Thermodynamical parameters Enthalpy(H) (kcal/mol) and Entropy(S) (cal/mol-K) of isolated solvents and all pure complexes

Fragments	H	S
EC	-1369.3	72.8
$Li^+(EC)$	-1293.6	83.2
$Li^+(EC)_2$	-2698.9	116.9
$Li^+(EC)_3$	-4090.4	142.2
$Li^+(EC)_4$	-5473.4	174.0
$Li^+(EC)_5$	-6849.9	214.6
DMC	-1530.2	82.5
$Li^+(DMC)$	-1449.0	90.6
$Li^+(DMC)_2$	-3012.2	124.5
$Li^+(DMC)_3$	-4562.4	158.1
$Li^+(DMC)_4$	-6100.8	216.8
$Li^+(DMC)_5$	-7636.7	251.3
PC	-1736.0	79.6
$Li^+(PC)$	-1662.2	89.8
$Li^+(PC)_2$	-3435.1	123.7
$Li^+(PC)_3$	-5193.2	154.5
$Li^+(PC)_4$	-6945.0	180.3
$Li^+(PC)_5$	-8687.2	231.3

TABLE 3.11: Gibbs free energy of clusters (energies in kcal/mol)

Fragments	G		
	S=EC	S=DMC	S=PC
$Li^+(S)+ 4S$	-6882.4	-7695.0	-8728.1
$Li^+(S)_2 + 3S$	-6906.7	-7713.5	-8751.3
$Li^+(S)_3 + 2S$	-6914.8	-7719.0	-8758.8
$Li^+(S)_4 + S$	-6916.2	-7720.2	-8758.5
$Li^+(S)_5$	-6913.9	-7711.6	-8756.2

energy of each cluster exhibit the opposite trend, being more important in the case of the $Li^+(DMC)_4$.

All previous results have been obtained in the gas phase. We have also decided to check that the structures do not change substantially by adding a dielectric background to account for bulk solvent and focused on the $Li^+(S)_4$ (S= EC, DMC and PC) structures. For each structure we have simulated the effect of solvation by adding a model describing the corresponding dielectric constant (ϵ=89,6, 3.1 and 64.9 for pure EC, DMC and PC respectively). The conductor-like screening model(COSMO) has been used for DFT optimisation calculation using GGA/PBE with TZP basis, and our results together with the corresponding solvent parameters are given in Table 3.12. As we expected, the obtained solvation energies are higher for systems which have higher dipole moment, like EC and PC systems, compared to DMC that is in general less polar. Also, the

TABLE 3.12: Parameters used for COSMO calculations and solvation energy of complexes ($Li^+(S)_4$) in kcal/mol

Parameters	EC	DMC	PC
ϵ	89.6	3.1	64.9
Radius(Å)	2.99	3.22	32.23
Solvation energy	-60.1	-33.0	-59.7

TABLE 3.13: Comparison of bond parameters between solvent clusters in gas and dielectric phase (bond lengths in angstrom, bond and dihedral angles in degree)

Parameters	$Li^+(EC)_4$		$Li^+(DMC)_4$		$Li^+(PC)_4$	
	Gas	Solvent	Gas	Solvent	Gas	Solvent
Bond length						
Li^+-O(=C)	1.951	1.967	1.945	1.937	1.954	1.939
O=C	1.215	1.226	1.234	1.231	1.217	1.228
C-O	1.352	1.345	1.335	1.336	1.348	1.341
Li^+-O=C(angle)	136.9	128.5	143.1	147.7	136.6	124.4
O-C(=O)-O(dihedral)	180.0	179.9	179.7	180.0	180.0	179.9
Charges						
Li^+	0.641	0.630	0.642	0.645	0.652	0.639
O(=C)	-0.564	-0.628	-0.638	-0.626	-0.570	-0.643
C(=O)	0.951	0.989	0.971	0.978	0.948	0.998

geometries , see Table 3.13, are not strongly affected. The overall arrangement stays the same around Li^+, just a few distances being affected, with variations of the order of 10^{-2} Å. In contrast, the Li^+-O=C bond angle is reduced for the EC and PC structures.

3.8 Solvent Mixtures

In Li-ion batteries research, several experimental and theoretical studies devoted to the interactions of Li^+ with pure and mixed carbonate-based electrolytes have already been published, the solvation structure and dynamics of lithium cations in these solvents is still a subject of debate. Therefore, we have considered the Li^+ ion in mixed binary and ternary carbonate-based solvents, and the results were discussed in the following section.

3.8.1 Binary Mixtures

In order to clarify the behaviour of binary mixtures we focus on the preferred tetra coordinated structures. We have considered three types of binary mixtures, $Li^+(EC)_m(PC)_n$, $Li^+(EC)_m(DMC)_n$ and $Li^+(PC)_m(DMC)_n$ (with : m+n=4). These complexes have been

TABLE 3.14: Structural parameters of Binary mixtures

Binary mixtures	r_{Li^+-O}(Å)		$r_{O=C}$ (Å)		$angle_{Li^+-O=C}$(°)		Dipole (D)
Ratio	S_1	S_2	S_1	S_2	S_1	S_2	
Li^+: EC(S_1) : PC(S_2)							
1:3:1	1.953	1.948	1.216	1.218	135.9	134.2	2.04
1:2:2	1.955	1.949	1.216	1.217	136.0	134.0	2.64
1:1:3	1.957	1.951	1.215	1.217	136.5	136.2	2.32
Li^+: EC(S_1) : DMC(S_2)							
1:3:1	1.943	1.921	1.216	1.231	138.9	160.8	6.18
1:2:2	1.972	1.910	1.214	1.231	136.6	156.4	7.19
1:1:3	1.943	1.921	1.216	1.231	138.9	160.8	8.70
Li^+: PC(S_1) : DMC(S_2)							
1:3:1	1.951	1.919	1.215	1.231	147.3	152.6	4.27
1:2:2	1.970	1.912	1.217	1.231	140.4	164.6	6.47
1:1:3	1.954	1.950	1.219	1.233	148.4	157.1	4.33

optimized using DFT with GGA/PBE functional at TZP basis. The optimized geometry bond parameters are illustrated in Table 3.14. As we can see in the Table, for $Li^+(EC)_m(PC)_n$ the variation in relative proportion of EC or PC in the first solvation shell of Li^+ does not change significantly distances, angles or dipoles values. The reason is that both EC and PC have similar dipoles and structures. In contrast, mixtures including DMC exhibit different bond lengths and bond angles, due to the totally different skeleton of DMC. Interestingly, we can clearly see from the Table that the bond between Li^+-O(=C) in DMC molecules is shorter compared to the corresponding EC and PC ones. Moreover, the same Li^+-O(=C) bond distance for EC and PC is elongated when DMC joins the solvation shell.

In Table 3.15 we report the vibrational analysis and the Mulliken charges for the studied binary complexes. Similar to the geometry discussion, also in this case EC and PC mixtures keep into constant values of both C=O and C-O frequencies modes and of mullikens charges, that do not really vary with the composition of the first solvation sphere. DMC containing structures show stronger variations. In general in presence of DMC in the first coordination sphere, the DMC molecule is the solvent molecule closest to the Li^+, and the corresponding oxygen of the carbonyl group has a higher negative charge compared to the EC and PC ones. The C=O frequency is in general around $100cm^{-1}$ lower for DMC thus confirming a weaker C=0 bond.

In order to understand the most favourable path transitions of one binary cluster to another binary clusters, we calculated the free energy of reactions which can be estimated by the following equation:

TABLE 3.15: Mulliken charges, Vibrational modes and Dipole moments of Binary mixtures

Binary mixtures	Charges(Li^+,O(=C))			$\nu_{C=O}(cm^{-1})$		$\nu_{C-O}(cm^{-1})$	
Ratio	Li^+	S_1	S_2	S_1	S_2	S_1	S_2
Li^+: EC(S_1) : PC(S_2)							
1:3:1	0.646	-0.567	-0.575	1775	1804	1174	1147
1:2:2	0.648	-0.565	-0.574	1776	1803	1174	1145
1:1:3	0.650	-0.564	-0.571	1775	1802	1174	1144
Li^+: EC(S_1) : DMC(S_2)							
1:3:1	0.651	-0.568	-0.611	1802	1701	1146	1194
1:2:2	0.647	-0.575	-0.612	1798	1705	1142	1193
1:1:3	0.659	-0.570	-0.615	1779	1709	1779	1709
Li^+: PC(S_1) : DMC(S_2)							
1:3:1	0.659	-0.563	-0.616	1796	1702	1160	1193
1:2:2	0.658	-0.569	-0.614	1789	1703	1174	1193
1:1:3	0.638	-0.568	-0.619	1772	1706	1163	1192

$$Li^+(S_1)_k(S_2)_l + (4-l).S_1 + (4-k).S_2 \rightarrow Li^+(S_1)_n(S_2)_m + (4-n).S_1 + (4-m).S_2 \quad (3.3)$$

where k + l = n + m = 4 and n, m, k, l = 1-3, were also estimated, in order to find the most favourable structure among the clusters with two types of solvents around lithium. The calculated values of enthalpy and entropy of all $Li^+(S_1)_k(S_2)_l$ clusters are given in Table 3.16, Gibbs free energy(G) values of $Li^+(S_1)_n(S_2)_m$ $+(4-n).S_1+(4-m).S_2$ clusters are reported in Table 3.17. The Li^+(EC)(PC) types complex results reveales that the possible combination of tetra coordinated cluster containing both EC and PC with the ratio of 50:50 $Li^+(EC)_2(PC)_2$ is the most preferable one, followed by $Li^+(EC)(PC)_3$. The least favourable complex is $Li^+(EC)_3(PC)$. These results suggest that EC and PC are equally coordinated to Li^+ ion and no selective solvation occur in these clusters. In contrast, in the cases of Li^+(EC)(DMC) and Li^+(PC)(DMC) type clusters the $Li^+(EC)_3$(DMC) and $Li^+(PC)_3$(DMC) are the most favourable ones, followed by $Li^+(EC)_2(DMC)_2$ and $Li^+(PC)_2(DMC)_2$. The less favourable cluster is the one with the highest concentration of DMC molecules. These results reveal that solvation is preferred with EC or PC molecules over DMC molecules in DMC- containing binary clusters. The Li^+(EC)(DMC) results are in good agreement with the ab initio study by Borodin and Smith [96], where the relative stabilities were based upon the energies of the complexes, and with the very recently study by Bhatt [197].

The average binding energy(BE) of all binary clusters have also been calculated by the following equation:

TABLE 3.16: Thermodynamical parameters Enthalpy(H) (kcal/mol) and Entropy(S) (cal/mol-K) binary complexes

Fragments	H	S
$Li^+(EC)_3(PC)$	-5842.1	167.2
$Li^+(EC)_2(PC)_2$	-6209.6	173.9
$Li^+(EC)(PC)_3$	-6576.9	180.3
$Li^+(EC)_3(DMC)$	-5632.2	182.1
$Li^+(EC)_2(DMC)_2$	-5790.4	186.2
$Li^+(EC)(DMC)_3$	-5946.2	204.9
$Li^+(PC)_3(DMC)$	-6734.5	193.1
$Li^+(PC)_2(DMC)_2$	-6524.7	209.5
$Li^+(PC)(DMC)_3$	-6314.5	204.7

$$\Delta E_{BE} = -\{E_{total}[Li^+(S1)_m(S2)_n] - E[Li^+] - mE[S1] - nE[S2]\}/(m+n) \quad (3.4)$$

where $E_{total}[Li^+(S1)_m(S2)_n]$ is the total energy of the binary clusters, $E[Li^+]$ is the energy of the Lithium ion, the S1 and S2 are the solvent molecules (EC, DMC, PC) and $E[S1], E[S2]$ are isolated solvent molecules energies m, n (n+m=4) are the number of solvent molecules of type S1 and S2 respectively.

The average binding energies of all binary mixtures are shown in Figure 3.10. The obtained results show that the binary complexes of Li^+(EC)(PC) types are more energetically stable than Li^+(EC)(DMC) and Li^+(PC)(DMC) complexes. The BE difference between the complexes such as Li^+(EC)(DMC) and Li^+(PC)(DMC) is only of a few kcal/mol. Interestingly, the BE of all binary complexes are energetically more stable

TABLE 3.17: Gibbs free energies (in kcal/mol) of clusters containing two types of solvents with Li^+ ion

Fragments	G
$Li^+(EC)_3(PC)$ + 1 EC + 3 PC	-12562.3
$Li^+(EC)_2(PC)_2$ + 2 EC + 2 PC	-12564.7
$Li^+(EC)(PC)_3$ + 3 EC + PC	-12563.5
$Li^+(EC)_3(DMC)$ + 1 EC + 3 DMC	-11741.7
$Li^+(EC)_2(DMC)_2$ + 2 EC + 2 DMC	-11737.3
$Li^+(EC)(DMC)_3$ + 3 EC + 1 DMC	-11735.0
$Li^+(PC)_3(DMC)$ + 1 PC + 3 DMC	-13358.6
$Li^+(PC)_2(DMC)_2$ + 2 PC + 2 DMC	-13354.7
$Li^+(PC)(DMC)_3$ + 3 PC + 1 DMC	-13350.4

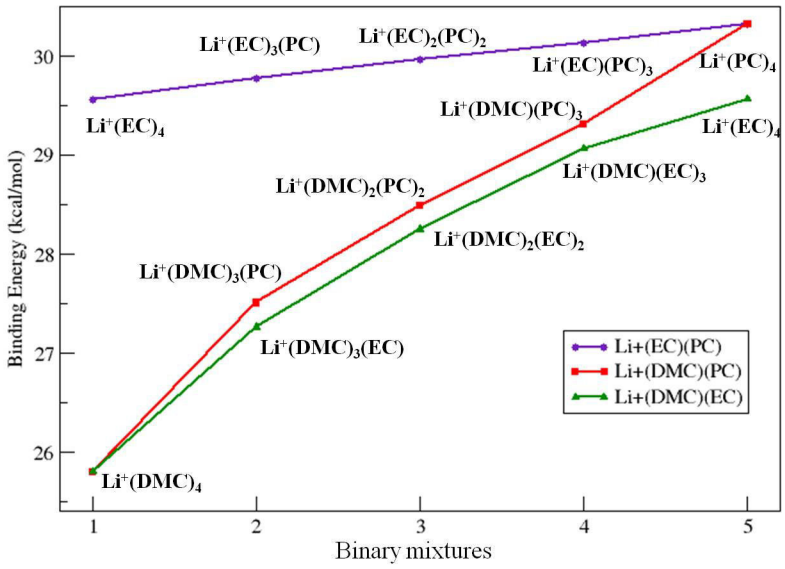

FIGURE 3.10: Calculated Binding Energies of all tetra coordinated Binary mixtures

than pure $Li^+(DMC)_4$. Therefore, the pure $Li^+(DMC)_4$ is hardly formed when two types of solvents are involved in the bulk solution.

3.8.2 Ternary Mixtures

Although, many studies have been devoted to binary mixtures, to best of our knowledge, this is the first study also focusing on ternary mixtures.

Structures of the optimized clusters for the $Li^+(EC)_n(PC)_m(DMC)_l$ with n+m+l=4 are shown in Figure 3.11. Pur results of structural parameters, Mulliken charges, vibrational modes and binding energies are presented in Table 3.18. Focusing on the asymmetry of solvents, bond angles and distances differ frpm those in the pure clusters. We can clearly seen from the Table, that DMC produces some changes on the solvation structures of Li^+ ion. Despite the higher negative charge on carbonyl oxygen in DMC molecule, it coordinates with Li^+ ion at a shorter distance if compared to Li^+-EC and Li^+-PC distances. The Li^+-O (=C) distance is almost the same as that in pure PC containing clusters, in all ternary clusters. However, the corresponding Li^+-O(=C) distance increases in $Li^+(EC)(PC)(DMC)_2$ clusters. But in the case of Li^+-O(=C) distance in DMC decreases around 0.2 Å as compared to $Li^+(DMC)_4$.

The angle Li^+-O=C increases in all clusters, as compared to their corresponding pure clusters due to different structure of solvents. The $Li^+(EC)(PC)_2(DMC)$ cluster has a lower positive charge on Li^+ ion and it is slightly higher in the other clusters. The same trend is also observed for carbonyl group charges. Also, no large changes are observed on the vibrational modes associated to C=O stretching and asymmetric C-O stretching.

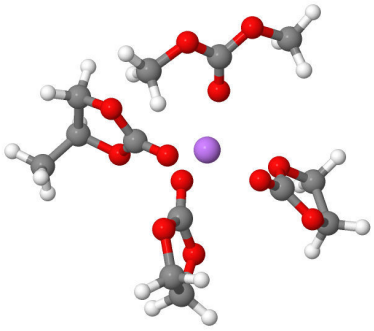

(a) $Li^+(EC)_2(PC)(DMC)$

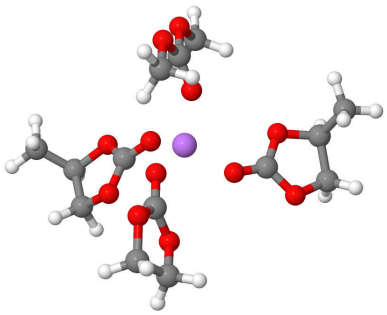

(b) $Li^+(EC)(PC)_2(DMC)$

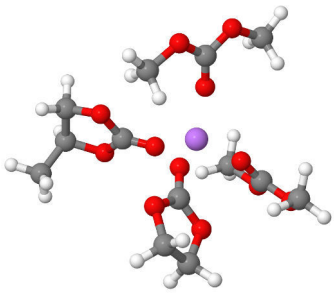

(c) $Li^+(EC)(PC)(DMC)_2$

FIGURE 3.11: Gas phase Optimized geometries of ternary clusters such as $Li^+(EC)_2(PC)(DMC)$, $Li^+(EC)(PC)_2(DMC)$ and $Li^+(EC)(PC)(DMC)_2$

The binding energy(BE) for all ternary clusters has been calculated by the following equation:

$$\Delta E_{BE} = -\{E_{total}[Li^+(EC)_l(DMC)_m(PC)_n] - E[Li^+] - lE[EC] - mE[DMC] - nE[PC]\}/(l+m+n) \quad (3.5)$$

where $E_{total}[Li^+(EC)_l(DMC)_m(PC)_n]$ is the total energy of the ternary clusters and $E[Li^+]$, $E[EC]$, $E[DMC]$, $E[PC]$ are the energy of the Lithium ion, isolated solvent molecules (EC, DMC, PC) and l, m, n (l+n+m=4) are the number of solvent molecules respectively. The average binding energy (BE) of all ternary mixtures are calculated using equation (3.5) and the values are presented in Table 3.18. According to the BE, the $Li^+(EC)(PC)_2(DMC)$ is more stable than $Li^+(EC)(PC)(DMC)_2$ cluster, but the difference is only about $\sim$ 1 kcal/mol. A similar result holds for the $Li^+(EC)_2(PC)(DMC)$ complex.

We have also calculated the HOMO-LUMO gap for all complexes which are shown in Figure 3.12. The HOMO-LUMO gap is comparatively low in $Li^+(EC)(PC)(DMC)_2$ and the $Li^+(EC)_2(PC)(DMC)$ cluster has a higher energy gap. From the Figure, the HOMO is mainly attributed to the DMC molecule rather than to EC and PC.

TABLE 3.18: Structural parameters, Mulliken charges, Vibrational modes and cacu-lated average Binding energies of Ternary mixture

Parameters	$Li^+(EC)_2(PC)(DMC)$	$Li^+(EC)(PC)_2(DMC)$	$Li^+(EC)(PC)(DMC)_2$
Bond distances (Å)			
Li^+-O(=C)			
EC	1.976, 1.942	1.957	1.990
PC	1.953	1.800, 1.957	1.955
DMC	1.923	1.908	1.916, 1.923
Bond angle in (°)			
Li^+-O=C			
EC	137.9, 140.5	142.2	146.9
PC	143.9	142.2, 142.3	145.5
DMC	160.1	154.0	163.0, 161.7
Mulliken charges			
Li^+	0.651	0.643	0.659
O(=C)-EC	-0.563, -0.574	-0.571	-0.558
O(=C)-PC	-0.562	-0.565, -0.573	-0.571
O(=C)-DMC	-0.610	-0.6107	-0.609, -0.6092
$\nu_{O=C}, \nu_{C-O}(cm^{-1})$			
EC	1800, 1156	1796, 1159	1793, 1163
PC	1800, 1156	1796, 1159	1793, 1163
DMC	1702, 1194	1700, 1193	1708, 1194
BE(kcal/mol)	-29.15	-29.31	-28.50

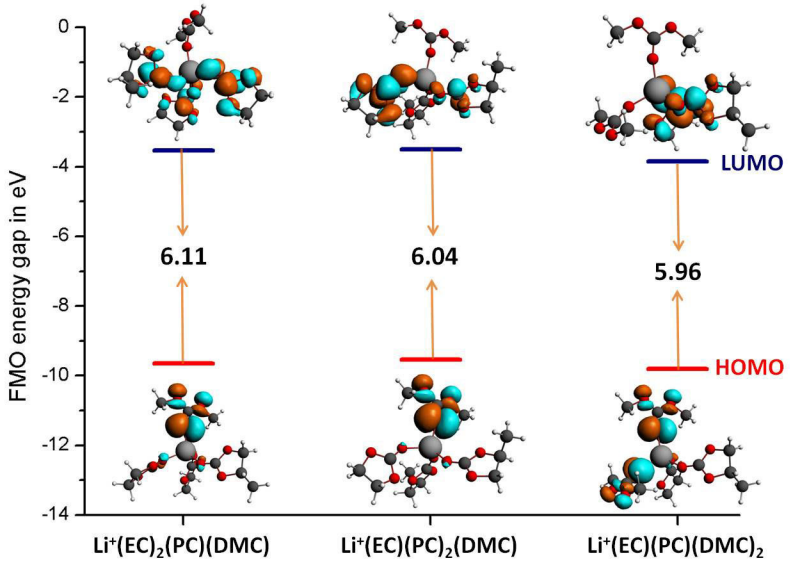

FIGURE 3.12: Frontier molecular orbitals energy gap and corresponding orbitals of ternary complexes

Finally, a free energy analysis similar to the one perfomed for the binary mixtures have also been performed for termary clusters. The results obtained, using the same methodology discussed above in the binary clusters, are presented in Tables 3.19 and 3.20. It can be seen that the clusters containing more EC molecules, $Li^+(EC)_2(PC)(DMC)$ seem

TABLE 3.19: Thermodynamical parameters such as Enthalpy(H) (kcal/mol) and Entropy(S) (cal/mol-K) values of ternary complexes

Fragments	H	S
$Li^+(EC)_2(DMC)(PC)$	-5999.3	189.0
$Li^+(EC)(DMC)_2(PC)$	-6157.0	202.5
$Li^+(EC)(DMC)(PC)_2$	-6367.2	188.9

to be the most favourable, followed by $Li^+(EC)(PC)_2(DMC)$ and eventually $Li^+(EC)(PC)(DMC)_2$ cluster. However the free energy changes for the transition paths between these clusters is very small, indicating that all these structures could possibly exist in the bulk phase.

TABLE 3.20: The calculated Gibbs free energies (in kcal/mol) of clusters containing three types of solvents with Li^+ ion

Fragments	G
$Li^+(EC)_2(DMC)(PC)$ + 2 EC + 3 PC + 3 DMC	-18781.2
$Li^+(EC)(DMC)_2(PC)$ + 3 EC + 3 PC + 2 DMC	-18779.2
$Li^+(EC)(DMC)(PC)_2$ + 3 EC + 2 PC + 3 DMC	-18780.3

3.9 Conclusions

Our DFT results have shown that the preferential interaction obtained between Li^+ ion with carbonyl oxygen atom of the all carbonate solvents, which is in agreement with all the previously reported experimental and theoretical studies. The estimated Gibbs free energies of the pure clusters, predicted a tetracoordinated lithium ion with four solvents are arranged in a tetrahedral environment. In the case of EC and DMC clusters, we found that $Li^+(EC)_4$ and $Li^+(DMC)_4$ to be the most stable. However, in the case of pure PC clusters, the energy difference of $Li^+(PC)_3$ and $Li^+(PC)_4$ is very small, indicated that both structure are exists in the bulk solution. Also, we showed that coordination 5 could not be achieved and that a fifth solvent molecule can be arranged only in the outer sphere or second solvation shell. The binding energy results demonstrate that the Li^+- EC and Li^+-PC clusters have the stronger bonds interactions respect to DMC ones. In the case of binary mixtures $Li^+(S_1)_n(S_2)_m$, (S_1, S_2 =EC, PC, DMC, with m+n=4), we have also in this case a conservation of the tetrahedral arrangement around Li^+ ion. The analysis of Gibbs free energy shows:

1. In the case of Li^+- (EC)(PC) clusters, the obtained results revealed that the tetracoordinated $Li^+(EC)_2(PC)_2$ is the most favourable one, followed by $Li^+(EC)(PC)_3$ and eventually $Li^+(EC)_3(PC)$ cluster, although the energy difference of these cluster are very small, therefore these three clusters are exists in the bulk solution. These results also suggested both EC and PC molecules approach the Li^+ ion with equal participation and there is no preferential solvation obtained.

2. In contrast in the case of Li^+- (EC)(DMC) clusters, we have predicted $Li^+(EC)_3(DMC)$ is the most favourable, followed by $Li^+(EC)_2(DMC)_2$ and $Li^+(EC)(DMC)_3$ being the least favourable.

3. Similarly, the same results were obtained for mixed Li^+- (PC)(DMC) clusters, like $Li^+(PC)_3(DMC)$ is the most favourable, followed by $Li^+(PC)_2(DMC)_2$ and $Li^+(PC)(DMC)_3$ is a least one.

4. For all binary mixtures results are coherent with a stronger interaction with PC and EC rather than DMC.

In the case of ternary mixtures $Li^+(EC)_l(DMC)_m(PC)_n$ with l+m+n=4, the cluster $Li^+(EC)_2(DMC)(PC)$ has been predicted to be the most favourable one, and followed by $Li^+(EC)(DMC)(PC)_2$ and eventually $Li^+(EC)(DMC)_2(PC)$ is the least stable among these clusters. The particular free energy changes for the transition paths between these clusters are very small, indicating that all these structures could possibly exist in the bulk phase.

4

Study of Counter Anion PF_6^- Effect on Li^+-EC, -DMC and -PC complexes

In the previous chapter we have discussed the coordination of EC, DMC and PC around Li^+ ion. In this chapter, we discuss about the role of the salt, and in particular the PF_6^- counter anion on the coordination sphere around Li^+. We focused our study on $Li^+(EC)_nPF_6^-$, $Li^+(DMC)_nPF_6^-$ and $Li^+(PC)_nPF_6^-$ clusters. A structural analysis and energetic have been performed and will be presented.

4.1 Optimization of PF_6^- Anion

In this section, we study the optimization of super halogen PF_6^- anion which, for the ground state, exists in octahedral geometry (O_h) . In agreement with previous studies [198–200], the optimized structure with GGA/PBE functional and TZP basis set is octahedral as shown in Figure 4.1. However, several bond lengths for P-F has been reported in the literature [201, 202]. For example, the X-ray crystallographic measurements found the bond distance of P-F is 1.568-1.592 Å in $(CH_3)_4NPF_6$ [201] and it was 1.555-1.556 in $P(C_6H_5)_4PF_6$ crystal [202]. In our structure the optimized bond length for the isolated molecule is 1.652 Å slightly greater than the above mentioned values.

The isolated PF_6^- anion exhibits 15 vibrational modes which can be accounted by the following formula:

$$\Gamma = a_{1g} + e_g + 2t_{1u} + t_{2g} + t_{2u}$$

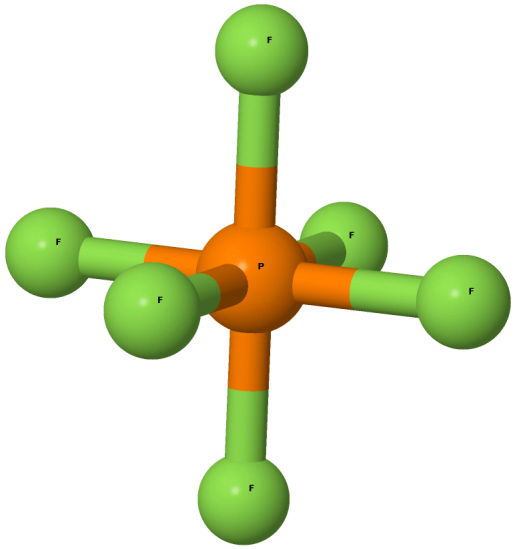

FIGURE 4.1: The isolated optimized geometry of PF_6^- anion

In these modes, $a_{1g}(\nu_1)$, $e_g(\nu_2)$ and $t_{2g}(\nu_5)$ are Raman active and $t_{1u}(\nu_3)$ and $t_{1u}(\nu_4)$ are IR active, but in the case t_{2u} mode is inactive. The experimental vibrational frequencies of PEO-$LiPF_6$ are $\nu_1 = 741$, $\nu_2 = 567$, $\nu_3 = 838$, $\nu_4 = 558$ and $\nu_5 = 470$ cm^{-1}. Our calculated frequencies are relatively underestimating the corresponding frequency values: $\nu_1 = 666.5$, $\nu_2 = 519.2$, $\nu_3 = 801.6$, $\nu_4 = 512.2$ and $\nu_5 = 425.6$ cm^{-1} . The optimized geometry Mulliken charges of P and F are 2.3160 and -0.5527 respectively.

4.2 Possible interactions between Li^+ and PF_6^- anion

For the Li^+ and PF_6^- interaction we foucused on three different approaches giving rise to monodentate interaction between Li^+ and one F atom, bidentate and tridentate. In Figure 4.2, we plotted the translational interaction energies, computed by imposing the symmetry C_{4V}(monodentate), C_{2V}(bidentate) and C_{3V}(tridentate) and freezing the PF_6^- geometry to the isolated one. At this levels we can see, the the tridentate interaction is comparatively more stable than other two configurations. The minimum energy obtained in tridentate complex with a distance of 1.4 Å where three F atoms are interacted by Li^+ ion, followed by the bidentate and eventually a monodentate complex.

4.3 Optimization of $LiPF_6$

In the following we searched for full optimized structures in the 3 symmetries. We obtained structures depicted in Figure 4.3. Nevertheless, just the C_{3V} symmetry configuration is a global minimum, with positive frequencies and lower energy. The C_{2V}

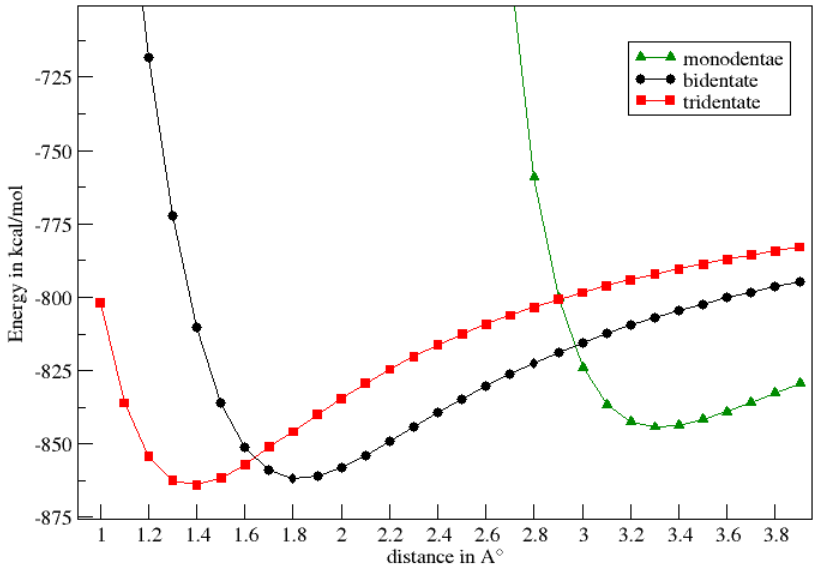

FIGURE 4.2: Calculated translational interaction energies between Li^+ and PF_6^- with respect to distances

(bidentate) symmetry structure has a slightly higher energy than C_{3V} (tridentate) structure, has and one imaginary frequency which indicates a saddle point. We do not achieve the ground state or transition state for the C_{4V} (monodentate) complex, and all calculation ended with at least 2 negative frequencies , and the obtained energetic values were higher respect to the tridentate or bidentate structures. Our results are in agreement with several theoretical studies [200, 203, 204] with different basis sets and functional or with correlated methods. Geometrical parameters for the C_{3V} minima and the C_{2V} transition state are presented Table 4.1. The complex energy has been calculated by optimized energy of $LiPF_6$ and isolated energy of Li^+ ion and PF_6^- at infinite separation. Considering the complex energies, the following order is obtained: tridentate >bidentate. Nevertheless, the difference in energy between such structure is relatively poor and of around 3 kcal/mol.

In this section, we take into account the above three interactions and the optimized structures are shown in Figure 4.3. The 3 interaction structures are having the following point groups: C_{4V}(monodentate), C_{2V}(bidentate) and C_{3V}(tridentate). Among three complexes, C_{3V} symmetry configuration has the global minimum or energetically more stable on the potential energy surface. The C_{4V} (monodentate) complex is a least stable, however it has two imaginary frequencies, indicating not a true minima structure. Moreover, another C_{2V}(bidentate) symmetry structure slightly has a higher energy than C_{3V}(tridentate) structure, though it has one imaginary frequency which indicates a saddle point. The stability of the $LiPF_6$ is found to be in the following order $C_{3V}(tri)$

$>C_{2V}(bi)$ $>C_{4V}(mono)$. Nevertheless, there are lot of studies had been done on the same analysis for these structures with various basis sets and electron correlation functions [200, 203, 204] results affect the energy values of the system, not affect the order of stability. Our optimized structural parameters are presented in Table 4.1. The complex energy has been calculated by optimized energy of $LiPF_6$ and isolated energy of Li^+ ion and PF_6^- at infinite separation. Considering the complex energies, the following order is obtained: tridentate >bidentate >monodentate. The energies of bidentate and tridentate geometries are relatively close, but in the case of monodentate the energy difference significantly larger than other two complexes which is around 15 kcal/mol. This relative energies are also suggested that the strong interaction is obtained in C_{3V} structure.

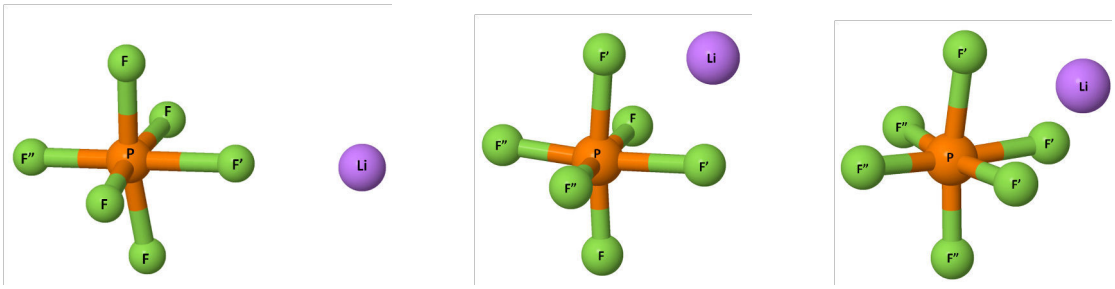

(a) C_{4V}(monodentate) (b) C_{2V}(bidentate) (c) C_{3V}(tridentate)

FIGURE 4.3: Three different optimized (interaction) structures of $LiPF_6$ complexes

As seen from the Figure 4.3, PF_6^- anion is highly distorted from its original octahedral geometry in most stable tridentate structure. The resulting bond length for Li-P is 2.432 Å in C_{3V} geometry which is slightly lower than C_{2V} geometry because of the strong interaction between Li^+ ion with F atom. This strong interaction makes Li-F'(closest to the Li^+ ion) bond length increases from bidentate to tridentate but P-F' bond decreases from 1.765 Å to 1.723 Å However, the bond length of P-F"(farthest F atom) slightly decrease. The charge transfer might be involved for this contraction which accounted from the Mulliken charge analysis. For example, the Mulliken charge of Li^+ in C_{3V} and C_{2V} are 0.815 and 0.806, respectively. The corresponding charges of closest F' atoms are -0.552 and -0.566, and the difference between Li and F atoms in C_{3V} (0.263) and C_{2V} (0.240). The Mulliken values also revealed that C_{3V} structure comparatively has strong interaction than other two structures.

4.4 Effect of PF_6^- anion in $Li^+(EC)_{1-3}$ Complexes

In this section, we discuss the effect of counter anion PF_6^- on the solvation structure of Li^+-EC clusters. Some structural parameters are collected in Table 4.2. In presence of the counter ion PF_6^- we have studied all structure from coordination 1 around Li^+ up to 4. The optimized geometries are shown in Figure 4.4 and the Li^+-EC complexes are

TABLE 4.1: Energies and Structural parameters and Charges of lipf complexes with C_{4V}, C_{2V} and C_{3V} geometries

Parameters	C_{2V} (bidentate)	C_{3V} (tridentate)
Complex Energy (kcal/mol)	-135.28	-138.11
Distances(Å)		
Li-P	2.650	2.432
Li-F'	1.775	1.881
P-F'	1.765	1.723
P-F	1.622	
P-F"	1.600	1.598
Angles in degree		
Li^+-F'-P	96.9	84.8
F'-P-F"	173.6	172.3
F-P-F	171.6	172.2
Charges(e)		
Li^+	0.806	0.815
P	2.220	2.226
F'	-0.566	-0.552
F	-0.483	
F"	-0.464	-0.461
Dipole moment/D	7.48	6.41

F' and F" are closest and farthest to Li^+

totally perturbed by the PF_6^- anion. The presence of the salt PF_6^-, breaks the linearity in the Li^+-O=C interaction angle giving an angle of 117.7° for the $Li^+(EC)PF_6^-$ system. From the Figure 4.4(a), we can see that the entire geometry of $Li^+(EC)PF_6^-$ has V shape which might result from an interaction of EC ring with the PF_6^- anion and the resulting angle between O -Li^+- P is around 125°. This interaction is mostly due to the fluorides Hydrogens bonds with the methyl groups of EC (with an average distance of 2.6 Å).

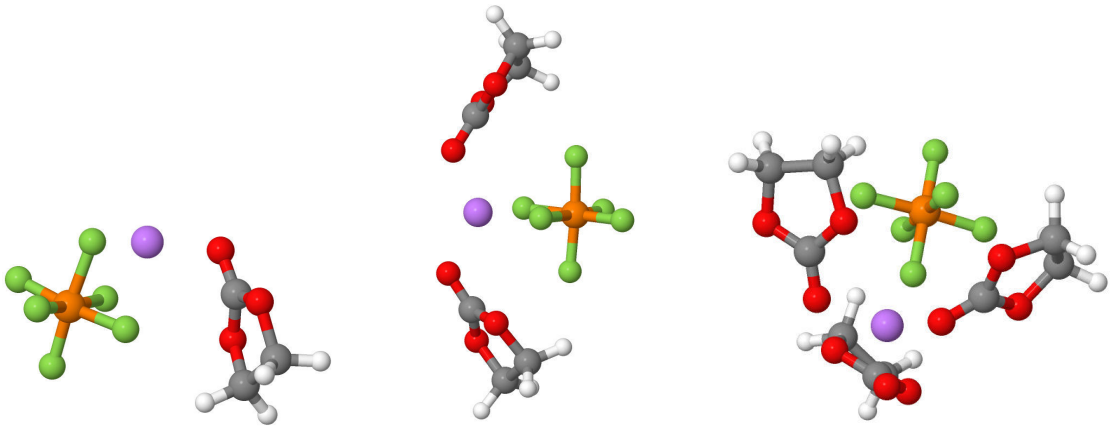

(a) $Li^+(EC)PF_6^-$ (b) $Li^+(EC)_2PF_6^-$ (c) $Li^+(EC)_3PF_6^-$

FIGURE 4.4: Optimized solvation structures of $Li^+(EC)_{1-3}PF_6^-$ complexes

From the Table 4.2, the distance between Li^+-O(=C) is 1.877 Å which is higher than pure or without PF_6^- anion (1.733 Å). Because, the strong interaction is obtained with Li^+ and carbonyl oxygen in Li^+(EC) cluster. However, the interaction is weaker after the coordination with strong negative PF_6^- anion. The C=O bond length is 1.224 Å which is lower as compared to Li^+(EC) (1.235 Å), this is due to the weaker interaction with Li^+ ion. The π character of C=O bond is not much affected in $Li^+(EC)PF_6^-$ cluster. The $LiPF_6$ have been interacted through bidentate way and the corresponding bond length is almost the same as isolated bidentate cluster (from Table 4.1). The P-F bond length also exhibits the same trend as $LiPF_6$ bidentate complex. While addition of EC molecule, the interaction is getting weaker therefore the $Li^+-O(=C)$ bond length become increases. For instance, the bond lengths of $Li^+(EC)_2PF_6^-$ and $Li^+(EC)_3PF_6^-$ are 1.916 Å and 1.953/1.966 Å, respectively.

As we have already seen in $Li^+(EC)_2$ complex in previous chapter where the Li^+ ion shares two EC molecule with an angle of 177.1°. But in the case of $Li^+(EC)_2PF_6^-$ complex, the Li^+ ion interact both EC molecule O=C groups and F atoms from PF_6^- and forms a trigonal linkage from Li^+ ion. However, the entire cluster geometry seems to be like boat shape configuration. This particular configuration could be formed from the strong interaction of hydrogen bonds as well as the positive character of EC ring which attract by F atoms. The strong hydrogen bond interaction obtained with EC molecule hydrogens and F atoms with the distance of around 2.5 Å. The corresponding angle between (C=)O- Li^+-O(=C) is 131.7 ° and Li^+-O=C angle is 120.6°. The angle of F-P-F also relaxed to 175.7°. The bidentate linkage have been obtained for $LiPF_6$ in $Li^+(EC)_2PF_6^-$. The $Li^+(EC)_3PF_6^-$ complex exhibits tetrahedral shape around Li^+ ion and all 3 EC molecules are arranged around the PF_6^- anion. The entire geometry coordination is almost similar to what we found in the first two complexes. Here, the 3 EC molecules hydrogens are interacted with F atoms in order to make the strong hydrogen bonds with a distances of 2.46 Å. The $LiPF_6$ interaction is also differ from other clusters and it deviates from bidentate interaction and forms an angle around 151.5° for Li^+-F'-P. The dipole moment decreases in complexes from $Li^+(EC)PF_6^-$ to $Li^+(EC)_3PF_6^-$.

In presence of PF_6^-, the Li^+-O(=C) bond distance is longer(1.877 Å) respect to the Li^+(EC) one (1.733 Å). Infact, in presence of the negative ion PF_6^- the stronger interaction is the Li^+/ PF_6^- one and the positive charge on Li^+ is lowered from such ionic interaction so that the interaction with EC dipole is lowered too. For such a reason The C=O bond length is less affected by the EC/ Li^+ interaction and the distance is 1.224 Å (which is 1.235 Å for Li^+(EC)) The $LiPF_6$ have been interacted through bidentate way and the corresponding bond length is almost the same as isolated bidentate cluster (from Table 4.1. The P-F bond length also exhibits the same trend as $LiPF_6$ bidentate complex. While addition of EC molecule, the interaction is getting weaker therefore the Li^+-O(=C) bond length become increases. For instance, the bond lengths

TABLE 4.2: Selected structural parameters of $Li^+(EC)_{1-3}$ with PF_6^- geometries (bond lengths in angstrom, bond and dihedral angles in degree)

Atoms	$Li^+(EC)PF_6^-$	$Li^+(EC)_2PF_6^-$	$Li^+(EC)_3PF_6^-$
Bonds			
Li^+-O(=C)	1.877	1.919	1.953/1.966
O=C	1.224	1.220	1.218
C-O	1.345	1.349	1.352
Li-P	2.680	2.822	3.576
Li-F'	1.855	1.950	1.985
P-F'	1.725	1.699	1.704
P-F"	1.605	1.613	1.622
Angles			
Li^+-O=C	117.7	120.6	121.2/122.6/117.0
F-P-F	174.3	175.7	179.4/177.1/176.9
Dihedral			
O-C(=O)-O	179.4	179.0	178.8
O-C-C-O	21.8	20.6	17.7
DPM/D	8.47	2.15	1.10

DPM = Dipole moment

of $Li^+(EC)_2PF_6^-$ and $Li^+(PC)_3PF_6^-$ are 1.916 Å and 1.953/1.966 Å respectively.

As we have already seen in $Li^+(EC)_2$ complex in previous chapter where theLi^+ ion shares two EC molecule with an angle of 177.1°. But in the case of $Li^+(EC)_2PF_6^-$ complex, the Li^+ ion interact , because of the interaction between methyls groups of EC and Fluorides atoms on PF_6^- the whole configuration seems to be like boat shape configuration. The strong hydrogen bond interaction obtained with EC molecule hydrogens and F atoms with the distance of around 2.5 Å. The corresponding angle between (C=)O-Li^+-O(=C) is 131.7° and Li^+-O=C angle is 120.6°. The angle of F-P-F also relaxed to 175.7°. The bidentate linkage have been obtained for $LiPF_6$ in $Li^+(EC)_2PF_6^-$. The $Li^+(EC)_3PF_6^-$ complex exhibits tetrahedral shape around Li^+ ion and all three EC molecules are arranged around the PF_6^- anion. The entire geometry coordination is almost similar to what we found in the first two complexes. Here, the three EC molecules hydrogens are interacted with F atoms in order to make the strong hydrogen bonds with a distance of 2.46 Å. The $LiPF_6$ interaction is also differ from other clusters and deviates from bidentate interaction and forms an angle around 151.5° for Li^+-F'-P. The dipole moment decreases in complexes from $Li^+(EC)PF_6^-$ to $Li^+(EC)_3PF_6^-$.

We also study the vibrational frequencies and Mulliken charges of $Li^+(EC)_{1\text{-}3}PF_6^-$ clusters and the values are collected in Table 4.3. Despite the structural changes of EC, the stretching frequency of C=O bond is also affected in the presence of PF_6^- anion. The C=O stretching frequency increases from $Li^+(EC)PF_6^-$ to $Li^+(EC)_3PF_6^-$, thus showing the lower interaction with the Li^+ charge by increasing the coordination number. Instead, we could expect C=O stretching frequency is higher in $Li^+(EC)PF_6^-$ as compared to pure $Li^+(EC)$ cluster, due to the weaker interaction in $Li^+(EC)PF_6^-$ retains the π

character of C=O bond, eventually has a higher frequency. Nevertheless, in the case of Li^+(EC) cluster, the C=O stretching frequency obtained around $1733cm^{-1}$ but it is $1750cm^{-1}$ in $Li^+(EC)PF_6^-$ cluster. This particular interaction is getting weaker upon addition of EC molecule results the C=O frequency increases. The reverse result is obtained for C-O asymmetric stretching which decreases in the presence of PF_6^- anion and substantially increases on going to higher EC content.

The analysis of Mulliken charges explains the charge distribution on the clusters and values are presented in Table 4.3. As seen from the Table, the positive charge on Li^+ increases with increasing EC molecules from 1 to 3. Initially, the Li^+ ion has +1 e and which is to be 0.766 e in $Li^+(EC)PF_6^-$ complex which is smaller than corresponding Li^+(EC) complex. The declining of charge on Li^+ is due to the charge transfer from F atoms. If we see the charges of closest F atoms in $Li^+(EC)PF_6^-$ complex, the values are -0.591 and -0.594 e, in which the charges exhibit bidentate $LiPF_6$ and the rest of the F atoms are nearly -0.501 e. The corresponding P charge is 2.404 e which is slightly higher than isolated value (2.3160 e) and which might arise due to the weakening of bond between F-P. This is also confirms the F atoms are involved in the charge transfer process preferably towards Li^+ ion. Although, the coordination of PF_6^- also affect the charges on EC molecule and negative charge on carbonyl oxygen is considerably higher than Li^+(EC) cluster. The positive charge on carbonyl carbon increases in the presence of counter anion. From the Table, the positive charge on Li^+ ion decreases from 1 EC to 3 EC containing clusters and increase the charge on P atom.

TABLE 4.3: Vibrational modes (in cm^{-1}) and Mulliken charges of $Li^+(EC)_{1-3}PF_6^-$ geometries

Atoms	$Li^+(EC)PF_6^-$	$Li^+(EC)_2PF_6^-$	$Li^+(EC)_3PF_6^-$
Modes			
O=C	1750	1774	1788
C-O	1163	1154	1145
Charges			
Li^+	0.766	0.722	0.680
P	2.404	2.443	2.497
O(=C)	-0.619	-0.609	-0.600
C(=O)	0.984	0.982	0.986

4.5 Effect of PF_6^- anion in $Li^+(DMC)_{1-3}$ Complexes

In this section, we will see the results of solvation structures of $Li^+(DMC)_{1\text{-}3}$ with counter PF_6^- anion and structural parameters are collected in Table 4.4. The corresponding optimized structures are shown in Figure 4.5. The $Li^+(DMC)PF_6^-$ cluster also perturbed due to the high negative charge of anion. Also in this case, the bond length of Li^+-O(=C) increases in the presence of PF_6^- anion, because of the lowering of the positive charge on Li^+, due to the stronger ionic interaction with the counterion.

The lower Li^+-O(=C) interaction makes the C=O bond distances shorter respect to the corresponding clusters without PF_6^-. For instance the C=O bond length is 1.212 Å for the isolated DMC, and goes to 1.235 in $Li^+(DMC)PF_6^-$ cluster and 1.252 in $Li^+(DMC)$. The same trend is observed in the higther coordinations. In the case of $Li^+(DMC)PF_6^-$ cluster, the Li^+- PF_6^- interaction have been arranged in a tridentate linkage and the corresponding bond length of Li-P is found to be 2.505 Å and the bond angle of F-P-F is of about 173.5°. We found a linear coordination in $Li^+(DMC)$ cluster, but in the case of $Li^+(DMC)PF_6^-$ cluster the resulting angle of Li^+-O=C is 147.7°. The bidentate linkage has been obtained in both $Li^+(DMC)_2PF_6^-$ and $Li^+(DMC)_3PF_6^-$ complexes and bond lengths are closely consistent with original bidentate value (2.650 Å) Hydrogen bonds also exist in these complexes between fluorides and methyls groups of DMC with average distance around 2.70 Å and they clearly influence the arrangement of the entire geometry. The $Li^+(DMC)_2PF_6^-$ and $Li^+(DMC)_3PF_6^-$ clusters exhibit almost trigonal and tetrahedral coordination with Li^+ ion and all complexes are having almost same dipole moment.

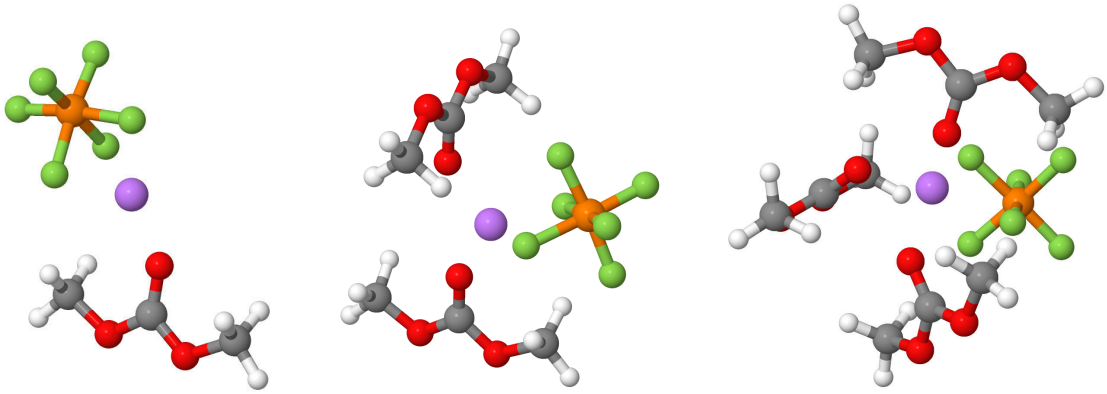

(a) $Li^+(DMC)PF_6^-$ (b) $Li^+(DMC)_2PF_6^-$ (c) $Li^+(DMC)_3PF_6^-$

FIGURE 4.5: Optimized solvation structures of $Li^+(DMC)_{1-3}PF_6^-$ complexes

We have also investigated vibrational modes and Mulliken charges of $Li^+(DMC)_{1\text{-}3}PF_6^-$ clusters and the values are collected in Table 4.5. The C=O stretching frequency has increased upon coordination of PF_6^- anion to $Li^+(DMC)$ which comes from the weaker interaction of Li^+ with O=C from DMC molecules. The π bond of C=O is remain almost unchanged in $Li^+(DMC)PF_6^-$, thus increasing the stretching frequency and the corresponding C=O bond has a shorter distance than in $Li^+(DMC)$. While the extra addition of DMC molecules the C=O frequency substantially increases and interaction between Li^+ and DMC molecules are getting lower is the reason for this change. However, the C-O asymmetric stretching frequency decreases in $Li^+(DMC)PF_6^-$ as compared to $Li^+(DMC)$ cluster and the same trend have also been observed at increasing DMC molecules.

As we have seen from the Table 4.5, the positive charge of Li^+ ion (+1 e) has dropped into 0.767 e in $Li^+(DMC)PF_6^-$ and obvious that the $Li^+(DMC)$ has a higher positive

TABLE 4.4: Structural parameters of $Li^+(DMC)_{1-3}$ with PF_6^- geometries (bond lengths in angstrom, bond and dihedral angles in degree)

Atoms	$Li^+(DMC)PF_6^-$	$Li^+(DMC)_2PF_6^-$	$Li^+(DMC)_3PF_6^-$
Bonds			
Li^+-O(=C)	1.861	1.900	1.970/2.065
O=C	1.235	1.231	1.229
C-O	1.331	1.341	1.339
Li-P	2.505	2.790	2.921
Li-F'	1.966	1.920	2.209/2.870
P-F'	1.725	1.718	1.687/1.987
P-F"	1.603	1.610	1.617
Angles			
Li^+-O=C	147.7	138.9	143.8/139.9/136.7
F-P-F	173.5	175.0	175.9
Dihedral			
O-C(=O)-O	179.9	178.1	178.3/179.1
DPM/D	9.05	8.75	9.07

DPM = Dipole moment

charge about 0.799 e . These results revealed that the substantial charge transfer obtained from the counter PF_6^- anion to Li^+ ion. However, this charge transfers also impact on the positive charge of P atom which means the P atom attributes higher positive charge than optimized $LiPF_6$ cluster. On the other hand, the weaker interaction of Li^+ with DMC molecules results the O in O=C groups possesses higher negative charge than Li^+(DMC) cluster. We have also received the same results in C(=O) atom. Nevertheless, we could expect unequal charges are obtained in $Li^+(DMC)_2PF_6^-$ and $Li^+(DMC)_3PF_6^-$ clusters, in which the DMC molecules has been arranged in a different orientation to Li^+ ion. Being the close arrangement of DMC molecules in both $Li^+(DMC)_2PF_6^-$ and $Li^+(DMC)_3PF_6^-$ clusters, where DMC molecules forms a strong hydrogen bonds with F atoms results the charge on P atom increases. The positive charge on Li^+ decreases upon addition of more DMC molecules.

TABLE 4.5: Vibrational modes (in cm^{-1} and Mulliken charges of $Li^+(DMC)_{1-3}PF_6^-$ geometries

Atoms	$Li^+(DMC)PF_6^-$	$Li^+(DMC)_2PF_6^-$	$Li^+(DMC)_3PF_6^-$
Modes			
O=C	1692	1708	1717
C-O	1309	1299	1290
Charges			
Li^+	0.767	0.754	0.721
P	2.398	2.436	2.4731
O(=C)	-0.638	-0.622/-0.653	-0.621/-0.633/-0.642
C(=O)	0.971	0.954/1.002	0.961/0.973/0.990

4.6 Effect of PF_6^- anion in $Li^+(PC)_{1-3}$ Complexes

In this section, we discuss about the results of $Li^+(PC)_{1\text{-}3}PF_6^-$ clusters and some structural parameters are presented in Table 4.6 and the corresponding optimized geometries are shown in Figure 4.6. Similar to the $Li^+(EC)_{1\text{-}3}PF_6^-$ clusters, the PC containing clusters also exhibit the same geometry structures. The Li^+-PC- PF_6^- clusters are also perturbed by the presence of the counterions. The typical distance of Li^+-O(=C) is 1.876 Å which is relatively higher than without PF_6^- anion. Moreover, the bond angle of Li^+-O=C is 117.3° in $Li^+(PC)PF_6^-$ which is more stretched than $Li^+(PC)$ (173.8°). We can clearly see from the Figure 4.6(a), the deviated bidentate linkage has been observed for $LiPF_6$ structure and the corresponding distance is about 2.680 Å for Li-P. Upon addition of a second PC, the distance of Li^+-O(=C) increases and C=O bond length decreases and the angle of Li+-O=C is become 121.1° in $Li^+(PC)_2PF_6^-$. For this structure, the $LiPF_6$ also forms a bidentate linkage with a distance of 2.832 Å. On the other hand, the usual hydrogen bonds has also obtained between Fluorine atoms with alkyl hydrogen of PC with a relative distance of 2.604 Å The dipole moment is dramatically decreased to 1.33 D in $Li^+(PC)_2PF_6^-$ from 9.08 D in $Li^+(PC)PF_6^-$. In the case of $Li^+(PC)_3PF_6^-$ complex, the Li^+-O(=C) distance eventually increases and although three sort of distance obtained in the range between 1.937 to 1.957 Å. The Li^+- PF_6^- interaction formed through monodentate linkage shows a distance of 3.694 Å. The corresponding Li-F' (by F we indicate the closest F to Li) distance also increases as expected. The dipole moment is slightly increases in $Li^+(PC)_3PF_6^-$ cluster.

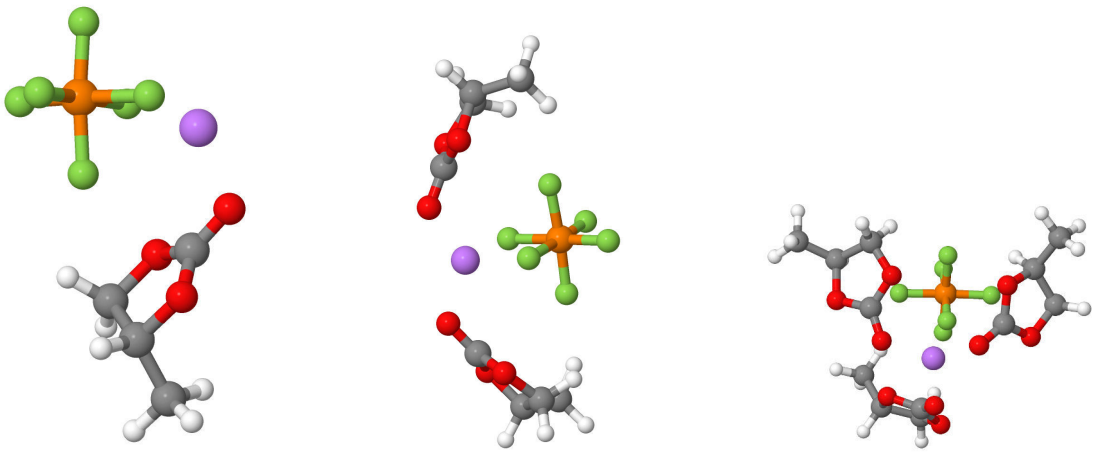

(a) $Li^+(PC)PF_6^-$ (b) $Li^+(PC)_2PF_6^-$ (c) $Li^+(PC)_3PF_6^-$

FIGURE 4.6: Optimized solvation structures of $Li^+(PC)_{1-3}PF_6^-$ complexes

We have also analysed vibrational modes and Mulliken charge changes on $Li^+(PC)_{1\text{-}3}PF_6^-$ and the results are presented in Table 4.7. The obtained results shows, as for previous structure with EC and DMC that the addition of PF_6^- anion to $Li^+(PC)$ cluster results to an increase of the stretching frequency of C=O. Also, the C-O frequency is affected

TABLE 4.6: Structural parameters of $Li^+(PC)_{1-3}$ with PF_6^- geometries (bond lengths in angstrom, bond and dihedral angles in degree)

Atoms	$Li^+(PC)PF_6^-$	$Li^+(PC)_2PF_6^-$	$Li^+(PC)_3PF_6^-$
Bonds			
Li^+-O(=C)	1.876	1.927	1.937/1.947/1.957
O=C	1.226	1.221	1.220
Li-P	2.680	2.832	3.694
Li-F'	1.857	1.956	2.034
P-F'	1.725	1.697	1.698
P-F"	1.608	1.614	1.622
Angles			
Li^+-O=C	117.3	121.1	124.2/121.0/118.4
F-P-F	174.3	176.1	177.2/179.5
Dihedral			
O-C(=O)-O	179.4	179.0	179.2
DPM/D	9.08	1.33	2.47

DPM = Dipole moment

by the presence of PF_6^- and decreases about $23cm^{-1}$ respect to the $Li^+(PC)$ value. The same trend is observed by adding a second or third PC.

It is quite obvious that the Mulliken charge also affected by the strong Li^+/ PF_6^- interaction. The overall positive charge on Li^+ decrease, respect to corresponding complexes without PF_6^-, and naturally it decrease also by increasing the number of PC.

TABLE 4.7: Vibrational modes (in cm^{-1} and Mulliken charges of $Li^+(PC)_{1-3}PF_6^-$ geometries

Atoms	$Li^+(PC)PF_6^-$	$Li^+(PC)_2PF_6^-$	$Li^+(PC)_3PF_6^-$
Modes			
O=C	1743	1767	1783
C-O	1381	1379	1343
Charges			
Li^+	0.764	0.722	0.688
P	2.405	2.491	2.543
O(=C)	-0.626	-0.615	-0.599/-0.607/-0.615
C(=O)	0.987	0.976	0.977/0.983/974

4.7 Stability of Clusters with anions

In order to provide the stability of clusters formation we analyse the thermodynamic parameters such as enthalpy, entropy and Gibbs free energy values which are shown in Table 4.8. From the Table values, we can clearly seen that for all complexes, with EC, PC or DMC the G values decreases by adding the solvents to the coordination sphere; Nevertheless the addition of a third EC, PC or DMC increase the G value. This means that in presence of PF_6^- linked to Li^+, the maximum coordination number of solvents

TABLE 4.8: Thermodyanmics parameters such as Enthalpy(H in kcal/mol), Entropy(S in cal/mol-K) and Gibbs free energy values (G in kcal/mol) of $Li^+(S)_{1-3}$ (S = Ec, DMC, PC) complexes with PF_6^- anion

Clusters	H	S	G
$LiPF_6$ + 3 EC	-4962.4	302.7	-5052.6
$Li^+(EC)PF_6^-$ + 2 EC	-4983.1	264.7	-5062.0
$Li^+(EC)_2PF_6^-$ + 1 EC	-4998.7	228.9	-5067.0
$Li^+(EC)_3PF_6^-$	-5006.4	193.8	-5064.2
$LiPF_6$ + 3 DMC	-5445.0	331.6	-5543.9
$Li^+(DMC)PF_6^-$ + 2 DMC	-5467.9	287.2	-5553.6
$Li^+(DMC)_2PF_6^-$ + 1 DMC	-5480.1	257.4	-5556.8
$Li^+(DMC)_3PF_6^-$	-5485.2	214.3	-5549.1
$LiPF_6$ + 3 PC	-6062.7	323.0	-6159.0
$Li^+(PC)PF_6^-$ + 2 PC	-6083.5	285.3	-6168.5
$Li^+(PC)_2PF_6^-$ + 1 PC	-6100.3	247.5	-6174.1
$Li^+(PC)_3PF_6^-$	-6108.3	200.7	-6168.1

groups in two, and the addition of a third one gets positive ΔG values for the reaction. Comparing the Thermodynamic values to the ones obtained in absence of PF_6^- we can conclude that :

1. in absence of salt counterions, we could achieve a coordination of four solvent molecules(either EC, PC and DMC) around Li^+.
2. the presence of PF_6^- in the coordination sphere has a strong impact on the effective charge on Li^+, and the maximum coordination number of carbonyls solvent is lowered to 2.

Also, in all complexes the enthalpy values are shown that the formation of larger number solvents containing clusters are more favourable, although the entropic term make the difference in these cases.

It is also interesting to analyse the energy for the following reactions in the Table 4.9 :

TABLE 4.9: Computed ΔG reaction values (kcal/mol) for the substitution of PF_6^- anion by one solvent molecule to the most stable $Li^+(S)_2PF_6^-$ (S=EC, DMC and PC)

Reactions	ΔG(kcal/mol)		
	S = EC	S = DMC	S = PC
$Li^+(S)_2PF_6^- + S \longrightarrow Li^+(S)_3 + PF_6^-$	54.5	78.2	61.2

The above reactions are used to explain the solvent ability to replace the PF_6^- anion in the solvation sphere. The positive ΔG free energy values (in Table 4.9) are demonstrated that the PF_6^- anion is strongly bound in the first solvation shell, it cannot be replaced by the another solvent molecule. The Li^+ ion prefers the interaction with salt anion

and to stay with lower coordination structure. Therefore, it should be stressed that in experimental LIBs devises the concentration of the salt in the electrolytes is around 1M, so that the concentration of the carbonates electrolytes are in strong predominance in solution. For that reason, both structures without PF_6^- (coordination number 4) and with PF_6^- (coordination number 2) are exists in the solution, and structure without salts represent the majority of the coordination of Li^+.

4.8 Conclusions

From the general point of view, our DFT results have predicted that the isolated PF_6^- anion has a perfect octahedral geometry, and we also studied the possible interactions with Li^+ ion. The Li^+ and PF_6^- ions forms three different interactions such as monodentate (C_{4V}), bidentate(C_{2V}) and tridentate (C_{3V}). The results revealed that the strong interaction (most stable) obtained in tridentate form, in which three fluorine atoms were coordinated to the Li^+ ion and the local structure also confirmed by frequency analysis. These results were in good agreement with previous theoretical works.

We have investigated the pure solvent clusters $Li^+(S)_{1\text{-}3}$ (S = EC, DMC and PC) in gas phase with PF_6^- anion, and the results suggested that the pure solvent clusters were totally perturbed in the presence of PF_6^- anion. In all the cases, the Li^+- Oc (carbonyl oxygen) distance increases due to the strong negative charge of PF_6^- anion, and the alkyl hydrogens from solvents forms hydrogen bonds with PF_6^- anion.

For all structures, in presence of PF_6^- in the coordination sphere the most favourable structure is $Li^+(S)_2PF_6^-$. The addition of a third S molecules is unfavourable (With positive ΔG vaules for the addition reaction). For all structures, in presence of PF_6^- in the coordination sphere the most favourable structure is $Li^+(S)_2PF_6^-$. The substitution of PF_6^- anion by a solvent molecule to form a coordination number three ($Li^+(S)_3$) is unfavourable (With positive ΔG values). The results suggested that Li^+ ion prefers the counter anion in the presence of salt and form a lower coordination. However, both structures without PF_6^- (coordination number 4) and with PF_6^- (coordination number 2) are exists in the solution.

5

Coupling DFT and MD

The aim of this chapter is to study the local solvation structure of Li^+ ion with carbonate solvents (EC, DMC and PC) at infinite dilution. We have discussed about the effective force fields that we used for this study. In the following, we have included the entire paper that we submitted to the journal.

5.1 What we need MD for?

Density functional theory (DFT) method is a good choice for the study of structural and electronic properties in chemistry as well as in physics. DFT is able to solve models with a system has relatively small size (for example below 60 to 70 atoms). The degree of accuracy also be achieved in small systems. In order to study system which contains hundreds or thousands of atoms, the DFT will not make it. Moreover, it mainly concerns on the isolated molecules, therefore, there is a possibility of finite size problems. Also, if we want to study the interaction between other molecules or atoms the DFT methods fail in this cases. Therefore, instead of solving Schrödinger equation to obtain the energy, the classical expression or force fields are used to account all intermolecular interactions. The interaction is treated in an atomic level which called as Molecular Dynamics(MD) simulation method. This MD take into account all intermolecular interaction even in large systems and also used to study the tedious system which can not be accessible experimentally. The MD result can give a detailed idea for structural properties, transport properties, and diffusion coefficients, etc.

The previous DFT chapter, the energetic results have shown that the preference of Li^+ to bind with the highly polar PC and EC molecules. Nevertheless, from an entropic point of view the addition of DMC molecules contributes to the decrease of the free energy of the clusters. In the investigated finite size clusters the energetic contribution seems to be the most important one. However, the small free energy differences observed for the transition paths leading from one cluster to the other indicate that the formation

of these clusters should be investigated at more extended length scales, in order to have a more realistic description of the effects taking place in the bulk liquid phase. This was the most important motivation to combine DFT calculations of isolated clusters with classical MD simulations at more extended length scales, in order to have a clearer picture about the solvation of Li^+ in pure and mixed organic carbonate-based solvents. We have discussed the MD results in the following sections.

5.2 Molecular Dynamics Simulation

In this section, we discuss about the simulation methods and systems that are used for this study. We have investigated the solvation structure of Li^+ ion at infinite dilution in EC, DMC and PC solvents by using classical molecular dynamics simulations. We have focused on the following systems that are formed by pure EC, DMC and PC with Li^+ ion and binary mixture EC:DMC in the 1:1 ratio and ternary mixture EC:DMC:PC with a molar ratio of 1:1:3, respectively.

In order to consider the dilute solution of Li^+ ion, the typical simulation box contains one Li^+ ion with 214 solvent molecules in the case of pure solvents and ternary mixtures, whereas in the case of binary mixture the one Li^+ ion is fixed with 213 solvent molecules. We have performed several trial runs in order to be sure for enough molecules to describe the solvation structure and also to avoid the possible finite size effects. The initial configurations of all simulated systems are prepared by using the Packmol software[205].

The equations of motion were integrated using a leapfrog-type Verlet algorithm with an integration time step of 1 fs[183]. The temperature has been fixed to 303.15 K and the pressure to 1 atm by coupling the systems to a Nose-Hoover thermostat and barostat with relaxation times of 0.2 and 0.5 ps, respectively[101, 206]. The rigid body equations of motion for EC and PC molecules were expressed in the quaternion formalism[183]. A cut-off radius of 9.0 Å has been applied for all Lennard-Jones interactions and long-range corrections have also been taken into account. To account for the long-range electrostatic interactions the standard Ewald summation technique has been used[183]. The simulation runs were performed using the DL_POLY simulation code [207]. The systems were equilibrated for 25 ns and a subsequent run of 15 ns was performed in each case, in order to calculate equilibrium properties

5.2.1 Effective Force Fields for EC, PC and DMC

The accurate force field can give the detailed interactions of intermolecular interactions between atoms. The intermolecular potential consists of short-range van der Waals interactions and long-range electrostatic interactions. The van der Waals interaction is called Lennard-Jones(LJ) potential which takes into account the interaction between two

non-bonding molecules or atoms with respect to the distance of separation. LJ equation consists of repulsive and attractive terms. And, the long-range electrostatic interaction or coulombic term also play a significant role in force fields. The intermolecular interaction energy are represented as follows:

$$E_{inter} = \sum_{i>j} \left\{ 4\varepsilon_{ij} \left[\left(\frac{\sigma_{ij}}{r_{ij}} \right)^{12} - \left(\frac{\sigma_{ij}}{r_{ij}} \right)^{6} \right] + \frac{q_i q_j}{4\pi\varepsilon_0 r_{ij}} \right\} \tag{5.1}$$

Where σ_{ij} is the distance at which the intermolecular particles at zero or equlibrium distance, and ε_{ij} is the depth of the potential well or strength of the interaction, i and j indicates the molecule1 and molecule2 respectively. r_{ij} is the distance between i^{th} and j^{th} atom. The coulombic term consists of q_i and q_j partial charges of atoms i and j respectively, ε_0 is vacuum permittivity. The geometric combining rule are used for σ_{ij} and ε_{ij} such that $\sigma_{ij} = (\sigma_{ii}\sigma_{jj})^{1/2}$ and $\varepsilon_{ij} = (\varepsilon_{ii}\varepsilon_{jj})^{1/2}$.

We have considered the previously reported force fields[69, 87] for our simulated systems and the corresponding parameters are collected in Table 5.1. The EC and PC solvent molecules were kept rigid during the simulation. In the case of DMC molecule, we consider as a flexible molecule due to existence of different conformers in the gas and liquid phase and intramolecular force filed has also been employed. Throughout this chapter, the EC, DMC and PC molecules are defined in the following: Oc for the carbonyl oxygen, O for the ether oxygen, Cc for carbonyl carbon, and C and H for the carbon and hydrogen of CH group respectively.

TABLE 5.1: Lennard-Jones parameters and Partial charges for the EC, DMC, PC and Li^+ molecules

Molecule	interaction center	σ(Å)	ε(kcal mol^{-1})	q/e
EC	Oc	2.96	0.210	-0.6452
	Cc	3.75	0.105	1.0996
	O	3.00	0.170	-0.4684
	C	3.50	0.066	0.0330
	H	2.50	0.030	0.1041
PC	Oc	2.96	0.210	-0.6378
	Cc	3.75	0.105	1.0489
	$O(CH_2)$	3.00	0.170	-0.4509
	O(CH)	3.00	0.170	-0.4120
	$C(H_2)$	3.50	0.066	-0.0040
	C(H)	3.50	0.066	0.0832
	$C(H_3)$	3.50	0.066	-0.3264
	H	2.50	0.030	0.1165
DMC	Oc	2.96	0.210	-0.6774
	Cc	3.75	0.105	1.0864
	O	3.00	0.170	-0.4478
	C	3.50	0.170	-0.4478
	H	2.50	0.030	0.1331
Li^+		1.46	0.191	1.0000

In the following page, we have attached the paper that we submitted to the journal and the paper contains both DFT and MD results.

5.3 The Published Version of Our Paper in The Journal of Physical Chemistry C

THE JOURNAL OF PHYSICAL CHEMISTRY C
Article
pubs.acs.org/JPCC

Li^+ Solvation in Pure, Binary, and Ternary Mixtures of Organic Carbonate Electrolytes

Ioannis Skarmoutsos,*[,†,‡,§] Veerapandian Ponnuchamy,[†,‡,§,∥,⊥] Valentina Vetere,[∥,⊥] and Stefano Mossa*[,†,‡,§]

[†]Université Grenoble Alpes, INAC-SPRAM, F-38000 Grenoble, France
[‡]CNRS, INAC-SPRAM, F-38000 Grenoble, France
[§]CEA, INAC-SPRAM, F-3800 Grenoble, France
[∥]Université Grenoble Alpes, LITEN-DEHT, F-38000 Grenoble, France
[⊥]CEA, LITEN-DEHT, F-38000 Grenoble, France

Supporting Information

ABSTRACT: Classical molecular dynamics (MD) simulations and quantum chemical density functional theory (DFT) calculations have been employed in the present study to investigate the solvation of lithium cations in pure organic carbonate solvents (ethylene carbonate (EC), propylene carbonate (PC), and dimethyl carbonate (DMC)) and their binary (EC−DMC, 1:1 molar composition) and ternary (EC-DMC-PC, 1:1:3 molar composition) mixtures. The results obtained by both methods indicate that the formation of complexes with four solvent molecules around Li^+, exhibiting a strong local tetrahedral order, is the most favorable. However, the molecular dynamics simulations have revealed the existence of significant structural heterogeneities, extending up to a length scale which is more than five times the size of the first coordination shell radius. Due to these significant structural fluctuations in the bulk liquid phases, the use of larger size clusters in DFT calculations has been suggested. Contrary to the findings of the DFT calculations on small isolated clusters, the MD simulations have predicted a preference of Li^+ to interact with DMC molecules within its first solvation shell and not with the highly polar EC and PC ones, in the binary and ternary mixtures. This behavior has been attributed to the local tetrahedral packing of the solvent molecules in the first solvation shell of Li^+, which causes a cancellation of the individual molecular dipole vectors, and this effect seems to be more important in the cases where molecules of the same type are present. Due to these cancellation effects, the total dipole in the first solvation shell of Li^+ increases when the local mole fraction of DMC is high.

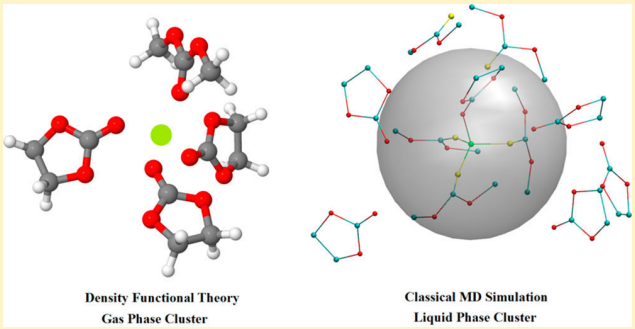

1. INTRODUCTION

In recent years the demand for portable power applications has been highly increased, thus giving a considerable impetus to the development of novel electrochemical devices, such as electric double-layer capacitors and lithium-ion batteries. Lithium-ion secondary batteries are very common in consumer electronics, such as laptop computers and cell phones, while they are also growing in popularity for automotive applications in order to decrease the greenhouse gas emissions in the atmosphere and, hence, to prevent global warming.[1−3] In general Li-ion batteries have been deployed so far in a wide range of energy storage applications, ranging from energy-type batteries of a few kilowatts per hour in residential systems with rooftop photovoltaic arrays to multimegawatt containerized ones, for the provision of grid ancillary services.

Li-ion cells mainly employ intercalation materials as positive and negative electrodes and aprotic electrolytes to conduct Li^+. The chemical nature of the electrodes determines the energy output, while the electrolyte affects the rate of the energy release by controlling mass transport properties within the battery.[1] The interactions between the electrolyte and the electrode materials are also very important, and the formation of electrified interfaces between them often dictates the performance of the device. An electrolyte should meet a list of minimal requirements in order to be used in such devices. In general it should be a good ionic conductor and electronic insulator, have a wide electrochemical window, exhibit electrochemical, mechanical, and thermal stability, and be environmentally friendly and inert to other cell components such as cell separators, electrode substrates, and cell packaging materials.

As mentioned above, the transport of Li^+ ions inside the electrolyte determines the rate of the energy transfer, which has been stored on the electrodes.[4] According to the literature the

Received: November 6, 2014
Revised: February 9, 2015

DOI: 10.1021/jp511132c
J. Phys. Chem. C XXXX, XXX, XXX−XXX

transport of Li^+ ions is controlled by a two-step mechanism involving the solvation of the ions by the solvent molecules, followed by the migration of the solvated ions.[5] A deeper understanding of the solvation of Li^+ ions may therefore act as a springboard toward the rational design of novel electrolytes with improved Li^+ conductivity.

By now, the most commonly employed strategy toward the rational design of electrolytes with optimal properties for battery applications is to use mixtures of cyclic and noncyclic organic carbonates.[6] In such a way the high dielectric constant of cyclic carbonates is combined with the low viscosity of acyclic carbonates ensuring good performances under low-temperature environments. On the other hand, the higher thermal stability of cyclic carbonates ensures a reasonable operating temperature range for the mixed solvent.

Although several experimental and theoretical studies devoted to the interactions of Li^+ with pure and mixed carbonate-based electrolytes have already been published, the solvation structure and dynamics of lithium cations in these solvents is still a subject of debate. Interestingly, even the determination of the coordination number around the lithium ions in pure carbonate-based solvents has not been definitely resolved.[7−18] While the generally accepted picture comprises a tetrahedral coordination of the carbonyl oxygen atoms around Li^+, some experimental and theoretical studies propose the existence of local structures exhibiting slightly higher coordination numbers. The dependence of this local coordination number on the ion concentration is also somehow controversial. However, it should be emphasized that designing experimental methods or theoretical models to analyze the experimental data in order to provide a direct measurement of the coordination number is an extremely complicated task.[7,19,20] On the other hand, since the validation of molecular simulation results strongly depends on the direct comparison with experimental data, the development of experimental methods proving a direct determination of the coordination number becomes indispensable in order to obtain a clear picture about the local structural effects in liquid solvents.

On the basis of the above considerations the aim of the present study is not to give a final answer to this particular problem. The main purpose is to provide some general insight concerning the differences in the solvation mechanisms of Li^+ in pure and mixed binary and ternary carbonate-based solvents, by employing molecular dynamics simulations and quantum chemical calculations. Also, recent advances in the investigation of the local solvation structure by means of both experimental and theoretical techniques will be discussed and compared with the findings of the present study. Such a discussion might be used as a springboard toward a better understanding of the solvation phenomena in these electrolytes, significantly improving the rational design of electrolytes for battery applications.

2. COMPUTATIONAL METHODS AND DETAILS

2.1. Density Functional Quantum Chemical Calculations. Quantum chemical calculations for several clusters of pure, binary, and ternary electrolytes including a lithium cation have been performed using the ADF software.[21] The density functional theory (DFT) has been employed for the optimization of structures, using the PBE GGA[22] functional and a TZP (core double-ζ, valence triple-ζ, polarized) slater-type orbital (STO) basis set. Our calculations for some representative clusters have revealed that the basis set superposition error (BSSE) corrections[23] are negligibly small. A similar observation has also been pointed out in recent DFT studies.[24,25] Frequency analysis has been carried out for each structure ensuring the absence of imaginary modes and confirming each structure as a minimum on the potential energy surface. Zero-point energy (ZPE) corrections have been also taken into account. Thermodynamic quantities such as the entropy, enthalpy, and free energy of the investigated clusters have been estimated at the temperature of 298.15 K.

2.2. Molecular Dynamics Simulations. In the present study the solvation structure of Li^+ at infinite dilution in pure and mixed carbonate-based solvents has been investigated via classical molecular dynamics (MD) simulations. The selected pure solvents were ethylene carbonate (EC), propylene carbonate (PC), and dimethyl carbonate (DMC). The binary EC−DMC mixture with a molar composition 1EC:1DMC and the ternary EC−DMC−PC one with 1EC:1DMC:3PC molar composition were also studied.

Inside each simulation cubic box, one lithium cation was placed among 215 solvent molecules in the case of the pure solvents and the ternary mixture, whereas in the case of the binary mixture it was placed among 214 solvent molecules. Trial runs with larger system sizes have verified that the employed number of molecules is sufficient in describing the solvation structure of Li^+, avoiding in this way any possible artifacts arising from finite size effects. The initial configurations of the simulated systems were prepared by using the *Packmol* software.[26]

The force fields employed in the simulations were adopted from previous studies.[27,28] The intermolecular interactions in these models are represented as pairwise additive with site−site 12-6 Lennard-Jones plus Coulomb interactions. The EC and PC molecules were kept rigid during the simulations (intramolecular geometries can be found in the Supporting Information). It should be mentioned that when investigating the solvation of Li^+ in pure solvents test simulations were also performed using a flexible potential model[28] for EC. It was observed that the local structure and orientation around Li^+ in pure EC was not significantly affected compared to the case of the rigid model. This is possibly due to the fact that the rigid framework of cyclic carbonates is not significantly distorted by the presence of the intramolecular vibrational motions and therefore does not affect the packing of these molecules inside the solvation shell of Li^+.

In the case of DMC, due to the existence of different conformers in the gas and liquid phase,[29−31] an intramolecular force field has been also employed. The intramolecular interactions have been represented in terms of harmonic angle bending and cosine series for dihedral angle internal rotations, whereas the bond lengths have been kept rigid by employing a modified version of the SHAKE[32,33] algorithm. The parameters of the intramolecular force field used are also presented in the Supporting Information. Due to the absence of a rigid framework, which is present in cyclic carbonates, intramolecular torsional motions could play an important role in the packing of DMC molecules. It should be noted however that conformational transitions were not detected on the time scale of our simulations.

As pointed out in the Introduction, the generally accepted picture comprises a tetrahedral coordination of the carbonyl oxygen atoms around Li^+. The potential models used in the presented study predict such local structures,[27,28] and for this reason they were selected to be employed in the simulations.

DOI: 10.1021/jp511132c
J. Phys. Chem. C XXXX, XXX, XXX−XXX

Results obtained with different potential models already published in the literature will be also discussed together with the findings of the present study.

The equations of motion were integrated using a leapfrog-type Verlet algorithm with an integration time step of 1 fs.[34] The temperature has been fixed to 303.15 K and the pressure to 1 atm by coupling the systems to a Nose–Hoover thermostat and barostat with relaxation times of 0.2 and 0.5 ps, respectively.[35,36] The rigid body equations of motion for EC and PC molecules were expressed in the quaternion formalism.[34] A cutoff radius of 9.0 Å has been applied for all Lennard-Jones interactions, and long-range corrections have also been taken into account. To account for the long-range electrostatic interactions the standard Ewald summation technique has been used.[34] The simulation runs were performed using the DL_POLY simulation code.[37] The systems were equilibrated for 25 ns, and a subsequent run of 15 ns was performed in each case, in order to calculate equilibrium properties.

3. RESULTS AND DISCUSSION

3.1. Relative Stability of Isolated Clusters. By employing DFT calculations, using the methodologies described in Section 2.1, a wide range of clusters of the type $Li(S)_n^+$ (where S = EC, PC, DMC and n = 1–5) were optimized. Thermodynamic parameters, such as the enthalpy, entropy, and binding energy of these clusters, have been also estimated,[38,39] based upon the calculation of the total partition function resulting from the contribution of the translational, rotational, and vibrational degrees of freedom.[39] The binding energies of these clusters have been expressed in terms of the equation

$$\mathrm{BE} = E(\mathrm{Li(S)}_n^+) - E(\mathrm{Li}^+) - nE(\mathrm{S}) \quad (1)$$

In order to provide an estimation of the preferable coordination number around the lithium cation, the most favorable path between these clusters $Li(S)_n^+$ has to be determined in terms of free energy changes. To do so, the free energies of the aggregates $Li(S)_n^+ + m\mathrm{S}$ ($n + m$ = constant = 5 in this case) were estimated, in order to define the aggregate exhibiting the lowest free energy value. In this way, if the fragment $Li(S)_n^+ + m\mathrm{S}$ has the lowest free energy value, all paths of the type

$$\mathrm{Li(S)}_k^+ + l\cdot\mathrm{S} \rightarrow \mathrm{Li(S)}_n^+ + m\cdot\mathrm{S}, \quad k + l = n + m \quad (2)$$

will exhibit a negative free energy change ΔG, thus indicating that all possible paths leading to the cluster $Li(S)_n^+$ are favorable, and therefore, this cluster could be considered the most preferable one in terms of the free energy changes. Note that the paths depicted in eq 2 can correspond to both additions or subtractions of solvent molecules from one particular cluster leading to another, depending on the relative difference $m - l$. If $m - l < 0$, then the transition is being achieved through solvent addition, otherwise through solvent subtraction.

All the calculated values of enthalpy, entropy, and binding energy of the investigated $Li(S)_n^+$ clusters, together with the free energy values of the $Li(S)_n^+ + m\mathrm{S}$ aggregates, are presented in Tables 1 and 2. From the results obtained it can be clearly seen that in the cases of EC and DMC the predicted most favorable structures correspond to a tetracoordinated lithium cation. Similar conclusions have been drawn in the DFT study of Bhatt et al., studying the solvation of Li^+ in EC.[24] In the case of PC the free energy difference for the path going from $Li(PC)_3^+$ to $Li(PC)_4^+$ is very small. This is an indication that although the $Li(PC)_3^+$ cluster has been predicted to be the most favorable one both structures could possibly exist in the bulk phase. The optimized structures for $Li(EC)_4^+$, $Li(PC)_3^+$, and $Li(PC)_4^+$, as well as for $Li(DMC)_4^+$, are shown in Figures 1–3. From the data presented in Table 1, it might be also seen that in the cases of the tetracoordinated clusters the binding energies decrease in the order $E(Li(PC)_4^+) > E(Li(EC)_4^+) > E(Li(DMC)_4^+)$, which is reasonable taking into account that the dipole moments of PC, EC, and DMC molecules decrease

Table 1. Thermodynamical Parameters and Binding Energies of Li^+–Solvent Clusters (H and BE Are in kcal/mol and S in cal mol^{-1} K^{-1})[a]

clusters	H	BE	S
EC	−1369.3		72.8
$Li^+(EC)$	−1293.6	−47.6	83.2
$Li^+(EC)_2$	−2698.9	−83.1	116.9
$Li^+(EC)_3$	−4090.4	−104.6	142.2
$Li^+(EC)_4$	−5473.4	−118.2	174.0
$Li^+(EC)_5$	−6849.9	−126.9	214.6
DMC	−1530.2		82.5
$Li^+(DMC)$	−1449.0	−42.1	90.6
$Li^+(DMC)_2$	−3012.2	−74.0	124.5
$Li^+(DMC)_3$	−4562.4	−92.9	158.1
$Li^+(DMC)_4$	−6100.8	−103.2	216.8
$Li^+(DMC)_5$	−7636.7	−108.5	251.3
PC	−1736.0		79.6
$Li^+(PC)$	−1662.2	−49.5	89.8
$Li^+(PC)_2$	−3435.1	−85.3	123.7
$Li^+(PC)_3$	−5193.2	−106.5	154.5
$Li^+(PC)_4$	−6945.0	−121.3	180.3
$Li^+(PC)_5$	−8687.2	−128.8	231.3

[a]H = Enthalpy, BE = Binding Energy, S = Entropy.

Table 2. Gibbs Free Energy of Clusters (kcal/mol)

	G		
clusters	S = EC	S = DMC	S = PC
$Li^+(S) + 4S$	−6882.4	−7695.0	−8728.1
$Li^+(S)_2 + 3S$	−6906.7	−7713.5	−8751.3
$Li^+(S)_3 + 2S$	−6914.8	−7719.0	−8758.8
$Li^+(S)_4 + S$	−6916.2	−7720.2	−8758.5
$Li^+(S)_5$	−6913.9	−7711.6	−8756.2

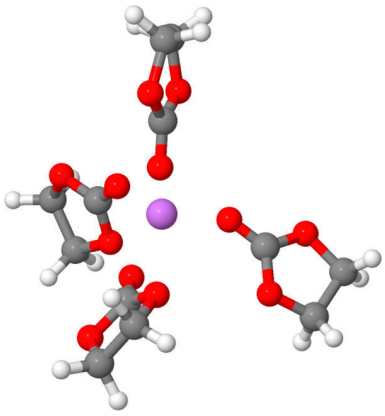

Figure 1. Structure of the optimized $Li(EC)_4^+$ cluster.

DOI: 10.1021/jp511132c
J. Phys. Chem. C XXXX, XXX, XXX–XXX

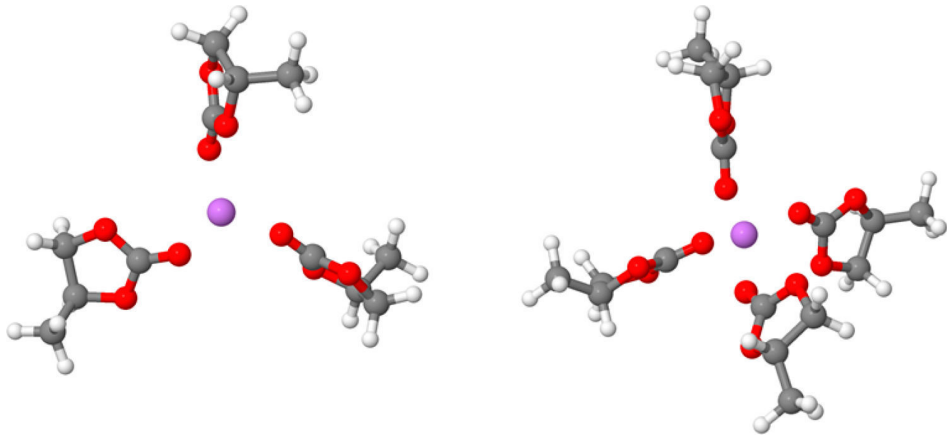

Figure 2. Structure of the optimized $Li(PC)_3^+$ and $Li(PC)_4^+$ clusters.

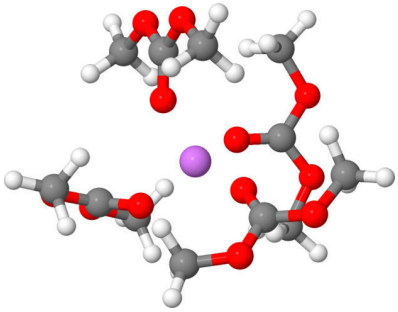

Figure 3. Structure of the optimized $Li(DMC)_4^+$ cluster.

in the same order (5.6, 5.3, and 0.35 D, respectively). It should be also noted that the entropic contributions to the free energy of each cluster exhibit the opposite trend, being more important in the case of the $Li(DMC)_4^+$.

Considering that the tetracoordinated structure is the most preferable one, the same calculations have been performed for clusters of the type $Li(S_1)_n(S_2)_m^+$, where S_1 = EC, S_2 = DMC, and $n + m = 4$. The free energy changes for the transitions

$$Li(S_1)_k(S_2)_l^+ + (4 - k)\cdot S_1 + (4 - l)\cdot S_2 \rightarrow Li(S_1)_n(S_2)_m^+ + (4 - n)\cdot S_1 + (4 - m)\cdot S_2 \quad (3)$$

where $k + l = n + m = 4$ and $n, m, k, l = 1-3$, were also estimated, in order to find the most favorable structure among the clusters with two types of solvents around lithium. The calculated values of enthalpy, entropy, and binding energy of the investigated $Li(S_1)_n(S_2)_m^+$ clusters, together with the free energy values of the $Li(S_1)_n(S_2)_m^+ + (4 - n)S_1 + (4 - m)S_2$ aggregates, are presented in Tables 3 and 4. The results obtained reveal that among all the possible combinations of tetracoordinated clusters containing both EC and DMC the most preferable is $Li(EC)_3(DMC)^+$, followed by $Li(EC)_2(DMC)_2^+$, and eventually the $Li(EC)(DMC)_3^+$ is the least favorable among these three clusters. This finding is in agreement with both ab initio studies by Borodin and Smith,[40] where the relative stabilities were based upon the energies of the complexes and with the very recently reported study by Bhatt and O'Dwyer.[25] The structures of the optimized clusters are presented in Figure 4.

Table 3. Thermodynamical Parameters and Binding Energies of $Li^+(EC)_n(DMC)_m$ ($n + m = 4$) Clusters (H and BE Are in kcal/mol and S in cal mol^{-1} K^{-1})[a]

clusters	H	BE	S
$Li^+(EC)_3(DMC)$	−5632.2	−116.3	182.1
$Li^+(EC)_2(DMC)_2$	−5790.4	−113.0	186.2
$Li^+(EC)(DMC)_3$	−5946.2	−109.1	204.9

[a]H = Enthalpy, BE = Binding Energy, S = Entropy.

Table 4. Gibbs Free Energies (in kcal/mol) of Clusters Containing Two Types of Solvents

clusters	G
$Li^+(EC)_3(DMC)$ + EC + 3DMC	−11741.7
$Li^+(EC)_2(DMC)_2$ + 2EC + 2DMC	−11737.3
$Li^+(EC)(DMC)_3$ + 3EC + DMC	−11735.0
$Li^+(EC)_4$ + 4DMC	−11744.2
$Li^+(DMC)_4$ + 4EC	−11729.4

Finally, a similar analysis was performed for the clusters $Li(S_1)_n(S_2)_l(S_3)_m^+$ (S_1 = EC, S_2 = DMC, S_3 = PC), containing EC, DMC, and PC solvent molecules. The structures of the optimized clusters are presented in Figure 5. From the results obtained using the same methodology discussed above, which are presented in Tables 5 and 6, it can be seen that the cluster $Li(EC)_2(DMC)(PC)^+$ seems to be the most favorable one, followed by $Li(EC)(DMC)(PC)_2^+$ and finally by $Li(EC)(DMC)_2(PC)^+$. However, the free energy changes for the transition paths between these clusters are very small, indicating that all these structures could possibly exist in the bulk phase. Also the free energy changes for the transition paths leading to the $Li(EC)_4^+$ and $Li(PC)_4^+$ clusters are very small. It has also been found that the transitions from clusters containing only EC and DMC to clusters with three types of solvent molecules, by substitution of one EC or DMC molecule with a PC one, are favorable in terms of the free energy changes. The substitution of a DMC molecule has been found to be more favorable than the substitution of an EC one. In general the above findings indicate that the presence of PC contributes to the stabilization of the clusters. This fact can be also supported by the calculated binding energies of the tetracoordinated clusters, which are plotted together in Figure 6.

Interestingly, from Tables 4 and 6 it can also be seen that the presence of DMC contributes to the increase of the entropy and therefore to the decrease of the free energy of the clusters containing more than one solvent type. Therefore, although

DOI: 10.1021/jp511132c
J. Phys. Chem. C XXXX, XXX, XXX−XXX

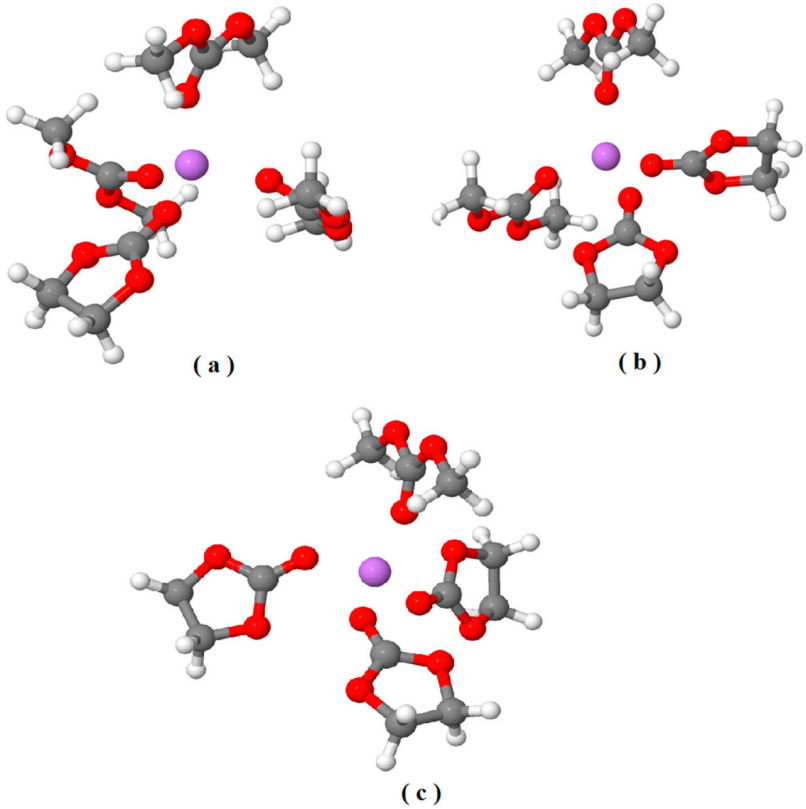

Figure 4. Structure of the optimized: (a) $Li(EC)(DMC)_3^+$, (b) $Li(EC)_2(DMC)_2^+$, and (c) $Li(EC)_3(DMC)^+$ clusters.

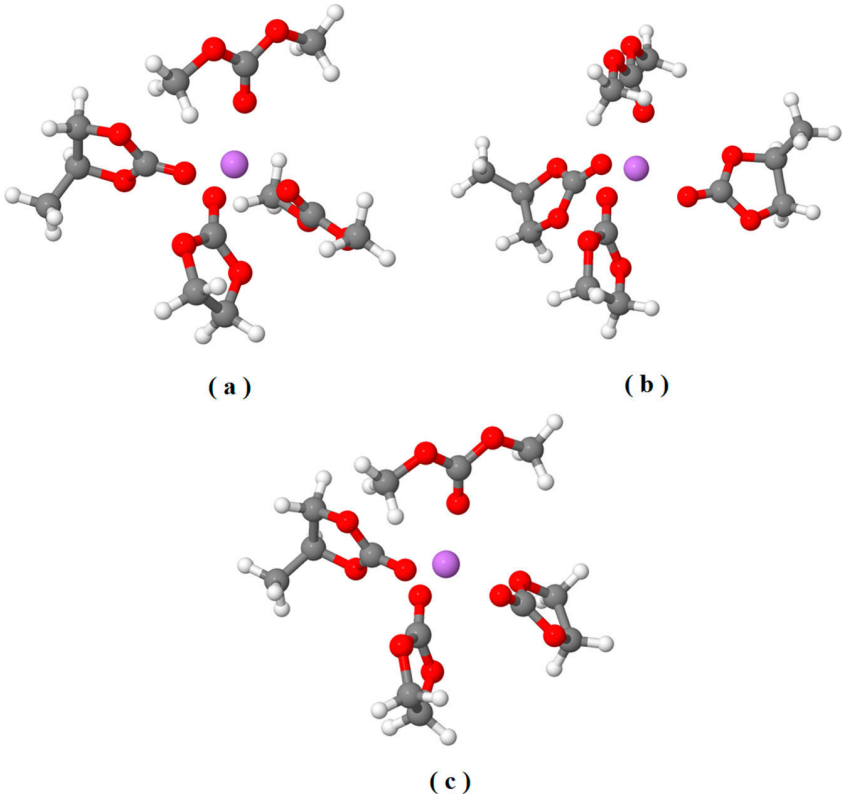

Figure 5. Structure of the optimized: (a) $Li(EC)(PC)(DMC)_2^+$, (b) $Li(EC)(PC)_2(DMC)^+$, and (c) $Li(EC)_2(PC)(DMC)^+$ clusters.

from an energetic point of view the preference of Li^+ to bind with the highly polar PC and EC molecules is undoubtful, from an entropic point of view the addition of DMC molecules contributes to the decrease of the free energy of the clusters. In

DOI: 10.1021/jp511132c
J. Phys. Chem. C XXXX, XXX, XXX−XXX

Table 5. Thermodynamical Parameters and Binding Energies of $Li^+(EC)_l(DMC)_m(PC)_n$ ($l + m + n = 4$) Clusters (H and BE Are in kcal/mol and S in cal mol^{-1} K^{-1})[a]

clusters	H	BE	S
$Li^+(EC)_3(DMC)(PC)$	−5999.3	−116.6	189.0
$Li^+(EC)(DMC)_2(PC)$	−6157.0	−114.0	202.5
$Li^+(EC)(DMC)(PC)_2$	−6367.2	−117.2	188.9

[a]H = Enthalpy, BE = Binding Energy, S = Entropy.

Table 6. Gibbs Free Energies (in kcal/mol) of Clusters Containing Three Types of Solvents

clusters	*G*
$Li^+(EC)_2(DMC)(PC)$ + 2EC + 3PC + 3DMC	−18781.2
$Li^+(EC)(DMC)_2(PC)$ + 3EC + 3PC + 2DMC	−18779.2
$Li^+(EC)(DMC)(PC)_2$ + 3EC + 2PC + 3DMC	−18780.3
$Li^+(EC)_4$ + 4DMC + 4PC	−18783.3
$Li^+(DMC)_4$ + 4EC + 4PC	−18768.5
$Li^+(PC)_4$ + 4EC + 4DMC	−18781.7

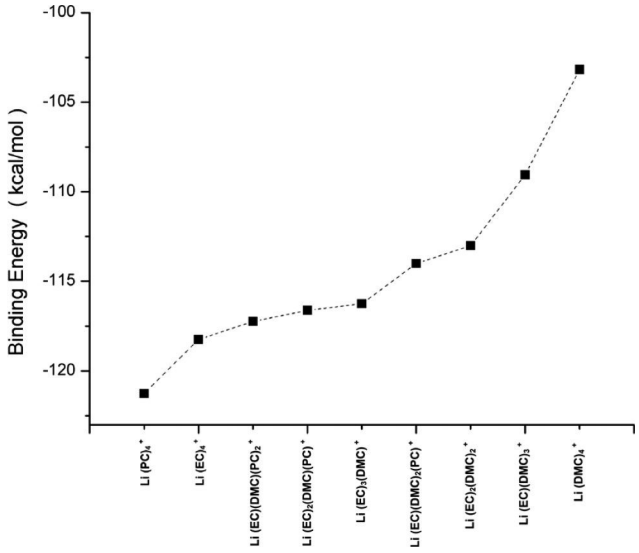

Figure 6. Calculated binding energies of the optimized tetracoordinated Li^+ clusters.

the investigated finite size clusters the energetic contribution seems to be the most important one. However, the small free energy differences observed for the transition paths leading from one cluster to the other indicate that the formation of these clusters should be investigated at more extended length scales, in order to have a more realistic description of the effects taking place in the bulk liquid phase. This was the most important motivation to combine DFT calculations of isolated clusters with classical MD simulations at more extended length scales, in order to have a clearer picture about the solvation of Li^+ in pure and mixed organic carbonate-based solvents.

3.2. Liquid Solvation Structure. *3.2.1. Local Structural Inhomogeneities.* By analyzing the trajectories obtained by the classical MD simulations described in section 2.2, the local structure around Li^+ was investigated for all the selected pure and mixed solvents. The local structure was analyzed in terms of the most representative atom−atom pair radial distribution functions (prdfs). The results obtained indicate a preferential interaction of Li^+ with the carbonyl oxygen atom (O_C) of the carbonate molecules, which is in agreement with all the previously reported experimental and theoretical studies. The calculated Li^+-O_C prdfs between Li^+ and the carbonyl oxygen atoms of EC, PC, and DMC in the pure, binary, and ternary solvents are presented in Figure 7.

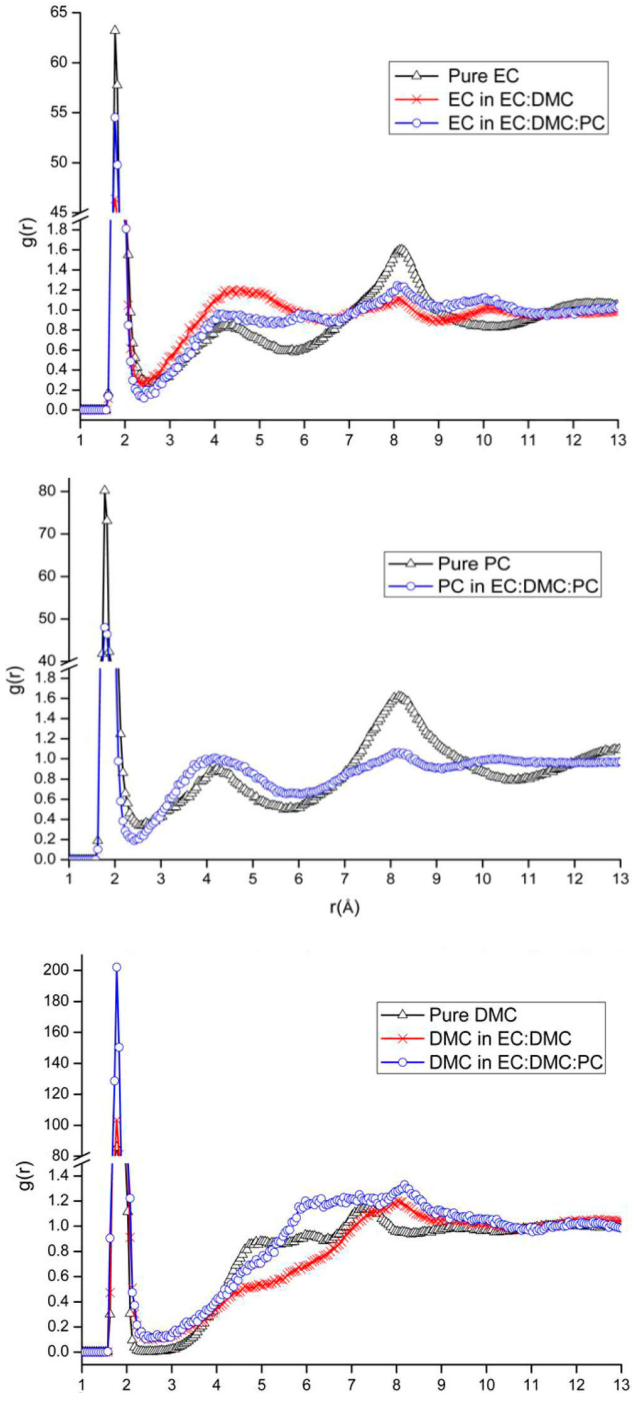

Figure 7. Calculated Li^+-O_c radial distribution functions.

One of the main features of the calculated prdfs is the existence of a high intensity peak located at 1.8 Å in all cases. In the cases of the pure solvents, the amplitude of this first peak decreases in the order $g(r)_{max}^{DMC} > g(r)_{max}^{PC} > g(r)_{max}^{EC}$. In the cases of the binary and ternary mixtures, the amplitude increases significantly in the case of DMC and decreases in

DOI: 10.1021/jp511132c
J. Phys. Chem. C XXXX, XXX, XXX−XXX

the cases of EC and PC. The high amplitude of the first peak of the Li^+-O_c prdf in the case of DMC indicates a strong interaction between Li^+ and the DMC molecules. The position of the first minimum, which determines the size of the first solvation shell, is located at about 2.6 Å in the case of the pure solvents and the binary mixture and at about 2.4 Å in the case of the ternary one. In order to estimate the number of solvent molecules around Li^+ in all the investigated systems, the local coordination numbers of each type of solvent were calculated as a function of the distance from the lithium cation, and they are presented in Figure 8. The values of the peak positions and amplitudes of the calculated prdfs together with the first minimum position and the corresponding coordination numbers for the first solvation shell are presented in Table 7.

From all these data it can be concluded that the solvation shell of Li^+ consists of four solvent molecules, and this situation does not change in the cases of the binary and ternary solvent mixtures. At this point it should be mentioned that several MD simulation studies[27,28,40−47] of the solvation of Li^+ in pure carbonate solvents have given different estimations of the coordination number corresponding to the first solvation shell of Li^+. In particular, whereas some potential models predict a solvation shell of Li^+ which consists of four solvent molecules,[27,28,40−42] other force fields predict a higher coordination number.[43,45] The potential models predicting higher coordination numbers also exhibit a strong dependence of the obtained coordination number on the salt concentration. From the shape of the obtained prdfs, it is also clear that there are significant local structural inhomogeneities in the system. These structural fluctuations are reflected in the behavior of the prdfs, which reveal the presence of well-structured second and third coordination shells. Eventually they reach the homogeneous limit, obtaining values close to unity, only at length scales longer than 15 Å.

In the cases of mixtures of organic carbonate solvents only a limited number of studies[40,45,48] have focused on the solvation of Li^+ in binary mixtures. Also, to the best of our knowledge, this is the first simulation study devoted to the solvation of Li^+ in ternary mixtures of carbonate-based solvents. In binary and ternary mixtures, beyond the estimation of the coordination number of the primary solvation shell around lithium, the mixed composition of the shell is also of interest. The local compositional fluctuations in a spherical shell around Li^+ can be characterized in terms of the corresponding local mole fractions of each type of solvent.[49] For instance, in a ternary mixture of solvents with indices *i*, *j*, *k* the local mole fraction of solvent *k* around Li^+ is expressed as

$$X_k(r) = \frac{n_k(r)}{n_i(r) + n_j(r) + n_k(r)} \quad (4)$$

In eq 4, $n_k(r)$ is the coordination number of solvent *k* corresponding to a spherical shell of radius *r* around Li^+. In a similar way, all the local mole fractions for the different types of solvents in the binary and ternary mixture around Li^+ have been calculated and are presented in Figure 9. The coordination number considered in the present calculations corresponds to the carbonyl oxygen atoms of each solvent around Li^+. The results obtained from the present MD simulations actually reveal that in the cases of binary and ternary mixtures there is a high concentration of DMC in the first solvation shell of Li^+. The existence of significant compositional fluctuations around Li^+ can also be observed. As a result of these fluctuations, the

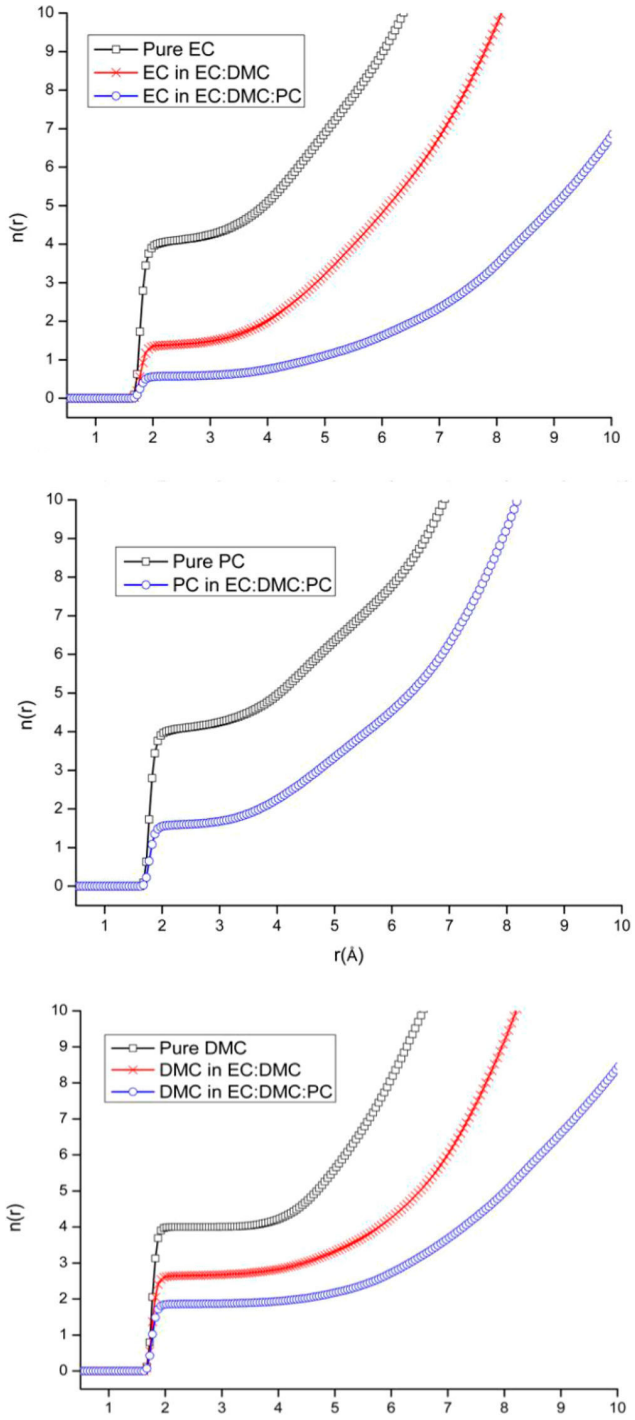

Figure 8. Calculated Li^+-O_c local coordination numbers.

structure around Li^+ could be described in terms of a short-range structure (up to 4−5 Å from Li^+) where the composition is rich in DMC and by a longer-range structure where in the case of the binary solvent mixture the composition is rich in EC and in the case of the ternary one is rich in PC. At larger length scales, in the range of about 15 Å from the lithium cation, the local mole fractions of each solvent reach the corresponding bulk value. From Figure 9 it can also be observed that the typical length scale of these fluctuations around Li^+ is slightly more extended in the case of the ternary mixture than in the binary one.

DOI: 10.1021/jp511132c
J. Phys. Chem. C XXXX, XXX, XXX−XXX

Table 7. Peak Positions and Amplitudes of the Calculated prdfs, Together with the First Minimum Position and the Corresponding Coordination Numbers for the First Solvation Shell of Li^+

system	EC	PC	DMC	EC:DMC (1:1)	EC:DMC:PC (1:1:3)
first peak position- amplitude	1.78 Å 63.19	1.78 Å 80.20	1.78 Å 85.58	Li^+ – EC: 1.78 Å 46.36 Li^+ – DMC: 1.78 Å 103.29	Li^+ – EC: 1.78 Å 54.51 Li^+ – DMC: 1.78 Å 202.09 Li^+ – PC: 1.78 Å 48.03
first minimum position	2.58 Å	2.53 Å	2.58 Å	Li^+ – EC: 2.53 Å Li^+ – DMC: 2.58 Å	Li^+ – EC: 2.43 Å Li^+ – DMC: 2.43 Å Li^+ – PC: 2.43 Å
coordination number (first shell)	4.13	4.12	4.00	Li^+ – EC: 1.41 Li^+ – DMC: 2.66	Li^+ – EC: 0.58 Li^+ – DMC: 1.86 Li^+ – PC: 1.60

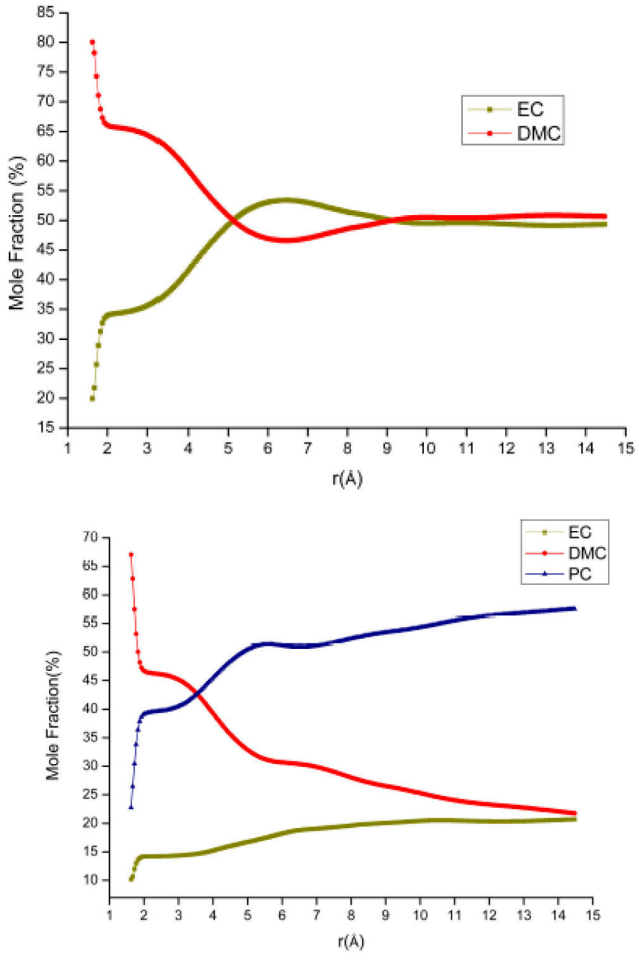

Figure 9. Local mole fractions (%) of EC, PC, and DMC as a function of the distance from the lithium cation in the binary and ternary mixtures.

The findings of the MD simulations regarding the composition of the first solvation shell of Li^+ in binary and ternary mixtures could be in contradiction with the results obtained by the DFT calculations. However, it should be pointed out that the first shell structure predicted in the MD simulations could be the result of local structural correlations between the first, second, and third solvation shells which exhibit completely different compositions. Indeed, the collective effects arising due to the interactions between regions of different density and composition could possibly stabilize the local structure observed inside the first solvation shell of Li^+. These are clearly not taken into account in the cases of the DFT calculations, where isolated clusters have been investigated. To perform a meaningful comparison between MD and DFT results in cases where significant structural fluctuations are present, extended far beyond the first solvation shell, the use of larger size clusters in DFT calculations seems to be needed.

To obtain a more detailed picture of the multiple different local microstructures observed in the first solvation shell of Li^+, an analysis of the different clusters $Li(S_1)_n(S_2)_l(S_3)_m^+$ (S_1=EC, S_2=DMC, S_3=PC, n,l,m= 0−4 and n+l+m=4) observed inside this shell was performed for the binary and ternary solvent mixtures. The relative populations of these are shown in Figure 10. In the binary mixture, the most prominent clusters inside the first solvation of Li^+ are the $Li(EC)(DMC)_3^+$ and the $Li(EC)_2(DMC)_2^+$, with the first exhibiting almost double occurrence probability. There is also a small fraction of clusters (7.2%) where Li^+ is pentacoordinated. About 80% of these five-coordinated Li^+ complexes consist of two EC and three DMC molecules and 19% of three EC and two DMC molecules, and an almost negligible 1% fraction consists of one EC and four DMC molecules. In the ternary mixture the most prominent clusters are $Li(EC)(DMC)_2(PC)^+$ and $Li(DMC)_2(PC)_2^+$, having though non-negligible fractions of $Li(EC)(DMC)(PC)_2^+$, $Li(DMC)_3(PC)^+$, and $Li(DMC)(PC)_3^+$, and a smaller one corresponding to the $Li(EC)_2(DMC)_2^+$ cluster. It should

DOI: 10.1021/jp511132c
J. Phys. Chem. C XXXX, XXX, XXX−XXX

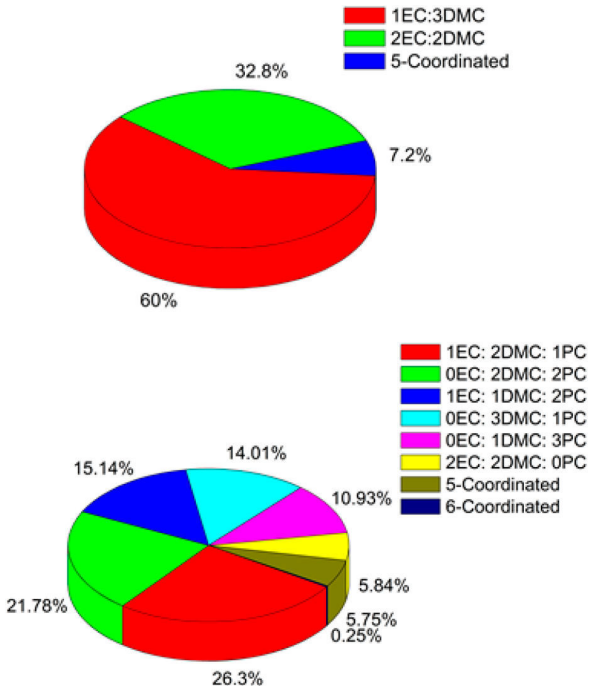

Figure 10. Fractions of the $Li(EC)_n(DMC)_{4-n}^+$ and $Li(EC)_n(PC)_m(DMC)_{4-n-m}^+$ clusters in the binary and ternary mixture.

be noted that almost half of the observed clusters with four solvent molecules (49.7%) do not contain EC at all, whereas DMC is involved in the formation of all of them. PC is absent in only 6.2% of the total fraction of clusters with four solvent molecules. There is also a fraction 5.75% of clusters with five solvent molecules and an almost negligible one (0.25%) of clusters where Li^+ is hexacoordinated.

Interestingly, such a discrepancy between the results obtained by MD and DFT calculations has been also reported by Borodin and Smith.[40] In their study, Borodin and Smith performed a MD simulation of a solution of $LiPF_6$ in an equimolar EC−DMC binary mixture (EC + DMC:Li = 11.8) using a polarizable potential model. The coordination number of DMC in the first solvation shell of Li^+ was higher than the coordination number of EC. This is in contrast with the results reported by Tenney and Cygan,[43] favoring the presence of EC in the first solvation shell of Li^+ in a low concentration $LiPF_6$ solution in a binary equimolar EC−DMC mixture. However, there is a significant difference between the potential models employed in these two MD simulation studies. The potential model used by Borodin and Smith[40] mainly predicts tetracoordinated Li^+ complexes inside its first solvation shell, whereas in the case of the simulation reported by Tenney and Cygan[45] the solvation shell of Li^+ mainly consists of five or six solvent molecules. The potential model used in the presented study also favors local structures with four solvent molecules around Li^+. This observation was an additional motivation to search for possible correlations between the formation of a local tetrahedral structure and the preference of Li^+ to form a first solvation shell mainly consisting of DMC molecules.

3.2.2. First Solvation Shell Orientational Ordering. The local tetrahedral structure around lithium can be investigated in terms of the tetrahedral order parameter, q.[50] This parameter q provides information about the extent to which a particle and its four nearest neighbors adopt a tetrahedral arrangement and is defined as

$$q = 1 - \left\langle \frac{3}{8} \sum_{j=1}^{3} \sum_{k=j+1}^{4} \left(\cos \phi_{jik} + \frac{1}{3} \right)^2 \right\rangle \quad (5)$$

In this equation ϕ_{jik} corresponds to the angle formed by the vectors $\vec{r}_{ij}$ and $\vec{r}_{ik}$, connecting the lithium cation i with the oxygen atoms of two of its four nearest neighbors j, k. Using this definition, $q = 1$ in a perfect tetrahedral network and $q = 0$ in an ideal gas.[48] Kumar et al.[51] have also suggested that an entropic term associated with this local tetrahedral order around a particle can be calculated from the probability distribution of the tetrahedral order parameter $P(q)$

$$S_{tetr} = \frac{3}{2} \cdot K_B \int \ln(1 - q) \cdot P(q) \cdot dq \quad (6)$$

We note that, in general, the entropy of a fluid can be expressed in terms of several contributions arising from the integrals over multiparticle correlation functions.[52−54] However, our analysis revealed that orientational entropy plays a crucial role in the stabilization of the local solvation shell structures, and hence we have focused on this particular aspect of orientational order and entropy. Also Kumar et al.[51] have proposed that in systems exhibiting significant local tetrahedral orientational order the tetrahedral entropy captures the most important contributions arising from configurational orientational correlations[54] and therefore offers a rather simpler way to investigate the entropy associated with such kinds of local structures.

The normalized distributions $P(q)$ have been calculated for all the simulated systems and are presented in Figure 11. The

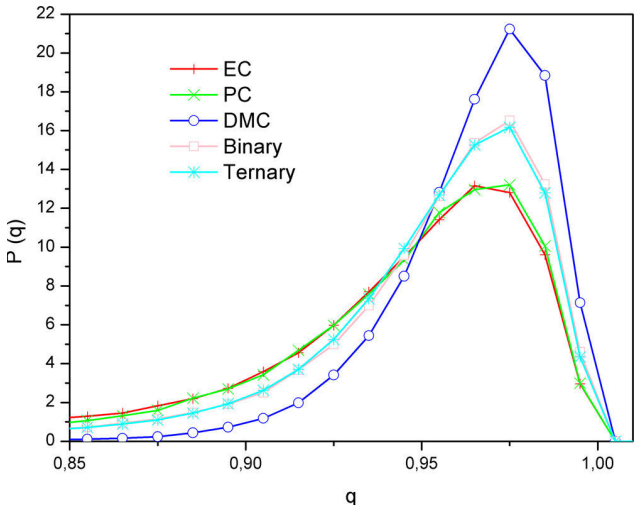

Figure 11. Normalized distribution of the tetrahedral order parameter around Li^+ in all the investigated solvents.

Table 8. Average Values of q and S_{tetr}/K_B per Lithium Cation Obtained by the MD Simulations

system	EC	PC	DMC	EC:DMC (1:1)	EC:DMC:PC (1:1:3)
$\langle q \rangle$	0.934	0.932	0.964	0.948	0.947
S_{tetr}/K_B	−4.56	−4.52	−5.29	−4.87	−4.84

DOI: 10.1021/jp511132c
J. Phys. Chem. C XXXX, XXX, XXX−XXX

average values of q and S_{tetr} are shown in Table 8. From the shape of these distributions it can be seen that there is a very significant tetrahedral local ordering around Li^+ in all cases, and the addition of cosolvents does not significantly distort this structural order. The average values of q are in the range of about 0.93−0.96 in all cases, very close to the ideal tetrahedron value. Whereas there is no significant difference in the average values of q, the calculated value of S_{tetr} is noticeably lower in the case of the pure DMC solution, signifying that from an entropic point of view the presence of DMC contributes to the stabilization of the local tetrahedral structure around Li^+.

As has been pointed out by one of the authors in a previous publication,[55] given the additive property of the integral in eq 6, the contributions of different cluster structures to the calculated S_{tetr} value can be easily extracted. By using the fractions χ_{nlm} of the different cluster structures $Li(S_1)_n(S_2)_l(S_3)_m^+$ (S_1 = EC, S_2 = DMC, S_3 = PC), already shown in Figure 10, the tetrahedral entropic term S_{tetr} per lithium cation is given by $S_{tetr} = \Sigma_{nlm}\chi_{nlm} \cdot S_{tetr}^{nlm}$, where the contribution of each cluster state is

$$S_{tetr}{}^{nlm} = \frac{3}{2} \cdot K_B \int \ln(1 - q) \cdot P^{nlm}(q) \cdot dq \quad (7)$$

In this equation $P^{nlm}(q)$ is the normalized probability density distribution of the tetrahedral order parameter q corresponding to a cluster $Li(S_1)_n(S_2)_l(S_3)_m^+$ inside the first solvation shell of Li^+. The calculated values of S_{tetr}^{nlm} corresponding to all the tetracoordinated Li^+ clusters observed during the simulations of the dilute solutions of Li^+ in the pure, binary, and ternary solvents are presented in Figure 12. In general it can be

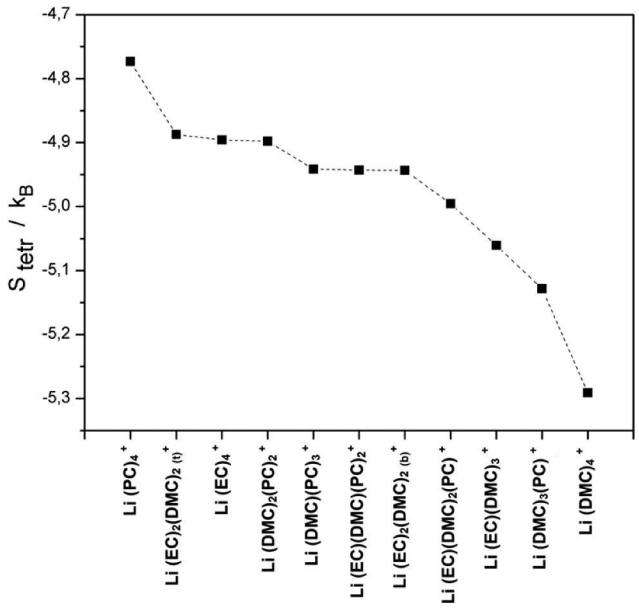

Figure 12. Calculated values of S_{tetr}^{nlm} corresponding to all the tetracoordinated Li^+ clusters observed in the pure, binary, and ternary solvents.

observed that the clusters having a high fraction of DMC molecules (three and four molecules) exhibit a higher tetrahedrality, which is reflected in the lower values of S_{tetr}^{nlm}. Interestingly there is also a small difference in the S_{tetr}^{nlm} values of the clusters $Li(EC)_2(DMC)_2^+$ observed in the binary and ternary solvent mixtures, the $Li(EC)_2(DMC)_{2(b)}^+$ and $Li(EC)_2(DMC)_{2(t)}^+$ clusters, respectively. This is a clear indication of the effect of the second solvation shell structure, which is different in the binary and ternary solvent mixtures, on the stabilization of the local structure observed in the first solvation shell. This observation further supports our previous statements that the use of larger size clusters in DFT calculations is required in cases where there are significant structural fluctuations, extended far beyond the first solvation shell.

It should be mentioned that previous experimental studies, using electrospray ionization and mass spectrometry (ESI-MS) techniques,[56] have predicted a stronger preference of Li^+ to bind with EC than with DMC in binary EC−DMC solvents. This preference has been attributed to the stronger ion dipole interactions between Li^+ and EC molecules. However, the authors in that study pointed out that their results have been extracted from measurements of isolated clusters formed by two solvent molecules only instead of four. This difference has been attributed to the relative depletion of free solvent molecules at high salt concentrations or to a possible partial desolvation, during which the loosely bound molecules in the $Li(S)_4^+$ clusters (S: solvent) could be lost before the solvated species ever reach the aperture of the spectrometer.

Borodin and Smith[40,57] pointed out in their study, where they observed a slight preference for Li^+ to bind with DMC, that the composition of the Li^+ solvation can be different in the gas and liquid phases. Takeuchi et al.[42] have come to similar conclusions about the Li^+ binding patterns to a PF_6^- anion. Another issue, which has not been discussed in the previous ESI-MS investigation, is the importance of the presence of the anions in the stabilization of the Li^+ solvation shell. The investigated solutions had a high salt concentration, and therefore the presence of the anions could strongly affect the preferential binding of Li^+ with the solvent molecules. The preferential solvation around Li^+ in binary and ternary mixtures is a quite complicated issue, and besides the relative permittivity and donicity of the cyclic and acyclic components of the mixed solvent,[56] salt concentration possibly plays a very important role. This statement is also supported by the findings of Borodin and Smith,[40] where the presence of PF_6^- anions in the solvation shell around Li^+ strongly affects the preferential binding of Li^+ with the cyclic and acyclic solvent molecules. This was the main reason why in the presented study dilute solutions of Li^+ were selected to be investigated, to focus more on the effects arising just due to the individual cation−solvent and solvent−solvent interactions. However, the anion concentration effect on the local solvation structure of mixed electrolyte solvents is a very important topic and will be the subject of a forthcoming study.

In general the preferential solvation around Li^+ is being discussed in terms of the strength of individual pair cation−dipole interactions. In this sense, the observed preferential solvation of Li^+ by the nonpolar DMC molecules instead of the highly polar EC and PC molecules seems to be problematic. To obtain a deeper insight, having in mind that collective effects might play a very important role in the solvation phenomena in condensed phases, the total dipole of the solvent molecules inside the solvation shell of Li^+ was calculated as

$$\vec{M}_{sh} = \sum_i \vec{\mu}_i, \text{ with } r_{i-Li} \leq r_c \quad (8)$$

These local collective dipole moments, corresponding to the sum of the individual molecular dipoles of the solvent molecules which are inside the first solvation shell of Li^+,

DOI: 10.1021/jp511132c
J. Phys. Chem. C XXXX, XXX, XXX−XXX

have been extracted by analyzing the trajectories of the classical MD simulations.

It should be also noted that although the effects arising from induction interactions are not taken into account in the classical simulations, in contrast with *ab initio* methods, the atomic charges and molecular geometries used in the classical force fields have been extracted from high level *ab initio* calculations[27,58] and predict dipole moments which are slightly higher than those reported experimentally for the gas phase. This is a very common approach to build effective classical potential models for liquid simulations, since due to polarization effects the dipole moments in the liquid phase are slightly higher than the gas phase ones. The effective potential models used also predict with a very good accuracy a wide range of properties of the neat liquid solvents.[27,58]

In eq 8, r_c = 2.6 Å is the distance determining the size of the solvation shell taken into account in the calculations. The calculated normalized probability density distributions $P(M_{sh})$ of the magnitude of the total dipole $M_{sh} = |\vec{M}_{sh}|$ for all the investigated systems are presented in Figure 13. From these

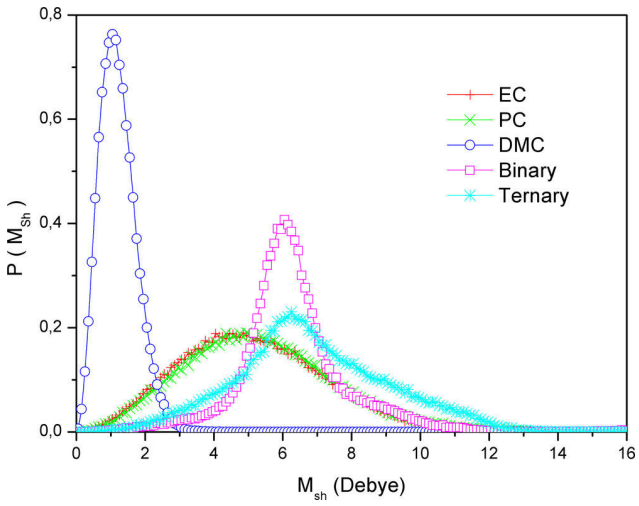

Figure 13. Calculated normalized probability density distributions $P(M_{sh})$ of the magnitude of the total dipole $M_{sh} = |\vec{M}_{sh}|$ inside the solvation shell of Li^+.

data it is clear that inside the first solvation shell of Li^+ in ternary and binary mixtures, which exhibits a high concentration of nonpolar DMC molecules, the total dipole of the solvent molecules is higher than in the cases where Li^+ is solvated by the highly polar EC and PC molecules. This finding signifies that the observed tetrahedral arrangement of the solvent molecules inside the solvation shell of Li^+ causes a cancellation of the individual molecular dipole vectors, and this cancellation is more important in the cases where molecules of the same geometry are present. When different types of solvent molecules are tetrahedrally packed inside the first solvation the resulting total dipole is higher, even though the fraction of the nonpolar DMC molecules is higher. As a result, the local environment around Li^+ becomes more polar when the fraction of DMC is higher. This observation clearly indicates that collective effects are very important in determining the local dielectric environment around a Li^+ cation, and the relative binding preferences should be determined on the basis of this collective dipole moment of the solvation shell and not in terms of pair ion−dipole interactions.

Before closing this section it would be useful to point out again that the experimental determination of the coordination number around the lithium ions in pure carbonate-based solvents has not been definitely resolved.[7−18] As it was mentioned in the Introduction, it should be however emphasized that designing experimental methods or theoretical models to analyze the experimental data in order to provide a direct measurement of the coordination number is an extremely complicated task.[7,19,20] Nevertheless, recent advances[59] in coupling theoretical methods with experiments to bias molecular simulations with experimental data tend to favor a tetrahedral-like structure, as also sophisticated polarizable models,[40] which predict a wide range of properties very close to the experimental ones. This was the main reason why a simple model, predicting a tetrahedral network around Li^+, was selected in the present treatment. In general, one of the most reliable experimental methods to extract information about the local structure in liquids is neutron diffraction. Only one neutron diffraction study of a 10 mol % solution of $LiPF_6$ in liquid PC has been reported up to now.[12] In this study the authors, by integrating the total radial distribution function $G(r)$ obtained by the diffraction experiments up to its first minimum, have estimated the coordination number around Li^+ to be 4.5. However, they have assumed that all the contributions to the total $G(r)$ at the short-range part up to 2.4 Å arise from the Li^+-O_c prdf. By inspecting the above-mentioned theoretical studies[40,59] and by performing a trial simulation of the same system, it became obvious that the Li^+-F prdf contributes to the shape of the total $G(r)$ at this short range. Therefore, a part of this 4.5 coordination number arises from the Li^+-F coordination number. However, the cation−anion coordination number at the same distance range is definitely smaller since the Li^+-F prdf and the corresponding coordination number provide information about the number of fluorine atoms inside the solvation shell of Li^+, which of course could belong to the same PF_6^- anion. As a consequence, it is very likely that the coordination number giving the total number of solvent molecules and anions around Li^+ should be smaller and could be even closer to four, or less. However, from that neutron diffraction study it is not possible to extract the separate contributions of the Li^+-O_c and Li^+-F prdfs in order to have a more accurate estimation of the total coordination number in the first solvation shell of Li^+. From this observation it becomes clear that even the interpretation of experimental data should be treated very carefully, and if it is also combined with reverse modeling techniques[60] it could provide even more valuable information.

4. CONCLUDING REMARKS

In the present study the solvation of Li^+ in pure carbonate-based solvents and their binary and ternary mixtures has been investigated, using a combination of quantum chemical DFT calculations and classical MD simulations. An analysis based on the changes in the free energy associated with the transitions between different types of clusters formed by the lithium cation and the solvent molecules has shown that the formation of complexes with four solvent molecules is the most favorable. In the cases of clusters containing EC and DMC molecules, the DFT calculations have predicted a preferential binding with EC rather than with DMC. For the clusters included at the same type EC, PC, and DMC molecules, although the $Li(EC)_2(DMC)(PC)^+$ has been predicted to be the most favorable one, the free energy changes for the transition paths

DOI: 10.1021/jp511132c
J. Phys. Chem. C XXXX, XXX, XXX−XXX

between several clusters are very small, indicating that all these structures could possibly exist in the bulk phase.

On the other hand the MD simulations have revealed the existence of significant structural heterogeneities, extending up to a length scale which is more than five times the size of the first shell radius. These heterogeneities are very important in the cases of the binary and ternary solvent mixtures, revealing very significant compositional inhomogeneities around a lithium cation. As a result of these fluctuations, the structure around Li^+ in the mixed solvents can be described in terms of a short-range structure (up to 4−5 Å from Li^+), where the composition is rich in DMC, and by a longer-range structure where in the case of the binary solvent mixture the composition is rich in EC and in the case of the ternary one is rich in PC. The local mole fractions of each solvent obtain their bulk values at more extended length scales, as it was mentioned above. This finding indicates that the collective effects arising due to the interactions between regions of different composition could possibly stabilize the local structure of the first solvation shell of Li^+.

In the DFT calculations of the finite size isolated clusters, although from an energetic point of view the preference of Li^+ to bind with the highly polar PC and EC molecules is undoubtful, from an entropic point of view the addition of DMC molecules contributes to the decrease of the free energy of the clusters. In these finite size clusters the energetic contribution seems to be the most important one. However, the small free energy differences observed for the transition paths leading from one cluster to the other indicate that the formation of these clusters should be investigated at more extended length scales in order to have a more realistic description of the effects taking place in the bulk liquid phase. The existence of significant structural fluctuations in the bulk liquid phases, extended far beyond the first solvation shell, signifies that to achieve a direct comparison between the MD and the DFT results the use of larger size clusters in DFT calculations seems to be more appropriate.

The MD simulations have also revealed that there is a very significant tetrahedral local ordering around Li^+ in all cases, and the addition of cosolvents does not distort this structural order. By calculating an entropic term associated with this local tetrahedral order around Li^+, it has also been revealed that the clusters having a high fraction of DMC molecules (three and four molecules) exhibit a higher tetrahedrality, which is reflected in the lower values of this entropic term. Therefore, from an entropic point of view the presence of DMC contributes to the stabilization of the local tetrahedral structure around Li^+.

A very interesting finding also revealed in the present study is that inside the first solvation shell of Li^+ in the ternary and binary mixtures, which exhibit a high concentration of nonpolar DMC molecules, the total dipole of the solvent molecules is higher than in the cases where Li^+ is solvated by the highly polar EC and PC molecules. The observed local tetrahedral packing of the solvent molecules in the first solvation shell of Li^+ causes a cancellation of the individual molecular dipole vectors, which seems to be more important in the cases where molecules of the same type are present. These collective effects are very important in determining the local permittivity around a Li^+ cation, and the relative binding preferences should be based upon this total dipole moment of the solvation shell and not in terms of the pair ion−dipole interactions, which is traditionally considered as the most important factor determining the preferential solvation in such systems. Further work is in progress to elucidate the impact of the above static structural features on dynamic and transport properties of the investigated electrolytes.

■ ASSOCIATED CONTENT

Supporting Information

The details of the inter- and intramolecular classical force fields employed in the present study are provided as a DL-POLY FIELD file. This material is available free of charge via the Internet at http://pubs.acs.org.

■ AUTHOR INFORMATION

Corresponding Authors

*E-mail: ioannis.skarmoutsos@cea.fr
*E-mail: stefano.mossa@cea.fr.

Notes

The authors declare no competing financial interest.

■ ACKNOWLEDGMENTS

The authors acknowledge financial support from ANR-2011 PRGE002-04 ALIBABA and DSM Energie CEA Program. Authors also acknowledge discussions with J.-S. Filhol.

■ REFERENCES

(1) Xu, K. Nonaqueous Liquid Electrolytes for Lithium-based Rechargeable Batteries. *Chem. Rev.* **2004**, *104*, 4303.
(2) Armand, M.; Tarascon, J. M. Building Better Batteries. *Nature* **2008**, *541*, 652.
(3) Kim, Y.; Goodenough, J. B. Challenges for Rechargeable Li Batteries. *Chem. Mater.* **2010**, *22*, 587.
(4) Besenhard, J. O.; Winter, M.; Yang, J.; Biberacher, W. Filming Mechanism of Lithium-Carbon Anodes in Organic and Inorganic Electrolytes. *J. Power Sources* **2005**, *54*, 228.
(5) Yuan, K.; Bian, H.; Shen, Y.; Jiang, B.; Li, J.; Zhang, Y.; Chen, H.; Zheng, J. Coordination Number of Li^+ in Nonaqueous Electrolyte Solutions Determined by Molecular Rotational Measurements. *J. Phys. Chem. B* **2014**, *118*, 3689.
(6) Eshetu, G. G.; Bertrand, J. P.; Lecocq, A.; Grugeon, S.; Laruelle, S.; Armand, M.; Marlair, G. Fire behavior of carbonates-based electrolytes used in rechargeable batteries with a focus on the role of the $LiPF_6$ and LiFSI salts. *J. Power Sources* **2014**, *269*, 804.
(7) Bogle, X.; Vazquez, R.; Greenbaum, S.; von Wald Cresce, A.; Xu, K. Understanding Li^+- Solvent Interaction in Nonaqueous Carbonate Electrolytes with ^{17}O NMR. *J. Phys. Chem. Lett.* **2013**, *4*, 1664−1668.
(8) Castriota, M.; Cazzanelli, E.; Nicotera, I.; Coppola, L.; Oliviero, C.; Ranieri, G. A. Temperature dependence of lithium ion solvation in ethylene carbonate-$LiClO_4$ solutions. *J. Chem. Phys.* **2003**, *118*, 5537−5541.
(9) Yuan, K.; Bian, H.; Shen, Y.; Jiang, B.; Li, J.; Zhang, Y.; Chen, H.; Zheng, J. Coordination Number of Li^+ in Nonaqueous Electrolyte Solutions Determined by Molecular Rotational Measurements. *J. Phys. Chem. B* **2014**, *118*, 3689−3695.
(10) Xu, K.; Lam, Y.; Zhang, S. S.; Jow, T. R.; Curtis, T. B. Solvation Sheath of Li^+ in Nonaqueous Electrolytes and Its Implication of Graphite/Electrolyte Interface Chemistry. *J. Phys. Chem. C* **2007**, *111*, 7411−7421.
(11) Smith, J. W.; Lam, R. K.; Sheardly, A. T.; Shih, O.; Rizzuto, A. M.; Borodin, O.; Harris, S. J.; Prendergast, D.; Saykally, R. J. X-Ray absorption spectroscopy of $LiBF_4$ in propylene carbonate: a model lithium ion battery electrolyte. *Phys. Chem. Chem. Phys.* **2014**, DOI: 10.1039/c4cp03240c.
(12) Kameda, Y.; Umebayashi, Y.; Takeuchi, M.; Wahab, M. A.; Fukuda, S.; Ishiguro, S.; Sasaki, M.; Amo, Y.; Usuki, T. Solvation structure of Li^+ in concentrated $LiPF_6$-propylene carbonate solutions. *J. Phys. Chem. B* **2007**, *111*, 6104−6109.

DOI: 10.1021/jp511132c
J. Phys. Chem. C XXXX, XXX, XXX−XXX

(13) Morita, M.; Asai, Y.; Yoshimoto, N.; Ishikawa, M. A Raman spectroscopic study of organic electrolyte solutions based on binary solvent systems of ethylene carbonate with low viscosity solvents which dissolve different lithium salts. *J. Chem. Soc., Faraday Trans.* **1998**, *94*, 3451−3456.
(14) Tsunekawa, H.; Narumi, A.; Sano, M.; Hiwara, A.; Fujita, M.; Yokoyama, H. Solvation and Ion Association Studies of $LiBF_4$-Propylenecarbonate-Trimethyl Phosphate Solutions. *J. Phys. Chem. B* **2003**, *107*, 10962−10966.
(15) Nie, M.; Abraham, D. P.; Seo, D. M.; Chen, Y.; Bose, A.; Lucht, B. L. Role of Solution Structure in Solid Electrolyte Interphase Formation on Graphite with $LiPF_6$ in Propylene Carbonate. *J. Phys. Chem. C* **2013**, *117*, 25381−25389.
(16) Li, Y.; Xiao, A.; Lucht, B. L. Investigation of solvation in lithium ion battery electrolytes by NMR spectroscopy. *J. Mol. Liq.* **2010**, *154*, 131−133.
(17) Kondo, K.; Sano, M.; Hiwara, A.; Takehiko, O.; Fujita, M.; Kuwae, A.; Iida, M.; Mogi, K.; Yokoyama, H. Conductivity and Solvation of Li^+ Ions of $LiPF_6$ in Propylene Carbonate Solutions. *J. Phys. Chem. B* **2000**, *104*, 5040−5044.
(18) Barthel, J.; Buchner, R.; Wismeth, E. FTIR Spectroscopy of Ion Solvation of $LiClO_4$ and LiSCN in Acetonitrile, Benzonitrile and Propylene Carbonate. *J. Solution Chem.* **2000**, *29*, 937−954.
(19) Buchner, R. Dielectric Spectroscopy of Solutions. In *Novel Approaches to the Structure and Dynamics of Liquids: Experiments, Theories and Simulations*; Samios, J., Durov, V. A., Eds.; Kluwer Academic Publishers: The Netherlands, 2004; p 265.
(20) Ravel, B.; Kelly, S. D. Difficult Chore of Measuring Coordination by EXAFS. *AIP Conf. Proc.* **2007**, *882*, 150−152.
(21) te Velde, G.; Bickelhaupt, F. M.; van Gisbergen, S. J. A.; Fonseca Guerra, C.; Baerends, E. J.; Snijders, J. G.; Ziegler, T. Chemistry with ADF. *J. Comput. Chem.* **2001**, *22*, 931−967.
(22) Perdew, J. P.; Burke, K.; Ernzerhof, M. Generalized gradient approximation made simple. *Phys. Rev. Lett.* **1996**, *77*, 3865−3868.
(23) Boys, S. F.; Bernardi, F. Calculation of Small Molecular Interactions by Differences of Separate Total Energies − Some Procedures with Reduced Errors. *Mol. Phys.* **1970**, *19*, 553.
(24) Bhatt, M. D.; Cho, M.; Cho, K. Interaction of Li^+ ions with ethylene carbonate (EC): Density Functional Theory calculations. *Appl. Surf. Sci.* **2010**, *257*, 1463−1468.
(25) Bhatt, M. D.; O'Dwyer, C. Density functional theory calculations for ethylene carbonate-based binary electrolyte mixtures in lithium ion batteries. *Curr. Appl. Phys.* **2014**, *14*, 349−354.
(26) Martínez, L.; Andrade, R.; Birgin, E. G.; Martínez, J. M. PACKMOL: A Package for Building Initial Configurations for Molecular Dynamics Simulations. *J. Comput. Chem.* **2009**, *30*, 2157−2164.
(27) Soetens, J. C.; Millot, C.; Maigret, B. Molecular Dynamics Simulation of $Li^+BF_4^-$ in Ethylene Carbonate, Propylene Carbonate and Dimethyl Carbonate Solvents. *J. Phys. Chem. A* **1998**, *102*, 1055−1061.
(28) Masia, M.; Probst, M.; Rey, R. Ethylene Carbonate-Li^+: A Theoretical Study of Structural and Vibrational Properties in Gas and Liquid Phases. *J. Phys. Chem. B* **2004**, *108*, 2016−2027.
(29) Katon, J. E.; Cohen, M. D. Conformational Isomerism and Oriented Polycrystal Formation of Dimethyl Carbonate. *Can. J. Chem.* **1974**, *52*, 1994−1996.
(30) Katon, J. E.; Cohen, M. D. The Vibrational Spectra and Structure of Dimethyl Carbonate and its Conformational Behavior. *Can. J. Chem.* **1975**, *53*, 1378−1386.
(31) Thiebaut, J. M.; Rivail, J. L.; Greffe, J. L. Dielectric Studies of non Electrolyte Solutions. *J. Chem. Soc., Faraday Trans.2* **1976**, *72*, 2024−2034.
(32) Smith, W.; Forester, T. R. Parallel macromolecular simulations and the replicated data strategy: II. The RD-SHAKE algorithm. *Comput. Phys. Commun.* **1994**, *79*, 63−77.
(33) Ryckaert, J. P.; Ciccotti, G.; Berendsen, H. J. C. Numerical integration of the Cartesian equations of motion of a system with constraints: molecular dynamics of n-alkanes. *J. Comput. Phys.* **1977**, *23*, 327−341.
(34) Allen, M. P.; Tildesley, D. J. *Computer Simulations of Liquids*; Oxford University Press: Oxford, 1987.
(35) Hoover, W. G. Canonical dynamics: Equilibrium phase-space distributions. *Phys. Rev. A* **1985**, *31*, 1695−1697.
(36) Hoover, W. G. Constant pressure equations of motion. *Phys. Rev. A* **1986**, *34*, 2499−2500.
(37) Smith, W.; Forester, T. R. DL_POLY_2.0: A general-purpose parallel molecular dynamics simulation package. *J. Mol. Graphics* **1996**, *14*, 136−141.
(38) McQuarrie, D. A.; Simon, J. D. *Molecular Thermodynamics*; University Science Books: Virginia, 1999.
(39) Swart, M.; Rösler, E.; Bickelhaupt, F. M. Proton Affinities of Maingroup-Element Hydrides and Noble Gases: Trends Across the Periodic Table, Structural Effects, and DFT Validation. *J. Comput. Chem.* **2006**, *27*, 1486.
(40) Borodin, O.; Smith, G. D. Quantum Chemistry and Molecular Dynamics Simulation Study of Dimethyl Carbonate: Ethylene Carbonate Electrolytes Doped with $LiPF_6$. *J. Phys. Chem. B* **2009**, *113*, 1763−1776.
(41) Takeuchi, M.; Kameda, Y.; Umebayashi, Y.; Ogawa, S.; Sonoda, T.; Ishiguro, S.; Fujita, M.; Sano, M. Ion-ion interactions of $LiPF_6$ and $LiBF_4$ in propylene carbonate solutions. *J. Mol. Liq.* **2009**, *148*, 99−108.
(42) Takeuchi, M.; Matubayashi, N.; Kameda, Y.; Minofar, B.; Ishiguro, S.; Umebayashi, Y. Free-Energy and Structural Analysis of Ion Solvation and Contact Ion-Pair Formation of Li^+ with BF_4^- and PF_6^- in Water and Carbonate Solvents. *J. Phys. Chem. B* **2012**, *116*, 6476−6487.
(43) Postupna, O. O.; Kolesnik, Y. V.; Kalugin, O. N.; Prezhdo, O. V. Microscopic Structure and Dynamics of $LiBF_4$ Solutions in Cyclic and Linear Carbonates. *J. Phys. Chem. B* **2011**, *115*, 14563−14571.
(44) Bhatt, M. D.; Cho, M.; Cho, K. Density Functional theory calculations and ab initio molecular dynamics simulations for diffusion of Li^+ within liquid ethylene carbonate. *Modelling Simul. Mater. Sci. Eng.* **2012**, *20*, 065004.
(45) Tenney, C. M.; Cygan, R. T. Analysis of Molecular Clusters in Simulations of Lithium-Ion battery Electrolytes. *J. Phys. Chem. C* **2013**, *117*, 24673−24684.
(46) Jorn, R.; Kumar, R.; Abraham, D. P.; Voth, G. A. Atomistic Modeling of the Electrode-Electrolyte Interface in Li-Ion Energy Storage Systems: Electrolyte Structuring. *J. Phys. Chem. C* **2013**, *117*, 3747−3761.
(47) Ganesh, P.; Jiang, D.; Kent, P. R. C. Accurate Static and Dynamic Properties of Liquid Electrolytes for Li-Ion Batteries from ab initio Molecular Dynamics. *J. Phys. Chem. B* **2011**, *115*, 3085−3090.
(48) Li, T.; Balbuena, P. Theoretical Studies of Lithium Perchlorate in Ethylene Carbonate, Propylene Carbonate, and Their Mixtures. *J. Electrochem. Soc.* **1999**, *146*, 3613−3622.
(49) Skarmoutsos, I.; Dellis, D.; Samios, J. Investigation of the local composition enhancement and related dynamics in supercritical CO_2-cosolvent mixtures: The case of ethanol in CO_2. *J. Chem. Phys.* **2007**, *126*, 224503.
(50) Errington, J. R.; Debenedetti, P. G. Relationship between structural order and the anomalies of liquid water. *Nature* **2001**, *409*, 318.
(51) Kumar, P.; Buldyrev, S. V.; Stanley, H. E. A tetrahedral entropy for water. *Proc. Natl. Acad. Sci. U.S.A.* **2009**, *106*, 22130−22134.
(52) Lazaridis, T.; Karplus, M. Orientational Correlations and entropy in liquid water. *J. Chem. Phys.* **1996**, *105*, 4294−4315.
(53) Lazaridis, T.; Paulaitis, M. E. Simulation studies of the hydration entropy of simple, hydrophobic solutes. *J. Phys. Chem.* **1994**, *98*, 635−642.
(54) Zielkiewicz, J. Two-particle Entropy and Structural Ordering in Liquid Water. *J. Phys. Chem. B* **2008**, *112*, 7810−7815.
(55) Guardia, E.; Skarmoutsos, I.; Masia, M. Hydrogen Bonding and Related Properties in Liquid Water: A Car-Parrinello Molecular

DOI: 10.1021/jp511132c
J. Phys. Chem. C XXXX, XXX, XXX−XXX

Dynamics Simulation Study. *J. Phys. Chem. B* **2014**, DOI: 10.1021/jp507196q.
(56) von Wald Cresce, A.; Xu, K. Preferential Solvation of Li^+ Directs Formation of Interphase on Graphitic Anode. *Electrochem. Solid-State Lett.* **2011**, *14*, A154−A156.
(57) Borodin, O. Molecular Modeling of Electrolytes. In *Electrolytes for Lithium and Lithium-Ion Batteries*; Jow, T. R., Xu, K., Borodin, O., Ue, M., Eds.; Modern Aspects of Electrochemistry 58; Springer: New York, 2014; pp 371−395.
(58) Soetens, J. C.; Millot, C.; Maigret, B.; Bakó, I. Molecular Dynamics simulation and X-Ray diffraction studies of ethylene carbonate, propylene carbonate and dimethyl carbonate in liquid phase. *J. Mol. Liq.* **2001**, *92*, 201−216.
(59) White, A. D.; Voth, G. A. Efficient and Minimal Method to Bias Molecular Simulations with Experimental Data. *J. Chem. Theory Comput.* **2014**, *10*, 3023−3030.
(60) Soper, A. K. Computer simulation as a tool for the interpretation of total scattering data from glasses and liquids. *Mol. Simul.* **2012**, *38*, 1171−1185.

DOI: 10.1021/jp511132c
J. Phys. Chem. C XXXX, XXX, XXX−XXX

6

Conclusions and Perspectives

We have investigated the most important component in batteries is called as electrolytes, which can be involved in transport properties, high energy densities, long cycle life and wide-range temperature applications etc . The carbonate solvents are playing important role in batteries. These electrolytes were studied using the combinations of both quantum chemical density functional theory (DFT) and classical Molecular Dynamics simulations. By studying the pure and mixture of carbonate solvent electrolytes with lithium salt, we have been able to demonstrate the most stable local structure around lithium ion, component of solvents in the first shell with particular compositions and the most preferable solvent.

In our study, we have considered the typical most commonly used solvents such as cyclic Ethylene carbonate(EC), Propylene carbonate(PC) and linear Dimethyl carbonate(DMC). The DFT calculations have been performed for pure systems $Li^+(S)_n$ (S=EC, DMC, PC and n = 1-5) and binary mixtures $Li^+(S_1)_n(S_2)_m$ (S_1, S_2 =EC, PC, DMC, with m+n=4), and ternary clusters $Li^+(EC)_l(DMC)_m(PC)_n$ with l+m+n=4. Moreover, the pure solvent clusters were also studied including the effect of PF_6^- anion. For MD simulations, we were considered the following systems at infinite dilution i) Pure solvent clusters with Li^+ ion ii) binary mixture EC:DMC with a equivalent molar composition of 1:1 with Li^+ ion and iii) the ternary mixture EC:DMC:PC with 1:1:3 molar ratio with Li^+ ion, respectively.

As based on the DFT results, the changes in the free energy during the transitions between different types of clusters formed by the lithium cation and the solvent molecules has shown that the formation of complexes with four solvent molecules is the most favourable. The solvents were arranged in a tetrahedral geometry which is observed in all cases such as pure and mixtures. In the case of Li^+ PC clusters, the smallest difference in free energies of $Li^+(PC)_3$ and $Li^+(PC)_4$ clusters suggest that both configurations could possibly exist in the bulk solution. Our results were adapted with several theoretical as well as experimental findings. In the cases of $Li^+(S)_5$ (S=EC, DMC, PC) clusters,

the fifth solvent molecules were arranged very far from the central Li^+ ion, explains the Li^+ ion can accommodate four molecules in the first solvation shell and extra molecules could participate in the second solvation shell and free energy also predicts the same as $Li^+(S)_4$ is most stable. We have predicted the $Li^+(S)_2PF_6^-$ cluster to be the most stable in the case of pure solvents with $LiPF_6$ salt and a solvent molecule can not replace the PF_6^- anion from the most stable $Li^+(S)_2PF_6^-$ cluster.

The same DFT free energy results in binary clusters found that $Li^+(EC)_2(PC)_2$ is most stable than other possible clusters in EC:PC mixtures, saying both EC and PC molecules approach the Li^+ ion with equal participation and there is no preferential solvation occurred. However, in both cases of Li^+ EC:DMC and Li^+ PC:DMC mixtures where the $(EC)_3(DMC)$ and $(PC)_3(DMC)$ clusters are more stable than other corresponding possible clusters. Therefore, our DFT calculations have predicted a preferential binding obtained with EC or PC rather than with DMC. In ternary mixtures, the cluster $Li^+(EC)_2(DMC)(PC)$ has been predicted to be the most favourable one, the free energy changes for the transition paths between several clusters are very small, indicating that all these structures could possibly exist in the bulk phase.

Our MD results have shown that the local solvation structure consists of four solvent molecules around Li^+ ion in a tetrahedral geometry. We have found the first peak separation of Li^+ Oc(carbonyl oxygen) at 1.78 Å which is almost comparable with DFT results where the typical distance is 1.93 Å. Due to the inhomogeneties around lithium ion in binary and ternary mixtures, the fluctuations could be described in terms of a short range structure (up to 4-5 Å from Li^+) where the composition is rich in DMC and by a longer-range structure where in the case of the binary solvent mixture the composition is rich in EC and in the case of the ternary one it is rich in PC. Such a finding indicates that the collective effects arising due to the interactions between regions of different composition could possibly stabilize the local structure of the first solvation shell of Li^+.

The MD simulations have also revealed that there is a very significant tetrahedral local ordering around Li^+ in all cases and the addition of cosolvents does not distort this structural order. By calculating an entropic term associated with this local tetrahedral order around Li^+, it has also been revealed that the clusters having a high fraction of DMC molecules (3 and 4 molecules) exhibit a higher tetrahedrality, which is reflected in the lower values of this entropic term. Therefore, from an entropic point of view the presence of DMC contributes to the stabilization of the local tetrahedral structure around Li^+.

A very interesting finding also revealed in the present study is that inside the first solvation shell of Li^+ in the ternary and binary mixtures, which exhibit a high concentration of non-polar DMC molecules, the total dipole of the solvent molecules is higher than in the cases where Li^+ is solvated by the highly polar EC and PC molecules. The observed local tetrahedral packing of the solvent molecules in the first solvation shell of Li^+

causes a cancellation of the individual molecular dipole vectors, which seems to be more important in the cases where molecules of the same type are present. These collective effects are very important in determining the local permittivity around a Li^+ cation and the relative binding preferences should be based upon this total dipole moment of the solvation shell and not in terms of the pair ion dipole interactions, which is traditionally considered as the most important factor determining the preferential solvation in such systems.

Most of our DFT results were comparable with MD results, but still our work also has some limitations. In the DFT calculations of the finite size isolated clusters, from an energetic point of view the preference of Li^+ to bind with the highly polar PC and EC molecules. However, the MD results found DMC is a most preferable solvent than EC and PC molecules. The finite size cluster effects in DFT could possibly affect the direct comparisons with MD results. In these finite size clusters the energetic contribution seems to be the most important one. Therefore, we have investigated the binary and ternary mixtures at more extended length scales in order to have a more realistic description of the effects taking place in the bulk liquid phase. The existence of significant structural fluctuations in the bulk liquid phases, extended far beyond the first solvation shell, signifies that to achieve a direct comparison between the MD and the DFT results the use of larger size clusters in DFT calculations seems to be more appropriate.

Finally, our perspective of work is to analyse the typical life time of the clusters in order to understand the transport properties of lithium ion. In our results, we have reported the second solvation is rich of EC concentration, probably it could be involved in the lithium ion transport. Therefore, if we could perform the DFT analysis including the second solvation shells, we could give a detailed description of the influence of second solvation shell. Indeed, the DFT calculations should be taken too much computational time in order to perform the optimization with around 120 atoms.

7

Chapitre 1: Introduction et motivations

Dans la première section de ce chapitre, nous décrivons brièvement les dispositifs les plus importants qui sont utilisés pour le stockage de l'énergie. Ensuite, nous nous concentrons principalement sur les batteries rechargeables, les batteries lithium-ion en particulier, et leurs principaux composants tels que l'électrolyte. Puis, nous établierons un aperçu général ainsi que l'état de l'art des propriétés et applications des différents solvants carbonate tels que le carbonate d'éthylène, le carbonate de diméthyle et les carbonates de propylène pures et en présence de sels, comme le $LiPF_6$. Dans les sections suivantes, nous allons présenter ce qui nous a poussé à introduire des mélanges de solvants et fournir un aperçu de la littérature la plus récente. Enfin, nous allons préciser nos principales motivations pour ce travail et donner un aperçu général du manuscrit.

Introduction

Une augmentation de la demande énergétique mondiale et les répercussions environnementales associées sont les questions les plus importantes dans la société moderne. Dans les deux dernières décennies, la nécessité du stockage d'énergie efficace a augmenté de façon spectaculaire. En effet, des dispositifs tels que les voitures, les véhicules électriques, les téléphones cellulaires, les téléviseurs, sont utilisés dans la vie quotidienne, mais une fraction importante de l'énergie nécessaire à leur fonctionnement provient toujours de combustibles fossiles comme le pétrole, le gaz naturel ou le charbon. Malheureusement, ces classes de combustibles sont les plus importants responsables de la production des gaz à effet de serre, lequel nuit gravement à l'environnement. Afin de réduire la grande quantité d'émission de dioxyde de carbone dans l'atmosphère, les sources d'énergie de remplacement sont nécessaires. Différentes technologies ont été introduites dans le passé, tels que les cellules solaires, les batteries, les piles à combustible

et supercondensateurs. L'électricité verte ou les énergies renouvelables ont été générées avec succès à partir du vent ou de sources naturelles solaires, qui sont malheureusement en corrélation avec les conditions climatiques et donc fortement fluctuantes dans le temps. En conséquence, les grands dispositifs de stockage d'énergie à grande échelle sont maintenant fondamentale, pour stocker l'énergie sur de longues échelles de temps avec une bonne compatibilité avec l'environnement. La conversion d'énergie électrochimique est le domaine de recherche clé pour les sources d'énergie alternatives.

Les dispositifs de conversion et de stockage d'énergie électrochimique comprennent les piles à combustible, les batteries et les super condensateurs. Ces technologies sont largement utilisés dans plusieurs applications telles que les appareils portables, les transports, les industries [3–7]. Bien que les mécanismes de conversion d'énergie et la stratégie de stockage utilisés dans ces dispositifs sont différents, ils présentent des caractéristiques communes comme un processus fournissant l'énergie qui a lieu à l'inter-phase entre trois segments: anode, électrolyte et de cathode. Plus précisément, tous les dispositifs sont constitués par deux électrodes qui sont séparées par la solution d'électrolyte [3, 4, 6, 8, 9]. L'énergie chimique est convertie en énergie électrique par des réactions d'oxydo-réduction dans les piles et les piles à combustible. Dans le cas des supercondensateurs électrochimiques, l'énergie est stockée à partir de l'accumulation des charges à l'interface entre l'électrode et l'électrolyte, dans lequel il n'e se produit pas de réaction chimique. Dans ce qui suit, nous discutons brièvement la composition des matériaux, les mécanismes de conversion de l'énergie et le fonctionnement de tous les appareils.

Les piles à combustible [9] sont des dispositifs qui convertissent l'énergie chimique fournie comme un combustible en énergie électrique par une réaction chimique d'oxydation de l'oxygène. Nous montrons un exemple de pile à combustible à la [1] in Figure 7.1(b). Ce dispositif diffère sensiblement de batteries, nécessitant des sources constantes de combustibles et de l'oxygène pour que la réaction chimique se produise. Les piles à combustible fournissent de l'énergie avec une efficacité de plus de 80%, sont éco-compatibles et sont principalement utilisés dans les applications stationnaires [10] et les transports. L' électrolyte polymère (ou échange de protons) de piles à combustible à membrane (PEMFC) [11] est principalement utilisé dans les appareils fixes, de l'automobile et portables. Dans la PEMFC, la conductivité protonique élevée est obtenue en présence d'eau. Ses propriétés comprennent: stabilité à l'oxydation, électro-osmose, faible transport de l'eau et une faible conductivité électronique [8]. Le rôle de la PEMFC est qu'elle permet le transport des protons de l'anode à la cathode. Cette membrane est principalement constituée de polymères organiques contenant des groupes fonctionnels acides tels que sulfonique, carboxylique et des groupes d'acides phosphoniques. Dans laquelle, il se dissocie en présence d'eau pour permettre H_3O^+ transport des protons hydratés [11]. L'inconvénient principal d'une pile à combustible est qu'il ne peut produire de l'électricité en continu qu'aussi longtemps que le carburant est fourni. Les batteries

[1] http://en.wikipedia.org/wiki/Fuel-cell

sont donc nécessaires pour le stockage de l'électricité produite, comme nous le verrons ci-dessous.

Les piles primaires [8, 12] sont des dispositifs qui ne peuvent être utilisés qu'une seule fois et sont ensuite rejetés, car ils ne peuvent pas être rechargés en électricité, contrairement aux piles secondaires . Les réactions électrochimiques qui se produisent dans la cellule ne sont pas réversibles et la batterie cesse de fonctionner lorsque les réactions sont complètes. En 1860, Leclanché invente la première pile primaire, consistant en une cellule zinc-carbone[2], comme le montre la figure 7.1(a). Nature du dioxyde de manganèse noir de carbone a été employée en tant que cathode et l'électrolyte est une combinaison de chlorure d'ammonium et de zinc chlorure contenus dans une gaine en zinc. L'oxyde de manganèse synthétique a, par la suite, donné de meilleures performances que l'oxyde de manganèse naturel. Le carbone-zinc avec batterie chlorure de zinc pour électrolyte primaire a la même performance que le zinc-manganèse et est mieux vendu dans le monde entier à partir de 2003. L'alcaline hydroxyde électrolyte de potassium (KOH) en zinc-manganèse est principalement utilisé dans les batteries primaires, car il fournit une meilleure performance que la cellule carbone zinc. En outre, le même électrolyte a été utilisé dans de nombreux équipements électroniques et aussi plus fiable dans des applications de haute énergie. Il existe plusieurs type de cellules primaires: chlorure de thionyle de lithium, l'oxyde de zinc-argent, les cellules lithium-dioxyde de soufre. Les cellules primaires au lithium sont plus largement utilisées que les cellules alcalines, en raison de la densité d'énergie élevée. Le lithium métallique est utilisé comme anode dans les piles au lithium et la tension dépasse 3,7 V, en raison du fort potentiel négatif de lithium. L'inconvénient des cellules au lithium est une capacité de débit inférieure, en raison d'un électrolyte non aqueux à faible conductivité. L'interphase électrode solide (SEI) (isolant électroniquement film qui permet sélectivement le transport des ions lithium) peut facilement être formée dans les cellules au lithium. D'autres cellules primaires$Li-SOCl_2$ et $Li-SO_2$ sont utilisées dans des applications à large gamme de température ainsi que dans des applications telles que les transpondeurs, l'équipement militaires et l' électronique automobiles.

Récemment, *les condensateurs électrochimiques* [6] ou *ultra condensateurs* [13, 14] ont considérablement attiré l'attention en raison de leur densité de puissance élevée, leur long cycle de vie ((>100 000 cycles), leur charge et décharge rapide ainsi que leur puissance de sortie élevée. leur performance de livraison de puissance qui remplit parfaitement l'écart [15] entre les piles / cellules de carburant (stockage de haute énergie) et les condensateurs diélectriques traditionnels (puissance de sortie élevée) [14]. Ils agissent également en tant que dispositifs de stockage d'énergie temporaire, lorsqu'ils sont associés aux piles à combustible et aux batteries. Un super-condensateur électrochimique [3] est illustrée à la Figure 7.1(c) Il ya cependant quelques inconvénients, tels que les coûts

[2]http://www.daviddarling.info/encyclopedia/L/Leclanche-cell.html
[3]https://gigaom.com/2011/07/12/how-ultracapacitors-work-and-why-they-fall-short

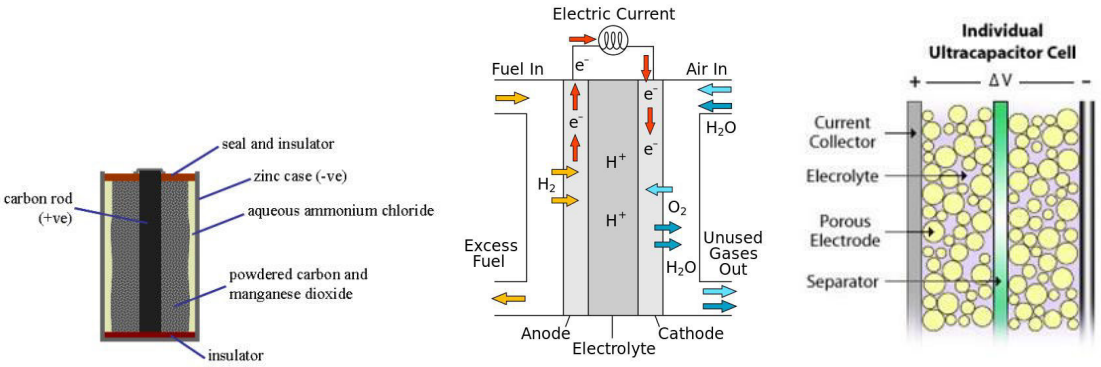

(a) Primaire (Leclanché) Cell (b) des Piles à Combustible (c) Condensateur

FIGURE 7.1: des dispositifs électrochimiques tels que a) la cellule primaire ou Leclanché, se compose d'une anode (tige de zinc) et la cathode une plaque de carbone entourée par du dioxyde de manganèse à remplissage et les électrodes ont été plongées dans une solution d'ammonium et de zinc chlorures b) Pile à combustible conductrice de protons c) Représentation schématique de supercondensateurs caractérisés par deux plaques métalliques appelés électrodes immergées dans un électrolyte

de production élevés et une faible densité énergétique. Deux grandes classes de condensateurs électrochimiques sont utilisés, super-condensateurs redox de pseudo-condensateur et condensateurs électriques à double couche (EDLC). La différence entre ces condensateurs est que les réactions redox réversibles comportent entre l'électrolyte et les espèces électro-actives sur la surface d'électrode en pseudo-condensateur mais aucune réaction dans EDLC [13].

Récemment, les condensateurs lithium-ion (LICs) ont attirés l'attention des chercheurs pour leur capacité à atteindre une densité d'énergie de niveau de batterie avec la densité de puissance des super-condensateurs. Toutefois, le déséquilibre cinétique des électrodes dans les LIC reste un problème et en vue de surmonter ce problème, du graphène fonctionnalisé est utilisé pour équilibrer la cinétique et conduit à un stockage du lithium [16]. En outre, les groupes fonctionnels d'oxyde de graphène cathode agissent avec des centres radicaux qui stockent le lithium à haut potentiel. [17]

Ce travail de thèse se concentre particulièrement sur les batteries lithium-ion secondaires que nous discutons dans la section suivante.

Piles Rechargeables

Parmi les différentes technologies de stockage, les batteries sont les dispositifs les plus efficaces et robustes. Les batteries convertissent l'énergie chimique en énergie électrique ou vice-versa, par des réactions chimiques d'oxydation-réduction réversibles. La première batterie rechargeable a été basée sur des electrodes nickel-cadmium (Ni-Cd) et le sel

alcalin (KOH) comme électrolyte [8]. Le métal Ni constitue l'électrode positive (cathode), dont la fonction est d'insérer / désinsérer les protons pendant le chargement / déchargement. La cathode Ni est en réalité une électrode de $Ni(OH)_2$. Le Cd constitue l'électrode négative (anode), qui fonctionne de manière réversible, et le produit de décharge est $Cd(OH)_2$. En raison de caractère toxique de Cd et une densité énergétique médiocre, ce dispositif a été remplacé par le nickel-métal hydrure (Ni-MH). Bien que, Ni-MH a une capacité de stockage d'énergie élevée pour une faible densité. Ceci n'a pas fonctionner correctement à des températures basses, cependant il a joué un rôle important dans l'évolution des véhicules électriques, des moteurs et pour le marché de l'appareil électronique portable.

En raison des inconvénients cités ci-dessus des piles au nickel-métal, un nouveau type de batterie est développé, la **pile au lithium**. En particulier, les batteries lithium-ion (LIB) ont été utilisées depuis quelques décennies et avec un succès particulier dans une large gamme de technologies, y compris les appareils électroniques portables et de nouvelles applications de l'automobile, en raison de leur efficacité énergétique élevée (>90 %), une bonne densité de stockage d'énergie, et une longue durée de cyclisme (>5000 de cycle). D'autres technologies explorées, tels que l'acide de plomb, le nickel-cadmium et nickel-hybride [2, 18–22] piles ont été démontrées être bien adaptées pour de telles applications, en raison de la faible densité énergétique par rapport aux batteries lithium-ion. La comparaison des densités d'énergie de différentes classes de batteries est présentée dans la Figure 7.2. Le développement de l'électrochimie de la Li-ion a été la plupart du temps en raison de son faible rayon ionique et de bas poids moléculaire, propriétés bénéfiques pour la diffusion. En outre, il a un faible potentiel redox $E^{\circ}(Li^{+}/Li) = -3.04V$ [23] par rapport à SHE (électrode standard hydrogène) de sorte qu'il peut facilement réduire. Ce processus cré une différence de potentiel entre les électrodes et le transport de lithium également obtenus. De plus le lithium est plus stable par rapport à des solvants non aqueux. Dans un premier temps, le lithium a été utilisé dans des batteries primaires, et après quelques décennies, il est maintenant le composant principal de batteries rechargeables [12]. La tension des capacités et l'exploitation de LIB sont 700-2400 mA.h et $\sim$ 3,6 V, respectivement. La température de fonctionnement du LIB varie entre °C [24]. Malheureusement, à basse température, (< 15 °C), la capacité devient assez faible, tandis que à haute température, (> 60 °C), la dégradation des matériaux d'électrode devient importante. Les pionniers Goodenough et Whittingham [25] avaient développé des matériaux pour la cathode des batteries lithium-ion en 1970. La première batterie au lithium-ion commerciale a été produite par Sony Co. en 1991 [26] et a été fondée sur LiCoO2 et la coke de pétrole. On montre un diagramme schématique d'une batterie lithium-ion sur la Figure 7.3(a).

Après 1991, le développement de la LIB a considérablement augmenté, en particulier au cours des deux dernières décennies. LIB sont exploitées dans des applications de haute densité énergétique et leur potentiel est étudié pour une utilisation sur véhicules

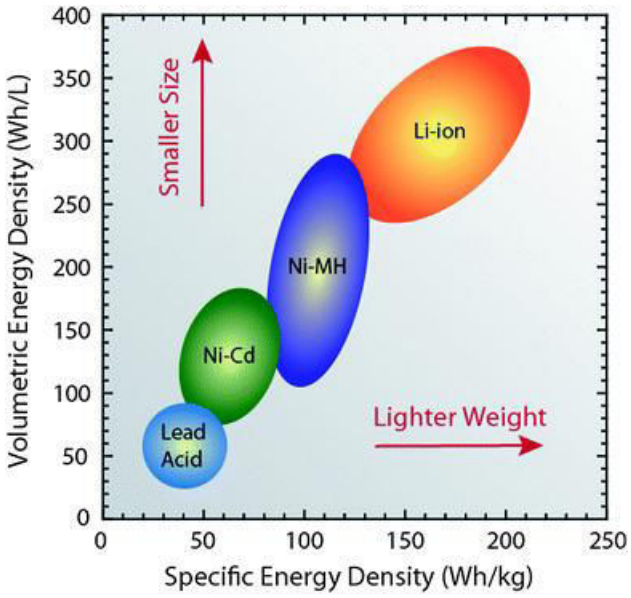

FIGURE 7.2: Comparaison des technologies de batteries rechargeables en fonction de densités d'énergie volumique et spécifiques. Figure de la référence [1]

électrique (EV), électrique hybride (HEV) et Plug-in Hybrid (PHEV) [24], en remplacement de la combustion interne des moteurs (IC) qui utilise des combustibles fossiles, diesel ou essence, pour produire de l'électricité.

Une batterie au lithium-ion normale est composée d'un carbone négatif (généralement en graphite) et d'une anode d'oxyde métallique en couche solide (par exemple $LiT^{M}O_2$, où T est un métal de transition) en tant que cathode. Ces deux électrodes sont les sources de réactions chimiques et sont séparées par un électrolyte (lithium-ion milieu conducteur), qui se compose de sels de lithium (par exemple, $LiPF_6$) et les solvants organiques (par exemple, le carbonate d'éthylène). Les réactions sont démarrées lorsque les électrodes sont connectées à une charge externe et le flux d'électrons se produit à partir de l'anode vers la cathode. En inversant le processus, la batterie peut être rechargée par l'application d'un courant extérieur. Pendant la charge, les ions lithium sont desintercalés (intercalation hôte) à partir de la cathode (par exemple, en couches $LiCoO_2$[27]) qui intercale entre les couches de graphite qui passe à travers l'électrolyte. La décharge est un processus inverse.

Durant l'intercalation / désintercalation, les réactions se produisent dans l'électrolyte, qui se décompose et forme l'électrolyte solide entre phases (SEI) [28–34]. Le SEI est formée à la surface de l'anode de graphite, où le graphite est transformé en une autre forme LiCx, où LiC_6 est le plus haut degré d'intercalation. Les SEI ont été étudiées à l'aide de rayons X et elles comprenent des composés tels que l'oxalate de lithium ($Li_2C_2O_4$), le méthylate de lithium ($LiOCH_3$) et de succinate de lithium ($LiO_2CCH_2CH_2CO_2Li$) [35] respectivement. En outre, la performance de l'anode de graphite est largement déterminée par les caractéristiques spécifiques du film SEI. De nombreux facteurs permettent de contrôler la composition chimique du SEI, par exemple, le choix des solvants

et du sel de l'électrolyte, la température de fonctionnement, la nature de la surface, le type d'anode etc. La couche SEI empêche la corrosion de surface à l'électrode, réaction de décomposition de l'électrolyte. Au cours de l'étude de la formation de la couche de SEI, le carbonate d'éthylène solvant est impliqué dans la formation ultérieure SEI. Un contrôle en profondeur de la composition, la morphologie et la structure du SEI sont nécessaires afin de concevoir de meilleurs électrodes et compositions d'électrolyte [27], ce qui est l'objectif le plus important dans la technologie LIB.

Dans les *piles métal-air*, les réactions de désintercalation et d'intercalation affectent la densité énergétique des batteries au lithium-ion. Cette problématique a entraîné le développement d'une approche, batteries métal-air alternative [36–40]. Dans ces piles, le matériau d'intercalation de cathode est remplacé par de l'oxygène réaction catalytique de réduction (ORR) et la réaction de dégagement d'oxygène (OER). Les batteries métal-air telles que les batteries Li-air et air-Zn sont largement utilisées en raison de leur haute densité d'énergie, leur respect de l'environnement et leur faible coût. Une batterie Li-air [4] est illustré à la Figure 7.1(b).

Elle génèrent de l'électricité par une réaction d'oxydoréduction entre le métal et de l'oxygène dans l'air. Les batteries métal-air sont également confrontées à des problèmes comme une faible efficacité de l'anode, une densité d'énergie limitée de la cathode, et une propension élevée à la corrosion de l'anode en contact avec l'électrolyte. La formation d'hydroxydes, d'oxydes métalliques et d'autres espèces qui se accumulent à la surface de l'anode empêche le processus de décharge. Dans la section suivante, nous verrons les électrolytes.

Électrolytes dans Batteries: Fondements

Les électrolytes sont une composante essentielle pour tous les dispositifs électrochimiques décrits ci-dessus. Les électrolytes sont constitués par des sels (solutés) dissous dans des solvants et ils agissent en tant que milieu conducteur qui transfère les charges ou les ions entre les électrodes. Les performances des dispositifs dépendent à la fois de l'électrolyte et des matériaux d'électrode. Le matériau de l'électrolyte doit être compatible chimiquement avec les électrodes pour éviter des problèmes de stabilité et les réactions chimiques qui ont lieu, il faut contrôler à la fois la quantité d'électrolyte et la vitesse de l'énergie libérée vers les électrodes. En outre, des electrolytes doivent être hautement stable ou complètement inerte lors du contact avec la surface de l'électrode, sinon ils ne parviennent pas à produire des densités d'énergie élevées. La vitesse de la décomposition des réactions réductrice et oxydante est contrôlée par la concentration d'électrolyte.

Afin de développer de meilleurs électrolytes quelques questions devraient être examinées [12]: *1)* plage de température pour la stabilité. Par exemple, le solvant EC est solide à la

[4] http://www.transportation.anl.gov/features/2009-Li-air-batteries.html

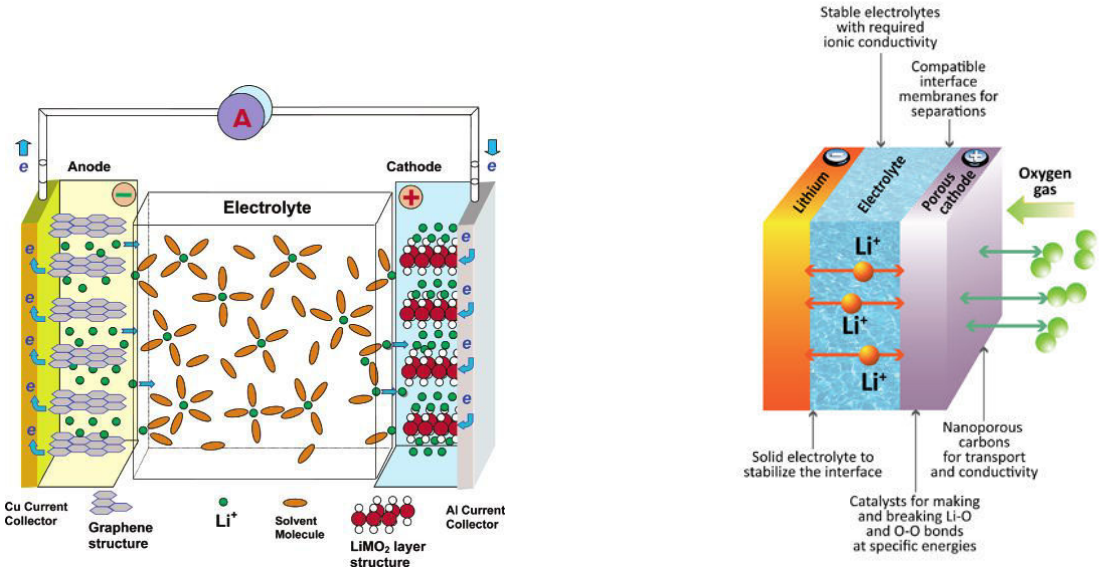

(a) au lithium-ion (b) Batterie Lithium-Air

FIGURE 7.3: piles au lithium types: a) Schéma de la batterie au lithium-ion (LIB) constitué de l'électrode positive (composé de Li-intercalation et l'électrode négative (de carbone graphitique) séparées par l'électrolyte, figure de référence [2], b) de la batterie Li-air se compose de cathode à air catalytique qui fournit de l'oxygène, un électrolyte, et une anode de lithium)

température ambiante, ce qui affecte donc la conductivité et la réactivité du sel, par exemple, $LiPF_6$; *2)* inflammabilité, il est donc crucial d'examiner les problèmes de sécurité; *3)* l'efficacité du solvant à dissoudre les sels de lithium; et *4)* une perte considérable de la concentration de lithium-ion à électrolyte, car les ions lithium sont impliqués dans la formation de SEI. L'électrolyte doit répondre à de nombreuses exigences, comme étant neutre pour l'environnement, inerte envers les substrats d'électrodes et le séparateur de cellules, hautement efficaces pour l'oxydation et la décomposition réductrice, et montrer une bonne conductivité ionique.

Électrolytes dans les Batteries: Les électrolytes sont en interaction étroite avec les deux électrodes et jouent un rôle crucial dans la LIB. Ils fournissent le milieu conducteur d'ions de la batterie au lithium-ion, où le Li^+ navettes entre les électrodes. Les electrolytes doivent être caractérisées d'une stabilité chimique élevée, qui empêche la décomposition lorsque oxydant à la cathode ou à l'anode réduction. Certaines propriétés importantes, comme la non-toxicité, bas point de fusion, point d'ébullition élevé, l'absence de réaction explosive, sont nécessaires pour un bon électrolyte afin d'être appliqués aux batteries. Trois types d'électrolytes ont été utilisés dans des piles: *aqueux*, *non aqueux* et *solide*.

Untextitélectrolyte aqueux est constitué d'un acide fort ou une base, en raison de la polarité ceux ci existent plus que des ions positifs et négatifs comme en solution. Ces électrolytes sont stables en particulier sur certaines gammes de tension, tandis que au-delà de ces limites, ils commencent à se décomposer. La stabilité de la tension fournie

est contrôlée par le degré de pureté de la composition de l'électrolyte. Des conductivités ioniques élevées peuvent être obtenues dans des électrolytes aqueux quand la constante diélectrique et le pouvoir solvatant des matériaux sont raisonnablement élevés.

Des électrolytes non aqueux sont formés par des solvants de carbonate de lithium avec des sels communs tels que $LiBF_4$, $LiClO_4$, $LiPF_6$, $LiAsF_6$, LiTFSI (lithium bis (trifluorométhane sulfonyl) d'iodure) et LiBOB (lithium bis-borate oxalato). La conductivité des électrolytes non aqueux est dans la gamme de 10^{-2}-10^{-3} Scm^{-1}. Plus précisément, ces électrolytes sont aprotique non aqueux (incapable d'agir comme donneurs de protons) des solvants organiques, combinées avec des sels de lithium. Ils sont caractérisés par une faible toxicité, un point de fusion bas, une bonne conductivité ionique et la stabilité électrochimique vers les électrodes. Les deux classes d'électrolytes qui ont été utilisées dans les piles sont: *i)* des carbonates d'alkyle linéaire (carbonate de diméthyle (DMC), le carbonate de méthyle éthyle (EMC), et le carbonate de diéthyle (DEC)) et *ii)* des carbonates d'alkyle cycliques (carbonate d'éthylène (EC), le carbonate de vinylène (VC), et le carbonate de propylène (PC)). Un grand nombre d'études ont été consacrées à leur décomposition, propriétés électrochimiques, et la formation et la structure de la première couche de solvatation autour des ions lithium [33, 41–44]. En raison de la constante diélectrique plus faible et du plus faible pouvoir solvant de certains solvants, la formation de paires d'ions est augmentée, ce qui entraîne une conductivité ionique plus faible. En effet, dans ce cas, les ions sont liés les uns aux autres et ne diffusent plus librement en solution. l'heure actuelle, des mélanges de solvants de compositions différentes sont utilisées pour améliorer la conductivité, et pour obtenir de bonnes performances à faible température. Les solvants purs et mélanges de solvants sont discutés dans les sections suivantes.

Des carbonates tels que PC et EC n'ont pas réussi à être utilisés comme solvants dans les batteries lithium-air en raison de leur réaction de décomposition avec O_2. En particulier, super-oxydes ou des radicaux sont formés pendant la réduction initiale de O_2 [45]. Des composés à base d'éther-moins volatils tels que l'éther diméthylique (DME) ou plus électrolytes composé d'éther ont été préférés comme de bons candidats pour les batteries lithium-air [46, 47].

Au-delà des carbonates, des liquides de silicium ont également reçu une attention considérable. Plusieurs études ont porté sur les électrolytes de carbonate modifié [48–50], siloxanes et silyléther [35, 51, 52] et de l'éthylène glycol [53–55] composés. Au lieu de solvants carbonate mixte avec des sels de lithium, les électrolytes polymères et copolymères ont également été envisagées, constitué par du poly (oxyde d'ethylene) (PEO) et des sels de lithium ($LiPF_6$ ou $LiCF_3SO_3$)[56–58].

Au cours des 15 dernières années, les liquides ioniques (IL) [59–61] ont attiré autant d'attention que les électrolytes de batteries lithium-ion. En effet, l'ILS sont des alternatives intéressantes aux solvants organiques dans les batteries en raison de leurs propriétés uniques telles que la stabilité électrochimique, une toxicité faible voir nulle,

une faible inflammabilité, des propriétés de faible pression de vapeur saturante, une densité de charge élevée et une polarité accordable. Les ILs avec une température de fusion supérieure ou proche de la température ambiante sont appelés à température ambiante liquides ioniques (RTILs). Ces ILs sont des molécules chargées et en plus d'autres avantages, ils ont une viscosité relativement élevée qui affectera la conductivité ionique. Ils sont entièrement composés de cations avec des amines de base tels que pyridinium, imidazolium, pyridinium, pyrrolidinium et morpholinium [62–64]. L'anion peut être inorganique comme BF_4^-, PF_6^-, CN^- ou AsF_6^-. Les propriétés de l'IL appuient également sur la nature des substituants qui affecte la solubilité du sel et la conductivité ionique. Les longueurs de chaîne alkyle [62] ou ramifiée de longueur de chaîne augmente la conductivité de l'IL jusqu'à une $mScm^{-1}$.

L'effet particulier des interactions ion-ion, la distribution de charge moléculaire et de formes moléculaires sont les principales propriétés de l'IL en solution comme aux interfaces. Contrairement à ce qui se passe dans les solvants normaux, les effets à paire d'ions ne sont pas prédominantes dans l'ILS, et donc la conductivité molaire s'élève à 0,1 Scm^2mol^{-1}. ILs ont également une faible constante diélectrique et pression de vapeur saturante. Les ILs montrent, cependant, une sensibilité à l'humidité, propriétés associées avec des atomes d'halogène et une viscosité modérément forte.

Différentes classes de ILs sont utilisées dans une grande fenêtre électrochimique et peuvent atteindre des densités élevées de charge. Un certain nombre pratiquement infini d'électrolytes IL peut être produit, en mélangeant différents ILs ou de mélange avec d'autres ILs solvants polaires organiques ou inorganiques.

Dans la section suivante, nous commençons notre discussion sur les solvants organiques les plus utilisés dans des applications comme composant principal d'électrolytes.

Solvants et Sels Organiques

Dans cette section, nous discuterons brièvement des solvants purs, que nous avons pris en considération dans ce travail, EC, DMC et PC, et de leurs propriétés physiques. Nous discuterons également des travaux antérieurs sur l'interaction carbonate Li^+. En particulier, nous allons d'abord se concentrer sur la bibliographie rapportant le calcul essentiellement théorique sans sel spécifique en grappes pures. Ensuite, nous allons présenter les résultats supplémentaires mettant en évidence le rôle joué parles sels choisis parmi les sels de lithium ($LiPF_6$ choisis, $LiClO_4$, $LiBF_4$, et autres).

Propriétés physiques du carbonate d'éthylène (EC), du diméthyle Carbonate (DMC) et du carbonate de propylène (PC)

Parmi tous les solvants organiques, les plus largement utilisés en LIB sont cycliques et sont des carbonates linéaires. En particulier, le solvant EC est très couramment utilisé en tant que composant principal dans des électrolytes, en raison de son moment dipolaire élevé (4,9 D), de sa constante diélectrique ($\varepsilon \sim 89$), et de sa miscibilité avec la plupart des solvants non aqueux [65, 66]. Certaines propriétés physiques du EC sont présentées dans le Tableau 7.1. A température ambiante EC est solide (température de point de fusion 36.4°), il est donc mélangé avec d'autres solvants de carbonate afin d'abaisser la température globale du point de fusion. Dans la plupart des cas, un petit pourcentage de carbonates linéaires, comme le DMC, est ajouté à EC pour transformer le mélange obtenu en liquide à la température ambiante. DMC est choisi en raison de sa faible viscosité, de son point d'ébullition bas et des a faible constante diélectrique (les valeurs sont indiquées dans le Tableau 7.1. La combinaison de EC et DMC á différentes concentrations forme un mélange homogène caractérisé par une faible viscosité et une conductivité ionique élevée. Ce mélange est stable jusqu'à 5,0 V à la surface de la cathode.

Le solvant de PC est un autre carbonate cyclique attrayant, caractérisé par une constante diélectrique ($\varepsilon \sim 64.9$) plus élevée que celle des carbonates linéaires. La conductivité ionique et la stabilité statique sur une large plage de températures, font du PC un des solvants favoris pour le lithium. Le PC est une molécule de noyau à cinq éléments, comme le EC avec un groupe méthyle supplémentaire dans la chaîne latérale. Cependant, le PC se comporte différemment du EC. Par exemple, plusieurs études ont montré que le EC joue un rôle important dans la formation des interfaces solides électrolytiques (SEI), assurent une protection particulière, notamment la protection des anodes en graphite face á la décomposition supplémentaire. Les SEI sont formé lors de la première charge lente d'une batterie, et la qualité de ses structures impacte fortement la durée de vie du système. En revanche, dans les systèmes ne contenant que au PC pur, les SEI sont effectivement formées sur la surface de l'électrode en graphite [67]. En outre, le PC est susceptible de subir une réaction de réduction suite á le transfert d'un électron unique [68] à partir du lithium qui impacte l'efficacité cyclique du système. Malgré ces problèmes, la molécule de PC a également été considérée comme un solvant prometteur en raison de sa forte stabilité anodique. En fait, la première batterie commercialisée (produit par Sony et co.) a été développée sur la base d'une électrolyte solvant PC. La structure et quelques propriétés physiques du PC sont présentées dans le Tableau 7.1. D'après les données indiquées dans le tableau, le PC semble avoir une viscosité légèrement supérieure à celle du EC, le PC ne peut donc pas abaisser la viscosité du EC comme le DMC.

Dans les dernières décennies, plusieurs travaux expérimentaux et théoriques ont été publiés sur les propriétés de coordination du EC, du PC et du DMC avec des ions Li^+.

TABLE 7.1: Structure, formule chimique, la constante diélectrique, la viscosité et Point de fusion (Mp) et Point d'ébullition (Bp) des solvants tels que EC, DMC et PC

Solvent	Structure	Constante diélectrique, ε	Viscosité η (cP)	Mp/Bp (°C)
EC	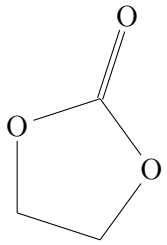	89	1.85	36.4/248
($C_3H_4O_3$)			(40° C)	
DMC	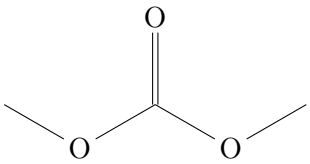	3.1	0.78	4.6/91
($C_3H_6O_3$)			(30° C)	
PC	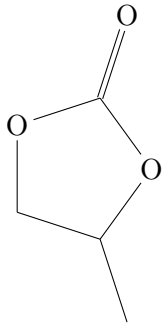	64	2.53	-48.8/242
($C_4H_6O_3$)			(30° C)	

En fait, la compréhension des propriétés de solvatation d'électrolytes carbonate avec Li^+ est cruciale pour comprendre un certain nombre de phénomènes physiques se produisant dans LIB, comme les propriétés de transport, de la stabilité dans l'environnement redox, et phénomènes de dégradations. Par exemple, Masia et al., [69] ont étudié la structure de solvatation de Li^+ par des molécules EC, en utilisant des méthodes DFT et MD. Les résultats de DFT ont montré que le complexe quadri coordonné $Li^+(EC)_4$ est une espèce dominante. De même, ils ont également trouvé le même nombre de coordination ($Li^+(EC)_4$) dans les simulations MD. Un résultat similaire a été obtenu par Wang et al., [70] dans une étude DFT, ce qui confirme l'espèce $Li^+(EC)_4$ est le complexe le plus stable pour $Li^+(EC)_{1\text{-}4}$ série. Ils ont également étudié $Li^+(DMC)_{1\text{-}3}$ complexes et ont constaté que $Li^+(DMC)_3$ est la série la plus stable. En outre, ils ont également étudié l'addition et la réaction de substitution des conformations la complexes mélangés avec des solvants EC et DMC: on peut conclure que l'addition de DMC au $Li^+(EC)_n$ avec n = 1 à 3 complexes est favorable, alors que la substitution de DMC au $Li^+(EC)_2$ complexe est interdit.

Selon Hiroto et al. [71], des études sur EC avec ion Li^+ par AIMD (dynamique moléculaire ab-initio), nitrent que l'ion Li^+ est solvaté par quatre molécules de la EC

dans la première couche de solvatation. Dans le cas du $Li^+(EC)_5$, seules quatre molécules sont coordonnées avec les ions Li^+ pendant que la 5 ème molécule se déplacé avec une distance moyenne de 5,09 Å à partir de l'ion Li^+. Des résultats similaires ont été obtenus par Cho et al., [72] par des calculs DFT. Dans les deux documents, les auteurs concluent que l'indice de coordination maximale dans la première sphère de solvatation est 4 et que les EC molécules supplémentaires peuvent être uniquement disposées dans la seconde couche de solvatation.

Mahesh et al., [73] a étudié l'ion Li^+ avec EC solvant par simulation DFT et MD. Les énergies libres de Gibbs ont été calculées en utilisant B3LYP/6-311++G(d,p) sur la réaction d'addition des EC à $Li^+(EC)_n$ (où n = 0-5) grappe donne des valeurs négatives ou des réactions spontanées pour $Li^+(EC)_{1\text{-}4}$ grappes et valeur positive Δ G pour le $Li^+(EC)_5$ complexe. Par conséquent, ils ont conclu que la formation d'une couche de coordination avec cinq molécules est énergétiquement défavorable. En outre, la simulation a révélé que le AIMD coordination est 4 pour Li^+ ion autour de ∼4 Å. Ils ont également signalé qu'il n'y a pas un déchange de molécules EC une fois la structure de solvatation formée. Les mêmes auteurs ont également publiés dans la suite des travaux [74] pour les complexes de PC que $Li^+(PC)_3$ est le composant principal, en calculant lénergie libre de Gibbs. Des calculs de la chaleur de formation et de lénergie libre de Gibbs, ils ont conclu que EC agit comme un meilleur solvant que le PC. Utilisation de la même discussion sur les énergies ΔG , avec différentes approches DFT, Balbuena et al., [34] et Wang et al., s'accordent sur les mêmes conclusions, confirmant ainsi un nombre maximum de coordination de 4 pour $Li^+(EC)_n$ solvatation et expliquant qu'il est peu probable que $Li^+(PC)_4$ existe et que $Li^+(PC)_2$, $Li^+(PC)_3$ sont les principaux composants de la solution.

Généralement, les électrolytes classiques consistent un sel de lithium comme $LiPF_6$, $LiClO_4$, $LiBF_4$ etc., et un mélange binaire ou ternaire de carbonates.

Mélange de Solvants Organiques

Parmi une variété d'électrolytes solvants pour les LIB, des mélanges de carbonates contenant EC sont principalement utilisés avec succès, pour les raisons suivantes: i*i)* même à forte concentration de sel (jusqu'à 1,0 M), la molécule EC peut facilement dissoudre les sels de lithium, en raison de sa constante diélectrique élevée; *ii)* un point bas de l'électrolyte de fusion; *iii)* une faible viscosité d'électrolytes de carbonate linéaires avec une stabilité chimique, le transport ionique et la permittivité diélectrique améliores ; *iv)* une conductivité ionique élevée à température ambiante, qui est supérieure à la limite de$10^{-3}\Omega^{-1}cm^{-1}$ [75, 76]. Cela impacte grandement la performance de la batterie et est compatible avec la tension de la batterie. Les compositions de mélange sont utilisées dans une large gamme de températures de fonctionnement ainsi que pur des applications de stockage et les performances de la cellule. Le choix de l'électrolyte est une

étape cruciale pour développer de meilleurs dispositifs conventionnels. Par conséquent, la constante diélectrique élevée de EC molécule est mélangée à la fois avec un solvant carbonate liquide (tels que les carbonates linéaires) et un PC (carbonate cyclique) pour surmonter ces problèmes. Les Ures Mixtes ternaires ont été utilisées pour améliorer les performances à basse température des batteries. Un mélange de EC et DMC avec $LiPF_6$ permet un plus grand nombre de processus de charge-décharge sans perte de capacité.

Dans les deux dernières décennies, des travaux de recherche très étendues ont été publiés en se concentrant sur la EC contenant des électrolytes. Avant les années 1970, le EC a été utilisé comme co-solvant dans les électrolytes, afin d'obtenir une bonne conductivité ionique. Dans les années 1970, une petite quantité de PC a été ajouté, afin d'abaisser le point de molécule EC résultant en une haute conductivité ionique de mélange dans la solution pure. En début des années 1990, des LIB classiques utilisés avec des solvants EC et en dépit des EC point d'ébullition élevé, de petites quantités de différents co-solvants ont été ajoutées, y compris PC, THF (tétrahydrofuranne), DEE (diéthoxyéthane). Ces solvants ne remplissent pas de manière satisfaisante, en raison du fait que PC provoque des réactions secondaires qui affectent la capacité irréversible des LIB. En outre, un solvant éther est instable lors de l'oxydation à la cathode chargée. Après 1994, Tarascon et Guyomard [77, 78] ont constaté que la molécule carbonate de DMC linéaire agit comme un meilleur co-solvant avec la EC pour former un électrolyte efficace.

En effet, l'addition de carbonate linéaire DMC a l'EC forme des mélanges homogènes obtenus en diminuant la température de EC de fusion [78, 79]. En conséquence, la viscosité EC devient très faible, améliorant les mécanismes de transport d'ions et, par conséquent, augmentant la conductivité ionique. L'ajout du EC et PC solvants dans des proportions adaptées a également été utilisé pour abaisser le point de l'électrolyte de fusion, en raison de la haute permittivité et de la faible température de pointe de fusion (-49°) [80] du solvant PC. Le développement et l'amélioration des batteries lithium-ion implique encore de surmonter les limites des mélanges binaires ci-dessus, en raison principalement de la faible stabilité thermique de solvants et de la pression de vapeur élevée. ce jour, de nombreux travaux de recherche ont été publiés dans divers mélanges avec différents sels que nous discutons ci-dessous. Certains résultats peuvent dépendre non seulement du choix du mélange de l'électrolyte mais également des sels. Pour cette raison, nous allons discuter de la bibliographie pour chaque sel dans des paragraphes distincts.

EC,PC,DMC + $LiClO_4$

De précédentes études expérimentales de spectroscopie Raman réalisées par Hyodo et al., [81] en 1989, ont porté sur la structure locale de solvatation d'ions Li^+ dans EC et PC avec le sel $LiClO_4$. Ils ont proposé un nombre de coordination de l'ordre de 4 pour Li^+ dans EC avec une concentration élevée de 1M $LiClO_4$, et ce nombre devient 4,9 à

une concentration plus faible de 0,1 M $LiClO_4$. Par ailleurs, ils ont également examiné des mélanges EC-PC. Ils ont rapporté 3,3 molécules de EC et 0,7 molécules de PC à concentration élevée (5:1). D'autres part, la coordination des molécules Li^+-EC diminue lorsque lorsque le ratio molaire de PC augmente. Au ratio 1:1, le nombre de molécules EC coordinées avec Li^+ est 1,9 (sur un nombre total de coordination de 3,8), signifiant que, dans ce cas, à la fois EC et PC sont liés à Li^+ dans un ratio 50:50, et il n'y a pas de solvatation préférentielle dans la première couche de solvatation. Néanmoins, les études théoriques de Klassen et al., [76], étudiant la chaleur lors de la formation des réactions de l'ion Li^+ avec EC et PC, montrèrent que EC/ Li^+ a une énergie de solvatation plus forte que PC/ Li^+. Ils conclurent que EC solvate sélectivement Li^+ dans les solutions EC/PC/ $LiClO_4$. De plus, les études de DFT et MD sur $LiClO_4$ avec EC, PC et en mélange, par Balbuena et al. [82], démontrèrent que EC tend à substituer PC dans la première couche de solvatation. Ils démontrèrent également que les molécules de EC ont un nombre de coordination de 4,1 avec $LiClO_4$ dans des solutions diluées, mais augmente à 3,8 dans des solutions concentrées. De plus, les nombres de coordination sont de 4 et 4,4 dans des mélanges EC-PC avec des ratios respectivement de 1:1 et 3:1. Dans la première couche de solvatation, ils trouvèrent 38% de PC lié avec l'ion Li^+ dans le mélange 1:1, et 16% dans le mélange 3:1.

La solvatation d'ion lithium dans EC avec $LiClO_4$ a été étudiée par Cazzanelli et al. [83], utilisant des techniques NMR, avec une concentration définie par le ratio R=[Li^+]/[EC]. Ils ont trouvé un nombre de solvatation d'environ 7 à la concentration R=0,1, alors qu'à une concentration plus élevée (R = 0,33), le complexe de Li^+-EC formée avec $\sim$ 3 molécules de solvant. La plupart des travaux cités ci-dessus suggèrent donc que la coordination est d'environ 4 pour $Li^+(EC)_n$. En revanche, Huang et al., [84] ont étudié la solvatation de $LiClO_4$ dans EC par spectroscopie Raman et IR, et suggèrent que le nombre moyen de solvatation des ions Li^+ dans EC est de 6. En outre, Matsuda et al., [85] ont mesuré la solvatation de Li^+ ion dans EC et PC avec $LiClO_4$ par ionisation électrospray spectroscopie de masse (ESI-MS) et ont montré que $Li^+(EC)_2$ et $Li^+(EC)_3$ sont les principales espèces de solvatation dans une solution 1 mM $LiClO_4$. Des résultats similaire ont été obtenu pour des molécules PC.

En 2002 Inaba et al., [86] ont étudié l'effet en tant que co-solvents du carbonate linéaire (DEC et DMC) sur des solutions basée sur EC, avec 1 M $LiClO_4$, par microscopie à force atomique (AFM). Ils ont rapporté que 4,6 est le nombre de solvatation apparente de Li^+-EC et ce nombre de solvatation diminue à 4,2 (3,1 EC + 1,1 DEC) et à 3,1 (2,9 EC + 0,2 DMC) dans les solutions EC: DEC (1: 1) et EC: DMC (1:1) respectivement. Leurs résultats ont révélé que la molécule EC participe principalement dans la première couche de solvatation plus que les carbonates linéaires.

EC, PC, DMC + $LiBF_4$

Les simulations moléculaires dynamiques de Soetens et al., [87], ont porté sur le sel $LiBF_4$ dans EC, DMC et PC. Ils réalisèrent des simulations sur Li^+-(EC), Li^+-(DMC) et Li^+-(PC) à différentes températures, dans des boîtes de simulation contenant 214 molécules de solvant pour un Li^+ et un BF_4^-, correspondant à la concentration 0,1 M . Ils ont montré que l'enveloppe de solvatation typique est formée par EC et PC autour de Li^+, avec un nombre de coordination de quatre. D'autre part, les études MD de Prezhdo et al., [88] ont signalé que six molécules individuelles de carbonate (EC, PC et DMC) peuvent coordonner autour de l'ion Li^+ à faible concentration (0,1 M) de $LiBF_4$. La coordination diminue à 5 à la concentration de 1 M. Ils ont également décrit l'enveloppe de solvatation pour les mélanges binaires. En particulier dans des mélanges PC-DME, l'ion lithium se coordonne avec six molécules de PC, en raison de l'absence du groupe C=O dans du DME. Dans le cas de mélanges EC-DMC, il a été trouvé que 5 EC et une molécule DMC solvatent l'ion Li^+. A des concentrations plus élevées, ils ont également trouvé une certaine interaction avec le contre-anion. En particulier, ils ont discuté que le contre-anion BF_4^- agit comme un monodentaté dans des mélanges de PC-DME, et en tant que ligand bidenté dans des mélanges EC-DMC. Sono et al., [89] ont étudié la solvatation des ions Li^+ dans des solutions de PC avec le sel $LiBF_4$, par des techniques de RMN et Raman. Ils ont rapporté que Li^+ ions est lié à 1,08 molécules de PC, à une concentration de plus de 1 M. Ce petit nombre de coordination est la preuve d'une formation plus importante de paires de contact-ion de Li^+- BF_4^-. Des études récentes sur $LiBF_4$ dans du PC par Sono et al., [90] ont montré que à une concentration de 1M, la coordination totale peut être attribuée comme 2,66 pour Li^+-O(PC) et 1,38 pour Li^+-F (BF_4-). Le nombre de coordination de Li^+-PC augmente à 3,14 à une concentration de 0,5 M, tandis que celui de Li^+-F diminue à 0,91, ce qui signifie que l'interaction du contre ion BF_4^- est plus faible dans la première enveloppe de solvatation.

EC, PC, DCM + LiTFSI

Borodin et Smith et al., [91] ont étudié la solvatation et le transport des ions Li^+ dans EC en utilisant des simulations MD. Ils ont estimé le sel LiTFSI (lithium bis trifluorométhane sulfonimide) pour l'ion Li^+ et étudié le système à 313 K. Ils ont rapporté que 2.7 à 3.2 molécules de EC et de 0,67 à 1,05 anions TFSI sont liés à l'ion Li^+ dans la première couche de solvatation. Toutefois, environ 3,8 molécules EC solvatées à Li^+ dans les électrolytes complètement dissociées avec une distance de RDF typique de la Li-O (= C EC) $\sim$ 1.95 Å pour toutes les concentrations.

EC, PC, DMC + $LiPF_6$

Morita et al., [92] , à l'aide de la spectroscopie Raman, analysèrent la solvatation d'ions Li^+ pour 3 concentrations différentes de sel $LiPF_6$ dans EC. Ils ont trouvé des nombres de coordination de 4,4, 4,1 et 3,9, correspondant aux trois concentrations pour $LiPF_6$ de 0,5M, 1,0M et 1,5M respectivement. Pour le mélange EC:DMC dans 1 M de $LiPF_6$ ils ont obtenu un nombre de coordination total de 4,1, qui comprend 3,0 molécules de EC et 1.1 de DMC. A partir de ce résultat, ils ont conclu que la coordination de EC avec l'ion Li^+ est préféré à celui de DMC.

Tasaki et al., [93] et des études de calcul sur l'association d'un sel $LiPF_6$ avec une variété de solvants, conclurent que les nombres de solvatation de EC, PC et DMC sont 3,53, 3,46 et 2,84 et les distances de Li^+ correspondantes sont 2,06, 2,05 et 2,05, respectivement. En outre, ils ont montré que l'ion PF_6^- participe également à la solvatation de la couche autour de l'ion Li^+. Sono et al., [89] ont étudié la solvatation des ions Li^+ dans des solutions de PC avec le sel $LiPF_6$ par des techniques de NMR et Raman et ont rapporté que l'ion Li^+ est lié à 4,3 molécule de PC dans la solution diluée. Ils ont également montré que, à concentration plus élevée (2,5 M), le rapport de PC/ Li^+ est 4, et près de 25% des molécules de PC sont libres dans la solution. Cependant, ils ont également obtenu l'orientation déformée (distorted orientation) de PC aux ions Li^+. A la plus forte concentration 3,29 M, le ratio PC/ Li^+ a diminué à 2,85. Ils ont également signalé dans des papiers ultérieurs sur le même sel $LiPF_6$ [94] que le nombre de coordination est de 3 pour le groupe de li PC / Li^+ 1 M concentration.

Sono et al., [90] se sont préoccupés de l'interaction ion-ion de $LiPF_6$ et $LiBF_4$ dans des solutions de PC. Les résultats montrent que la solution PC/ $LiPF_6$ a une conductivité ionique plus élevée par rapport à celles $LiBF_4$, et ils ont attribué ce phénomène à une faible formation de paires d'ions. Le nombre moyen de solvatation d'un sel $LiPF_6$ à 1M dans du PC se trouve être 3,72. A une concentration de 0,5M, le nombre de solvatation est déterminé à 3,97, ce qui indique qu'il y a moins de paires d'ions formées que dans le cas à 1M. Dans les deux cas, l'ion PF_6^- agit en tant que ligand monodenté.

Une étude de diffraction des neutrons de solution de $LiPF_6$ dans du PC réalisée par Yasuhiro et al., [95] a révélé que 4,5 molécules de PC sont fortement liées à l'ion Li^+ dans la première couche de solvatation (10% molaire du $LiPF_6$ en solution dans PC). Des études détaillées de la chimie quantique et de simulation MD ont également été publiées par Borodine et al. [96], sur les propriétés de solvatation de mélanges binaires de solvants EC et DMC avec $LiPF_6$. La boîte typique de simulation MD contient 480 molécules de solvant avec 1M $LiPF_6$, et les simulations ont été effectuées à différentes températures. Les résultats ont révélé que 3,8 molécules de EC sont présentes dans la première couche de solvatation (définie par un rayon de 2,8 Å coupé) à 298 K. A température plus élevée (333 K), le nombre de solvatation de EC est réduit à 3,3. Un nombre de coordination de 2,7 est obtenue pour DMC avec $LiPF_6$ à 1 M, ce qui est légèrement plus faible

que dans le cas avec EC. Dans le cas de mélanges binaires EC:DMC (1:1), les mêmes auteurs ont trouvé une enveloppe de solvatation avec une teneur plus élevée de DMC que EC. Dans la première couche, cependant, il y a encore une contribution considérable provenant du contre-anion PF_6^-. Dans le même travail ils ont également présenté une discussion intéressante sur le rôle joué par la conformation du DMC, et ont montré que, par exemple, le complexe Li^+-DMC préfère une conformation cis-trans pour le fragment DMC que celui cis-cis. Néanmoins, ils ont constaté que le complexe EC 3 DMC (cis-cis)/ Li^+ est plus stable que les espèces EC_4/ Li^+, et que EC_3DMC (cis-trans)/ Li^+ est moins stable que EC_4/ Li^+ en raison des interactions dipôle-dipôle défavorables.

Des études théoriques de Ganesh et al., [97] sur EC et PC et $LiPF_6$ montrent une distance typique entre Li-O (= C) denviron ∼1.94 Å dans PC et ∼ 1,92 Å EC à 310 K (400 K). A plus haute température (400 K), l'enveloppe de solvatation dEC est non sphérique. La distance moyenne Li^+- PF_6^- est environ 6,0 dans les EC et ∼ 9.0 au PC. Egalement les auteurs ont montré que a divers températures (310-400K) si pour PC la coordination autour du Li^+ est constante avec 4 molécules coordonnées, pour EC le nombre de coordination varie (4-6)

Kang Xu [98] ont effectuée des expériences de NMR ^{17}O sur les melanges EC et DMC avec 1 M $LiPF_6$, et ont constatée que un maximum de six molécules EC peut coordonner le ion Li^+. Egalement la même expérience sur le mélange EC: DMC (50:50 avec 1 M $LiPF_6$) montre que près de 70% de la sphère de coordination est constitué de DMC.

Sur la base de simulations de MD, Tenney et al [99] ont étudié le nombre de solvatation Li^+ en présence de EC, DMC et dans le mélange EC: DMC, avec le sel $LiPF_6$. Ces résultats montrent que le nombre de coordination varie avec la concentration et la température. A très faible concentration de 0,1 M $LiPF_6$, le nombre de coordination de EC autour Li^+ est de 5.2, 5.0 et 4.2 à 300 K, 350 K, 400 K, respectivement. Ainsi, à une concentration déterminée, les nombres de coordination diminuent lorsque la température augmente. A 1 M $LiPF_6$, le nombre de solvatation apparente de EC est de 4 à température ambiante (300 K), mais il diminué à 2,9 à une température supérieure 400 K. Cet effet a été expliqué par l'observation expérimentale que, à température plus élevée, le contre-anion PF_6^- est présent dans la première couche de solvatation ainsi diminuant le nombre de EC a 2,9. En effets, à 400K lenveloppe de solvatation est formée par 2,9 EC et 1,6 PF_6^- autour de l'ion Li^+. Pour DMC, le nombre de coordination typique est de 2,3 à 1,0 M (300K) et augmente légèrement à 2,6 à une concentration inférieure (0,1 M).

Au même temps, les auteurs ont analysé la variation des nombres de coordination des couples Li^+- PF_6^- en variant la concentration. Par exemple, dans le cas de pur EC ($LiPF_6$- EC), le nombre de coordination Li^+- PF_6^- est de 0,4 pour une solution 0,1 M et 1,1 à 1 M (à 300 K). Toutefois, dans le cas de DMC pur ($LiPF_6$- DMC),la coordination est de 1,7 à 0.1M et 2.1 à 1 M. Dans le cas du mélange binaire 1EC: 1DMC (300 K), les

nombres de coordination dEC et DMC sont 3,0 et 2,6 à 0,1 M de $LiPF_6$, et ces valeurs tombent à 1,6 à 1 M de $LiPF_6$.

Motivation et Vue d'ensemble

Dans les travaux suivants de ma thèse, jai concentre mon étude sur les électrolytes typiques EC, PC et DMC qui sont largement utilisé dans les développements expérimentaux récents. Comme nous avons présenté dans les paragraphes précédents, plusieurs études ont déjà été publiées sur ces électrolytes mais un certain écart entre les résultats expérimentaux et théoriques reste, et le rôle des différents mélanges carbonates dans la sphère de solvatation de Li^+ est encore l'objet de débats. Dun point de vue expérimental, divers nombres de coordination ont était observé et beaucoup des résultats sont contrastants. Malgré les nombreux études expérimentales et théoriques consacrées aux interactions de Li^+ avec des électrolytes à base de carbonates purs et mixtes, la structure et la dynamique de solvatation des cations lithium dans ces solvants nest pas encore bien comprise et même la détermination de l'indice de coordination autour des ions lithium dans des solvants à base de carbonate-pures n'a pas été définitivement résolu. Alors que l'image généralement acceptée comprend une coordination tétraédrique des atomes d'oxygène carbonyle autour de Li^+ élevés [76, 83, 86, 87, 89, 90, 92, 95, 97], certaines études expérimentales et théoriques proposent l'existence de structures locales présentant nombres de coordination [84, 88, 98, 99, 101] qui peut aller jusqu'à six.

La dépendance de ce numéro de coordination locale à la concentration d'ions est également quelque peu controversé. Toutefois, il convient de souligner que la conception de méthodes expérimentales ou des modèles théoriques pour analyser les données expérimentales, en vue de fournir une mesure directe de l'indice de coordination est une tche extrêmement compliquée. D'autre part, la validation des résultats de simulation moléculaire dépend fortement de la comparaison directe avec les données expérimentales. Le développement de méthodes expérimentales prouvant une détermination directe du nombre de coordination devient indispensable afin d'obtenir une image claire sur les effets structurels locaux dans les solvants liquides.

En outre, il est intéressant de mieux comprendre le rôle du DMC dans les mélanges binaires EC/DMC et ternaires EC/DMC/PC qui sont très utilisés dans les récents développements et jamais été explorée d'un point de vue théorique.

Ce travail est consacré à l'étude de la solvatation du Li^+ par divers carbonates et leurs mélanges. Après une présentation des approches théoriques utilisées dans ce travail, chapitre 2, nous présenterons au chapitre 3, les calculs DFT pour les clusters purs formés par un seul solvant avec le lithium-ion $Li^+(S)_n$ (S = EC, DMC et PC, n = 1-5). Dans le même chapitre, nous allons également décrire et analyser les résultats DFT obtenus pour mélanges binaires $Li^+(S_1)_n(S_2)_m$, (S_1, S_2 = EC, PC, DMC, avec m+n=4) et ternaires

$Li^+(EC)_l(DMC)_m(PC)_n$ avec l+m+n=4. En particulier, nous allons essayer de décrire les structures, la coordination autour de Li^+, la liaison et interaction. Egalement les propriétés thermodynamiques seront discuté avec une analyse de la stabilité et de régime préférentiel. Le rôle du sel, $LiPF_6$, sera discuté dans le chapitre 4. En particulier, nous allons discuter de la modification de la première couche de solvatation par la présence du contre-ion PF_6^-. Dans le chapitre 5, les résultats DFT seront couplées avec des résultats de MD obtenus sur EC/Li^+, DMC/Li^+, PC/Li^+ et mélangé EC binaire: DMC/Li^+ (1: 1) et ternaire solvant EC:DMC:PC/Li^+ (1:1:3) . à partir des résultats MD, nous allons rationaliser les résultats, y compris les fonctions de distribution radiale, nombres de coordination, fractions molaires locales et les distributions dipolaires etc.

8

Chapitre 2: Techniques Numériques

Le chapitre 2 décrit les méthodes de computationnelles utilisées dans ce travail. Nous montrons la formulation de la théorie de la densité fonctionnelle (DFT) et simulations de dynamique moleculaire des approches. En particulier, nous avons également expliqué l'Densité Amsterdam fonctionnelle (ADF) de formalisme que nous avons utilisé dans nos calculs DFT.

9

Chapitre 3: Etude de Lithium ion Coordination avec Solvants des Carbonates

Le chapitre 3 est consacré à l'étude DFT de la solvatation de l'ion Li^+ dans les solvants EC, PC et DMC. Plus particulièrement, les structures $Li^+(S)_{1\text{-}4}$ (S = EC, PC, DMC) ont été étudiées. Par la suite, nous avons examiné les structures de solvants binaires tels que $Li^+(EC)_m(PC)_n$, $Li^+(EC)_m(DMC)_n$ et $Li^+(PC)_m(DMC)_n$ dans lesquelles m+n = 4, suivie de l'étude de clusters de solvants mixtes $[Li^+(EC)_l(PC)_m(DMC)_n]$ (l + m + n = 4). Nos résultats DFT ont montré l'interaction préférentielle obtenu entre l'ion Li^+ et un atome d'oxygène de carbonyle de tous les solvants de carbonate, ce qui est en accord avec toutes les études expérimentales et théoriques précédentes. Les énergies libres de Gibbs estimées des clusters purs, prédisaient un ion lithium tétracoordiné avec quatre solvants agencés dans un environnement tétraédrique. Dans le cas des clusters EC et DMC, nous avons constaté que $Li^+(EC)_4$ et $Li^+(DMC)_4$ est le plus stable. Toutefois, dans le cas des clusters PC pures, la différence d'énergie de $Li^+(PC)_3$ et $Li^+(PC)_4$ est très faible, ce qui indique que les deux structures existent dans la solution. En outre, nous avons montré que la coordination 5 n'a pas pu être atteinte et qu'une cinquième molécule de solvant ne peut être organisé que dans la sphère extérieure ou seconde couche de solvatation. Les résultats de l'énergie de liaison démontrent que les clusters Li^+-EC et Li^+-PC ont les plus fortes interactions de liaison par rapport aux clusters DMC. Dans le cas de mélanges binaires $Li^+(S_1)_n(S_2)_m$, (S_1, S_2 = EC, PC, DMC, avec m + n = 4), nous avons aussi dans ce cas une conservation de l'arrangement tétraédrique autour de l'ion Li^+. L'analyse de l'énergie libre de Gibbs montre:

1. Dans le cas des clusters Li^+-(EC)(PC), les résultats obtenus ont révélé que $Li^+(EC)_2(PC)_2$ tétracoordonné est le plus favorable, suivie par les clusters $Li^+(EC)PC)_3$ et, éventuellement, $Li^+(EC)_3(PC)$, bien que la différence d'énergie de ces clusters soit très petite. C'est

pourquoi ces trois clusters existent en solution. Ces résultats ont également suggéré que les deux molécules EC et PC approchent l'ion Li^+ avec une participation égale et il n'y a pas de solvatation préférentielle obtenue.

2. En revanche, dans le cas des clusters Li^+-(EC)(DMC), nous avons prédit que $Li^+(EC)_3(DMC)$ est le plus favorable, suivie par $Li^+(EC)_2(DMC)_2$ et $Li^+(EC)(DMC)_3$ étant le moins favorable.

3. Similairement, les mêmes résultats ont été obtenus pour les clusters mixtes Li^+-(PC)(DMC), $Li^+(PC)_3(DMC)$ étant le plus favorable, suivie par $Li^+(PC)_2(DMC)_2$ et $Li^+(PC)(DMC)_3$ étant le moins favorable.

4. Pour tous les mélanges binaires les résultats sont cohérents avec une interaction plus forte avec PC et EC plutôt que DMC.

Dans le cas de mélanges ternaires $Li^+(EC)_l(DMC)_m(PC)_n$ avec l+m+n=4, le cluster $Li^+(EC)_2(DMC)(PC)$ a été prédit pour être le plus favorable, et suivie par $Li^+(EC)(DMC)(PC)_2$ et éventuellement $Li^+(EC)(DMC)_2(PC)$ est le moins stable parmi ces clusters. Les changements d'énergie libre particuliers pour les chemins de transition entre ces clusters sont très faibles, ce qui indique que toutes ces structures pourraient éventuellement exister dans la phase.

10

Chapitre 4: Etude de Contre-anion PF_6^- Effet sur Li^+ -EC, -DMC et complexes -PC

Dans le chapitre 4, nous avons discuté le rôle du sel, et en particulier le contre-anion PF_6^- sur la sphère de coordination autour de Li^+. Nous avons concentré notre étude sur les clusters $Li^+(EC)_nPF_6^-$, $Li^+(DMC)_nPF_6^-$ et $Li^+(PC)_nPF_6^-$. Une analyse structurale et énergétique a été effectuée et les résultats sont présentés ci-dessous. Du point de vue général, nos résultats DFT ont prédit que l'anion PF_6^- isolé a une géométrie octaédrique parfaite, et nous avons également étudié les interactions possibles avec l'ion Li^+. Les ions Li^+- PF_6^- forment trois interactions différentes telles que le monodentate (C_{4V}), bidentate (C_{2V}) et tridentate (C_{3V}). Les résultats ont révélé que l'interaction forte (le plus stable) est obtenue sous forme tridentate, dans lequel trois atomes de fluor sont coordonnés à l'ion Li^+. La structure locale a également été confirmée par l'analyse de fréquence. Ces résultats sont en accord avec des travaux théoriques précédents. Nous avons étudié les clusters de solvant pur $Li^+(S)_{1\text{-}3}$ (S = EC, DMC et PC) en phase gazeuse avec l'anion PF_6^-, et les résultats suggèrent que les clusters de solvant pur ont été totalement perturbé en présence de l'anion PF_6^-. Dans tous les cas, la distance Li^+- Oc (oxygène carbonyle) augmente en raison de la forte charge négative de l'anion PF_6^-, et les hydrogènes alkyles des solvants forment des liaisons hydrogène avec l'anion PF_6^-. Pour toutes les structures en présence de PF_6^- dans la sphère de coordination, la structure la plus favorable est $Li^+(S)_2PF_6^-$. L'addition d'une troisième molécule de S est défavorable (avec des valeurs de Δ G positifs pour la réaction d'addition). Pour toutes les structures en présence de PF_6^-- dans la sphère de coordination, la structure la plus favorable est $Li^+(S)_2PF_6^-$. La substitution de l'anion PF_6^- par une molécule de solvant pour former un numéro de coordination trois ($Li^+(S)_3$) est défavorable (avec des valeurs positives de Δ G). Les résultats suggèrent que l'ion Li^+ préfère le contre-anion en présence de sel et forme une coordination plus faible. Cependant, les deux structures

sans PF_6^- (numéro de coordination 4) et avec PF_6^- (coordination numéro 2) existent dans la solution.

11

Chapitre 5: Accouplement DFT et MD

Ce chapitre 5 est d'étudier la structure des ions Li^+ avec des solvants de carbonate (EC, DMC et PC) solvatation locale à une dilution limitée. Nous avons discuté sur les champs de force efficaces que nous avons utilisé pour cette étude. En outre, nous avons inclus l'ensemble du document que nous avons publié dans la revue.

12

Conclusions et Perspectives

Nous avons étudié l'élément le plus important dans les batteries est appelé comme électrolytes, qui pouvoir être impliqués dans les propriétés de transport, des densités d'énergie élevées, longue durée de vie et les applications de température large plage etc. Les solvants de carbonate jouent rôle important dans les batteries. Ces électrolytes ont été étudiés en utilisant les combinaisons de la théorie fonctionnelle de la densité chimique quantique (DFT) et classiques simulations de dynamique moléculaire. En étudiant le pur et le mélange d'électrolytes solvants carbonate avec du sel de lithium, nous ont été en mesure de démontrer la structure locale plus stable autour de lithium-ion, un composant des solvants dans la première coque avec des compositions particulières et le solvant le plus préférable. Dans notre étude, nous avons considéré les solvants typiques les plus couramment utilisés tels que le carbonate cyclique d'éthylène (EC), le carbonate de propylène (PC) et linéaire carbonate de diméthyle (DMC). Les calculs ont été effectués DFT pour les systèmes purs $Li^+(S)_n$ (S = EC, DMC, PC et n = 1 à 5) et les mélanges binaires $Li^+(S_1)_n(S_2)_m$(S_1, S_2 = EC, PC, DMC, avec m + n = 4), les clusters et ternaires $Li^+(EC)_l(DMC)_m(PC)_n$ avec l + m + n = 4. En outre, les agrégats de solvant purs ont également été étudiés, y compris l'effet de la PF_6^- anion. Pour les simulations MD, nous étions considérés comme les systèmes suivants à dilution infinie *i)* des pôles de solvant pur avec ion Li^+ *ii)* de mélange binaire EC: DMC avec une composition équivalent molaire de 1: 1 avec ion Li^+ et *iii)* le mélange ternaire EC: DMC: PC avec 1: 1: 3 avec un rapport molaire d'ions Li^+, respectivement. Comme sur la base des résultats DFT, les variations de l'énergie libre pendant les transitions entre les différents types de groupes formés par le cation lithium et les molécules de solvant ont montré que la formation de complexes avec quatre molécules de solvant est le plus favorable. Les solvants ont été disposés dans une géométrie tétraédrique qui est observée dans tous les cas comme pur et mélanges. Dans le cas des grappes Li^+-PC, la plus petite différence dans les énergies libres de $Li^+(PC)_3$ et $Li^+(PC)_4$ pôles suggèrent que les deux configurations peuvent éventuellement exister dans la solution en vrac. Nos résultats ont été adaptés avec plusieurs théorique ainsi que les résultats expérimentaux.

Dans les cas de $Li^+(S)_5$(S = EC, DMC, PC) grappes, les cinquième molécules de solvant ont été organisées très loin de l'ion central Li^+, explique l'ion Li^+ peut accueillir quatre molécules dans la première couche de solvatation et des molécules supplémentaires pourraient participer à la deuxième couche de solvatation et énergie libre prédit également la même que $Li^+(S)_4$ est plus stable. Nous avons prédit la $Li^+(S)_2PF_6^-$ cluster pour être le plus stable dans le cas de solvants purs avec du sel $LiPF_6$ et une molécule de solvant ne peut pas remplacer l'anion PF_6^- de la plus stable $Li^+(S)_2PF_6^-$ cluster. Les mêmes DFT résultats libres d'énergie en grappes binaires ont constaté que $Li^+(EC)_2(PC)_2$ est plus stable que les autres grappes possibles en EC: mélanges de PC, en disant la EC et molécules de PC se approchent de la ions Li^+ avec une participation égale et il n'y a pas solvatation préférentielle se est produite. Cependant, dans les deux cas de Li^+- EC: DMC et Li^+- PC: DMC mélanges où le $(EC)_3$(DMC) et $(PC)_3$(DMC) grappes sont plus stables que les autres grappes possibles correspondant. Par conséquent, nos calculs DFT ont prédit une liaison préférentielle obtenue avec EC ou un PC plutôt qu'avec DMC. Dans les mélanges ternaires, le cluster $Li^+(EC)_2$(DMC)(PC) a été prévu pour être le plus favorable, les changements énergétiques gratuits pour les chemins de transition entre plusieurs grappes sont très faibles, ce qui indique que toutes ces structures pourraient éventuellement exister dans la phase brute. Nos résultats ont montré que la MD de la structure de solvatation locale se compose de quatre molécules de solvant autour de l'ion Li^+ dans une géométrie tétraédrique. Nous avons trouvé le premier pic de séparation de Li^+- Oc (carbonyle oxygène) à 1,78 Å qui est presque comparable avec des résultats DFT où la distance typique est 1,93 Å. En raison des inhomogénéités autour lithium-ion dans des mélanges binaires et ternaires, les fluctuations pourraient être décrites en termes de structure de courte portée (jusqu'à 4-5 Å de Li^+) lorsque la composition est riche en DMC et par une structure à plus long terme où dans le cas du mélange de solvants binaire la composition est riche en EC et dans le cas de la ternaire il est riche en PC. Un tel résultat indique que les effets collectifs résultant en raison des interactions entre les régions de composition différente pourrait éventuellement stabiliser la structure locale de la première couche de solvatation de Li^+. Les simulations de MD ont également révélé qu'il ya une commande très importante tétraédrique locale autour Li^+ dans tous les cas et l'ajout de co-solvants ne fausse pas cet ordre structurel. En calculant un terme entropique associé à cet ordre tétraédrique locale autour de Li^+, il a également été révélé que les groupes ayant une fraction élevée de molécules DMC (3 et 4 molécules) présentent une tetrahedrality supérieur, qui se reflète dans les valeurs inférieures de cette entropique terme. Par conséquent, d'un point de vue entropique la présence de DMC contribue à la stabilisation de la structure tétraédrique locale autour de Li^+. Un résultat très intéressant également révélé dans la présente étude est que l'intérieur de la première enveloppe de solvatation de Li^+ dans les mélanges ternaires et binaires, qui présentent une forte concentration de molécules de DMC non polaires, le dipôle total des molécules de solvant est supérieur à celui du cas où Li^+ est solvaté par les molécules EC et PC fortement polaires. L'emballage tétraédrique locale observée des

molécules de solvant dans la première couche de solvatation de Li^+ provoque une annulation des vecteurs dipolaires moléculaires individuels, ce qui semble être plus important dans les cas où les molécules du même type sont présents. Ces effets collectifs sont très importantes dans la détermination de la permittivité locale autour d'un cation Li^+ et les préférences de liaison relatives devrait être fondée sur ce moment total de dipôle de l'enveloppe de solvatation et non en termes des interactions dipolaires paire d'ions, qui est traditionnellement considéré comme le plus facteur important qui détermine la solvatation préférentielle dans de tels systèmes. La plupart de nos résultats DFT étaient comparables avec des résultats MD, mais notre travail a également certaines limites. Dans les calculs DFT de la taille finie groupes isolés, d'un point de vue énergétique la préférence de Li^+ se lier avec le PC et les molécules fortement polaires EC. Cependant, les résultats trouvés MD, DMC est un solvant particulièrement préférable que les molécules EC et de PC. Les effets de grappe de taille finie dans DFT pourraient éventuellement affecter les comparaisons directes avec des résultats MD. Dans ces groupes de taille finie la contribution énergique semble être le plus important. Par conséquent, nous avons étudié les mélanges binaires et ternaires à des échelles de longueur plus longues afin d'avoir une description plus réaliste des effets qui ont lieu dans la phase liquide en vrac. L'existence de fluctuations structurelles importantes dans les phases liquides en vrac, se est étendue bien au-delà de la première couche de solvatation, signifie que pour atteindre une comparaison directe entre le rapport de gestion et la DFT résulte l'utilisation de plus grandes grappes de taille dans les calculs DFT semble être plus approprié. Enfin, notre point de vue du travail est d'analyser le temps de vie typique des grappes afin de comprendre les propriétés de transport des ions de lithium. Dans nos résultats, nous avons rapporté la deuxième solvatation est riche de la concentration EC, probablement il pourrait être impliquée dans le transport d'ions de lithium. Par conséquent, si nous pouvions effectuer l'analyse DFT y compris les secondes coques de solvatation, nous pourrions donner une description détaillée de l'influence de la seconde couche de solvatation. En effet, les calculs DFT doivent être pris beaucoup de temps de calcul afin de réaliser l'optimisation avec environ 120 atomes.

Bibliography

[1] Brian J. Landi, Matthew J. Ganter, Cory D. Cress, Roberta A. DiLeo, and Ryne P. Raffaelle. Carbon nanotubes for lithium ion batteries. *Energy Environ. Sci.*, 2: 638–654, 2009. doi: 10.1039/B904116H. URL http://dx.doi.org/10.1039/B904116H.

[2] Kang Xu. Nonaqueous liquid electrolytes for lithium-based rechargeable batteries. *Chemical reviews*, 104(10):4303–417, October 2004. ISSN 0009-2665. URL http://www.ncbi.nlm.nih.gov/pubmed/15669157.

[3] Masataka Wakihara and Osamu Yamamoto. *Lithium ion batteries: fundamentals and performance*. John Wiley & Sons, 2008.

[4] Walter van Schalkwijk and Bruno Scrosati. *Advances in lithium-ion batteries*. Springer, 2002.

[5] Gholam-Abbas Nazri and Gianfranco Pistoia. *Lithium batteries: science and technology*. Springer Science & Business, 2008.

[6] Antonino Salvatore Aricò, Peter Bruce, Bruno Scrosati, Jean-Marie Tarascon, and Walter Van Schalkwijk. Nanostructured materials for advanced energy conversion and storage devices. *Nature materials*, 4(5):366–377, 2005.

[7] Michel Armand and J-M Tarascon. Building better batteries. *Nature*, 451(7179): 652–657, 2008.

[8] Martin Winter and Ralph J. Brodd. What are batteries, fuel cells, and supercapacitors? *Chemical Reviews*, 104(10):4245–4270, 2004. doi: 10.1021/cr020730k. URL http://pubs.acs.org/doi/abs/10.1021/cr020730k.

[9] Yan-Jie Wang, Jinli Qiao, Ryan Baker, and Jiujun Zhang. Alkaline polymer electrolyte membranes for fuel cell applications. *Chem. Soc. Rev.*, 42:5768–5787, 2013. doi: 10.1039/C3CS60053J. URL http://dx.doi.org/10.1039/C3CS60053J.

[10] K.D. Kreuer. On the development of proton conducting polymer membranes for hydrogen and methanol fuel cells. *Journal of Membrane Science*, 185(1):29 – 39, 2001. ISSN 0376-7388. doi: http://dx.doi.org/10.

1016/S0376-7388(00)00632-3. URL http://www.sciencedirect.com/science/article/pii/S0376738800006323. Membrances in Fuel Cells.

[11] C Laberty-Robert, K Valle, F Pereira, and C Sanchez. Design and properties of functional hybrid organic–inorganic membranes for fuel cells. *Chemical Society Reviews*, 40(2):961–1005, 2011.

[12] M Rosa Palacín. Recent advances in rechargeable battery materials: a chemists perspective. *Chemical Society Reviews*, 38(9):2565–2575, 2009.

[13] Li Li Zhang and X. S. Zhao. Carbon-based materials as supercapacitor electrodes. *Chem. Soc. Rev.*, 38:2520–2531, 2009. doi: 10.1039/B813846J. URL http://dx.doi.org/10.1039/B813846J.

[14] Guoping Wang, Lei Zhang, and Jiujun Zhang. A review of electrode materials for electrochemical supercapacitors. *Chem. Soc. Rev.*, 41:797–828, 2012. doi: 10.1039/C1CS15060J. URL http://dx.doi.org/10.1039/C1CS15060J.

[15] Celine Largeot, Cristelle Portet, John Chmiola, Pierre-Louis Taberna, Yury Gogotsi, and Patrice Simon. Relation between the ion size and pore size for an electric double-layer capacitor. *Journal of the American Chemical Society*, 130(9): 2730–2731, 2008. doi: 10.1021/ja7106178. URL http://dx.doi.org/10.1021/ja7106178. PMID: 18257568.

[16] Haegyeom Kim, Kyu-Young Park, Jihyun Hong, and Kisuk Kang. All-graphene-battery: bridging the gap between supercapacitors and lithium ion batteries. *Scientific reports*, 4, 2014.

[17] Haegyeom Kim, Hee-Dae Lim, Sung-Wook Kim, Jihyun Hong, Dong-Hwa Seo, Dae-chul Kim, Seokwoo Jeon, Sungjin Park, and Kisuk Kang. Scalable functionalized graphene nano-platelets as tunable cathodes for high-performance lithium rechargeable batteries. *Scientific reports*, 3, 2013.

[18] Doron Aurbach, Mikhail D. Levi, Elena Levi, and Alexander Schechter. Failure and Stabilization Mechanisms of Graphite Electrodes. *The Journal of Physical Chemistry B*, 101(12):2195–2206, March 1997. ISSN 1520-6106. doi: 10.1021/jp962815t. URL http://pubs.acs.org/doi/abs/10.1021/jp962815t.

[19] a Robert Armstrong, Daniel W Tee, Fabio La Mantia, Petr Novák, and Peter G Bruce. Synthesis of tetrahedral LiFeO2 and its behavior as a cathode in rechargeable lithium batteries. *Journal of the American Chemical Society*, 130(11):3554–9, March 2008. ISSN 1520-5126. doi: 10.1021/ja077651g. URL http://www.ncbi.nlm.nih.gov/pubmed/18284239.

[20] Qing Wang, Nick Evans, Shaik M Zakeeruddin, Ivan Exnar, and Michael Grätzel. Molecular wiring of insulators: charging and discharging electrode materials for

high-energy lithium-ion batteries by molecular charge transport layers. *Journal of the American Chemical Society*, 129(11):3163–7, March 2007. ISSN 0002-7863. doi: 10.1021/ja066260j. URL http://www.ncbi.nlm.nih.gov/pubmed/17326635.

[21] J M Tarascon and M Armand. Issues and challenges facing rechargeable lithium batteries. *Nature*, 414(6861):359–67, November 2001. ISSN 0028-0836. doi: 10.1038/35104644. URL http://www.ncbi.nlm.nih.gov/pubmed/11713543.

[22] Ken Tasaki. Solvent decompositions and physical properties of decomposition compounds in Li-ion battery electrolytes studied by DFT calculations and molecular dynamics simulations. *The journal of physical chemistry. B*, 109(7):2920–33, February 2005. ISSN 1520-6106. doi: 10.1021/jp047240b. URL http://www.ncbi.nlm.nih.gov/pubmed/16851305.

[23] Vinodkumar Etacheri, Rotem Marom, Ran Elazari, Gregory Salitra, and Doron Aurbach. Challenges in the development of advanced li-ion batteries: a review. *Energy Environ. Sci.*, 4:3243–3262, 2011. doi: 10.1039/C1EE01598B. URL http://dx.doi.org/10.1039/C1EE01598B.

[24] M. V. Reddy, G. V. Subba Rao, and B. V. R. Chowdari. Metal oxides and oxysalts as anode materials for li ion batteries. *Chemical Reviews*, 113(7):5364–5457, 2013. doi: 10.1021/cr3001884. URL http://pubs.acs.org/doi/abs/10.1021/cr3001884.

[25] M Stanley Whittingham and Arthur H Thompson. Intercalation and lattice expansion in titanium disulfide. *The Journal of Chemical Physics*, 62(4):1588–1588, 1975.

[26] T Nagaura and K Tozawa. Lithium ion rechargeable battery. *Prog. Batteries Solar Cells*, 9:209, 1990.

[27] Antonino Salvatore Arico, Peter Bruce, Bruno Scrosati, Jean-Marie Tarascon, and Walter van Schalkwijk. Nanostructured materials for advanced energy conversion and storage devic es. *Nat Mater*, 4(5):366–377, May 2005. ISSN 1476-1122. doi: 10.1038/nmat1368. URL http://dx.doi.org/10.1038/nmat1368.

[28] L.D. Xing, C.Y. Wang, M.Q. Xu, W.S. Li, and Z.P. Cai. Theoretical study on reduction mechanism of 1,3-benzodioxol-2-one for the formation of solid electrolyte interface on anode of lithium ion battery. *Journal of Power Sources*, 189(1):689–692, April 2009. ISSN 03787753. doi: 10.1016/j.jpowsour.2008.08.076. URL http://linkinghub.elsevier.com/retrieve/pii/S0378775308017643.

[29] D Aurbach, K Gamolsky, B Markovsky, Y Gofer, M Schmidt, and U Heider. On the use of vinylene carbonate (VC) as an additive to electrolyte solutions for Li-ion batteries. *Electrochimica Acta*, 47(9):1423–1439, February 2002. ISSN 00134686.

doi: 10.1016/S0013-4686(01)00858-1. URL http://linkinghub.elsevier.com/retrieve/pii/S0013468601008581.

[30] Kang Xu, Guorong V. Zhuang, Jan L. Allen, Unchul Lee, Sheng S. Zhang, Philip N. Ross, and T. Richard Jow. Syntheses and characterization of lithium alkyl mono- and dicarbonates as components of surface films in li-ion batteries. *The Journal of Physical Chemistry B*, 110(15):7708–7719, 2006. doi: 10.1021/jp0601522. URL http://pubs.acs.org/doi/abs/10.1021/jp0601522. PMID: 16610865.

[31] Kang Xu, Unchul Lee, Shengshui Zhang, Mark Wood, and T. Richard Jow. Chemical analysis of graphite/electrolyte interface formed in libob-based electrolytes. *Electrochemical and Solid-State Letters*, 6(7):A144–A148, 2003. doi: 10.1149/1.1576049. URL http://esl.ecsdl.org/content/6/7/A144.abstract.

[32] X. Zhang, P. N. Ross, R. Kostecki, F. Kong, S. Sloop, J. B. Kerr, K. Striebel, E. J. Cairns, and F. McLarnon. Diagnostic characterization of high power lithium-ion batteries for use in hybrid electric vehicles. *Journal of The Electrochemical Society*, 148(5):A463–A470, 2001. doi: 10.1149/1.1362541. URL http://jes.ecsdl.org/content/148/5/A463.abstract.

[33] Yixuan Wang, Shinichiro Nakamura, Makoto Ue, and Perla B. Balbuena. Theoretical studies to understand surface chemistry on carbon anodes for lithium-ion batteries: reduction mechanisms of ethylene carbonate. *Journal of the American Chemical Society*, 123(47):11708–11718, 2001. doi: 10.1021/ja0164529. URL http://pubs.acs.org/doi/abs/10.1021/ja0164529. PMID: 11716728.

[34] Yixuan Wang and Perla B. Balbuena. Theoretical Insights into the Reductive Decompositions of Propylene Carbonate and Vinylene Carbonate: Density Functional Theory Studies. *The Journal of Physical Chemistry B*, 106(17): 4486–4495, May 2002. ISSN 1520-6106. doi: 10.1021/jp014371t. URL http://pubs.acs.org/doi/abs/10.1021/jp014371t.

[35] Lingzhi Zhang, Leslie Lyons, Jocelyn Newhouse, Zhengcheng Zhang, Megan Straughan, Zonghai Chen, Khalil Amine, Robert J. Hamers, and Robert West. Synthesis and characterization of alkylsilane ethers with oligo(ethylene oxide) substituents for safe electrolytes in lithium-ion batteries. *J. Mater. Chem.*, 20:8224–8226, 2010. doi: 10.1039/C0JM01596B. URL http://dx.doi.org/10.1039/C0JM01596B.

[36] Zhong-Li Wang, Dan Xu, Ji-Jing Xu, and Xin-Bo Zhang. Oxygen electrocatalysts in metal-air batteries: from aqueous to nonaqueous electrolytes. *Chem. Soc. Rev.*, pages –, 2014. doi: 10.1039/C3CS60248F. URL http://dx.doi.org/10.1039/C3CS60248F.

[37] Fangyi Cheng and Jun Chen. Metal-air batteries: from oxygen reduction electrochemistry to cathode catalysts. *Chem. Soc. Rev.*, 41:2172–2192, 2012. doi: 10.1039/C1CS15228A. URL http://dx.doi.org/10.1039/C1CS15228A.

[38] Jun Lu, Li Li, Jin-Bum Park, Yang-Kook Sun, Feng Wu, and Khalil Amine. Aprotic and aqueous lio2 batteries. *Chemical Reviews*, 114(11):5611–5640, 2014. doi: 10.1021/cr400573b. URL http://pubs.acs.org/doi/abs/10.1021/cr400573b.

[39] Moran Balaish, Alexander Kraytsberg, and Yair Ein-Eli. A critical review on lithium-air battery electrolytes. *Phys. Chem. Chem. Phys.*, 16:2801–2822, 2014. doi: 10.1039/C3CP54165G. URL http://dx.doi.org/10.1039/C3CP54165G.

[40] Zhong-Li Wang, Dan Xu, Ji-Jing Xu, and Xin-Bo Zhang. Oxygen electrocatalysts in metal–air batteries: from aqueous to nonaqueous electrolytes. *Chemical Society reviews*, 2014.

[41] Lidan Xing and Oleg Borodin. Oxidation induced decomposition of ethylene carbonate from dft calculations - importance of explicitly treating surrounding solvent. *Phys. Chem. Chem. Phys.*, 14:12838–12843, 2012. doi: 10.1039/C2CP41103B. URL http://dx.doi.org/10.1039/C2CP41103B.

[42] James M. Vollmer, Larry A. Curtiss, Donald R. Vissers, and Khalil Amine. Reduction mechanisms of ethylene, propylene, and vinylethylene carbonates: A quantum chemical study. *Journal of The Electrochemical Society*, 151(1):A178–A183, 2004. doi: 10.1149/1.1633765. URL http://jes.ecsdl.org/content/151/1/A178.abstract.

[43] Vyacheslav S. Bryantsev and Mario Blanco. Computational study of the mechanisms of superoxide-induced decomposition of organic carbonate-based electrolytes. *The Journal of Physical Chemistry Letters*, 2(5):379–383, 2011. doi: 10.1021/jz1016526. URL http://pubs.acs.org/doi/abs/10.1021/jz1016526.

[44] Ken Tasaki, Alexander Goldberg, and Martin Winter. On the difference in cycling behaviors of lithium-ion battery cell between the ethylene carbonate- and propylene carbonate-based electrolytes. *Electrochimica Acta*, 56(28):10424 – 10435, 2011. ISSN 0013-4686. doi: http://dx.doi.org/10.1016/j.electacta.2011.05.112. URL http://www.sciencedirect.com/science/article/pii/S0013468611008565. Selected Papers from the 61st {ISE} Meeting, Nice, France, 2010.

[45] Wu Xu, Vilayanur V. Viswanathan, Deyu Wang, Silas A. Towne, Jie Xiao, Zimin Nie, Dehong Hu, and Ji-Guang Zhang. Investigation on the charging process of li2o2-based air electrodes in lio2 batteries with organic carbonate electrolytes. *Journal of Power Sources*, 196(8):3894 – 3899, 2011. ISSN 0378-7753. doi: http://dx.doi.org/10.1016/j.jpowsour.2010.12.065. URL http://www.sciencedirect.com/science/article/pii/S0378775310022731.

[46] Stefan A. Freunberger, Yuhui Chen, Nicholas E. Drewett, Laurence J. Hardwick, Fanny Bard, and Peter G. Bruce. The lithiumoxygen battery with ether-based electrolytes. *Angewandte Chemie International Edition*, 50(37):8609–8613, 2011. ISSN 1521-3773. doi: 10.1002/anie.201102357. URL http://dx.doi.org/10.1002/anie.201102357.

[47] Gabriel M. Veith, Nancy J. Dudney, Jane Howe, and Jagjit Nanda. Spectroscopic characterization of solid discharge products in liair cells with aprotic carbonate electrolytes. *The Journal of Physical Chemistry C*, 115(29):14325–14333, 2011. doi: 10.1021/jp2043015. URL http://pubs.acs.org/doi/abs/10.1021/jp2043015.

[48] Takashi Takeuchi, Satoshi Noguchi, Hideyuki Morimoto, and Shin ichi Tobishima. Carbonate-modified siloxanes as solvents of electrolyte solutions for rechargeable lithium cells. *Journal of Power Sources*, 195(2):580 – 587, 2010. ISSN 0378-7753. doi: http://dx.doi.org/10.1016/j.jpowsour.2009.07.042. URL http://www.sciencedirect.com/science/article/pii/S0378775309012233.

[49] X.J. Wang, H.S. Lee, H. Li, X.Q. Yang, and X.J. Huang. The effects of substituting groups in cyclic carbonates for stable {SEI} formation on graphite anode of lithium batteries. *Electrochemistry Communications*, 12(3):386 – 389, 2010. ISSN 1388-2481. doi: http://dx.doi.org/10.1016/j.elecom.2009.12.041. URL http://www.sciencedirect.com/science/article/pii/S1388248110000020.

[50] Yasuhiro Takei, Kazuhiko Takeno, Hideyuki Morimoto, and Shin ichi Tobishima. Effects of nonaqueous electrolyte solutions mixed with carbonate-modified siloxane on chargedischarge performance of negative electrodes for secondary lithium batteries. *Journal of Power Sources*, 228(0):32 – 38, 2013. ISSN 0378-7753. doi: http://dx.doi.org/10.1016/j.jpowsour.2012.11.096. URL http://www.sciencedirect.com/science/article/pii/S0378775312017715.

[51] Zonghai Chen, H. H. Wang, D. R. Vissers, Lingzhi Zhang, R. West, L. J. Lyons, and K. Amine. Kinetic investigation of the solvation of lithium salts in siloxanes. *The Journal of Physical Chemistry C*, 112(6):2210–2214, 2008. doi: 10.1021/jp076744h. URL http://pubs.acs.org/doi/abs/10.1021/jp076744h.

[52] Lingzhi Zhang, Zhengcheng Zhang, Scott Harring, Megan Straughan, Rachel Butorac, Zonghai Chen, Leslie Lyons, Khalil Amine, and Robert West. Highly conductive trimethylsilyl oligo(ethylene oxide) electrolytes for energy storage applications. *J. Mater. Chem.*, 18:3713–3717, 2008. doi: 10.1039/B806290K. URL http://dx.doi.org/10.1039/B806290K.

[53] Hiroshi Nakahara, Sang-Young Yoon, and Steven Nutt. Effect of an additive to polysiloxane-based electrolyte on passive film formation on a graphite electrode. *Journal of Power Sources*, 158(1):600 – 607, 2006. ISSN 0378-7753. doi: http:

//dx.doi.org/10.1016/j.jpowsour.2005.09.050. URL http://www.sciencedirect.com/science/article/pii/S0378775305013467.

[54] Hiroshi Nakahara and Steven Nutt. Compounds in solid electrolyte interface (sei) on carbonaceous material charged in siloxane-based electrolyte. *Journal of Power Sources*, 160(2):1355 – 1360, 2006. ISSN 0378-7753. doi: http://dx.doi.org/10.1016/j.jpowsour.2006.02.088. URL http://www.sciencedirect.com/science/article/pii/S0378775306004253. Special issue including selected papers presented at the International Workshop on Molten Carbonate Fuel Cells and Related Science and Technology 2005 together with regular papers.

[55] Hiroshi Nakahara, Manabu Tanaka, Sang-Young Yoon, and Steven Nutt. Electrochemical and thermal stability of a siloxane-based electrolyte on a lithium transition metal oxide cathode. *Journal of Power Sources*, 160(1):645 – 650, 2006. ISSN 0378-7753. doi: http://dx.doi.org/10.1016/j.jpowsour.2006.01.084. URL http://www.sciencedirect.com/science/article/pii/S0378775306001558.

[56] F Croce, GB Appetecchi, L Persi, and B Scrosati. Nanocomposite polymer electrolytes for lithium batteries. *Nature*, 394(6692):456–458, 1998.

[57] D.R. MacFarlane, P.J. Newman, K.M. Nairn, and M. Forsyth. Lithium-ion conducting ceramic/polyether composites. *Electrochimica Acta*, 43 (1011):1333 – 1337, 1998. ISSN 0013-4686. doi: http://dx.doi.org/10.1016/S0013-4686(97)10039-1. URL http://www.sciencedirect.com/science/article/pii/S0013468697100391.

[58] Binod Kumar, Stanley J Rodrigues, and Lawrence G Scanlon. Ionic conductivity of polymer-ceramic composites. *Journal of The Electrochemical Society*, 148(10): A1191–A1195, 2001.

[59] Colin D. Hubbard, Peter Illner, and Rudi van Eldik. Understanding chemical reaction mechanisms in ionic liquids: successes and challenges. *Chem. Soc. Rev.*, 40:272–290, 2011. doi: 10.1039/C0CS00043D. URL http://dx.doi.org/10.1039/C0CS00043D.

[60] Heiko Niedermeyer, Jason P. Hallett, Ignacio J. Villar-Garcia, Patricia A. Hunt, and Tom Welton. Mixtures of ionic liquids. *Chem. Soc. Rev.*, 41:7780–7802, 2012. doi: 10.1039/C2CS35177C. URL http://dx.doi.org/10.1039/C2CS35177C.

[61] Maxim V Fedorov and Alexei A Kornyshev. Ionic liquids at electrified interfaces. *Chemical reviews*, 114(5):2978–3036, 2014.

[62] Maciej Galiski, Andrzej Lewandowski, and Izabela Stpniak. Ionic liquids as electrolytes. *Electrochimica Acta*, 51(26):5567 – 5580, 2006. ISSN 0013-4686. doi: http://dx.doi.org/10.1016/j.electacta.2006.03.016. URL http://www.sciencedirect.com/science/article/pii/S0013468606002362.

[63] Zhi-Bin Zhou, Hajime Matsumoto, and Kuniaki Tatsumi. Cyclic quaternary ammonium ionic liquids with perfluoroalkyltrifluoroborates: Synthesis, characterization, and properties. *Chemistry – A European Journal*, 12(8):2196–2212, 2006. ISSN 1521-3765. doi: 10.1002/chem.200500930. URL http://dx.doi.org/10.1002/chem.200500930.

[64] Eliana Quartarone and Piercarlo Mustarelli. Electrolytes for solid-state lithium rechargeable batteries: recent advances and perspectives. *Chem. Soc. Rev.*, 40: 2525–2540, 2011. doi: 10.1039/C0CS00081G. URL http://dx.doi.org/10.1039/C0CS00081G.

[65] M. L; Ahuja. S. C; Mandal. H. G Lakhanpul. No Title. *Indian Journal of Chemistry*, 102:928, 1978.

[66] Ashwini K Srivastava, Rajesh A Samant, and Snehal D Patankar. Ionic Conductivity in Binary Solvent Mixtures. 2. Ethylene Carbonate + Water at 25 C. *Journal of Chemical & Engineering Data*, 41(3):431–435, January 1996. ISSN 0021-9568. doi: 10.1021/je950207l. URL http://pubs.acs.org/doi/abs/10.1021/je950207l.

[67] J.O. Besenhard and H.P. Fritz. Cathodic reduction of graphite in organic solutions of alkali and nr4+ salts. *Journal of Electroanalytical Chemistry and Interfacial Electrochemistry*, 53(2):329 – 333, 1974. ISSN 0022-0728. doi: http://dx.doi.org/10.1016/S0022-0728(74)80146-4. URL http://www.sciencedirect.com/science/article/pii/S0022072874801464.

[68] D. Aurbach, M. L. Daroux, P. W. Faguy, and E. Yeager. Identification of surface films formed on lithium in propylene carbonate solutions. *Journal of The Electrochemical Society*, 134(7):1611–1620, 1987. doi: 10.1149/1.2100722. URL http://jes.ecsdl.org/content/134/7/1611.abstract.

[69] Marco Masia, Michael Probst, and Rossend Rey. Ethylene CarbonateLi + : A Theoretical Study of Structural and Vibrational Properties in Gas and Liquid Phases. *The Journal of Physical Chemistry B*, 108(6):2016–2027, February 2004. ISSN 1520-6106. doi: 10.1021/jp036673w. URL http://pubs.acs.org/doi/abs/10.1021/jp036673w.

[70] Yixuan Wang and Perla B. Balbuena. Theoretical studies on cosolvation of Li ion and solvent reductive decomposition in binary mixtures of aliphatic carbonates. *International Journal of Quantum Chemistry*, 102(5):724–733, 2005. ISSN 0020-7608. doi: 10.1002/qua.20466. URL http://doi.wiley.com/10.1002/qua.20466.

[71] Hiroto Tachikawa and Shigeaki Abe. Solvent Stripping Dynamics of Lithium ion solvated by ethylene carbonates: A direct ab-initio molecular (AIMD) Study. *Electrochimica Acta*, 120:57–64, February 2014. ISSN 00134686. doi: 10.1016/j.

electacta.2013.12.054. URL http://linkinghub.elsevier.com/retrieve/pii/S0013468613024948.

[72] Mahesh Datt Bhatt, Maenghyo Cho, and Kyeongjae Cho. Interaction of Li+ ions with ethylene carbonate (EC): Density functional theory calculations. *Applied Surface Science*, 257(5):1463–1468, December 2010. ISSN 01694332. doi: 10.1016/j.apsusc.2010.08.073. URL http://dx.doi.org/10.1016/j.apsusc.2010.08.073http://linkinghub.elsevier.com/retrieve/pii/S0169433210011517.

[73] Mahesh Datt Bhatt, Maenghyo Cho, and Kyeongjae Cho. Density functional theory calculations and ab initio molecular dynamics simulations for diffusion of Li + within liquid ethylene carbonate. *Modelling and Simulation in Materials Science and Engineering*, 20(6):065004, September 2012. ISSN 0965-0393. doi: 10.1088/0965-0393/20/6/065004. URL http://stacks.iop.org/0965-0393/20/i=6/a=065004?key=crossref.07f7d60dc5074ea12e091cb856bb1d53.

[74] Mahesh Datt Bhatt, Maenghyo Cho, and Kyeongjae Cho. Conduction of li+ cations in ethylene carbonate (ec) and propylene carbonate (pc): comparative studies using density functional theory. *Journal of Solid State Electrochemistry*, 16(2):435–441, 2012.

[75] Shin-ichi Tobishima and Akihiko Yamaji. Electrolytic characteristics of mixed solvent electrolytes for lithium secondary batteries. *Electrochimica Acta*, 28(8):1067–1072, 1983. ISSN 0013-4686. doi: http://dx.doi.org/10.1016/0013-4686(83)80010-3. URL http://www.sciencedirect.com/science/article/pii/0013468683800103.

[76] B Klassen, R Aroca, M. Nazri, and G. A. Nazri. Raman Spectra and Transport Properties of Lithium Perchlorate in Ethylene Carbonate Based Binary Solvent Systems for Lithium Batteries. *The Journal of Physical Chemistry B*, 102(24):4795–4801, June 1998. ISSN 1520-6106. doi: 10.1021/jp973099d. URL http://pubs.acs.org/doi/abs/10.1021/jp973099d.

[77] D. Guyomard and J. M. Tarascon. Rechargeable li1+x mn2o4/carbon cells with a new electrolyte composition: Potentiostatic studies and application to practical cells. *Journal of The Electrochemical Society*, 140(11):3071–3081, 1993. doi: 10.1149/1.2220987. URL http://jes.ecsdl.org/content/140/11/3071.abstract.

[78] J TARASCON and D GUYOMARD. New electrolyte compositions stable over the 0 to 5 V voltage range and compatible with the Li1+xMn2O4/carbon Li-ion cells. *Solid State Ionics*, 69(3-4):293–305, August 1994. ISSN 01672738. doi: 10.1016/0167-2738(94)90418-9. URL http://www.sciencedirect.com/science/article/pii/0167273894904189http://linkinghub.elsevier.com/retrieve/pii/0167273894904189.

[79] D. Guyomard. Rechargeable Li[sub 1+x]Mn[sub 2]O[sub 4]Carbon Cells with a New Electrolyte Composition. *Journal of The Electrochemical Society*, 140(11): 3071, 1993. ISSN 00134651. doi: 10.1149/1.2220987. URL http://jes.ecsdl.org/cgi/doi/10.1149/1.2220987.

[80] Gianfranco Pistoia, Mario De Rossi, and Bruno Scrosati. Study of the Behavior of Ethylene Carbonate as a Nonaqueous Battery Solvent. *Journal of The Electrochemical Society*, 117(4):500, 1970. ISSN 00134651. doi: 10.1149/1.2407550. URL http://jes.ecsdl.org/cgi/doi/10.1149/1.2407550.

[81] Shi-Aki Hyodo and Katsuaki Okabayashi. Raman intensity study of local structure in non-aqueous electrolyte solutionsI. Cation-solvent interaction in LiClO4/ethylene carbonate. *Electrochimica Acta*, 34(11):1551–1556, November 1989. ISSN 00134686. doi: 10.1016/0013-4686(89)87040-9. URL http://linkinghub.elsevier.com/retrieve/pii/0013468689870409.

[82] Tao Li. Theoretical Studies of Lithium Perchlorate in Ethylene Carbonate, Propylene Carbonate, and Their Mixtures. *Journal of The Electrochemical Society*, 146(10):3613, 1999. ISSN 00134651. doi: 10.1149/1.1392523. URL http://jes.ecsdl.org/cgi/doi/10.1149/1.1392523.

[83] Marco Castriota, Enzo Cazzanelli, Isabella Nicotera, Luigi Coppola, Cesare Oliviero, and Giuseppe Antonio Ranieri. Temperature dependence of lithium ion solvation in ethylene carbonateLiClO[sub 4] solutions. *The Journal of Chemical Physics*, 118(12):5537, 2003. ISSN 00219606. doi: 10.1063/1.1528190. URL http://scitation.aip.org/content/aip/journal/jcp/118/12/10.1063/1.1528190.

[84] Zhaoxiang Wang, Biying Huang, Rongjian Xue, Liquan Chen, and Xuejie Huang. Ion association and salvation studies of liclo4/ethylene carbonate electrolyte by raman and infrared spectroscopy. *Journal of The Electrochemical Society*, 145 (10):3346–3350, 1998. doi: 10.1149/1.1838810. URL http://jes.ecsdl.org/content/145/10/3346.abstract.

[85] Yoshiharu Matsuda, Tsuyoshi Fukushima, Hiroyuki Hashimoto, and Ryuichi Arakawa. Solvation of Lithium Ions in Mixed Organic Electrolyte Solutions by Electrospray Ionization Mass Spectroscopy. *Journal of The Electrochemical Society*, 149(8):A1045, 2002. ISSN 00134651. doi: 10.1149/1.1489687. URL http://jes.ecsdl.org/cgi/doi/10.1149/1.1489687.

[86] Soon-ki Jeong, Minoru Inaba, Yasutoshi Iriyama, Takeshi Abe, and Zempachi Ogumi. Surface film formation on a graphite negative electrode in lithium-ion batteries: AFM study on the effects of co-solvents in ethylene carbonate-based solutions. *Electrochimica Acta*, 47(12):1975–1982, May 2002. ISSN 00134686.

doi: 10.1016/S0013-4686(02)00099-3. URL http://linkinghub.elsevier.com/retrieve/pii/S0013468602000993.

[87] Jean-Christophe Soetens, Claude Millot, and Bernard Maigret. Molecular Dynamics Simulation of Li + BF 4 - in Ethylene Carbonate, Propylene Carbonate, and Dimethyl Carbonate Solvents. *The Journal of Physical Chemistry A*, 102 (7):1055–1061, February 1998. ISSN 1089-5639. doi: 10.1021/jp972457+. URL http://pubs.acs.org/doi/abs/10.1021/jp972457%2B.

[88] O O Postupna, Y V Kolesnik, O N Kalugin, and O V Prezhdo. Microscopic structure and dynamics of LiBF4 solutions in cyclic and linear carbonates. *The journal of physical chemistry. B*, 115(49):14563–71, December 2011. ISSN 1520-5207. doi: 10.1021/jp206006m. URL http://www.ncbi.nlm.nih.gov/pubmed/21995517.

[89] Kazutaka Kondo, Mitsuru Sano, Akio Hiwara, Takehiko Omi, Miho Fujita, Akio Kuwae, Masauu Iida, Koichi Mogi, and Haruhiko Yokoyama. Conductivity and Solvation of Li + Ions of LiPF 6 in Propylene Carbonate Solutions. *The Journal of Physical Chemistry B*, 104(20):5040–5044, May 2000. ISSN 1520-6106. doi: 10.1021/jp000142f. URL http://pubs.acs.org/doi/abs/10.1021/jp000142f.

[90] Munetaka Takeuchi, Yasuo Kameda, Yasuhiro Umebayashi, Sari Ogawa, Takaaki Sonoda, Shin-ichi Ishiguro, Miho Fujita, and Mitsuru Sano. Ionion interactions of LiPF6 and LiBF4 in propylene carbonate solutions. *Journal of Molecular Liquids*, 148(2-3):99–108, September 2009. ISSN 01677322. doi: 10.1016/j.molliq.2009.07.003. URL http://linkinghub.elsevier.com/retrieve/pii/S0167732209001536.

[91] Oleg Borodin and Grant D Smith. LiTFSI structure and transport in ethylene carbonate from molecular dynamics simulations. *The journal of physical chemistry. B*, 110(10):4971–7, March 2006. ISSN 1520-6106. doi: 10.1021/jp056249q. URL http://www.ncbi.nlm.nih.gov/pubmed/16526738.

[92] Masayuki Morita, Yoshiko Asai, Nobuko Yoshimoto, and Masashi Ishikawa. A Raman spectroscopic study of organic electrolyte solutions based on binary solvent systems of ethylene carbonate with low viscosity solvents which dissolve different lithium salts. *Journal of the Chemical Society, Faraday Transactions*, 94(23):3451–3456, 1998. ISSN 09565000. doi: 10.1039/a806278a. URL http://xlink.rsc.org/?DOI=a806278a.

[93] Ken Tasaki. Computational Study of Salt Association in Li-Ion Battery Electrolyte. *Journal of The Electrochemical Society*, 149(4):A418, 2002. ISSN 00134651. doi: 10.1149/1.1456533. URL http://jes.ecsdl.org/cgi/doi/10.1149/1.1456533.

[94] Hajime Tsunekawa, Akiko Narumi, Mitsuru Sano, Akio Hiwara, Miho Fujita, and Haruhiko Yokoyama. Solvation and ion association studies of libf4propylenecarbonate and libf4propylenecarbonatetrimethyl phosphate solutions. *The Journal of Physical Chemistry B*, 107(39):10962–10966, 2003. doi: 10.1021/jp0300546. URL http://pubs.acs.org/doi/abs/10.1021/jp0300546.

[95] Atetegeb Meazah Haregewoin, Ermias Girma Leggesse, Jyh-Chiang Jiang, Fu-Ming Wang, Bing-Joe Hwang, and Shawn D. Lin. A combined experimental and theoretical study of surface film formation: Effect of oxygen on the reduction mechanism of propylene carbonate. *Journal of Power Sources*, 244:318–327, December 2013. ISSN 03787753. doi: 10.1016/j.jpowsour.2013.01.030. URL http://linkinghub.elsevier.com/retrieve/pii/S0378775313000530.

[96] Oleg Borodin and Grant D Smith. Quantum chemistry and molecular dynamics simulation study of dimethyl carbonate: ethylene carbonate electrolytes doped with LiPF6. *The journal of physical chemistry. B*, 113(6):1763–76, February 2009. ISSN 1520-6106. doi: 10.1021/jp809614h. URL http://www.ncbi.nlm.nih.gov/pubmed/19146427.

[97] P Ganesh, De-en Jiang, and P R C Kent. Accurate static and dynamic properties of liquid electrolytes for Li-ion batteries from ab initio molecular dynamics. *The journal of physical chemistry. B*, 115(12):3085–90, March 2011. ISSN 1520-5207. doi: 10.1021/jp2003529. URL http://www.ncbi.nlm.nih.gov/pubmed/21384941.

[98] Xavier Bogle, Rafael Vazquez, Steven Greenbaum, Arthur von Wald Cresce, and Kang Xu. Understanding Li + Solvent Interaction in Nonaqueous Carbonate Electrolytes with 17 O NMR. *The Journal of Physical Chemistry Letters*, 4(10): 1664–1668, May 2013. ISSN 1948-7185. doi: 10.1021/jz400661k. URL http://pubs.acs.org/doi/abs/10.1021/jz400661k.

[99] Craig M. Tenney and Randall T. Cygan. Analysis of Molecular Clusters in Simulations of Lithium-Ion Battery Electrolytes. *The Journal of Physical Chemistry C*, 117(47):24673–24684, November 2013. ISSN 1932-7447. doi: 10.1021/jp4039122. URL http://pubs.acs.org/doi/abs/10.1021/jp4039122.

[100] Munetaka Takeuchi, Nobuyuki Matubayasi, Yasuo Kameda, Babak Minofar, Shinichi Ishiguro, and Yasuhiro Umebayashi. Free-energy and structural analysis of ion solvation and contact ion-pair formation of Li(+) with BF4(-) and PF6(-) in water and carbonate solvents. *The journal of physical chemistry. B*, 116(22):6476–87, June 2012. ISSN 1520-5207. doi: 10.1021/jp3011487. URL http://www.ncbi.nlm.nih.gov/pubmed/22616851.

[101] Kaijun Yuan, Hongtao Bian, Yuneng Shen, Bo Jiang, Jiebo Li, Yufan Zhang, Hailong Chen, and Junrong Zheng. Coordination number of li+ in nonaqueous

electrolyte solutions determined by molecular rotational measurements. *The Journal of Physical Chemistry B*, 118(13):3689–3695, 2014.

[102] E. Schrdinger. Quantisierung als eigenwertproblem. *Annalen der Physik*, 384(4): 361–376, 1926. ISSN 1521-3889. doi: 10.1002/andp.19263840404. URL http://dx.doi.org/10.1002/andp.19263840404.

[103] M. Born and R. Oppenheimer. Zur quantentheorie der molekeln. *Annalen der Physik*, 389(20):457–484, 1927. ISSN 1521-3889. doi: 10.1002/andp.19273892002. URL http://dx.doi.org/10.1002/andp.19273892002.

[104] Peter Ring and Peter Schuck. *The nuclear many-body problem*. Springer, 2004.

[105] E. Fermi. Eine statistische methode zur bestimmung einiger eigenschaften des atoms und ihre anwendung auf die theorie des periodischen systems der elemente. *Zeitschrift fr Physik*, 48(1-2):73–79, 1928. ISSN 0044-3328. doi: 10.1007/BF01351576. URL http://dx.doi.org/10.1007/BF01351576.

[106] LH Thomas. On the capture of electrons by swiftly moving electrified particles. *Proceedings of the Royal Society of London. Series A*, 114(768):561–576, 1927.

[107] Robert G Parr and Weitao Yang. *Density-functional theory of atoms and molecules*, volume 16. Oxford university press, 1989.

[108] Eberhard KU Gross and Reiner M Dreizler. *Density functional theory*. Springer, 1995.

[109] R G Parr. Density functional theory. *Annual Review of Physical Chemistry*, 34 (1):631–656, 1983. doi: 10.1146/annurev.pc.34.100183.003215. URL http://dx.doi.org/10.1146/annurev.pc.34.100183.003215.

[110] Tom. Ziegler. Approximate density functional theory as a practical tool in molecular energetics and dynamics. *Chemical Reviews*, 91(5):651–667, 1991. doi: 10.1021/cr00005a001. URL http://pubs.acs.org/doi/abs/10.1021/cr00005a001.

[111] P. Geerlings, F. De Proft, and W. Langenaeker. Conceptual density functional theory. *Chemical Reviews*, 103(5):1793–1874, 2003. doi: 10.1021/cr990029p. URL http://pubs.acs.org/doi/abs/10.1021/cr990029p.

[112] P. Hohenberg and W. Kohn. Inhomogeneous electron gas. *Phys. Rev.*, 136:B864–B871, Nov 1964. doi: 10.1103/PhysRev.136.B864. URL http://link.aps.org/doi/10.1103/PhysRev.136.B864.

[113] W. Kohn and L. J. Sham. Self-consistent equations including exchange and correlation effects. *Phys. Rev.*, 140:A1133–A1138, Nov 1965. doi: 10.1103/PhysRev.140.A1133. URL http://link.aps.org/doi/10.1103/PhysRev.140.A1133.

[114] Ann E. Mattsson. In pursuit of the "divine" functional. *Science*, 298(5594):759–760, 2002. doi: 10.1126/science.1077710. URL http://www.sciencemag.org/content/298/5594/759.short.

[115] D. M. Ceperley and B. J. Alder. Ground state of the electron gas by a stochastic method. *Phys. Rev. Lett.*, 45:566–569, Aug 1980. doi: 10.1103/PhysRevLett.45.566. URL http://link.aps.org/doi/10.1103/PhysRevLett.45.566.

[116] John P Perdew and Alex Zunger. Self-interaction correction to density-functional approximations for many-electron systems. *Physical Review B*, 23(10):5048, 1981.

[117] J Harris and RO Jones. The surface energy of a bounded electron gas. *Journal of Physics F: Metal Physics*, 4(8):1170, 1974.

[118] David C Langreth and John P Perdew. The exchange-correlation energy of a metallic surface. *Solid State Communications*, 17(11):1425–1429, 1975.

[119] J Harris. Adiabatic-connection approach to kohn-sham theory. *Physical Review A*, 29(4):1648, 1984.

[120] John P Perdew and Yue Wang. Pair-distribution function and its coupling-constant average for the spin-polarized electron gas. *Physical Review B*, 46(20):12947, 1992.

[121] John P Perdew and Yue Wang. Accurate and simple analytic representation of the electron-gas correlation energy. *Physical Review B*, 45(23):13244, 1992.

[122] SH Vosko, Ll Wilk, and M Nusair. Accurate spin-dependent electron liquid correlation energies for local spin density calculations: a critical analysis. *Canadian Journal of Physics*, 58(8):1200–1211, 1980.

[123] Axel D Becke. Density-functional exchange-energy approximation with correct asymptotic behavior. *Physical Review A*, 38(6):3098, 1988.

[124] John P Perdew, JA Chevary, SH Vosko, Koblar A Jackson, Mark R Pederson, DJ Singh, and Carlos Fiolhais. Atoms, molecules, solids, and surfaces: Applications of the generalized gradient approximation for exchange and correlation. *Physical Review B*, 46(11):6671, 1992.

[125] John P Perdew, Kieron Burke, and Matthias Ernzerhof. Generalized gradient approximation made simple. *Physical review letters*, 77(18):3865, 1996.

[126] Atom PBE revPBE Exact. Comment on generalized gradient approximation made simple. 1998.

[127] BHLB Hammer, Lars Bruno Hansen, and Jens Kehlet Nørskov. Improved adsorption energetics within density-functional theory using revised perdew-burke-ernzerhof functionals. *Physical Review B*, 59(11):7413, 1999.

[128] John P Perdew, Adrienn Ruzsinszky, Gábor I Csonka, Oleg A Vydrov, Gustavo E Scuseria, Lucian A Constantin, Xiaolan Zhou, and Kieron Burke. Restoring the density-gradient expansion for exchange in solids and surfaces. *Physical Review Letters*, 100(13):136406, 2008.

[129] Adrienn Ruzsinszky, Gábor I Csonka, and Gustavo E Scuseria. Regularized gradient expansion for atoms, molecules, and solids. *Journal of Chemical Theory and Computation*, 5(4):763–769, 2009.

[130] Yan Zhao and Donald G Truhlar. Construction of a generalized gradient approximation by restoring the density-gradient expansion and enforcing a tight lieb–oxford bound. *The Journal of chemical physics*, 128(18):184109, 2008.

[131] Andrew R. Leach. *Molecular modelling: principles and applications*. Pearson Education, 2001.

[132] E.J. Baerends, D.E. Ellis, and P. Ros. Self-consistent molecular hartreefockslater calculations i. the computational procedure. *Chemical Physics*, 2(1):41 – 51, 1973. ISSN 0301-0104. doi: http://dx.doi.org/10.1016/0301-0104(73)80059-X. URL http://www.sciencedirect.com/science/article/pii/030101047380059X.

[133] G. te Velde, F. M. Bickelhaupt, E. J. Baerends, C. Fonseca Guerra, S. J. A. van Gisbergen, J. G. Snijders, and T. Ziegler. Chemistry with adf. *Journal of Computational Chemistry*, 22(9):931–967, 2001. ISSN 1096-987X. doi: 10.1002/jcc.1056. URL http://dx.doi.org/10.1002/jcc.1056.

[134] G. te Velde and E. J. Baerends. Precise density-functional method for periodic structures. *Phys. Rev. B*, 44:7888–7903, Oct 1991. doi: 10.1103/PhysRevB.44.7888. URL http://link.aps.org/doi/10.1103/PhysRevB.44.7888.

[135] P. M. Boerrigter, G. Te Velde, and J. E. Baerends. Three-dimensional numerical integration for electronic structure calculations. *International Journal of Quantum Chemistry*, 33(2):87–113, 1988. ISSN 1097-461X. doi: 10.1002/qua.560330204. URL http://dx.doi.org/10.1002/qua.560330204.

[136] G. te Velde and E.J. Baerends. Numerical integration for polyatomic systems. *Journal of Computational Physics*, 99(1):84 – 98, 1992. ISSN 0021-9991. doi: http://dx.doi.org/10.1016/0021-9991(92)90277-6. URL http://www.sciencedirect.com/science/article/pii/0021999192902776.

[137] C. Fonseca Guerra, J. G. Snijders, G. te Velde, and E. J. Baerends. Towards an order-n dft method. *Theoretical Chemistry Accounts*, 99(6):391–403, 1998. ISSN 1432-881X. doi: 10.1007/s002140050353. URL http://dx.doi.org/10.1007/s002140050353.

[138] E. J. Baerends and P. Ros. Evaluation of the lcao hartreefockslater method: Applications to transition-metal complexes. *International Journal of Quantum Chemistry*, 14(S12):169–190, 1978. ISSN 1097-461X. doi: 10.1002/qua.560140814. URL http://dx.doi.org/10.1002/qua.560140814.

[139] J.G. Snijders, E.J. Baerends, and P. Ros. A perturbation theory approach to relativistic calculations. *Molecular Physics*, 38(6):1909–1929, 1979. doi: 10.1080/00268977900102941. URL http://dx.doi.org/10.1080/00268977900102941.

[140] E. van Lenthe, E. J. Baerends, and J. G. Snijders. Relativistic regular twocomponent hamiltonians. *The Journal of Chemical Physics*, 99(6), 1993.

[141] E. van Lenthe, E. J. Baerends, and J. G. Snijders. Relativistic total energy using regular approximations. *The Journal of Chemical Physics*, 101(11), 1994.

[142] E. van Lenthe, J. G. Snijders, and E. J. Baerends. The zeroorder regular approximation for relativistic effects: The effect of spinorbit coupling in closed shell molecules. *The Journal of Chemical Physics*, 105(15), 1996.

[143] E Van Lenthe, R Van Leeuwen, and EJ Baerends. Re la tivis t ic regular two-c omponen t hamiltonians. *International Journal of Quantum Chemistry*, 57:281–293, 1996.

[144] Louis Versluis and Tom Ziegler. The determination of molecular structures by density functional theory. the evaluation of analytical energy gradients by numerical integration. *The Journal of Chemical Physics*, 88(1), 1988.

[145] Liangyou Fan and Tom Ziegler. Application of density functional theory to infrared absorption intensity calculations on main group molecules. *The Journal of Chemical Physics*, 96(12), 1992.

[146] Georg Schreckenbach and Tom Ziegler. The calculation of nmr shielding tensors based on density functional theory and the frozen-core approximation. *International Journal of Quantum Chemistry*, 60(3):753–766, 1996. ISSN 1097-461X. doi: 10.1002/(SICI)1097-461X(1996)60:3⟨753::AID-QUA4⟩3.0.CO;2-W. URL http://dx.doi.org/10.1002/(SICI)1097-461X(1996)60:3<753::AID-QUA4>3.0.CO;2-W.

[147] Georg Schreckenbach and Tom Ziegler. Calculation of nmr shielding tensors based on density functional theory and a scalar relativistic pauli-type hamiltonian. the application to transition metal complexes. *International Journal of Quantum Chemistry*, 61(6):899–918, 1997. ISSN 1097-461X. doi: 10.1002/(SICI)1097-461X(1997)61:6⟨899::AID-QUA3⟩3.0.CO;2-R. URL http://dx.doi.org/10.1002/(SICI)1097-461X(1997)61:6<899::AID-QUA3>3.0.CO;2-R.

[148] S. K. Wolff and T. Ziegler. Calculation of dft-giao nmr shifts with the inclusion of spin-orbit coupling. *The Journal of Chemical Physics*, 109(3), 1998.

[149] Cory C. Pye and Tom Ziegler. An implementation of the conductor-like screening model of solvation within the amsterdam density functional package. *Theoretical Chemistry Accounts*, 101(6):396–408, 1999. ISSN 1432-881X. doi: 10.1007/s002140050457. URL http://dx.doi.org/10.1007/s002140050457.

[150] Tom K. Woo, Luigi Cavallo, and Tom Ziegler. Implementation of the imomm methodology for performing combined qm/mm molecular dynamics simulations and frequency calculations. *Theoretical Chemistry Accounts*, 100(5-6):307–313, 1998. ISSN 1432-881X. doi: 10.1007/s002140050391. URL http://dx.doi.org/10.1007/s002140050391.

[151] S. J. A. van Gisbergen, J. G. Snijders, and E. J. Baerends. A density functional theory study of frequencydependent polarizabilities and van der waals dispersion coefficients for polyatomic molecules. *The Journal of Chemical Physics*, 103(21), 1995.

[152] S. J. A. van Gisbergen, V. P. Osinga, O. V. Gritsenko, R. van Leeuwen, J. G. Snijders, and E. J. Baerends. Improved density functional theory results for frequencydependent polarizabilities, by the use of an exchangecorrelation potential with correct asymptotic behavior. *The Journal of Chemical Physics*, 105(8), 1996.

[153] S. J. A. van Gisbergen, J. G. Snijders, and E. J. Baerends. Calculating frequency-dependent hyperpolarizabilities using time-dependent density functional theory. *The Journal of Chemical Physics*, 109(24), 1998.

[154] S.J.A. van Gisbergen, J.G. Snijders, and E.J. Baerends. Application of time-dependent density functional response theory to raman scattering. *Chemical Physics Letters*, 259(56):599 – 604, 1996. ISSN 0009-2614. doi: http://dx.doi.org/10.1016/0009-2614(96)00858-5. URL http://www.sciencedirect.com/science/article/pii/0009261496008585.

[155] S. J. A. van Gisbergen, J. G. Snijders, and E. J. Baerends. Accurate density functional calculations on frequency-dependent hyperpolarizabilities of small molecules. *The Journal of Chemical Physics*, 109(24), 1998.

[156] Erik van Lenthe, Andreas Ehlers, and Evert-Jan Baerends. Geometry optimizations in the zero order regular approximation for relativistic effects. *The Journal of Chemical Physics*, 110(18), 1999.

[157] Tom Ziegler and Arvi Rauk. A theoretical study of the ethylene-metal bond in complexes between copper(1+), silver(1+), gold(1+), platinum(0) or platinum(2+) and ethylene, based on the hartree-fock-slater transition-state method. *Inorganic Chemistry*, 18(6):1558–1565, 1979. doi: 10.1021/ic50196a034. URL http://pubs.acs.org/doi/abs/10.1021/ic50196a034.

[158] Tom Ziegler and Arvi Rauk. Carbon monoxide, carbon monosulfide, molecular nitrogen, phosphorus trifluoride, and methyl isocyanide as .sigma. donors and .pi. acceptors. a theoretical study by the hartree-fock-slater transition-state method. *Inorganic Chemistry*, 18(7):1755–1759, 1979. doi: 10.1021/ic50197a006. URL http://pubs.acs.org/doi/abs/10.1021/ic50197a006.

[159] Keiji Morokuma. Molecular orbital studies of hydrogen bonds. iii. c=oho hydrogen bond in h2coh2o and h2co2h2o. *The Journal of Chemical Physics*, 55(3), 1971.

[160] Kazuo Kitaura and Keiji Morokuma. A new energy decomposition scheme for molecular interactions within the hartree-fock approximation. *International Journal of Quantum Chemistry*, 10(2):325–340, 1976. ISSN 1097-461X. doi: 10.1002/qua.560100211. URL http://dx.doi.org/10.1002/qua.560100211.

[161] R. S. Mulliken. Electronic population analysis on lcaomo molecular wave functions. i. *The Journal of Chemical Physics*, 23(10), 1955.

[162] R. S. Mulliken. Electronic population analysis on lcaomo molecular wave functions. iv. bonding and antibonding in lcao and valencebond theories. *The Journal of Chemical Physics*, 23(12), 1955.

[163] F. Matthias Bickelhaupt, Nicolaas J. R. van Eikema Hommes, Clia Fonseca Guerra, and Evert Jan Baerends. The carbonlithium electron pair bond in (ch3li)n (n = 1, 2, 4). *Organometallics*, 15(13):2923–2931, 1996. doi: 10.1021/om950966x. URL http://pubs.acs.org/doi/abs/10.1021/om950966x.

[164] F.L. Hirshfeld. Bonded-atom fragments for describing molecular charge densities. *Theoretica chimica acta*, 44(2):129–138, 1977. ISSN 0040-5744. doi: 10.1007/BF00549096. URL http://dx.doi.org/10.1007/BF00549096.

[165] Kenneth B. Wiberg and Paul R. Rablen. Comparison of atomic charges derived via different procedures. *Journal of Computational Chemistry*, 14(12):1504–1518, 1993. ISSN 1096-987X. doi: 10.1002/jcc.540141213. URL http://dx.doi.org/10.1002/jcc.540141213.

[166] S. H. Vosko, L. Wilk, and M. Nusair. Accurate spin-dependent electron liquid correlation energies for local spin density calculations: a critical analysis. *Canadian Journal of Physics*, 58(8):1200–1211, 1980. doi: 10.1139/p80-159. URL http://dx.doi.org/10.1139/p80-159.

[167] John P. Perdew and Wang Yue. Accurate and simple density functional for the electronic exchange energy: Generalized gradient approximation. *Phys. Rev. B*, 33:8800–8802, Jun 1986. doi: 10.1103/PhysRevB.33.8800. URL http://link.aps.org/doi/10.1103/PhysRevB.33.8800.

[168] John P. Perdew. Density-functional approximation for the correlation energy of the inhomogeneous electron gas. *Phys. Rev. B*, 33:8822–8824, Jun 1986. doi: 10.1103/PhysRevB.33.8822. URL http://link.aps.org/doi/10.1103/PhysRevB.33.8822.

[169] A. D. Becke. Density-functional exchange-energy approximation with correct asymptotic behavior. *Phys. Rev. A*, 38:3098–3100, Sep 1988. doi: 10.1103/PhysRevA.38.3098. URL http://link.aps.org/doi/10.1103/PhysRevA.38.3098.

[170] C Lee, W Yang, and RG Parr. Phys. l rev. b 37, 785 (1988);(b) ad becke. *Phys. Rev. A*, 38:3098, 1988.

[171] C. G. BROYDEN. The convergence of a class of double-rank minimization algorithms: 2. the new algorithm. *IMA Journal of Applied Mathematics*, 6(3):222–231, 1970. doi: 10.1093/imamat/6.3.222. URL http://imamat.oxfordjournals.org/content/6/3/222.abstract.

[172] Liangyou Fan and Tom Ziegler. Optimization of molecular structures by selfconsistent and nonlocal densityfunctional theory. *The Journal of Chemical Physics*, 95(10), 1991.

[173] Liangyou Fan and Tom Ziegler. Application of density functional theory to infrared absorption intensity calculations on transition-metal carbonyls. *The Journal of Physical Chemistry*, 96(17):6937–6941, 1992. doi: 10.1021/j100196a016. URL http://pubs.acs.org/doi/abs/10.1021/j100196a016.

[174] J. L. Pascual-Ahuir, E. Silla, J. Tomasi, and R. Bonaccorsi. Electrostatic interaction of a solute with a continuum. improved description of the cavity and of the surface cavity bound charge distribution. *Journal of Computational Chemistry*, 8(6):778–787, 1987. ISSN 1096-987X. doi: 10.1002/jcc.540080605. URL http://dx.doi.org/10.1002/jcc.540080605.

[175] Andreas Klamt. Conductor-like screening model for real solvents: A new approach to the quantitative calculation of solvation phenomena. *The Journal of Physical Chemistry*, 99(7):2224–2235, 1995. doi: 10.1021/j100007a062. URL http://pubs.acs.org/doi/abs/10.1021/j100007a062.

[176] A. Klamt and G. Schuurmann. Cosmo: a new approach to dielectric screening in solvents with explicit expressions for the screening energy and its gradient. *J. Chem. Soc., Perkin Trans. 2*, pages 799–805, 1993. doi: 10.1039/P29930000799. URL http://dx.doi.org/10.1039/P29930000799.

[177] Maurizio Cossi, Nadia Rega, Giovanni Scalmani, and Vincenzo Barone. Energies, structures, and electronic properties of molecules in solution with the c-pcm solvation model. *Journal of Computational Chemistry*, 24(6):669–681, 2003. ISSN 1096-987X. doi: 10.1002/jcc.10189. URL http://dx.doi.org/10.1002/jcc.10189.

[178] Juan Luis Pascual-Ahuir and Estanislao Silla. Gepol: An improved description of molecular surfaces. i. building the spherical surface set. *Journal of Computational Chemistry*, 11(9):1047–1060, 1990. ISSN 1096-987X. doi: 10.1002/jcc.540110907. URL http://dx.doi.org/10.1002/jcc.540110907.

[179] Estanislao Silla, Iaki Tun, and Juan Luis Pascual-Ahuir. Gepol: An improved description of molecular surfaces ii. computing the molecular area and volume. *Journal of Computational Chemistry*, 12(9):1077–1088, 1991. ISSN 1096-987X. doi: 10.1002/jcc.540120905. URL http://dx.doi.org/10.1002/jcc.540120905.

[180] Jacopo Tomasi, Benedetta Mennucci, and Roberto Cammi. Quantum mechanical continuum solvation models. *Chemical Reviews*, 105(8):2999–3094, 2005. doi: 10.1021/cr9904009. URL http://pubs.acs.org/doi/abs/10.1021/cr9904009.

[181] Loup Verlet. Computer" experiments" on classical fluids. i. thermodynamical properties of lennard-jones molecules. *Physical review*, 159(1):98, 1967.

[182] Denis J Evans. On the representatation of orientation space. *Molecular Physics*, 34(2):317–325, 1977.

[183] Mike P Allen, Dominic J Tildesley, et al. Computer simulation of liquids. 1987.

[184] Shūichi Nosé. A molecular dynamics method for simulations in the canonical ensemble. *Molecular physics*, 52(2):255–268, 1984.

[185] William G Hoover. Canonical dynamics: equilibrium phase-space distributions. *Physical Review A*, 31(3):1695, 1985.

[186] Michele Parrinello and Aneesur Rahman. Polymorphic transitions in single crystals: A new molecular dynamics method. *Journal of Applied physics*, 52(12): 7182–7190, 1981.

[187] C. J. Brown. The crystal structure of ethylene carbonate. *Acta Crystallographica*, 7(1):92–96, January 1954. ISSN 0365-110X. doi: 10.1107/S0365110X54000175. URL http://scripts.iucr.org/cgi-bin/paper?S0365110X54000175.

[188] C. L. Angell. The infra-red spectra and structure of ethylene carbonate. *Transactions of the Faraday Society*, 52(1178):1178, 1956. ISSN 0014-7672. doi: 10.1039/tf9565201178. URL http://xlink.rsc.org/?DOI=tf9565201178.

[189] Pedro M. Matias, G.A. Jeffrey, Lavinia M. Wingert, and John R. Ruble. Single crystal neutron diffraction analysis (15 K) and ab initio molecular orbital calculations for ethylene carbonate. *Journal of Molecular Structure: THEOCHEM*, 184(3-4):247–260, February 1989. ISSN 01661280. doi: 10.1016/0166-1280(89)85094-8. URL http://linkinghub.elsevier.com/retrieve/pii/0166128089850948.

[190] Irene Wang, Chester O. Britt, and James E. Boggs. The Planarity of the Ring Atoms in Ethylene Carbonate. *Journal of the American Chemical Society*, 87(21): 4950–4951, November 1965. ISSN 0002-7863. doi: 10.1021/ja00949a045. URL http://pubs.acs.org/doi/abs/10.1021/ja00949a045.

[191] Jean-Christophe Soetens, Claude Millot, Bernard Maigret, and Imre Bak. Molecular dynamics simulation and xray diffraction studies of ethylene carbonate, propylene carbonate and dimethyl carbonate in liquid phase. *Journal of Molecular Liquids*, 92(3):201 – 216, 2001. ISSN 0167-7322. doi: http://dx.doi.org/10.1016/S0167-7322(01)00192-1. URL http://www.sciencedirect.com/science/article/pii/S0167732201001921.

[192] Jose L Alonso, Rinaldo Cervellati, Alessandra Degli Esposti, David G Lister, and Paolo Palmieri. Microwave spectrum and ab initio computations for ethylene carbonate. Part 1.?Conformation and ring inversion. *Journal of the Chemical Society, Faraday Transactions 2*, 82(3):337, 1986. ISSN 0300-9238. doi: 10.1039/f29868200337. URL http://xlink.rsc.org/?DOI=f29868200337.

[193] J. E. Katon and M D Cohen. The Vibrational Spectra and Structure of Dimethyl Carbonate and its Conformational Behavior. *Canadian Journal of Chemistry*, 53 (9):1378–1386, May 1975. ISSN 0008-4042. doi: 10.1139/v75-191. URL http://www.nrcresearchpress.com/doi/abs/10.1139/v75-191.

[194] Hugo Bohets and Benjamin J. van der Veken. On the conformational behavior of dimethyl carbonate. *Physical Chemistry Chemical Physics*, 1(8):1817–1826, 1999. ISSN 14639076. doi: 10.1039/a901046g. URL http://xlink.rsc.org/?DOI=a901046g.

[195] D. Labrenz and W. Schrer. Conformational analysis of symmetric carbonic acid esters by quantum chemical calculations and dielectric measurements. *Journal of Molecular Structure*, 249(24):327 – 341, 1991. ISSN 0022-2860. doi: http://dx.doi.org/10.1016/0022-2860(91)85078-H. URL http://www.sciencedirect.com/science/article/pii/002228609185078H.

[196] OKIMASA OKADA. Conformational analysis of liquid dimethyl carbonate by molecular dynamics calculations. *Molecular Physics*, 93(1):153–158, 1998. doi: 10.1080/002689798169546. URL http://www.tandfonline.com/doi/abs/10.1080/002689798169546.

[197] Mahesh Datt Bhatt and Colm O'Dwyer. Density functional theory calculations for ethylene carbonate-based binary electrolyte mixtures in lithium ion batteries. *Current Applied Physics*, 14(3):349–354, March 2014. ISSN 15671739. doi: 10.1016/j.cap.2013.12.010. URL http://linkinghub.elsevier.com/retrieve/pii/S1567173913004513.

[198] Gregory S. Tschumper, Justin T. Fermann, and Henry F. Schaefer. Structures, thermochemistry, and electron affinities of the pfn and pfn series, n=16. *The Journal of Chemical Physics*, 104(10), 1996.

[199] Christoph Klmel, Gottfried Palm, Reinhart Ahlrichs, Michael Br, and Alexander I. Boldyrev. Ab initio study of structure, stability and ionization potentials of the anions pf6 and p2f11. *Chemical Physics Letters*, 173(23):151 – 156, 1990. ISSN 0009-2614. doi: http://dx.doi.org/10.1016/0009-2614(90)80069-P. URL http://www.sciencedirect.com/science/article/pii/000926149080069P.

[200] Oleg Borodin, Grant D. Smith, and Richard L. Jaffe. Ab initio quantum chemistry and molecular dynamics simulations studies of lipf6/poly(ethylene oxide) interactions. *Journal of Computational Chemistry*, 22(6):641–654, 2001. ISSN 1096-987X. doi: 10.1002/jcc.1033. URL http://dx.doi.org/10.1002/jcc.1033.

[201] Y. Wang, L. D. Calvert, and S. K. Brownstein. The structure of tetramethylammonium hexafluorophosphate. *Acta Crystallographica Section B*, 36(6):1523, Jun 1980. doi: 10.1107/S0567740880006498. URL http://dx.doi.org/10.1107/S0567740880006498.

[202] P.J. Hay and W.R. Wadt. Ab initio effective core potentials for molecular calculations. potentials for k to au including the outermost core orbitale. *The Journal of Chemical Physics*, 82(1):299–310, 1985. URL http://www.scopus.com/inward/record.url?eid=2-s2.0-27344448074&partnerID=40&md5=45923a6871b942ca1d5553b4c5423571. cited By (since 1996)7765.

[203] R. Aroca, M. Nazri, G.A. Nazri, A.J. Camargo, and M. Trsic. Vibrational spectra and ion-pair properties of lithium hexafluorophosphate in ethylene carbonate based mixed-solvent systems for lithium batteries. *Journal of Solution Chemistry*, 29 (10):1047–1060, 2000. ISSN 0095-9782. doi: 10.1023/A:1005151220893. URL http://dx.doi.org/10.1023/A%3A1005151220893.

[204] Xiaopeng Xuan, Jianji Wang, and Hanqing Wang. Theoretical insights into pf6 and its alkali metal ion pairs: geometries and vibrational frequencies. *Electrochimica Acta*, 50(20):4196 – 4201, 2005. ISSN 0013-4686. doi: http://dx.doi.org/10.1016/j.electacta.2005.01.045. URL http://www.sciencedirect.com/science/article/pii/S0013468605000940.

[205] Leandro Martínez, R Andrade, Ernesto G Birgin, and José Mario Martínez. Packmol: A package for building initial configurations for molecular dynamics simulations. *Journal of computational chemistry*, 30(13):2157–2164, 2009.

[206] William G Hoover. Constant-pressure equations of motion. *Physical Review A*, 34 (3):2499–2500, 1986.

[207] W Smith and TR Forester. Dl_poly_2. 0: A general-purpose parallel molecular dynamics simulation package. *Journal of Molecular Graphics*, 14(3):136–141, 1996.